Technische Universität München

TUM School of Engineering and Design

# A multipronged study on improved wind farm operation with emphasis on wind farm aerodynamics

**Emmanouil Marios Nanos**

Vollständiger Abdruck der von der TUM School of Engineering and Design der Technischen Universität München zur Erlangung des akademischen Grades eines

**Doktors der Ingenieurwissenschaften (Dr.-Ing.)**

genehmigten Dissertation.

| | |
|---|---|
| Vorsitzender: | Prof. Dr.-Ing. Manfred Hajek |
| Prüfer der Dissertation: | Prof. Dr. Carlo L. Bottasso |
| Zweiter Prüfer der Dissertation: | Prof. Dr. Vasilis A. Riziotis |

Die Dissertation wurde am 25.08.2021 bei der Technischen Universität München eingereicht und durch die TUM School of Engineering and Design am 10.11.2021 angenommen.

Technische Universität München
Fakultät für Maschinenwesen
Lehrstuhl für Windenergie
Boltzmannstraße 15
D-85748 Garching bei München
Germany
Tel.: +49 (0) 89 / 289 – 16681
Fax.: +49 (0) 89 / 289 – 16611
Email: info@wind.tum.de
Web: www.wind.mw.tum.de

## ABSTRACT

This dissertation presents a study on several interconnected aspects of the operation of wind farms with emphasis on the role of wind farm aerodynamics on improving wind farm operation.
The work begins with a review of the Key Performance Indicators currently used by the wind energy industry to evaluate the operation and maintenance practices of wind farms. These KPIs are grouped by stakeholders and aspects of wind farm O& M and are evaluated for their effectiveness based on proposed criteria. Then the study proposes a concise set of KPIs in an attempt to standardize the evaluation of wind farm operation among the various wind energy industry stakeholders.
Next, the dissertation deals with ways of improving wind farm operation and, in particular, wind farm power yield. The study explores the potential of wind farm control methods to improve wind farm power production by demonstrating the application of such a controller in an actual scaled wind farm consisting of six scaled wind turbines. The implementation of the wind farm controller lead to substantial power gains. Furthermore, in the context of this dissertation the implementation of a reduced order wind farm model is attempted and the model is validated with the use of wind tunnel data.
The importance of wind tunnel studies of wind farm aerodynamics towards the improvement of wind farm operation is highlighted in this dissertation. To this purpose, a scaled wind turbine model with a rotor diameter of 0.6 m was designed and extensively characterized. The scaled wind turbine is compact enough to allow for various types of wind farm aerodynamics studies, i.e. deep array configurations, complex terrain etc. Additionally, its aerodynamic performance and functionality make it a suitable platform for the validation of wind farm control algorithms. In the context of this dissertation, the scaled wind turbine model was used, coupled with CFD simulations, in several studies: i)evaluate the similarity of a scaled wake with the one shed from a full scale machine, ii)study the interaction of wind turbine wake with complex terrain, and iii)assess the vertical wake deflection as a means of increasing wind farm power yield.
Further, the present study proposes a novel way of implementing vertical wake steering, as a means of improving floating wind farm operation. The method is based on differential ballast control of the semi-submersible platforms that support the wind turbines. The proposed method was evaluated in terms of power gains for a 2 turbine cluster with wind tunnel measurements and CFD simulations. Results showed that for the tested configuration the method can have a positive effect. It was also found that the geometry of the platform and the turbine orientation can have a significant effect on power output. The method was also assessed on the additional loading that it may cause on the platform-turbine structure with hydro-aero-servo-elastic simulations of a 10 MW machine. Results showed that, when used in good weather conditions and below the rated wind speed, turbine tilting has very limited effects, mostly on fatigue loads.
The dissertation concludes that the improvement of wind farm operation is a multi disciplinary effort. It was shown that wind farm control, and in particular wake steering, can improve wind farm operation. It was also shown that scaled wind turbine models can play an important role as intermediate step between the introduction of concepts and the testing of these concepts in the field, which ultimately decides which concepts will be implemented on utility wind farms.

# ACKNOWLEDGMENTS

This section is devoted to all those who contributed, one way or another, to the completion of this dissertation. First of all, I want to thank my supervisor, Carlo, who believed in me and supported me throughout this journey. His impact goes beyond this Thesis. Working with him was a privilege as I could benefit from his technical expertise, his rare ability to transfer knowledge and his amazing skill to distill the important things from an ocean of information. What is more, I can't wait to visit him in Paros next summer. Next, I would like to thank all the people that I collaborated with. First, I would like to thank Vasilis, Marinos, Spyros and Dimitris from NTUA. They not only helped me during my first steps in research, but they also proved to be excellent collaborators during my time at TUM. Next, I would like to thank Prof. Alessandro Croce for hosting me for 4 moths and for his help in the execution of some very interesting tests in POLIMI, where I also received precious help from Prof. Alex Zanotti, Luca, Gabrielle and Donato. Last but not least, I would like to thank Florian Heckmeier for his support in the wind tunnel experiments performed at TUM and the excellent collaboration we had for the Praktikum.

I would also like to thank the whole team at UTD in Texas. First to Professor Mario Rotea for initiating and supporting the collaboration between TUM and UTD. Next, Dr. Valerio Iungo for his scientific support, for doing me the honor to be the first external user of his wind tunnel and for his entertaining stories. My special thanks and wishes to Dr. Kyle Jones, with whom I spend countless hours in the wind tunnel setting up the experiments. I will remember, apart from his technical skills, his expertise in sodas, smoked ribs and our shared passion for The Office.

Further, I would like to thank all my fellow ESR as well as the supervisors of the AWESOME project. We spent together three wonderful years, I gained thanks to them broad knowledge on wind energy. Of course, this was combined with many travels and lots of fun.

An important chapter in the book of my adventure in TUM belongs to the students I had the honor to work with. I learned a lot from all the students who participated in the Praktikum as well as the students who completed their Thesis under my supervision, hence, I thank them all. I would like to make special reference to three students with whom I collaborated for more than a year. They had priceless contribution to the work I present hereafter and, I believe, we had great time as well. My special thanks to Nady Kheirallah, Johanne Robke and Kutay Yilmazlar. My deepest thanks also to my colleague at Dornier, Daniel Bitzer, who helped me with the proofreading of the Thesis.

A well deserved spot on these Acknowledgments and in my heart belongs to my colleagues at the LWE. I would like to thank Filippo, for mentoring me during my first years at TUM and for sharing amazing trips to Milano, Franz for being such a great role model( and for helping me translate the Thesis abstract), Marta for the numerous life lessons she gave me and Elli for having the patience to deal with my countless trips, contracts and invoices all these years. My deepest thanks to Stefan for being so positive, to Johannes, and Robin for his precious internet security life hacks. I feel myself privileged for meeting the best representatives of Chinese culture, Jesse and Chengyu. I would also like to thank the new starters Robert, Abhinav and Doruk. Moreover, I want to thank Vlaho who, despite having left many years ago, he still remains in my heart a LWE member and my first friend in Munich. Last but not least, my special thanks to Helena and Carlo. Their diligence, passion for wind energy, devotion to the task has always been a source for inspiration for me. Next to that, the countless

Pepenero nights, the push-up Thursdays, the FFFs, the Galla dinners and all the other things that (due to space limitation) should not been written here gifted me some amazing memories.
Next, I would like to thank all my friends in Greece who are like a second family to me. Their support goes beyond this Thesis. My deepest thanks to the Mech. Mech.: Apostolis, Christos, Chris, Georgios, Manolis, Jason, Stathis, Katerina, Eleni. I would also like to thank my childhood friends: Konstantinos, Kostas, Asterios, Magda, Marilena, Nantia, Eleni and Marios. Last but not least, I would like to thank all my friends in Munich and, especially, Marina who supported me through the last, and most intense, stage of my PhD.
This section could not have a different epilogue other than a cordial gratitude to my beloved family: my parents Georgia and Giorgos, my brother Panagiotis, my sister in law Eleni, the little ones, Giorgos and Zoe and all cousins, aunts and uncles.
I would like to devote this Thesis especially to my parents. Apart from giving me all the love and support I could ask for, they taught me a very important lesson: it is not enough to understand the world, we should always try to make it better. They deserve the happiness, relief and pride that accompany the completion of this Thesis as much as I do, if not more.

# Contents

CHAPTER 1

# Introduction

It is beyond doubt that we have entered an era of rapid technological transformations and a massive introduction of artificial intelligence and digitalization in both industry and our every day lives. The energy sector, being of high strategic importance, could not be left out of this transformation. In this context, any developments in the renewable energy sector will have multiple effects. First, any further increase in the use of renewable energy will considerably decrease humanity's CO2 footprint and slow down the damage human activity causes on the environment. What is more, further penetration of renewables in the energy mix means less dependency on oil or natural gas producing countries. Last but not least, renewable energy paves the road for the decentralized and clever electricity generation architecture that will from a completely new status quo in the economics of energy and, due to the importance of this sector, to the economy in general.
In light of the above, it is no surprise that renewable energy and, in particular, wind energy has experienced steady and rapid growth over the last few decades (Fig. 1.1). Even though Europe and the USA were the pioneers in incorporating wind into the energy mix, we can see that China has the greatest growth and is today the greates producer of wind energy electricity in the world (Fig. 1.2).
However, that is only one side of the coin. The other side is that electricity generated from renewables remains only a small portion of the electricity provided today. This is likely to change as current policies set ambitious goals. The European Commission predicts that by 2050 the electricity coming from renewables (which are mainly wind and solar energy sources) will account for 50% of the total energy production in Europe [1], while the International Energy Agency, being more optimistic, predicts that by 2040 renewables will cover 50% of the word's electricity demands [2]. It is clear that in order to achieve these goals advancements in wind energy technology, the largest representative of renewable energy sources, are absolutely essential. This is the framework in which this dissertation was carried out.

## 1.1 Advancements in wind energy technology

Based on the fast growth of the wind energy sector presented above, it is reasonable to conclude that there has been considerable progress made in wind energy technology over the last several decades. It is beyond the scope of this introduction to conduct an exhaustive review of the evolution of the different wind turbine sub systems. Such reviews, can be found in the relevant books [3]. Nevertheless, it is insightful to contemplate how turbine size and rated power have evolved over the years and examine the journey from solid aluminum blades of a few meters length to machines with 100 m fiberglass blades. In [4] in 1980 the authors believed that wind turbines of more than 3 MW were technically impossible, a statement that probably reflects the maturity of the industry at that time.
The technological advancements that lead to a tremendous improvement in the efficiency and rated power of wind turbines span most aspects of these machines. However, one could emphasize some of them that played a quite crucial role. First and foremost, is the aerodynamic design of the wind turbine rotors. One of the most significant developments in this field was the design of wind turbine tailored airfoils, instead of airfoils that were already used in other aeronautical applications which, for

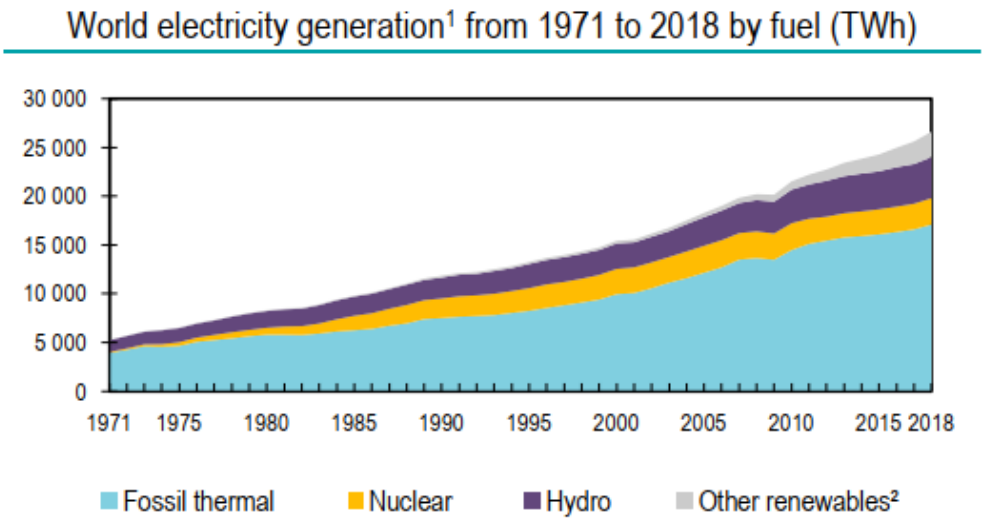


**Figure 1.1:** World electricity generation by type from 1971 to 2018 [2].

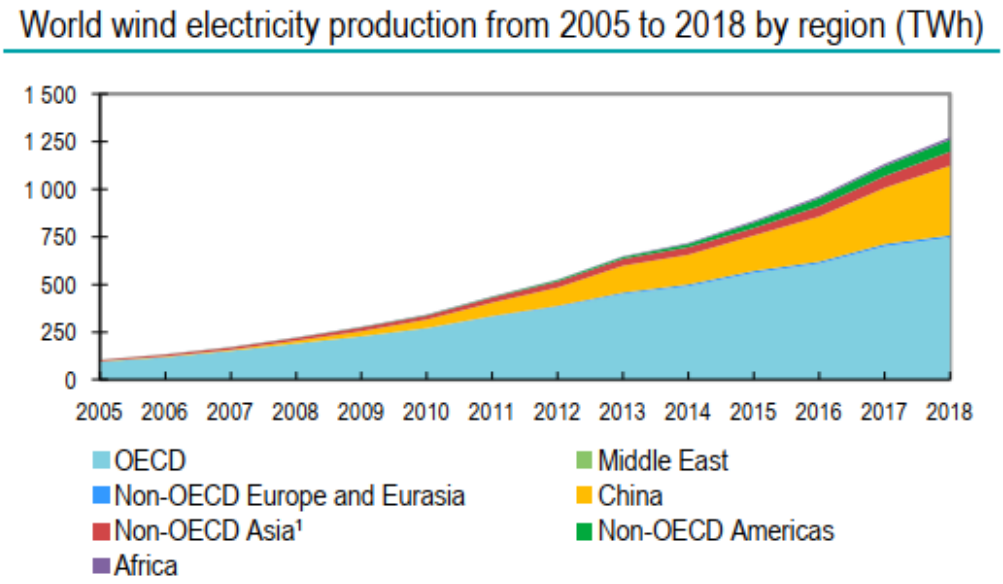


**Figure 1.2:** World wind electricity production by region from 2005 to 2018 [2].

various reasons, did not perform very well in wind turbine applications. Moreover, the adoption of variable speed rotors instead of fixed speed ones, enabled the wind turbines to work at their maximum efficiency for a broader range of wind speeds and, therefore, vastly increased their annual energy production figures.
Another key improvement came from our improved understanding of the structural behaviors of the machines in combination with the use of advanced materials. In the 80s, it was still unclear which configuration was the best and research projects on new machines were split between horizontal, vertical, one bladed, two bladed and three bladed machines. The last two decades wind turbine manufacturers and research institutions have agreed on the horizontal three bladed upwind configuration, even though this could again change in light of new technologies and further developments. The convergence to one configuration increased, as expected, our understanding of such structures and lead to improved designs and manufacturing techniques resulting in larger, more efficient and more reliable machines. Of course, one should not neglect the research and development efforts done in other critical parts of the turbine such as the drivetrain, generator, cabling, foundations etc.
In addition to ongoing research in the aforementioned fields, over the last years several new topics on the turbine level have emerged. For example, multi-disciplinary optimization methods are being developed by several research groups in an effort to build tools that will enable the industry to design machines optimized holistically, after taking into consideration all of the aspects of wind turbine design and operation (aerodynamics, structure, transport, maintenance, lifetime etc.) [5]. In addition, smarter ways of extracting more information about the flow or the wind turbine status are being developed and can further improve turbine operation and increase lifetime. Most importantly, a new approach on how to improve wind energy efficiency has gained attention during the last decade, according to which, the emphasis is given to the plant operation level instead of the individual turbine level.

It is well known that wind energy production sites are organized in clusters of wind turbines, namely wind farms, in order to minimize installation and maintenance costs. Therefore, even though the cell of the wind farm is the wind turbine, it is more appropriate to correlate wind energy efficiency with wind plant efficiency. However, a wind turbine operating inside a wind farm does not perform in the same manner as it would if it were a standalone machine. This happens because of the interaction between wind turbines and the wakes of their neighbouring ones. The wakes shed from the turbine rotors are flow regions with increased turbulence intensity and reduced kinetic energy. When the wake of an upstream machine interacts with a wind turbine placed downstream, the downstream turbine experiences increased loads and a reduced power yield [6]. Wind farm developers take this interaction into consideration during the planning stage, for example when deciding the precise location of the turbines within the wind farm. However, this prominent interaction is currently not accounted for in wind turbine operations. In other words, wind turbines are designed and operate as if they were isolated.
It is known by now that this way of operating is sub-optimal and that, even without any improvement on the single turbine efficiency, the total efficiency of a wind plant can be increased considerably if these effects are factored in. The task of improving the wind energy efficiency on a plant level has been tackled in various ways: improved maintenance strategies, development of energy storage technologies, smart grid platforms etc. However, the most radical, according to the author opinion, is the introduction of wind farm control algorithms.
Modern wind turbines are actively controlled with three control degrees of freedom: blade pitch angle, yaw angle, and generator torque demand. The aim of the turbine control algorithms is to maximize the power yield of the turbine in a variety of wind conditions (wind direction, wind speed) and to protect it from damage in case of a technical malfunction or extreme weather conditions. On the other hand, wind farm control is based on the simple idea of tuning the aforementioned turbine parameters based on a cost function that optimizes wind plant instead of turbine performance. The term performance

includes power yield, turbine fatigue and wind plant revenue. Wind farm control algorithms could also be used beyond the wind plant, providing grid ancillary services, such as frequency response for short-term power balancing or voltage support for distribution networks.

As explained above, the problems arise from the interaction of the turbines with the wake of their neighbouring ones. Therefore, wind farm control is based on wake manipulation strategies, which can be split into two main categories: wake redirection and axial induction techniques. Wake redirection aims to redirect the flow laterally or vertically, by applying forces to the flow normal to the main wind direction. This can be achieved by either rotor misalignment with respect to the flow or by individual pitch control. The second category of wake manipulation methods is based on modifying, statically or dynamically, the induction factor of the rotor.

This new approach, according to which the wind plant is the epicenter of research and development, is also served by this dissertation through 8 publications, which are referred to in the text hereafter as (**Papers I-VIII**). The topic is tackled from different aspects and in different depths but the common denominator is the improved operation of a wind farm.

## 1.2 Research topics and innovative content

As elaborated in the previous section, improved wind farm operation & maintenance is the framework in which this dissertation developed. One could make the legitimate statement that this framework includes countless aspects and each one of them could be a topic for a dissertation. The present study, indeed, touches on a plethora of aspects that can be grouped in three bigger research topics that follow a deductive course: it starts with the definition of wind farm operation & maintenance, the key performance indicators of improved O& M that are already in use and the recommendation of new ones. Next, it deals with the topic of wind farm modeling and control by a novel experimental application of wind farm control, a first implementation and comparison against experimental data of a wake model and a numerical/experimental assessment of wake redirection techniques. Then, it goes deeper into the study of wind farm aerodynamics and wake physics by developing a sophisticated experimental tool of study and by presenting some applications of this tool in some aspects of wind farm/turbine wakes.

### 1.2.1 Improved wind farm operation

As covered extensively in the previous sections, wind energy has recently experienced substantial increase in installed capacity and in its energy mix penetration. The rapid development of wind energy projects has increased the number of competitors in the market. Even the oldest wind farm developers and operators have only few years of experience from large projects. Under this prism, it is not strange that there is no solid agreement between the various wind energy stakeholders about the metrics that can show how good the operation of a wind farm is and are called key performance indicators [7].
The issue of non-uniformity in the key performance indicators used in the wind farm operations was the main problem that arose from the joint industry workshop (JIW) organized in the context of the Advanced Wind Energy System Operation and Maintenance Expertise (AWESOME) project, in which a number of industrial and academic partners from the wind energy sector participated. This problem was publicly addressed for the first time in Paper I, which gives a full list of the KPIs used by the various wind farm stakeholders during O& M. What's more, the study proposed several basic characteristics for performance metrics in order to gauge their suitability as a key performance indicator. According to this analysis, it was determined that a KPI should be: relevant, specific, measurable, comparable,

traceable in time and standardized. In the last part of the study the enlisted KPIs were evaluated against the desired KPI characteristics and against the needs of each stakeholder. This resulted in a compact list of KPIs that cover the whole spectrum of needs for wind farm O& M.
One of the categories of KPIs, particularly interesting for wind farm operators, was wind farm performance. While time-based availability was the most common KPI, the study points out the importance of energy-based availability as well. Since wind is not always the same in strength or direction, energy based availability gives a more accurate picture of a wind farm efficiency. This KPI, however, is quite difficult to measure and raised two questions. Firstly, how much energy is really available within the wind farm at each moment and secondly, what portion of this energy could be captured by the wind farm if all turbines were to work at their maximum efficiency? None of these questions have a straightforward answer, nevertheless, it is known that there may be benefits on the wind farm level if, at least some of, the turbines were deliberately not working at their maximum efficiency for the sake of plant efficiency. This leads to the discussion of the next research topic: wind farm control and modeling.

### 1.2.2 Wind farm control and modeling

As mentioned previously, the proposed tools for implementing wind farm control algorithms are wake steering and the alteration of the induction factor. Changing the induction factor means that the turbine operates at a lower than the optimum power coefficient, even below rated wind speed. This is achieved by altering the blade pitch angle, the rotor speed, or both.
This wind farm control method was first proposed in the late 80s [8], where the authors altered by trial and error the wind turbine rotor speed, resulting in a small power gain. In the study of 2007 [9], the authors ran an optimization algorithm to find the optimum induction factor for each turbine of a real wind farm. Their simulations showed an overall power gain of 0.5% even though for some wind directions the gain was considerably higher. In [10] the authors combined rotor speed and pitch angle changes to reduce the induction factor. For a row of 6 turbines with longitudinal spacing of 6 rotor diameters, they reported a maximum power gain of 10%. In [11] the authors compared a gradient based optimization against a game theoretic approach for optimizing the power of the Princess Amalia Wind Park, which contains 60 turbines. They conclude that the gradient based method converged faster and that both methods resulted in higher total plant output even though they do not report how significant the power gain was. In [12], the performance of an engineering model was compared against a high order wind farm model when it comes to induction based wind farm control. It was found that there were significant discrepancies between them. The study concluded that the power gains on a wind plant that employs axial induction control demonstrate high dependency on atmospheric conditions and wind farm configuration. The authors suggest that these characteristics substantially affect wake recovery and expansion, so that they should be taken into account as there are cases that axial induction control methods are unsuitable. On a similar note, wind tunnel tests performed in [13, 14] showed that the energy lost from the upstream machine cannot be recovered by downstream machines through axial induction control methods. Last but not least, a study performed recently [15] used an optimization code and wake modeling, which were validated with field data collected over a period of six months. The study concluded that there was a plant power gain increase of few percent when taking into account all the wind directions that were present during data sampling period.
The studies mentioned above employ static induction control methods.This means that once the optimization algorithms (regardless which kind of optimization method is used) converge to an optimum set-point for each turbine, the turbines remain at this set-point unless there are changes in the ambient conditions. This method is based primarily on extracting less energy from some turbines

in order to increase the energy extraction for others and, consequently, for the whole wind farm.
An alternative to static axial induction is the dynamic axial induction method, which aims at enhancing wake mixing and recovery downstream of a wind turbine and, thus, increasing the available kinetic energy for the wind turbines further downstream. This is achieved by periodically changing the axial induction factor, i.e. the controller asks for a sinusoidal blade pitch profile which excites the flow in specific frequencies. This method was first introduced in [16]. In [17] the authors performed Large Eddy Simulations (LES) of a 50 turbine wind farm and used a conjugate-gradient optimization method. The authors report a 16% increase in wind farm power which was attributed to the drastic increase of Reynolds stresses within the wake.

While all the previous studies were conducted in simulation environment, the work presented in [18] combined wind tunnel experiments and aeroelastic simulations to demonstrate that periodic dynamic induction control (DIC) can benefit wind farm power output. Last but not least, a novel way of controling wakes that involves dynamically changing the wind turbine set-point was proposed in [19]. In this LES study, the authors used individual pitch control to give the wake a helical shape, which increased wake mixing and recovery. The authors claim power gains similar to DIC and yaw redirection but with less significant variation from the operating range for which turbines are designed.
Even though static axial induction techniques were the first to be tested with regards to their effectiveness in a wind farm control context, there is a consensus among the research community [12, 18, 20] that the wake steering method has greater potential. As a result, there is an increasing interest and, consequently, number of studies on wake steering related topics.
One of the first studies [21] in 2003 explored experimentally the possibility of increasing the power capture of a cluster of two turbines by yawing the first machine. This study was the first demonstration that this method can be effective. Another experimental study [22], in 2011, claimed a total gain of about 12% for a cluster of two turbines. It was also concluded that the power gain for the two turbines strongly depends on the spacing between them and their operating conditions. In the two studies mentioned so far the turbines were yawed manually, i.e. there was no use of any kind of closed loop controller.
In **Paper II** of the present dissertation there was for the first time a real demonstration of a wind farm closed loop controller. In this study, a wind farm comprised of three turbines was placed in a wind tunnel. The scaled wind turbines where fully controllable (pitch, yaw, torque). Apart from the individual turbine controllers, there was also a controller running in a wind farm level. For the wind farm controller, a gradient-based extremum seeking control algorithm was implemented with the goal of maximizing the wind farm power yield with the use of yaw-based wake steering. The outcome of this study was a 15% increase in wind farm power output with respect to the baseline case without the wind farm controller. This power gain corresponds to the specific inflow condition and wind farm set-up used in this experiment. In [23] the authors simulated three different wind farm configurations, comprised of six full scale machines, in LES environment. They also ran an optimization algorithm that was based on the predictions of a reduced order engineering wind farm model FLORIS. Results showed that for all wind farm configurations a power increase, up to 13% in some cases, was possible using the model predictions.
In **Paper III** of this dissertation, two methods for lateral wake steering were assessed. The first was yaw misalignment and the second was wake steering through individual pitch control. The methods were assessed both numerically (LES simulations) and experimentally (wind tunnel measurements). The results showed a very good agreement between simulations and experiments and both confirmed that yaw misalignment is a very effective way of redirecting the wake. Conversely, individual pitch control was shown not to be. On top of that, it was shown that individual pitch control caused considerably increased loads on the turbine, so that it was concluded that this method is not suitable for lateral wake steering.
In [24], the authors coupled the wake model FLORIS with the wind plant simulation tool WISDEM to

study the Annual Energy Production (AEP) of the Princess Amalia Wind Park. The study was twofold as the authors attempted to optimize the layout of the wind farm in order to both reduce losses due to wake effects and to minimize those losses when the wind farm is in operation through the use of wake steering. Results showed that AEP can be increased up to 3.7% for the already wake-optimized layout wind farm while the combined increase was 5.3%. In a more recent study [25], the authors placed 5 scaled wind turbines models in an atmospheric boundary layer wind tunnel. The authors tested 210 different scenarios with different yaw angle distributions among the wind turbine models. These scenarios were split into three control strategies of differing complexity. The first strategy involved yawing of only the first machine. For the second strategy all machines, apart from the last one, are yawed to the same yaw angle and for the third strategy each machine could be set to any yaw angle independently from the others. Results showed that the third, more complicated, strategy yielded the greatest power increase (17%) while the simplest strategy lead to power increase of 4%, which is still not negligible.
Despite the positive results of the aforementioned studies, the fact that the wind direction was constant is a weak point and the suitability of such methods under varying wind directions should be addressed. This is done in [26] [27] where the authors tested, among other things, the effectiveness of a wind farm controller under varying wind direction, which was realized by rotating the wind tunnel turntable. Results show that with increasing wind direction uncertainty the power gain from the use of the wind farm controller, decreases, yet it is always positive.
Last but not least, some recent studies [28–30] have demonstrated the effectiveness of wake steering in field experiments using full scale wind turbines. In [29] the authors used two of the five wind turbines of a utility wind farm. They superimposed yaw misalignment on the first turbine and measured the total power production of the two turbines. Then they compared those results with the predictions of the wake model FLORIS. Results showed an around 4% improvement on the two turbine cluster power production and very good agreement between the FLORIS predictions and the field measurements. In [30] the study was extended to a different pair of wind turbines and included additional wind directions. Results showed an overall 6.5% reduction in the wake losses and confirmed the good agreement between field data and FLORIS predictions.
With regards to vertical wake steering, articles on this topic are far more scarce. The reason for this is the difficulties involved in the implementation of this method as there is no readily available mechanism like in the lateral steering case. Nevertheless, there are some studies that have addressed the topic.
In a wake mitigation control strategies comparison with LES in [31] the authors concluded that vertical wake deflection through rotor tilt is even more beneficial than lateral wake deflection for a two turbine cluster. In [32] LES simulations of a cluster of two and three wind turbines were run. Results revealed a maximum 8% plant power increase for the two turbine case and 13% for the three turbine case.
Although the two previous studies presented very promising results they did not address the issue of the implementation of vertical wake steering. This was done in **Paper VIII**, where a novel way of implementing vertical wake steering for offshore wind energy was presented. More specifically, it is proposed to use ballast water and the active ballast control system that is already installed on semi-submersible floating platforms to tilt the platform, and the rotor, and thus deflect the wake vertically. An assessment of the method in terms of platform kinematics, power gain for a cluster of two turbines and additional loads on the turbine was made, and concluded that this method has potential and should be further investigated. Last but not least, in [33] it was shown that apart from the multiplying effect on power gain that multiple rows of turbines have, the presence of multiple columns can also multiply the positive effect of rotor tilt on plant power gain.

It is clear from the discussion above that the implementation of wind farm control requires, to some extent, knowledge of the flow within the wind farm. This knowledge could be gained from either field measurements or LES simulations. Both of these methods are irreplaceable when it comes to

expanding our knowledge of the flow within a wind farm. However, they are both inappropriate when, for example, model predictive control needs to be implemented because they are either expensive (field measurements) or computationally demanding (LES). For this reason, there is an increased interest in reduced order engineering wake models.
The fidelity of these models is much lower than LES since their simplicity does not allow them to capture the full physics of the flow. Nevertheless, with appropriate assumptions and clever incorporation of the relevant physics, engineering models have proven to be very useful. Probably the first engineering wake model is the Modified Park [34] which is an improvement of the model presented in [35]. This model, based on the momentum balance, assumes linear expansion of the wake and a wind speed deficit that depends only on the turbine thrust coefficient. The Frandsen model, introduced in [36] is more elaborated and incorporates wake merging effects and the effect of the atmospheric boundary layer on the wakes. In [37] a wind plant model, named FLORIS, which is particularly suitable for wind farm control, was presented. This model combines the Jensen formulation for the wake expansion and velocity deficit, with several enhancements to better capture the wake behavior. Additionally, there are expressions included for wake deflection and for the superposition of multiple wakes. The model parameters require data in order to be calibrated to the specific wind turbines and ambient flow conditions. Since FLORIS was developed with wind farm control in mind it has been quite popular in the last 5 years and since its introduction it has been used in several studies. **Paper IV** presents an adaptation of the FLORIS model together with a demonstration of parameter identification through wind tunnel experiments. The data was taken from a scaled three turbine wind farm for which wake and power measurements were made for all three turbines. A subset of the available experimental data was used to identify the FLORIS parameters. Then, FLORIS was used to calculate the wake and power of the wind farm, and to compare those quantities against another subset of experimental data. The correlation was found to be quite good apart from the power predictions for the last turbine. Nevertheless, the model was capable of correctly predicting the optimum yaw angle of the two first turbines for wind farm power maximization. In [38] the authors used FLORIS to improve the power output of a 6 turbine wind farm under strongly-time-varying inflow conditions achieving an instantaneous 11% and an average 1.4% power improvement. What is more, FLORIS has also been augmented by adding several deflection models, velocity deficit models, inflow conditions classes etc. [39]. Moreover, in [40] the authors augmented the model with some additional parameters which were tuned using SCADA data from an operational wind farm. In this way they were able to incorporate into the model phenomena (secondary steering, orographic effects etc.) that were not originally taken into account.
This literature review on wind farm control and modeling, although not exhaustive, gives an overview of the evolution and trends on the topic. One could conclude that static axial induction techniques have not shown the necessary potential when it comes to wind farm power maximization, yet they could potentially benefit other forms of wind farm control like lifetime management, grid services etc. Regarding dynamic axial induction, it has proved itself to be effective in increasing wind farm power capture but is associated with a substantial increase in fatigue loads. However, the general category of wake-mixing techniques that aim at catalyzing wake recovery is a promising field that may lead to further advancements in the future.
Wake redirection techniques have proven to be effective and, therefore, are being studied in more depth. Even though the vast majority of studies are focused on increasing the power capture of a wind farm, it should be noted that these methods could also help mitigating fatigue loads associated with wake-turbine interaction. In any case, wind farm control techniques will only be of any use if accurate and computationally cheap wind farm flow models become available. There has been important progress made also on this front, yet the models available do not capture the flow behavior adequately. The only way to improve these models is to better understand the physics that govern wind farm/wake flows. Only Then will it be possible to make informed assumptions and simplifications.

Equally important is to have sufficient experimental data upon which one could validate or reject new formulations. Therefore, the study of the wind turbine/farm flows and in particular the provision of reliable experimental data is of paramount importance. This is the following, and last, topic addressed in the present dissertation.

### 1.2.3 Wind turbine/farm aerodynamics

The study of wind turbine aerodynamics goes back to the beginning of the 20$^{th}$ century, long before the first utility wind turbines, with the works of Betz [41] and Joukowsky [42] on propeller aerodynamics. In addition, the formulation of the blade-element momentum theory (BEM), which is the foundation of rotor design theory used by the industry, was introduced by Glauert [43] in 1935. Since then, there have been plenty of studies on wind turbine and wind farm flows that have addressed a broad range of topics. One of the most significant characteristics of the wake is its division into two distinct regimes [6]: the near wake and the far wake. The near wake region is influenced by the turbine geometry such as blade shape, nacelle, hub etc. The flow distribution within this region is heterogeneous and complex. The effect of turbine geometry on the flow in the far wake region is negligible. The governing factors in this region are the more fundamental quantities such as the thrust and the torque applied from the turbine to the flow and ambient flow conditions. There is no sharp distinction that can be made between the near and far wake but it is generally agreed that this happens around 2 to 3 rotor diameters downstream of the turbine.
The near wake most important features are the vortex structures that are shed from the tip and root of the blades as well as from the hub. Even though these vortex structures can mainly be seen in the near wake, they have attracted research interest as their behavior can also affect the far wake. For example, the breakdown of tip vortices is associated with the entrainment of higher energy flow into the wake, which is known as the wake recovery mechanism [44]. Therefore, a large number of articles study these root [45–47], tip [48–50] and hub [51–53] vortices.
The far wake is more interesting from a wind farm point of view. As the spacing between turbines in a farm ranges between 3 & 12 rotor diameters, this is the part of the wake that interacts with other turbines. Some of the points of interest regarding the far wake are the velocity deficit profile which has been studied with field experiments [51, 53, 54], wind tunnel experiments [27, 55] and numerical simulations [56, 57], the wake recovery [58, 59] and turbulence intensity [60–62]. The popularity of wind farm control using lateral wake redirection has directed many researchers to study the wake structure and behavior under yawed conditions. The main focus has been the deflection of the wake [63–65], yet the irregular shape of the wake that a yawed wind turbine sheds has also been investigated in several research works [66–68]. In **Paper VI** the wake of a scaled wind turbine was studied under yawed conditions for two different inflows, one turbulent and one laminar. Results showed that, unlike wake recovery, the deflection of the wake center was insensitive to the ambient turbulence intensity. Moreover it was shown that the maximum wake deflection does not occur at the wake center as had also been recently suggested in [65].
Most of the aforementioned works were focused on the wake of a single wind turbine. There are, however, plenty of studies which consider full wind farms focusing either on what happens within the wind farm or moving to higher level where the whole wind farm is treated as a single entity and the main point of interest is its interaction with the mesoscale meteorological phenomena.
In any case, the above summary is by no means complete as the bibliography on this topic is very broad. A good review can be found in the reviews by Vermeer et al. [6] and Bastankha and Porté - Agel [69].

Wind tunnel testing has been indispensable in the study of wind turbine and wind farm flows. In fact, many of the aforementioned studies were experimental and, in particular, wind tunnel studies.

The rapid increase of computational power and, the development of numerical methods that came with it, do not make wind tunnel testing obsolete. On the contrary, now there is an even higher demand for ways to validate numerical schemes, aerodynamic models or wind farm control algorithms. It is beyond doubt that the best way to test and validate wind farm models and wind farm control strategies is through real applications in field tests. This, however, is extremely complex for many reasons. Firstly, it is extremely expensive to develop full scale experimental set-ups or to take utility scale wind turbines from the production line. Secondly, the inflow conditions are not controlled which means that the desired test conditions rarely occur, increasing the time needed to validate or reject proposed models. Thirdly, field tests require wind turbine characteristics or wind farm operational data that, more often than not, is confidential and their owners, who are usually not the developers of these new methods, are not willing to share. This is where wind tunnel testing comes into play and can bridge the gap by providing relatively cheap, controlled and reliable data. One could argue that it is not always possible to match the physics of the full scale phenomena in a wind tunnel. Although this is a valid argument, this problem can be addressed in several ways. Firstly, it is usually not necessary to match the whole spectrum of physical phenomena that occur in full scale but only a fraction of them. For example, the Coriolis effect, although present in atmospheric flows, has a negligible effect on the behavior of tip vortices, therefore, it may safely be neglected in a wind tunnel study whose purpose is the study of tip vortex behavior. Secondly, when it comes to validating numerical codes, it is usually enough to provide reliable input and output data even if this data cannot be scaled up directly. For example, simplified wake models that work based on conservation of momentum can be credibly validated with wind tunnel data even if the scaled rotors do not match the full physics of the utility scale rotors.
For all the above reasons, it is no surprise that wind tunnel testing is more popular today than ever within the wind energy research community and that scaled wind turbine models are becoming very popular. They have been used for a great variety of research goals like studying the effects of thermal stability on the wake of a wind turbine [27, 70] or how the inflow and operating conditions influence the development of the wake [50, 71–74]. Scaled wind turbine models have also been used for wind turbine/farm control tests [26, 75, 76].

Despite the widespread use of scaled wind turbine models the last decade, the articles that give an in-depth description of the used wind turbine models are scarce. In [75] the authors describe the development of a 2 m scaled wind turbine model. This model is aero-servo-elasticly scaled and tries to match a 3 MW full scale model as regards to the relative placement of the principal natural frequencies of the drive-train and the tower with respect to the rotor rotating frequency and its harmonics. What is more, the control logic and hardware of the model is similar to full scale ones. The authors also present some applications of this model that are related to wind turbine control such as emergency shut down manoeuvres and individual pitch control for load alleviation. In [74] the authors describe the development of a 0.58 m wind turbine model. The model rotor was designed with use of BEM and is equipped with active pitch control by a way of a sliding mechanism. For the most part, the authors focus on the performance of the closed loop torque controller that the model is equipped with. In [77] and [55] the authors give a thorough description of the development of a 0.15 cm wind turbine model while they also characterize the aerodynamic performance and the wake. The model features a cambered plate blade which gives a maximum $C_P$ of 0.4 at a tip speed ratio 4 that is, however, low compared to typical full scale machines. Regarding wake characterization, the authors presented a variety of flow characteristics such as mean velocities, turbulence intensity, turbulent fluxes and wake meandering while they also quantified the loads that the model wake would induce on a downstream machine in case of wind farm tests. In addition, in [78] the authors designed two scaled wind turbine rotors, one of 0.45 m and one of 0.225 m. The performance of the two rotors was measured in the wind tunnel and compared against 1D BEM and 3D CFD simulations with the goal of evaluating the suitability of BEM design methods for low Reynolds rotors. In [79] the authors perform an analytical

discussion about the rotor scaling process while in [80] a new approach for designing scaled wind turbine rotors, where the goal is to match wake behavior, is presented.
**Paper V** presents an extensive discussion about the design and characterization of a novel scaled wind turbine model with a 0.6 m rotor. The novelty of this miniature model is twofold. First, it is the combination of compact size with extensive control and measurement capabilities. More specifically the model is pitch, torque and yaw actuated and supports most of the wind turbine and wind farm control strategies that have been proposed so far. At the same time, it is equipped with bending and torsion sensors on its shaft and tower allowing, apart from the typical thrust and power measurements, for the testing of advanced wind sensing methodologies [81]. At the same time, its compact size makes it suitable for wind farm control tests on deep array multi column wind farm configurations and for studies on the wind turbine-complex terrain interactions. The second point of novelty is its rotor design, which matches the normalized circulation distribution along the blade of a reference full scale machine. In this way, as shown in [79, 80] the wake of the scaled model will be similar to the wake of a full scale machine. The characterization of the model showed that its maximum power coefficient is around 0.41 for a tip speed ratio of 7.5 and thrust coefficient of 0.75. The wake of the model was characterized extensively in many different aspects, e.g. velocity deficit, wake deflection, added turbulence intensity, and compared against other scaled wind turbine models, CFD and popular empirical models.
The new miniature model (G06) was used, in the context of this dissertation, to study some more specialized topics in the area of wind turbine/farm aerodynamics. First, to assess the behavior of a wind turbine placed on complex terrain and second to evaluate the potential of vertical wake deflection for wind farm control.

Complex terrain is known to, in some cases, severly disturb the inflow of a wind farm. Speed-ups, increased turbulence and high vertical and horizontal shear are some of the effects that complex 3D topography can have. The models that are currently in use cannot adequately capture these phenomena [82,83] despite some recent endeavors to introduce wind farm models with improved performance on complex terrain [84]. Therefore, the predictions of the AEP of new wind farm and/or the fatigue loads on the turbines can divert from the actual ones. Since a large portion of future onshore wind plants will be installed in complex terrain, this topic is of significant importance.
There are many studies on the flow around hills that deal with the topic from a meteorological point of view [85–89] either experimentally or numerically. There are also a non-negligible number of CFD studies that address the topic from a wind plant perspective [90–92], while some others combine CFD with wind tunnel data [83, 93–95]. The aforementioned experimental studies include only the terrain in their experimental set-ups. When it comes to combining experimentally terrain and wind turbine there are only a handful of studies [96, 97] that, however, make use of very simplified terrain and wind turbine models. Last but not least, there are studies that have used field data obtained by either met-masts or drones [98, 99]. **Paper VII** presents the first experimental study that employs scaled copy of real complex terrain together with the sophisticated scaled wind turbine model presented in **Paper V** and **Paper VI**. The goal of the study was firstly to demonstrate the credibility of such an experimental set-up and, secondly, to provide an initial set of turbine wake data that could be compared with the flat terrain cases. The complex terrain was a scaled model of a real test site with a scaling factor of 1:200 and had dimensions $6 \times 1 \times 13.5$ m, which makes it the largest terrain model that has been tested in a wind tunnel. The edges of the terrain model were optimized through CFD simulations in order to minimize the formation of vortices that could affect the wake measurements. The entire set-up was evaluated against flow similarity criteria and blockage effects and found to be credible for wind tunnel measurements with a small correction for blockage effects (5%) being necessary. The PIV measurements of the turbine inflow and wake revealed a strong vertical component around 1 diameter upstream the turbine and slightly weaker wake recovery compared to the flat terrain case.

The vertical wake deflection, as discussed earlier, has not been studied extensively due to the associated technical difficulties in its implementation. Therefore, most of the studies focus only on the effects of rotor tilting mainly in the wind farm power. In **Paper VIII** a more comprehensive study of vertical wake steering is presented.
Firstly, the study shows the effects of tilt misalignment on a two turbine cluster using LES simulations of the G06 scaled model. There are two points of differentiation between the analysis presented in this paper and the ones found in the literature: i) the LES were validated against wind tunnel data of the same set-up, ii) the analysis included turbine spacing that is more relevant for offshore wind applications. Results agree with previous observations that deflection of the wake towards the ground is more beneficial in terms of wind farm power gains. In the cases tested in this paper, the power gain for the cluster of two turbines spaced 12 diameters apart was approximately 3%. It was also found that, for the specific turbine set-up, vertical wake steering was more beneficial than lateral wake steering.
Secondly, the paper proposes a novel yet technically feasible way to implement wake steering in floating wind turbines. The idea is based on the fact that semi-submersible platforms, that are the most popular support concept, already employ ballast system to ensure the horizontal position of the platform. Such a system could be employed to impose a pitch misalignment to the platform and, subsequently, to the turbine rotor. An initial sizing of such a system is attempted and a rough estimation of the cost of this method from an energetic point of view with application in two different platforms presented.
Moreover, the impact of the proposed method on ultimate and fatigue loads is evaluated through hydro-aero-servo-elastic simulations of a full scale platform with a 10 MW turbine on it that was pitched by 20 and -20 degrees. Results show a small effect on fatigue loads mainly on tower base bending and drivetrain torsion loads of 2% and 5%, respectively. As for the ultimate loads, the simulations revealed that, for the tested structure, the implementation of this method has no effect on them, provided that it is used under normal sea state and below rated wind speed conditions.
Additionally an initial estimation of the time scale that this system can work was performed. It was found that for an optimum tilt angle of $-15^{\circ}$, the system required approximately 10 minutes to reach that position. It is clear that this control of freedom is slower than, for example, lateral wake deflection. In addition, one or the other method may be more beneficial based on the inflow conditions. Therefore, one may not consider tilt as a substitute for yaw control, but as a complementary method that could work in synergy with lateral wake deflection in a wind farm.

## 1.3 Publications

This section summarizes the 8 publications that appear in this dissertation, while Fig. 1.3 gives an overview of the dissertation structure in terms of both publications and content.
Section 1.3.1 lists them together with their corresponding references.

**Paper I** addresses the issue of defining improved O& M for wind farms. One of the problems is the non-uniformity in the use of key performance indicators (KPI) when assessing the performance of a wind farm. It presents an overview of the various stakeholders related to the development and operation of wind farms along with a list of key performance indicators used by them. The paper establishes the key characteristics of an efficient KPI. Based on those characteristics, the study proposes a set of KPIs for each stakeholder.
Next, the dissertation deals with wind farm control and modeling as tools for improved wind farm operation. **Paper II** demonstrated the first experimental implementation of a wind farm closed-loop controller. The controller was implemented in a scaled wind farm of three machines placed in a wind tunnel. Using lateral wake steering through yaw misalignment the controller increased the

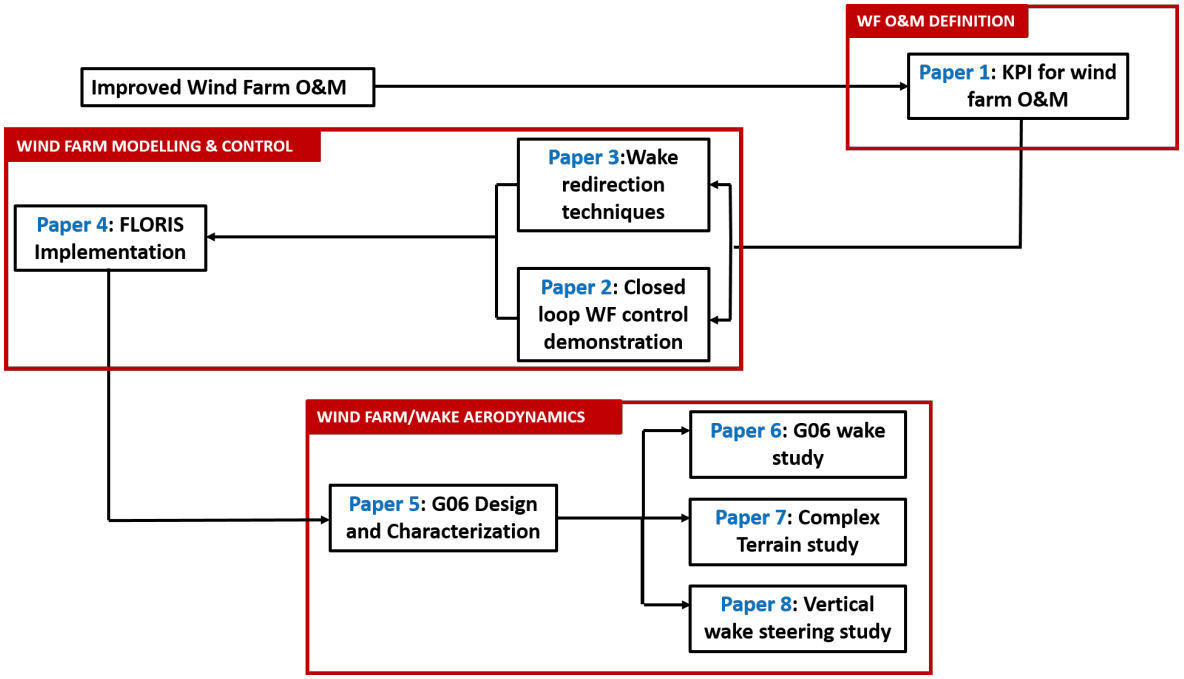


**Figure 1.3:** Schematic overview of the dissertation roadmap the distribution of papers among the research topics.

power output of the farm by 15% for specific turbine layout and inflow conditions. In **Paper III** two ways of redirecting the wake laterally were assessed by LES and wind tunnel tests. The paper showed good agreement between LES and wind tunnel tests and concluded that yaw misalignment is the only meaningful way of redirecting the wake laterally since individual pitch control was found to be ineffective. **Paper IV** implements a wind farm model (FLORIS). Using wind tunnel data of a scaled wind farm similar to the one in **Paper II** the parameters of the model were tuned. Then, the model predictions were compared against other sets of experimental data showing quite satisfactory agreement.

The last part of the dissertation touches on wind farm aerodynamics as a better understanding in this area is mandatory for implementing wind farm control strategies. **Paper V** presents the design and characterization of a novel scaled wind turbine (G06). This wind turbine model encompasses a compact design along with extensive sensorization and sophisticated rotor design aiming at realistic aerodynamic performance and wake behavior similar to full scale machines. G06 is extensively characterized in terms of aerodynamic performance and wake flow dynamics. It is concluded that the design was successful and the model can be used for a plethora of applications some of which are presented in the last three papers of the dissertation. **Paper VI** presents wake measurements of G06 in different wind tunnels and under diversified inflow conditions and yaw angles. Results show good agreement among the wind tunnels and the measuring techniques. It also showed the dependence of key wake quantities (velocity deficit, wake center trajectory etc.) on the inflow conditions. **Paper VII** presents the first ever wind tunnel study of a wind turbine on a complex terrain. G06 (described in **Paper V**) and a scaled copy of a real complex terrain were used for these experiments. Results showed that this experimental set-up can be reliably used for benchamarking measurements and numerical code validation. Last but not least, **Paper VIII** presents a novel way of implementing vertical wake steering in offshore wind applications using differential ballast control on a semi-submersible platform. The method is evaluated using both wind tunnel measurements and CFD simulations. Results show that, depending on the spacing of two turbines, the power gain was up to 3% for the tested layouts and

inflow conditions, when the wake is deflected towards the ground with 15 degree rotor tilt angle. In addition, the method was assessed with regards to platform kinematics revealing that reaching the optimum tilt angle requires, depending on the platform, from 7 to 20 minutes. Last but not least, the loads on the structure were also investigated through hydro-aero-servo-elastic simulations, concluding that the additional loads, for the tested platform case, are insignificant when the method is used in low wave sea state and under rated wind speeds.

### 1.3.1 List of publications

This section lists the publications that comprise this dissertation. Most of them have already been published in peer-reviewed journals apart from **Paper V** and **Paper VIII**, which have been submitted and accepted for review. For each publication, the corresponding chapter includes a summary and a description of each author's contribution. All paper manuscripts are included in the appendix of this Thesis.

- **Paper I**: E. Gonzalez, E. M. Nanos, H. Seyr, L. Valldecabres, N. Y. Yürüşen, U. Smolka, M. Muskulus, and J. J. Melero, "Key performance indicators for wind farm operation and maintenance," *Energy Procedia*, vol. 137, pp. 559 – 570, 2017. doi: https://doi.org/10.1016/j.egypro.2017.10.385

- **Paper II**: F. Campagnolo, V. Petrović, J. Schreiber, E. M. Nanos, A. Croce, and C. L. Bottasso, "Wind tunnel testing of a closed-loop wake deflection controller for wind farm power maximization," *Journal of Physics: Conference Series*, vol. 753, p. 032006, 2016. doi: 10.1088/1742-6596/753/3/032006

- **Paper III** : J. Wang, S. Foley, E. M. Nanos, T. Yu, F. Campagnolo, C. L. Bottasso, A. Zanotti, and A. Croce, "Numerical and experimental study of wake redirection techniques in a boundary layer wind tunnel," *Journal of Physics: Conference Series*, vol. 854, 2017. doi: 10.1088/1742-6596/854/1/012048.

- **Paper IV** : J. Schreiber, E. M. Nanos, F. Campagnolo, and C. L. Bottasso, "Verification and calibration of a reduced order wind farm model by wind tunnel experiments," *Journal of Physics: Conference Series*, vol. 854, p. 012041, 2017. doi: 10.1088/1742-6596/854/1/012041.

- **Paper V**: E. M. Nanos, C. L. Bottasso, F. Campagnolo, S. Letizia, G. V. Iungo, and M. A. Rotea, "Design, performance and wake characterization of a scaled wind turbine with closed-loop controls," *Wind Energ. Sci. Discuss.*, 2021. doi: 10.5194/wes-2021-66

- **Paper VI**: E. M. Nanos, J. Robke, F. Heckmeier, M. Cerny, K. Jones, V. Iungo, and C. L. Bottasso, "Wake characterization of a multipurpose scaled wind turbine model," *AIAA Scitech 2019 Forum*, 2019. doi: 10.2514/6.2019-2082

- **Paper VII**: E. Nanos, K. Yilmazlar, A. Zanotti, A. Croce, and C. Bottasso, "Wind tunnel testing of a wind turbine in complex terrain," *Journal of Physics: Conference Series*, vol. 1618, 2020. doi: 10.1088/1742-6596/1618/3/032041

- **Paper VIII**: E. M. Nanos, C. L. Bottasso, D. I. Manolas, and V. A. Riziotis, "Vertical wake deflection for floating wind turbines by differential ballast control," *Wind Energ. Sci. Discuss.*, 2021. doi: 10.5194/wes-2021-79

CHAPTER 2

# Methods

The present dissertation, due to its broadness, naturally encompasses a variety of research methods a summary of which will be presented in this section. The most extensively used research methods in this dissertation are the experimental ones, while numerical methods supplemented the work.
Section 2.1 summarizes the experimental apparatus, experimental objects and techniques that were used in this thesis, section 2.2 presents the numerical methods that were employed.

## 2.1 Experimental methods

### 2.1.1 Atmospheric boundary layer wind tunnels

Wind tunnels have been in use, in their earliest forms, since the beginning of the $18^{th}$ century and they became of paramount importance during the dawn of $20^{th}$ century when they were the main support tool for the newly born aeronautical industry. Nowadays, despite the development of numerical methods and the rapid increase in computational power they remain relevant. Their role as a bridge between numerical predictions and full scale experiments in addition to their importance in the validation of numerical schemes and engineering models make them indispensable to research.
Atmospheric boundary layer (ABL) wind tunnels are as special type of wind tunnel whose purpose is to accommodate experiments that require the presence of a boundary layer and atmospheric level of turbulence intensity. Their applicability is quite diversified varying from civil engineering (bridges, buildings etc.), urban architecture (ventilation) to atmospheric studies (pollutants dispersion etc.). Their main characteristics are low wind speeds and (relatively) long test sections. The test sections need to be long so they can allow for the development of a boundary layer. Most often, the length of the tunnel is still not enough so it is necessary to accelerate the development of the boundary layer with the use of special devices like spires and roughness elements. Careful design based on empirical equations of the geometry, size and positioning of these devices can result in the desired characteristics of the boundary layer like vertical profile of streamwise velocity and turbulence intensity or even more advanced quantities like turbulent length scales etc.
In the present dissertation, the experimental results were obtained from three different ABL wind tunnels, a fact that is quite remarkable considering the technical and logistical challenges that one needs to tackle when coupling an experimental object (scaled wind turbines) with an experimental facility (ABL wind tunnels). The ABL wind tunnels that were used are the Wind Tunnel C of the Institute of Aerodynamics at Technical University of Munich, the wind tunnel of the Politecnico di Milano and the Boundary Layer and Subsonic (BLAST) wind tunnel of University of Texas at Dallas.

The ABL wind tunnel at TUM has a test section of $21m$ long $\times$ $2.7m$ wide $\times$ $1.8m$ tall. It is a closed loop wind tunnel with a single fan of 210 kW power. In a clean configuration the minimum turbulence intensity is 0.5% while the maximum velocity at the test section can reach $30ms^{-1}$. The TUM wind tunnel was extensively used for testing and calibrating the scaled wind turbine models as well as for measuring the wake with hot wire probes in both laminar and turbulent/sheared wind inflow. For the

sheared inflow a set of spires and lego bricks were used as roughness elements.

The ABL at the Politecnico di Milano is a closed-circuit wind tunnel and is equipped with two test sections, one for low turbulence aeronautical test purpose and one massive $35m$ long × $13.84m$ wide × $3.84m$ tall boundary layer test section. The flow circulation is achieved by 14 fans with a total power of 1.5 MW. The wind speed at the ABL test section can reach $16ms^{-1}$ and the minimum turbulence intensity in a clean configuration is 2%. When enhancement of the boundary layer is desired, spires and concrete blocks are used as roughness elements. The Politecnico di Milano was used, in the context of this dissertation, mainly for the complex terrain study as well as for wake redirection assessment studies.

The majority of the wind tunnel data presented in this dissertation was obtained in the recently built ABL wind tunnel at UTD. It is also a closed circuit wind tunnel with a boundary layer test section that is $30m$ long × $2.8m$ wide × $2.1m$ tall. It is powered from a single stage axial flow fan with power of 255 kW. The maximum wind velocity at the test section is $35ms^{-1}$ while in a clean configuration the turbulence intensity is less than 0.1%. The UTD BLAST wind tunnel was used for most of the wake measurements presented in this dissertation as well as for most of the performance measurements for the characterization of the G06 scaled wind turbine aerodynamic performance.

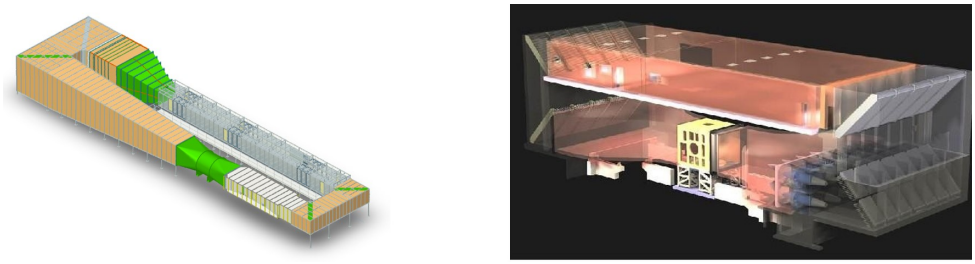

**Figure 2.1:** Left: UTD BLAST wind tunnel sketch. Right: POLIMI wind tunnel sketch.

### 2.1.2 Scaled wind turbine models

The core of this dissertation is the scaled wind turbines that were used not only to obtain the experimental data but they were also modeled in the numerical simulations. For the vast majority of the data presented in this dissertation, the scaled wind turbine G06 was employed while for the rest the scaled wind turbine model G1 [107] was used. In reality, the development of G06 is the main milestone as well as the main element of novelty of this dissertation and its analytically described in **Paper V**. Nevertheless, for the sake of the completeness of this section, a brief description of both models, G1 and G06 will be given in the following lines.

The G1 scaled wind turbine model was used in the studies presented in **Paper II**, **Paper III** and **Paper IV**. It was developed in 2014 and its main purpose was wind farm control studies. It is a three bladed upwind wind turbine with rigid blades made out of carbon fiber. The blades utilize one airfoil profile, the RG-14 which is low Reynolds airfoil originally conceived for sailplanes and the rotor has been designed to optimize $C_P$. It is equipped with active yaw, individual pitch and torque control, while it is possible to calculate the loads on the tower root and on the rotor shaft with the use of strain gauges. The main characteristics of the G1 are presented in table2.1 while an overview of its components and systems is given in Fig. 2.2.

The G06 scaled wind turbine model has a similar configuration to the G1, yet, with almost half its size and a re-design of its rotor in order to extend the capabilities for wind farm aerodynamics and control wind tunnel tests. As a result, it bears some similarities like the airfoil, which had been proved to work well for a scaled wind turbine model, the blade manufacturing method and the load cells on

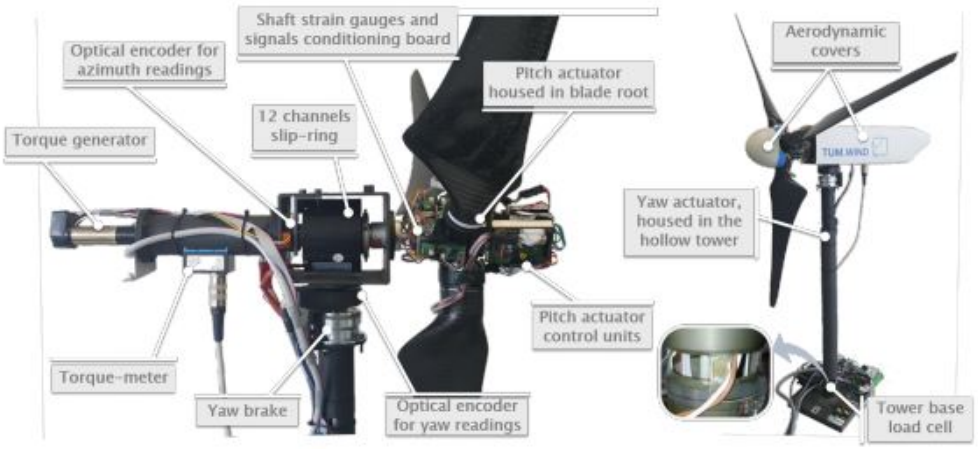


**Figure 2.2:** G1 layout.

**Table 2.1:** Basic characteristics of the G1

| | |
|---|---|
| Nr. of blades | 3 |
| Rotation | Clockwise |
| Airfoil | RG-14 |
| Rotor diameter | 1.1 m |
| Hub height | 0.64 m |
| Rated wind speed | 5 $ms^{-1}$ |
| Rated power | 45 W |
| Active pitch control | Yes (individual) |
| Active torque control | Yes |
| Active yaw control | Yes |

**Table 2.2:** Basic characteristics of the G06

| | |
|---|---|
| Nr. of blades | 3 |
| Rotation | Clockwise |
| Airfoil | RG-14 |
| Rotor diameter | 0.6 m |
| Hub height | 0.64 m |
| Rated wind speed | 10 $ms^{-1}$ |
| Rated power | 65 W |
| Active pitch control | Yes (collective) |
| Active torque control | Yes |
| Active yaw control | Yes (separate mechanism) |

the tower and the shaft. Despite being smaller than the G1, the G06 keeps most of the G1 functionality. This caused many technical challenges and in most cases different engineering solutions had to be made.
G06 is a three bladed upwind scaled wind turbine and it features rigid blades with a single airfoil profile made out of carbon fiber. The rotor is designed for maximizing the power coefficient while keeping the normalized circulation distribution equal to the one of a reference model, which is the DTU-10 MW turbine. This decision is based on the free vortex theory according to which the blades of a wind turbine can be replaced by vortex filaments of strength $\Gamma$ which is the circulation of each filament. In a steady state, where the circulation does not change over time, the wind velocity at any point in the field is a combination of the free stream velocity and the induced velocity of each filament that can be calculated with the Biot-Savart law and is based on the strength of the filament. Therefore, if the scaled model has the same normalized circulation distribution as a full scale machine, their wakes will be theoretically similar.
The G06 is equipped with collective pitch and torque control while the active yaw control is realized through a separate mechanism developed specifically for the G06. Loads on tower root and on the rotor shaft can be calculated with the use of strain gauges. The basic characteristics of G06 are presented in table 2.2 while an overview of its components is given in Fig2.3. This miniature model was used in the studies presented in **Paper VI**, **Paper VII**, **Paper VIII** while its development and characterization are the main topics of **Paper V**.

### 2.1.3 Measuring techniques

Following the diversity in experimental facilities used for this study, the measuring equipment that was used is also broad. There were basically two types of measurements: strain measurements and wind velocity measurements. The strain measurements enable the calculation of loads on the turbine (aerodynamic torque, thrust etc.) whilst the wind velocity measurements provide information about the wake of the wind turbines as well as, combined with the loads calculations, information about the performance of wind turbine models.

#### Strain gauges

Strain measurements were achieved via the use of strain gauges. Strain gauges are metallic foils that are adhered on structures. When the structure is under loading it deforms and together with it the strain gauge also deforms changing its resistance. The changes in resistance are quite small and to facilitate

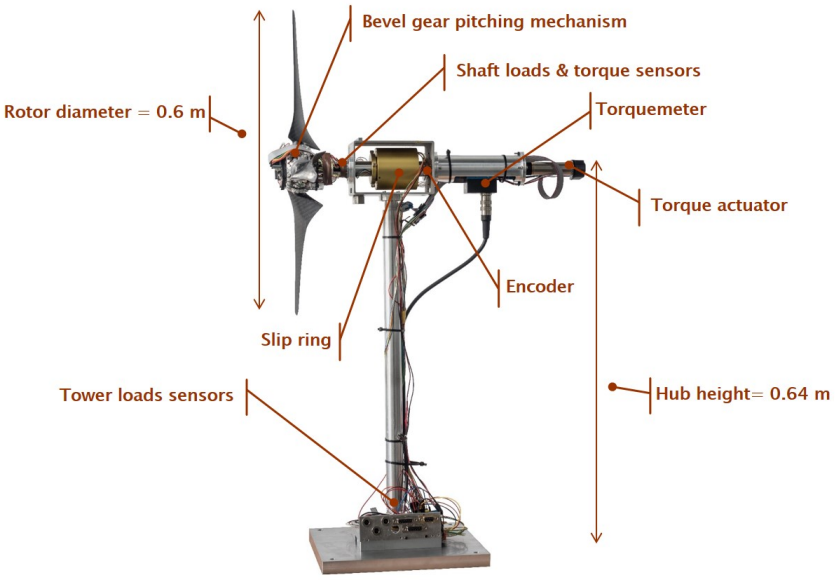


**Figure 2.3:** G06 configuration.

the measurement strain gauges are usually connected in a Wheatstone bridge which is comprised of four strain gauges (or even less, but in this case dummy resistors complete the Wheatstone bridge). When the Wheatstone bridge is under voltage excitation and all resistances are equal, the voltage output of the bridge is zero. However, any change in the resistance of any of the four bridge arms will result in a nonzero output voltage. By calibrating a strain gauge bridge, one can correlate the measured voltage with a stress value.

G1 and G06 share the same strain gauge configuration. Each one of these two machines has a full strain gauge bridge at the root of the tower for measuring bending strains, one full bridge at the rotor shaft measuring bending strains caused bending loads on the shaft and one full bridge at the rotor shaft measuring shear strains caused by torsion loads (i.e. aerodynamic torque).

The wind velocity measurements presented in this dissertation are accomplished via three different measurement techniques: hot wire anemometer, particle image velocimetry (PIV) and Pitot tube.

### Hot wire anemometry

Hot-wire anemometry is a measuring method that goes back almost 150 years and it is essentially a thermal transducer which can be used for measuring instantaneous point velocities. The working principle of this method is the following: a very thin metal wire is connected to a Wheatstone bridge which is excited by a voltage source. The current running through the wire heats it up to a specific temperature which for constant temperature anemometer (CTA), like the one used in this dissertation, remains the same. When the wire is placed inside a flow, the moving air cools it down and as a result its resistance change. This change is detected and the system adjusts the current running through the wire in order to compensate for the change in resistance and bring the temperature back to the fixed value (Fig. 2.5). The compensating values of current (or voltage) can be measured and correlated with velocity changes through a calibration process. The calibration takes place by mounting the wire in a calibration device where is subjected to known wind speed flow. The main advantages of this

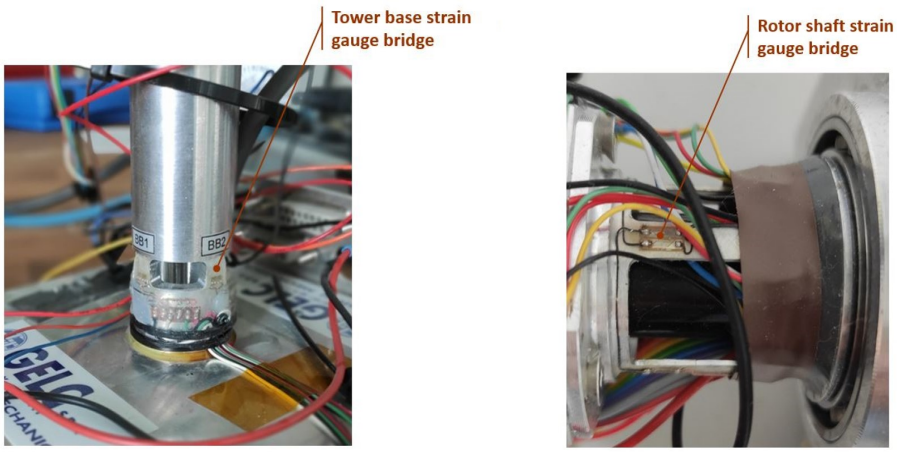


**Figure 2.4:** Strain gauges on the tower root (left) and rotor shaft (right) of the G06.

method are its simplicity, low uncertainty and its ability to sample at very high frequencies (up to 15 kHz) which makes it suitable for studying unsteady phenomena and turbulence. On the other hand, a drawback of this method is the fact that it is a point measurement technique, which means that the probe has to be traversed if information about the flow for more than one point is required. It is also an intrusive method which could affect the flow at the measurement position.
In the present dissertation a triple-wire probe was used. A triple-wire is equipped with three wires, hence it is able to detect wind speed in all three directions. The calibration process is similar to the one described above with the difference of having to calibrate the probe for many different cone angles (i.e. wind inflow directions).

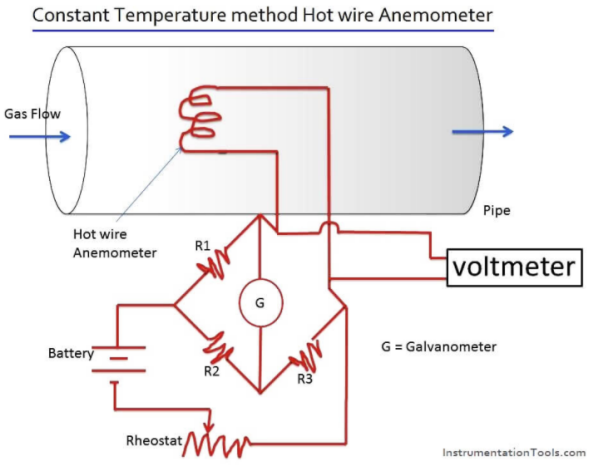


**Figure 2.5:** Sketch of constant temperature anemometer working principle. Source: www.instrumentationtools.com.

### Particle image velocimetry

The particle image velocimetry (PIV) is the most extensively used flow velocity measuring method in the present dissertation. PIV is a relatively new measuring technique as it was first introduced in the 80s. A very brief description of the method is the following [108]: the flow is seeded with small particles (usually olive oil droplets but this depends largely on the application) with diameters of $1-5\mu m$. A high power laser illuminates a window of the flow and a high speed camera takes a two subsequent pictures. By correlating the position of particle clouds between the two frames, and assuming that the particles are following the air flow, one can calculate the flow vectors within the window (Fig. 2.6). Sometimes one pair of images is not enough to reliably calculate the flow field within the whole measuring window and a statistical averaging of multiple pairs is necessary. Another important advantage of this method is that it gives a vector field within a plane and not just a point measurement. Moreover, the method is practically non-intrusive as the particles that are seeded into the flow, if chosen carefully, follow the flow without affecting it.

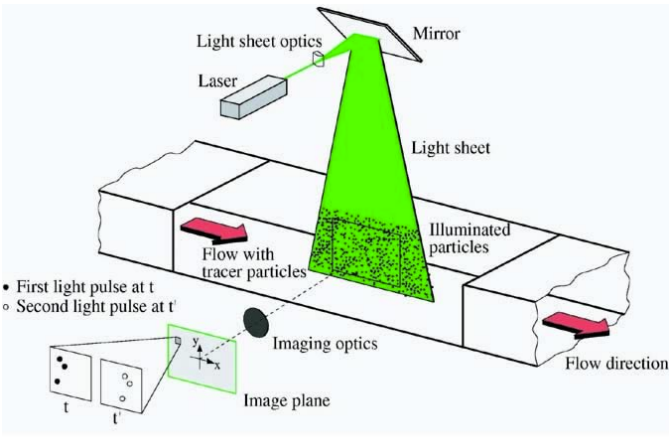


**Figure 2.6:** Sketch of PIV working principle. Source: www.dlr.de

Simple PIV can only measure the two in-plane velocity components. To overcome this shortcoming, it is possible to add another camera, in which case the method becomes stereo-PIV. It is also possible to use 4 cameras in total which is known as volumetric-PIV. In the case of stereo-PIV one can determine the three velocity components within a measuring plane. With volumetric-PIV it is possible to measure the flow field within a volume. In the case of stereo and volumetric PIV, the correct set-up of the equipment and the calibration process are quite difficult procedures which, if not done properly, can affect the quality of the measurements. What's more, since this technique relies on statistical image processing methods, the post-processing of the data is not always a straightforward process and it requires the right choice of one of the various post-processing methods.
In this dissertation, both the simple and stereo-PIV method were employed. The simple PIV tests were conducted in the POLIMI wind tunnel for the complex terrain studies (**Paper VII**) for which a sCMOS camera of 2 Mp and a 200 mJ/pulse laser were used (Fig. 2.7 left).

The stereo-PIV was employed in both of the wind tunnels in POLIMI and at UTD for the studies presented in **Paper V**, **Paper VI** and **Paper VIII** .The equipment was comprised of two sCMOS 5.5 Mp cameras, Scheimpflug adapters, 50 mm lenses and a 380 mJ/pulse laser (Fig.2.7 right). For each measuring plane 2000 pairs of images were taken to ensure convergence of the flow statistics.

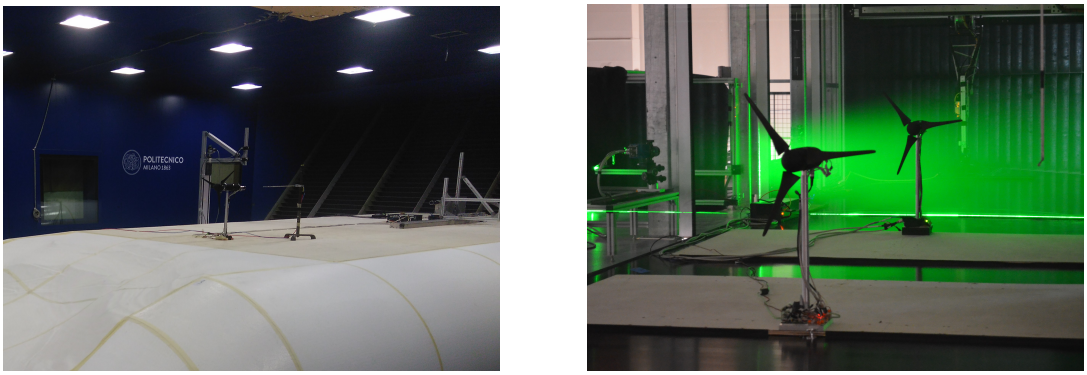

**Figure 2.7:** Left: Picture of the complex terrain experimental set-up. The G06, the camera and laser of the PIV system are also visible. Right: Picture of the UTD experimental set-up. Two G06, the cameras and the laser sheet of the PIV system are also visible.

### Pitot - static tube

Pitot tubes were used during all wind tunnel experiments as a method for determining the inflow wind speed at hub height. The Pitot tube can be used for calculating the flow speed at a single point by using the Bernoulli equation which states that if no work is added to the flow, the total pressure is equal to the sum of dynamic pressure and static pressure. The Pitot - static tube has one tube that is pointing directly into the fluid flow. The fluid that enters the tube, having nowhere to go, stagnates. At the same time, it has a port perpendicular to the flow where the air is moving freely. The tube and the static port are connected to a Manometer and the pressure difference between those two is equal to the dynamic pressure. The flow velocity can then be calculated if one knows the density of the flow (Fig. 2.8). Pitot - static tubes are very easy to use, do not require any calibration and are suitably economical.

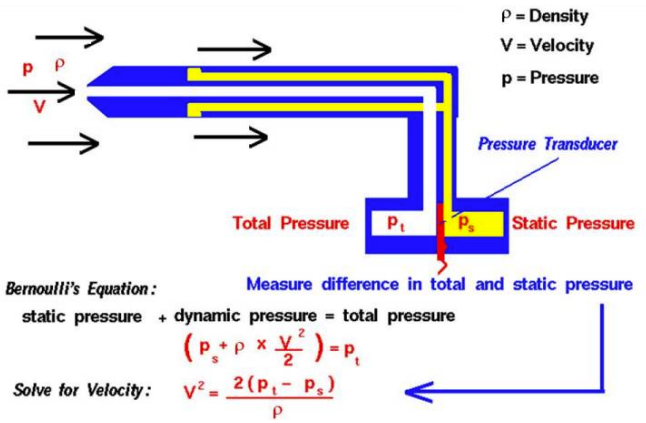


**Figure 2.8:** Schematic drawing of a pitot-static tube. Source: NASA, Glenn Research Center.

## 2.1.4 Wind turbine control system

The control system of the scaled wind turbines is not merely a data acquisition system. It has the architecture of a full scale commercial wind turbine controller and uses the same hardware while it was developed fully in house. Therefore, according to the author's opinion, it is worth mentioning in this section.

G1 and G06 share the same control system, as this was one of design requirements for the G06 which was developed after the G1. The core of the control system is an industrial standard Programmable Logic Computer (PLC) provided by Bachmann [109] shown in Fig. 2.9. This PLC is a modular controller that can be adapted to the user requirements. In this case, the controller consists of 5 modules. The heart of the controller is the CPU module where all the control applications run. Then there is a counter module which is useful for rpm measurement and synchronization with external software functions. There is a Controller Area Network (CAN) module which allows for CAN communication protocol and it is used for the pitch and yaw actuators. Last but not least there two analog input-output modules that are used for all the remaining sensors(strain gauges, Pitot , temperature etc.) and the torque actuator.
Regarding the control algorithms that run the wind turbine models, they follow a typical power controller based on [110], where the turbine operation is split to two distinct control regions: below rated wind speed and above rated wind speed. Below rated speed the blade pitch angle is kept fixed at its optimum value while the torque demand varies with the goal of keeping the optimum tip speed ratio. Above the rated wind speed, the torque demand is kept fixed while the collective blade pitch angle increases with increasing wind speed with the goal of limiting the produced power at the rated value.

**Figure 2.9:** Picture of the Bachmann PLC control system.

## 2.2 Numerical methods

Numerical methods supplemented the work that was done in this dissertation. In some cases, like the work presented in **Paper VIII**, numerical methods were the main tool of the study. In the context of the present dissertation, the term "numerical methods" encompasses three main areas: the numerical scheme that was used to simulate the flow dynamics, the methods to model nacelle, tower and blades of the wind turbine and the polar identification method.

### 2.2.1 Turbine numerical model

The rotor of the scaled wind turbine was modeled based on blade element theory. According to blade element theory, each rotor blade is divided into segments and each segment is treated independently as a 2D airfoil. The forces around each blade element are calculated based on tabulated airfoil polars that should either be pre-calculated with other numerical methods (e.g. panel methods) or measured. Since the method is using a sum of 2D airfoils to model a 3D body (blade), it is simpler and computationally cheap. Unavoidably, this simplification excludes 3D phenomena like centrifugal pumping or root and tip losses from the analysis. For some of them, empirical corrections can be applied to improve the accuracy of the method. Blade element theory is combined with momentum theory to

constitute the blade element momentum theory, which more comprehensively describes the blade-flow interaction.
Despite its simplicity, BEM method is reasonably accurate and represents the state of the art tool for the wind energy and helicopter industries. In this dissertation, the BEM method is implemented with the open source code FAST [111], which is a widely used code for commercial and research purposes. In the CFD simulations the FAST model of the G06 is also used as part of the implementation of the actuator-line method (ALM) [112]. The difference is that in the CFD simulation case, the induction on the flow is calculated by CFD instead of BEM according to the velocity sampling approach proposed in [113]. Hence, FAST and CFD are coupled using the SOWFA framework [114] for the implementation of the ALM method.
The inflow along the blade is computed in distinct stations using the integral approach and the results are used as an input from FAST, which calculates the aerodynamic forces at each station by interpolating lift and drag coefficients, which are stored in lookup tables and depend on angle of attack and Reynolds number. Then, the computed aerodynamic forces are projected back to the flow using a single Gaussian width value.
The nacelle and the tower are usually omitted in full scale CFD simulations. However, for scaled models like the G06, which have relatively large nacelles and towers with respect to their rotor diameter, these components have non-negligible effects on the flow, especially in the near wake region. Therefore, they are included in the simulations using the immersed boundary method [115, 116].

### 2.2.2 Polars identification

A direct consequence of the above is that the stored lift and drag coefficients are of paramount importance. This importance is further emphasized by the fact that the studies presented here use scaled wind turbine models that work at low Reynolds numbers, where polars calculation using traditional panel codes (like Xfoil [117]) are less accurate. In addition, small imperfections in the turbine rotor manufacturing process could result in different polars. Therefore, the polars used for these simulations are tuned following the methodology described in [118]. In a nutshell, first a large number of power and thrust measurements were collected. These measurements covered the whole operating regime of the scaled models in terms of angles of attack and Reynolds number. Next these data were used to tune the nominal polars (derived with Xfoil) using a maximum-likelihood criterion.

### 2.2.3 Large-eddy simulation

The computational fluid dynamics (CFD) simulations that were run for this dissertation were based on the large eddy simulation (LES) mathematical model which was proposed in the 60s [119]. LES resolve numerically only the higher length scales of the Navier-Stokes equations while they use models to get information about the smaller length scales of turbulence. This method is, in general terms, a compromise between direct numerical simulations (DNS), which resolve the whole spectrum of the Navier-Stokes equations but is computationally expensive, and the Reynolds averaged Navier Stokes (RANS) simulations which are time averaged and computationally cheap, but at the expense of lost information especially in parts of the flow with high time derivatives. As computational power increases, LES is widely adopted by the wind energy research community [67, 120] due to its inherent ability to better resolve features of the flows within wind farms.
The LES solver used in this Dissertation is based on the finite-volume method, which is using a standard Boussinesq PISO (Pressure Implicit with Splitting of Operator) incompressible formulation. The solver is implemented in OpenFOAM [121]. The spatial differencing is based on the Gamma method [122], which uses a higher level of upwinding in the near-wake region in order to enhance numerical stability.

The backward Euler scheme is used for the time marching, while the pressure equation is solved by the conjugate gradient method, which is preconditioned by a geometric-algebraic multi-grid. The velocity field, dissipation rate and turbulence kinetic energy are solved by the bi-conjugate gradient method. In this case, the diagonal incomplete LU factorization is used as preconditioner. Last but not least, the Smagorinsky turbulence model is used to model small scales of turbulence with a Smagorinsky constant equal to 0.16.

### 2.2.4 Precursor simulation

In all cases presented in this dissertation, the CFD copied the wind tunnel test set-up. The wind tunnel used here are, as described above, atmospheric boundary layer tunnels with relatively long test sections. The long test sections are necessary for allowing for enough space for the boundary layer development. However, the scaled wind turbines are placed in a part of the test section where the boundary layer has already developed.
The aim of the precursor simulation is to resolve the turbulent inflow generation process that takes place in the first part of the test section with the aim of matching the experimental inflow data. Once this goal is achieved, this inflow can be used for several wind farm or wind turbine CFD simulations without the need for simulating the whole wind tunnel test section every time.
The precursor simulations were performed for two wind tunnels, namely Politecnico di Milano and University of Texas at Dallas. The inflow velocity distribution $U_m(y,z)$ was measured 19.1 m downstream the entrance of the test section for the POLIMI wind tunnel and 22 m for the UTD wind tunnel. For the precursor simulation, a velocity distribution $U_P(y,z)$ was used at the entrance of the wind tunnel, while the spires and roughness elements (described in 2.1) were also modeled in the simulation. The precursors simulations were run iteratively, changing in each iteration the $U_P(y,z)$ until the velocity distribution of the simulation $U_S(y,z)$ matched the $U_m(y,z)$ at the measurement positions.

CHAPTER 3

# Definition of Improved Wind Farm O& M: Key performance indicators for wind farm operation and maintenance (Paper I)

## 3.1 Summary

This paper is dealing with the lack of well-defined metrics for the assessment of the wind farm operation and maintenance. First the relevant wind farm stakeholders are identified and their needs and interests are defined and split into five categories, namely Performance, Reliability, Maintenance, Finances and Safety. Next, a review of the existing metrics (Key Performance Indicators) that are used is presented. What is more, the paper explores the characteristics a KPI should have in order to fulfill its purpose in adequate manner. The paper concludes that these characteristics are: relevant, measurable, traceable in time.
The current KPIs are evaluated based on those characteristics and a compact set of KPIs is proposed that improves situational awareness of the wind farm stakeholders in all respective categories. It is also concluded that further validation with actual wind farm data is highly recommended to make a quantitative evaluation among different KPIs.

## 3.2 Contribution

For this peer-reviewed publication, the author of this dissertation shared equally the main research work, the interviewing part and the data analysis with Elena Gonzalez, Helene Seyr, Laura Valldecabres and Nurseda Y. Yürüşen. Ursula Smolka, Michael Muskulus and Julio Melero supervised the research work and provided important feedback. All authors contributed to the writing of this publication.

## 3.3 Reference

E. Gonzalez, E. M. Nanos, H. Seyr, L. Valldecabres, N. Y. Yürüşen, U. Smolka, M. Muskulus, and J. J. Melero, "Key performance indicators for wind farm operation and maintenance," *Energy Procedia*, vol. 137, pp. 559 – 570, 2017. doi: https://doi.org/10.1016/j.egypro.2017.10.385

CHAPTER 4

# Wind farm control and modeling: First demonstration of closed loop wind farm controller (Paper II)

## 4.1 Summary

This paper demonstrates the first application of a closed-loop wind farm controller, implemented on a cluster of scaled wind turbines in atmospheric boundary layer wind tunnel. The controller is a model-free gradient based extremum seeking algorithm. It is implemented on a cluster of three staggered scaled wind turbine models changing the yaw angle of the first two turbines with the aim of deflecting the wake away from the downstream machines in order to increase the cluster power.
At each step, the controller changes the yaw angle of a machine. At the end of each step, the gradient of the power output of the yawed machine and its closest neighbor is calculated. Based on the sign and magnitude of this gradient the controller calculates the next step. This procedure is followed for the two upstream machines until convergence.
The experimental results showed that the controller was able to reach the optimum yaw configuration of each turbine of the cluster, leading to a significant cluster power increase of more than 15% at the tested inflow conditions and cluster configuration. The advantage of a model-free controller, like the one tested here, is that there is no need for data to calibrate the model parameters. On the other hand, the model-free approach requires significant time to converge to the optimum solution.

## 4.2 Contribution

For this publication, the author of this dissertation assisted in conducting the wind tunnel experiments and performed part of the data post-processing and analysis. Filippo Campagnolo led the preparation and execution of the test campaign and the data analysis. Vlaho Petrovic implemented the wind farm controller on the wind turbine control software and assisted on the execution of the experiments and on the data analysis. Johannes Schreiber assisted in conducting the wind tunnel tests and to the data analysis. Alessandro Croce supervised the execution of the wind tunnel tests. Carlo L. Bottasso had the original idea of testing wind farm control algorithms in scaled wind farms, assisted in the interpretation of the results and supervised the whole research work. All authors provided important input to this research work through discussions, feedback and by writing the paper.

## 4.3 Reference

F. Campagnolo, V. Petrović, J. Schreiber, E. M. Nanos, A. Croce, and C. L. Bottasso, "Wind tunnel testing of a closed-loop wake deflection controller for wind farm power maximization," *Journal of Physics: Conference Series*, vol. 753, p. 032006, 2016. doi: 10.1088/1742-6596/753/3/032006

CHAPTER 5

# Wind farm control and modeling: Evaluation of wake redirection methods (Paper III)

## 5.1 Summary

The aim of the present paper is twofold. First to validate a numerical CFD framework using wind tunnel experiments and, second, to evaluate two wake redirection techniques: yaw misalignment and cyclic pitch control.
The experiments were conducted in a boundary layer wind tunnel employing stereo PIV and Hot Wire, while a LiDAR system was used to map the inflow velocity field in the wind tunnel test section. The numerical simulations used a high-fidelity LES lifting line model including the effect of nacelle and tower.
Comparisons between wind tunnel measurements and LES revealed acceptable agreement in terms of average velocities, turbulence intensity and Reynolds stresses. Moreover, the necessity for more accurate airfoil polars and the importance of including the nacelle and tower in the CFD model is also highlighted.
Regarding the evaluation of the redirection methods, it was shown the cyclic pitch control is not an efficient method to deflect the wake. On the other hand, it was validated that lateral wake deflection due to yaw misalignment can be effective.

## 5.2 Contribution

For this peer-reviewed publication, the author of this dissertation performed the wind tunnel experiments and conducted the data post-processing and analysis of the experimental data. Jiangang Wang led the research work and performed, together with Spencer Foley, the numerical simulations. Carlo L. Bottasso supervised the whole work. All authors provided important input to this research work through discussions, feedback and by writing the paper.

## 5.3 Reference

J. Wang, S. Foley, E. M. Nanos, T. Yu, F. Campagnolo, C. L. Bottasso, A. Zanotti, and A. Croce, "Numerical and experimental study of wake redirection techniques in a boundary layer wind tunnel," *Journal of Physics: Conference Series*, vol. 854, 2017. doi: 10.1088/1742-6596/854/1/012048

CHAPTER 6

# Wind farm control and modeling: Implementation and validation of a wind farm model (Paper IV)

## 6.1 Summary

This paper presents a first implementation of a FLORIS [37] based wind farm model. This model can be used for predicting the flow within a wind farm and, consequently, the wind farm power. First, the paper addresses the problem of identifying the model parameters using experimental data. To this purpose, wind tunnel measurements of isolated scaled wind turbines were used to identify the model parameters.
Next, the calibrated model is used to predict the optimum yaw angle of the two upstream turbines that maximize the power output of three wind turbine farm. The predictions of the model were compared against experimental data from wind tunnel measurements of an identical scaled wind farm.
Results showed that the model was capable of correctly defining the yaw angle distribution among the tree wind turbines that maximizes the wind farm power output despite some discrepancies on the absolute power predictions. Those discrepancies could be attributed to a number of factors, such as the insufficient modeling of wake recovery and lateral flow speed variations present in the wind tunnel.
Note: There is a typo in Eq. 5 of the published paper. The correct form of the equation is $C_T(\gamma) = \frac{1}{2} cos(\gamma)^2 (4\alpha(1-\alpha))$.

## 6.2 Contribution

For this peer-reviewed publication, the author of this dissertation implemented an initial version of the wind farm model, which was later expanded and completed by Johannes Schreiber. Additionally, he assisted in the execution of the wind tunnel experiments and conducted the data post-processing and analysis of the experimental data. Johannes Schreiber expanded the wind farm model, assisted in the execution of wind tunnel experiments and the data analysis. Carlo L. Bottasso assisted in the model formulation, the interpretation of the results and supervised the whole project. All authors provided important input to this research work through discussions, feedback and by writing the paper.

## 6.3 Reference

J. Schreiber, E. M. Nanos, F. Campagnolo, and C. L. Bottasso, "Verification and calibration of a reduced order wind farm model by wind tunnel experiments," *Journal of Physics: Conference Series*, vol. 854, no. 1, p. 012041, 2017. [Online]. Available: http://stacks.iop.org/1742-6596/854/i=1/a=012041

CHAPTER 7

# Wind farm/wake aerodynamics: Design and characterization of a scaled wind turbine model (Paper V)

## 7.1 Summary

This paper presents the design and characterization of the G06 scaled wind turbine model. G06 features compact size that allows for deep array wind farm control tests and employs novel rotor design for realistic aerodynamic performance and wake behavior. Additionally, it is highly sensorized allowing for a variety of test possibilities.
The as realistic as possible aerodynamic performance and wake behavior is ensured by the selection of appropriate low Reynolds airfoil and the matching of the normalized circulation distribution along the blade with respect to a full scale reference wind turbine.
After the discussion about the design methodology, the paper presents the performance characterization of the G06 as obtained from wind tunnel measurements. Results indicate that the model, given its size, has a good performance with $C_P$ of 0.41 and $C_T$ of 0.75 at rated wind speed. Results also showed that the performance in consistent among different rotors.
Regarding the wake behavior, an extensive analysis showed that the wake behavior is the expected and similar to other scaled models. What is more, the wake behavior is, to a large extend, in line with empirical models used for full scale machines. The wake is characterized not only with respect to first order flow statistics (like wake velocity) but also with respect to quantities that are, in most similar experimental studies, not presented in similar studies, such as turbulent fluxes and dissipation rate.

## 7.2 Contribution

For the peer-reviewed publication, the author of this dissertation designed the scaled wind turbine, prepared and executed the wind tunnel measurements and analyzed the experimental and numerical data. Carlo L. Bottasso defined the design methods and requirements for this scaled model and supervised the whole work. Filippo Campagnolo contributed to the design of G06, developed the rotor design code and performed the G1 wind tunnel measurements. Stefano Letizia assisted in the wind tunnel experiments and Valerio G. Iungo supervised the wind tunnel activities performed performed at UTD. Mario Rotea facilitated and supported the work at UTD. All authors provided important input to this research work through discussions, feedback and by writing the paper.

## 7.3 Reference

E. M. Nanos, C. L. Bottasso, F. Campagnolo, S. Letizia, G. V. Iungo, and M. A. Rotea, "Design, performance and wake characterization of a scaled wind turbine with closed-loop controls," *Wind Energ. Sci. Discuss.*, 2021. doi: 10.5194/wes-2021-66

CHAPTER 8

# Wind farm/wake aerodynamics: Wake measurements of the scaled wind turbine model (Paper VI)

## 8.1 Summary

This paper presents an initial wake characterization of the scaled wind turbine G06. In comparison with **Paper V**, which succeeds and extends the wake characterization, this paper focuses on basic wake properties (wake deflection, velocity deficit), analyzing their behavior under different inflow conditions and in different wind tunnels.
The wind tunnel tests were performed in two different wind tunnels using hot-wire in the one, and S-PIV in the other. Two inflow conditions were used, one with low turbulence and one with high turbulence and vertical shear. For both types of inflow, the conditions were comparable for the two wind tunnels.
Results confirmed the very strong dependence on inflow conditions highlighting the stronger wake recovery when the added turbulence intensity. On the other hand, wake redirection due to yaw misalignment was largely unaffected by the inflow conditions.
The analysis also revealed a very good agreement between measurements that were performed in different wind tunnels and with different measuring techniques.

## 8.2 Contribution

For the peer-reviewed publication, the author of this dissertation prepared and executed the wind tunnel measurements in TUM and UTD and analyzed the experimental data. Johanne Robke assisted to the preparation of the experiments at TUM and UTD and to the data analysis. Florian Heckmeier assisted to the conduction of the experiments at TUM, while Valerio Iungo and Kyle Jones assisted to the conduction of the experiments at UTD. Carlo L. Bottasso defined the G06 design requirements and methodology, contributed to the interpretation of the data and supervised the whole work. All authors provided important input to this research work through discussions, feedback and by writing the paper.

## 8.3 Reference

E. M. Nanos, J. Robke, F. Heckmeier, M. Cerny, K. Jones, V. Iungo, and C. L. Bottasso, "Wake characterization of a multipurpose scaled wind turbine model," *AIAA Scitech 2019 Forum*, 2019. doi: 10.2514/6.2019-2082

CHAPTER 9

# Wind farm/wake aerodynamics: Complex terrain study (Paper VII)

## 9.1 Summary

This paper presents a novel wind tunnel set-up for complex terrain wind turbine interaction studies. The paper describes the methodology that was followed to create a scaled copy of a real complex terrain test site and then presents a characterization of the flow around the terrain with and without a wind turbine.
To ensure a as realistic as possible flow around the scaled model of the complex terrain, flow similarity criteria were taken into account, i.e. Reynolds, Richardson, Eckert, Rosby and Prandtl numbers. The most relevant quantity for this application is Reynolds number, which is the largest found in the literature and way above the minimum threshold proposed in literature for Re-independent flow.
The final geometry of the scaled model of the complex terrain was refined using CFD simulations in order to minimize edge vortices that could develop and affect the turbine wake. Moreover, the CFD simulations were used to quantify the blockage effect of the terrain. It was found that a 5% correction should be applied to experimental results due to blockage effects. Next, the paper presents wake measurements of the terrain alone and the terrain together with the scaled wind turbine G06. Results revealed some of the effects the terrain has on the flow, even though its influence on the turbine wake (for the specific turbine position tested) was weak. The most noticeable effect was the weaker wake recovery observed for the turbine on a complex terrain in comparison with the same turbine on a flat terrain.

## 9.2 Contribution

For the peer-reviewed publication, the author of this dissertation initiated and supervised the design of the scaled complex terrain model, prepared and executed the wind tunnel measurements and analyzed the experimental data. Kutay Yilmazlar assisted to the preparation of the experiments and performed a big part of the terrain design. Alex Zanotti was responsible for the measuring equipment and the post-processing of the data. Alessandro Croce supervised the wind tunnel experiments in POLIMI. Carlo L. Bottasso had originally the idea of studying the turbine complex terrain interaction in a wind tunnel, contributed to the terrain design methodology and to the interpretation of the results and supervised the whole work. All authors provided important input to this research work through discussions and feedback.

## 9.3 Reference

E. Nanos, K. Yilmazlar, A. Zanotti, A. Croce, and C. Bottasso, "Wind tunnel testing of a wind turbine in complex terrain," *Journal of Physics: Conference Series*, vol. 1618, 2020. doi: 10.1088/1742-6596/1618/3/032041

CHAPTER 10

# Wind farm/wake aerodynamics: Vertical wake steering study (Paper VIII)

## 10.1 Summary

This paper presents a novel concept of wind farm control suitable for floating wind turbines. It introduces the idea of vertical wake steering with the use of differential ballast control on floating wind turbines. For this study a reference 10 MW wind turbine was used along with two reference platforms. First, the paper assesses the vertical wake steering in terms of power gain for a two wind turbine cluster with different values of the streamwise turbine spacing. The assessment is performed with LES simulations of the G06 scaled model, since the tested setup can be validated with experimental data, while previous studies have shown that G06 wake is similar to the one of the reference wind turbine. Results show that, for the tested configuration, deflecting the wake towards the sea surface leads to power gains of up to 3% for spacing between the turbines of 12D, while for smaller spacing the gains are greater.
In addition, hydro-aero-servo-elastic simulations of one of the full scale platforms together with the turbine show that the impact of platform pitching is rather small on fatigue and ultimate loads considering that this method is not utilized under severe sea state and wind speeds above rated.
Next, the paper presents an initial sizing of the system based on two examples of floating platforms. Results show that, in the tested conditions, the energy expenditure for pitching the front wind turbine in a two turbines array requires 10 to 30 minutes of pitched operation to break even. After that point, the energy gains are net profit.
The paper concludes that this idea has potential and is worth investigating further as a complementary method to other wind farm control techniques.

## 10.2 Contribution

For the peer-reviewed publication, the author of this dissertation performed the wind tunnel experiments, contributed to the CFD simulations, performed all the sizing analyses and contributed to the interpretation of the results. Carlo L. Bottasso devised the original idea of wake steering through differential ballast control, collaborated in the interpretation of the results and supervised the whole research. Dimitris Manolas and Vasilis Riziotis performed the hydro-aero-servo-elastic simulations and analyzed the corresponding data. All authors provided important input to this research work through discussions, feedback and by writing the paper.

## 10.3 Reference

E. M. Nanos, C. L. Bottasso, D. I. Manolas, and V. A. Riziotis, "Vertical wake deflection for floating wind turbines by differential ballast control," *Wind Energ. Sci. Discuss.*, 2021. doi: 10.5194/wes-2021-79

CHAPTER 11

# Discussion and conclusions

This dissertation tackles the issue of improved wind farm operation from different perspectives. With different levels of detail, the dissertation touches upon the definition of the improved wind farm operation, wind farm modeling and control and wind farm/wake aerodynamics. The methods used in this dissertation, following the broadness of the research topics addressed, are diversified. However, despite the variety of methods used, it should be pointed out that the biggest part of the dissertation is devoted to the development, validation and implementation of experimental techniques and tools, which, according to the authors opinion, are a vital and indispensable link in the chain of innovation transfer from the conceptual stage to real world application.

First, the dissertation addresses the lack of consensus among the various wind farm stakeholders about the metrics that should be used in the evaluation of the operation and maintenance of a wind farm. There is very limited published work on this issue and it is either not complete [124] or too specific and contains a large number of KPIs [125] so that it does not serve the purpose of providing a compact standardized set of metrics for the evaluation of a wind farm operation and maintenance. This dissertation attempts a first step towards the mitigation of this issue by identifying the needs and interests of the various wind farm stakeholders, defining the necessary properties that efficient KPIs should have and, finally, proposing a compact set of KPIs which cover most of the stakeholders of a wind farm.

Next, the dissertation touches on the wind farm modeling and control topics as one of the most promising methods to improve wind farm operation. Unlike plenty of studies that implemented wind farm controllers to increase the power output of a wind farm in a CFD environment in this dissertation there was a first actual demonstration of wind farm controller implemented on a scaled wind farm in a wind tunnel. More specifically, a cluster of three scaled wind turbine models were placed in a boundary layer wind tunnel. Then, the model-free closed loop wind farm controller altered the yaw angle of the models until it converged to an optimum yaw angle distribution among the models resulting in a up to 15% higher power yield.

Further, this dissertation demonstrated that wind tunnel data from scaled models can be used for calibrating and further validating wind farm models, as wake data from a boundary layer wind tunnel. More specifically, wake data from a wind farm configuration similar to the one described above was used for calibrating a wind farm model similar to FLORIS. Then, the model predictions were compared against other sets of data from the same wind farm. Despite the simplistic nature of the wind farm model, it could correctly predict the best yaw angle distribution for optimum power production after being calibrated with a small set of data.

So far the dissertation has demonstrated that scaled wind turbine models can accelerate the development of advanced wind farm control and wind farm modeling techniques in two ways. First, directly by providing test conditions and data suitable for the calibration and validation of these models. Second, by increasing the general understanding of wake and wind farm aerodynamics and, therefore, leading to more sophisticated incorporation of the relevant physics into reduced order models. The development of a scaled wind turbine model and its use on some wind farm and wake aerodynamic applications was the third topic of this dissertation.

The interest of the research community in scaled wind turbine models has increased over the last years for the reasons described above. One can find plenty of scientific articles [71, 73] that make use of scaled wind turbine models but few that describe their development. Among those, the models are either too big [75], which means that wake and/or wind farm studies are very difficult to conduct, or with limited capabilities and of simplistic design [27, 70]. This dissertation presents a miniature wind turbine model, which, in spite of its compact size, features the functionality of larger scaled wind turbine models. This model has a rotor of 0.6 m and, therefore, can be used for multiple types of wake studies like wind turbine-complex terrain interaction or deep array wind farm configurations with columns of 5-6 turbines. At the same time, it is equipped with sensors and actuators that make it also suitable for testing advanced wind sensing and wind farm control algorithms. The strongest point of the model is its rotor design, which, compared to similar size models, has been designed for maximum possible wake similarity with a full scale reference machine. The dissertation presents an extensive characterization of the model with regard to its aerodynamics performance and its wake flow characteristics. It has been shown that it has a high $C_P$ coefficient for a model of this size, while the thrust coefficient $C_T$ and the optimum tip speed ratio match the ones of full scale machines. Additionally, a thorough wake dynamics characterization, similar to ones which can only be found in very few other articles with less sophisticated models, was performed with the aim of deepening, at least incrementally, the current understanding of wake physics.
The G06 was also used, in the context of this dissertation, for two distinct wake studies. The first was about the interaction between wind turbine wake and complex terrain wake and the second was the potential of vertical wake steering for wind plant power maximization.
The interaction between wind turbines and complex terrain, even though of the utmost importance for onshore applications, has not been given the appropriate attention. There are some studies that are purely numerical [90–92], while the experimental ones use oversimplified terrain geometries and turbine models [96]. The study presented in this dissertation is a first attempt to couple a scaled copy of a real complex terrain with a sophisticated scaled wind turbine model. For this study the biggest terrain model found in the literature was designed and manufactured. Consequently, a lot of attention was given to the characteristics, such as size and geometry, the whole set-up should have in order to ensure credible measurements.
Last but not least, wind tunnel measurements of the G06, together with numerical simulations were used to assess the vertical wake steering as a wind farm control strategy. Vertical wake steering has received little attention due to the technical difficulties associated with its implementation. From the few articles that have been published so far, most of them are CFD studies while one is purely experimental [126]. In this dissertation both methods are combined together with hydro-aero-elastic simulations to assess the potential of vertical wake steering. Furthermore, the dissertation proposes a novel way for a, relatively, easy implementation of vertical wake steering suitable for floating wind turbines.

The most important contributions from the work described in this dissertation are presented in the following synopsis:

- First, the dissertation identifies the needs and interest of the various wind farm stakeholders when it comes the monitoring of a wind farm O& M. Then, it establishes the basic characteristics that key performance indicators, which are reliable, relevant, specific, comparable, traceable in time and standard. Last but not least, based on the needs of the stakeholders and the characteristics of a good KPI the dissertation recommends a compact list of KPIs that cover a big spectrum of wind farm O& M.

- Lateral wake steering through yaw misalignment is an effective method for wind farm control with the goal of power maximization. In addition, it was demonstrated through wind tunnel

experiments that even a simplified wind farm controller can substantially improve the farm power output. It was also shown that reduced order wake model can indeed predict the optimum operating point of a wind farm, and that even a small set of data is enough to properly calibrate them.

- It is shown that wind tunnel testing of scaled wind turbines is of fundamental importance and catalyzes the transfer of innovation from paper to full scale implementation. This dissertation contributes to this by presenting a detailed design and characterization of a miniature wind turbine. This wind turbine combined successfully the sophisticated aerodynamics and sensorization that can be found on bigger models, with a very compact size which allows for a big range of wind tunnel studies to be carried out. Undoubtedly, this model can be an invaluable tool for future studies on wind farm aerodynamics and control.

- The dissertation presented the design, development and a first application of a novel test set-up for the study of complex terrain - wind turbine interaction. All relevant flow similarity parameters were taken into account resulting in a terrain copy of a real test site with one of the highest Reynolds number that can found in literature coupled with a sophisticated scaled wind turbine. Apart from the flow similarity criteria, special attention was given to minimize finite geometry and wind tunnel blockage effects that are present in wind tunnel models.

- It is demonstrated that vertical wake deflection can be beneficial, and a technically feasible way of implementing it in floating wind farms with the use of differential ballast control is proposed. The study was expanded to turbine spacing that is more relevant for offshore wind plants, i.e. 12 rotor diameters apart. The aerodynamic analysis revealed that deflecting the wake towards the ground is more beneficial for the tested configuration, leading to power gain of up to 3% for a cluster of two turbines. What is more, hydro-aero-elastic simulations showed it has limited effects on fatigue loads and no impact on ultimate loads when the method is used in good weather (normal sea state) and for wind speeds below rated.

## 11.1 Outlook

As demonstrated in this dissertation, the improvement of wind farm operation and maintenance is a multi-variable effort and embraces many different research fields that have on one hand their own specific challenges, but on the other hand are interconnected and advancements on one assist advancements on the others.
This dissertation has attempted to bring the topics it touched a little bit forward. Nevertheless, there is still a lot to be done in all aspects before there is a considerable impact on commercial wind farms. Based on the work done and the exposure on the topics in the context of this dissertation, the following recommendations about future work can be made.
First, there is a need for further evaluation of the proposed key performance indicators for the wind farm operation and maintenance. The study presented in this dissertation, despite novel, is based on discussion with stakeholders in the context of a workshop and the suitability of the proposed KPIs, even though justifiable, is based on data found in literature. It is necessary to carry out dedicated case studies based on operational data of existing wind farms, possibly supplemented with numerical simulations to fill potential gaps. Dedicated means that the case studies will not just use KPIs for other research purposes (as has been done up until now) but the main topic of the study should be the KPIs themselves.
As for the wind farm control and modeling, next steps would be to couple wind farm models with model-based controllers. What is more, the robustness of wind farm control should be validated with

controllers and models being tested under higher degrees of uncertainty (wind direction changes and/or noisy data).

Regarding the design and characterization of the G06, further steps could include a detailed experimental and numerical assessment of the effect that this design methodology has on the similarity of the wake. Measurements in, even moderately, turbulent inflow show that most secondary flow quantities are filtered out relatively quickly and main effect present on the wake is the one of the average thrust. To move one step further in the characterization of the wake and the evaluation of the rotor design it is mandatory to perform high resolution, phase locked, S-PIV measurements in low turbulent inflow in order to capture, for example, the effect of the circulation distribution on the near wake. What is more, the whole operating envelope of sensors and actuators should be verified experimentally.

On a more general note regarding scaled wind turbines, it is necessary to standardize the design and characterization process. As explained extensively in this dissertation, there are very few articles in the literature with a thorough description of the design process and the characterization of the models and, even among those studies, there is little to no commonality between the models. Introducing reference scaled turbines, similar to what happens with full scale machines used in aeroelastic simulations, will boost their use and impact substantially.

Next, this dissertation proved the suitability of the experimental set-up for the complex terrain wind turbine interaction studies. The obvious next step would be to extend the measurements trying different wind turbine positions to parts of the terrain where its effect on the flow is more prominent. Moreover, the terrain should be also equipped with artificial vegetation, which is also present on the real test site, and assess its impact on the wind turbine inflow. Last but not least, the measurements should be coupled with LES simulations for validating the latter ones, which is, after all, one of the main goals for developing this experimental set up.

Finally, as for the vertical wake deflection by differential ballast control, the most critical next step would be to evaluate the method in offshore wind farm configurations which, typically, include multiple columns of 8-10 wind turbines, since most of the studies performed so far, including the one presented in this dissertation, consider columns of 2 to 3 machines. Additionally, a parametric study of the ambient wind and sea conditions influence on the effectiveness of this method should be performed.

From a turbine standpoint, it is necessary to understand better if and to what extend the tilting of a platform affects the turbine structure and other turbine subsystems like hydraulics or lubrication circuits. Equally important is to quantify the potential additional requirements that this method brings to the platform designs and to the anchoring system. Last but not least, all the aforementioned individual research objectives will have to be combined in cost-benefit study of this method.

[1] E. Commission, "Energy roadmap 2050," 2012.

[2] I. E. Association, "Key world energy statistics," 2020.

[3] T. Burton, D. Sharpe, N. Jenkins, and E. Bossanyi, *Wind energy handbook*. John Wiley & Sons, 2001. ISBN 0-471-48997-2

[4] G. Bergeles. Symeon, 1980. ISBN 978-960-7888-57-X

[5] P. Bortolotti, C. L. Bottasso, and A. Croce, "Combined preliminary–detailed design of wind turbines," *Wind Energy Science*, vol. 1, pp. 71–88, 2016. doi: 10.5194/wes-1-71-2016

[6] L. J. Vermeer, J. N. Sørensen, and A. Crespo, "Wind turbine wake aerodynamics," *Progress in Aerospace Sciences*, vol. 39, no. 6-7, pp. 467–510, 2003. doi: 10.1016/S0376-0421(03)00078-2

[7] H. Kerzner, "Project management metrics, KPIs, and dashboards," 2011.

[8] M. Steinbuch, W. W. de Boer, O. H. Bosgra, S. A. Peters, and J. Ploeg, "Optimal control of wind power plants," *Journal of Wind Engineering and Industrial Aerodynamics*, vol. 27, no. 1-3, pp. 237–246, jan 1988. doi: 10.1016/0167-6105(88)90039-6

[9] J. G. Schepers and S. P. van der Pijl, "Improved modelling of wake aerodynamics and assessment of new farm control strategies," *Journal of Physics: Conference Series*, vol. 75, no. 1, p. 012039, 2007. [Online]. Available: http://stacks.iop.org/1742-6596/75/i=1/a=012039

[10] J. S. González, M. B. Payán, and J. R. Santos, "Optimal control of wind turbines for minimizing overall wake effect losses in offshore wind farms," in *IEEE EuroCon 2013*, 2013, pp. 1129–1134. doi: 10.1109/EUROCON.2013.6625122

[11] P. M. Gebraad, F. C. Van Dam, and J. W. Van Wingerden, "A model-free distributed approach for wind plant control," in *Proceedings of the American Control Conference*. Institute of Electrical and Electronics Engineers Inc., 2013, pp. 628–633. doi: 10.1109/acc.2013.6579907

[12] J. Annoni, P. M. O. Gebraad, A. K. Scholbrock, P. A. Fleming, and J.-W. van Wingerden, "Analysis of axial-induction-based wind plant control using an engineering and a high-order wind plant model," *Wind Energy*, vol. 19, no. 6, pp. 1135–1150, jun 2016. [Online]. Available: http://doi.wiley.com/10.1002/we.1891. doi: 10.1002/we.1891

[13] J. Bartl and L. Sætran, "Experimental testing of axial induction based control strategies for wake control and wind farm optimization," *Journal of Physics: Conference Series*, vol. 753, no. 3, 2016. doi: 10.1088/1742-6596/753/3/032035

[14] F. Campagnolo, V. Petrovic, E. M. Nanos, W. Chun, and C. L. Bottasso, "Wind tunnel testing of power maximization control strategies applied to a multi-turbine floating wind power platform," in *International Ocean and Polar Engineering Conference*, 2016.

[15] E. Bossanyi and R. Ruisi, "Axial induction controller field test at Sedini wind farm," *Wind Energy Science Discussions*, pp. 1–27, 2020. doi: 10.5194/wes-2020-88

[16] C. H. Westergaard, "A method for improving large array wind park power performance through active wake manipulation reducing shadow effects," mar 2013.

[17] J. P. Goit and J. Meyers, "Optimal control of energy extraction in wind-farm boundary layers," *Journal of Fluid Mechanics*, vol. 768, pp. 5–50, 2015. [Online]. Available: https://doi.org/10.1017/jfm.2015.70. doi: 10.1017/jfm.2015.70

[18] J. A. Frederik, R. Weber, S. Cacciola, F. Campagnolo, A. Croce, C. Bottasso, and J.-W. van Wingerden, "Periodic dynamic induction control of wind farms: proving the potential in simulations and wind tunnel experiments," *Wind Energy Science*, vol. 5, no. 1, pp. 245–257, feb 2020. [Online]. Available: https://wes.copernicus.org/articles/5/245/2020/. doi: 10.5194/wes-5-245-2020

[19] J. A. Frederik, B. M. Doekemeijer, S. P. Mulders, and J. Wingerden, "The helix approach: Using dynamic individual pitch control to enhance wake mixing in wind farms," *Wind Energy*, vol. 23, no. 8, pp. 1739–1751, aug 2020. [Online]. Available: https://onlinelibrary.wiley.com/doi/abs/10.1002/we.2513. doi: 10.1002/we.2513

[20] F. Campagnolo, V. Petrović, C. L. Bottasso, and A. Croce, "Wind tunnel testing of wake control strategies," in *Proceedings of the American Control Conference*, vol. 2016-July. Institute of Electrical and Electronics Engineers Inc., jul 2016, pp. 513–518. doi: 10.1109/ACC.2016.7524965

[21] D. Medici and J. Å. Dahlberg, "Potential improvement of wind turbine array efficiency by active wake control (awc)," 2003, pp. 65–84.

[22] M. S. Adaramola and P. Å. Krogstad, "Experimental investigation of wake effects on wind turbine performance," *Renewable Energy*, vol. 36, no. 8, pp. 2078–2086, aug 2011. doi: 10.1016/j.renene.2011.01.024

[23] P. M. Gebraad, F. W. Teeuwisse, J. W. van Wingerden, P. A. Fleming, S. D. Ruben, J. R. Marden, and L. Y. Pao, "Wind plant power optimization through yaw control using a parametric model for wake effects-a cfd simulation study," *Wind Energy*, vol. 19, no. 1, pp. 95–114, 2016. doi: 10.1002/we.1822

[24] P. Gebraad, J. J. Thomas, A. Ning, P. Fleming, and K. Dykes, "Maximization of the annual energy production of wind power plants by optimization of layout and yaw-based wake control," *Wind Energy*, vol. 20, no. 1, pp. 97–107, jan 2017. [Online]. Available: http://doi.wiley.com/10.1002/we.1993. doi: 10.1002/we.1993

[25] M. Bastankhah and F. Porté-Agel, "Wind farm power optimization via yaw angle control: A wind tunnel study," *Journal of Renewable and Sustainable Energy*, vol. 11, no. 2, p. 023301, mar 2019. [Online]. Available: http://aip.scitation.org/doi/10.1063/1.5077038. doi: 10.1063/1.5077038

[26] F. Campagnolo, R. Weber, J. Schreiber, and C. L. Bottasso, "Wind tunnel testing of wake steering with dynamic wind direction changes," *Wind Energy Science*, vol. 5, pp. 1273–1295, 2020. doi: 10.5194/wes-5-1273-2020

[27] L. P. Chamorro and F. Porté-Agel, "A wind-tunnel investigation of wind-turbine wakes: boundary-layer tur- bulence effects," *Boundary-Layer Meteorol*, vol. 132, pp. 129–149, 2009.

[28] P. Fleming, J. Annoni, J. J. Shah, L. Wang, S. Ananthan, Z. Zhang, K. Hutchings, P. Wang, W. Chen, and L. Chen, "Field test of wake steering at an offshore wind farm," *Wind Energy Science*, vol. 2,

no. 1, pp. 229–239, may 2017. [Online]. Available: https://wes.copernicus.org/articles/2/229/2017/. doi: 10.5194/wes-2-229-2017

[29] P. Fleming, J. King, K. Dykes, E. Simley, J. Roadman, A. Scholbrock, P. Murphy, J. K. Lundquist, P. Moriarty, K. Fleming, J. Van Dam, C. Bay, R. Mudafort, H. Lopez, J. Skopek, M. Scott, B. Ryan, C. Guernsey, and D. Brake, "Initial results from a field campaign of wake steering applied at a commercial wind farm-Part 1," *Wind Energ. Sci*, vol. 4, pp. 273–285, 2019. [Online]. Available: https://doi.org/10.5194/wes-4-273-2019. doi: 10.5194/wes-4-273-2019

[30] P. Fleming, J. King, E. Simley, J. Roadman, A. Scholbrock, P. Murphy, J. K. Lundquist, P. Moriarty, K. Fleming, J. van Dam, C. Bay, R. Mudafort, D. Jager, J. Skopek, M. Scott, B. Ryan, C. Guernsey, and D. Brake, "Continued results from a field campaign of wake steering applied at a commercial wind farm – Part 2," *Wind Energy Science*, vol. 5, no. 3, pp. 945–958, 2020. [Online]. Available: https://wes.copernicus.org/articles/5/945/2020/. doi: 10.5194/wes-5-945-2020

[31] P. Fleming, P. M. Gebraad, S. Lee, J.-W. van Wingerden, K. Johnson, M. Churchfield, J. Michalakes, P. Spalart, and P. Moriarty, "Simulation comparison of wake mitigation control strategies for a two-turbine case," *Wind Energy*, vol. 18, no. 12, pp. 2135–2143, dec 2015. [Online]. Available: http://doi.wiley.com/10.1002/we.1810. doi: 10.1002/we.1810

[32] J. Annoni, A. Scholbrock, M. Churchfield, and P. Fleming, "Evaluating tilt for wind plants," *American Control Conference Seattle*, pp. 717–722, 2017.

[33] C. Cossu, "Replacing wakes with streaks in wind turbine arrays," no. August, pp. 1–12, 2020. [Online]. Available: http://arxiv.org/abs/2007.01617. doi: 10.1002/we.2577

[34] I. Katic, J. Højstrup, and N. Jensen, "A Simple Model for Cluster Efficiency," *European wind energy association conference and exhibition*, vol. 1, 1987.

[35] N. O. Jensen, *A note on wind generator interaction*, 1983. ISBN 87-550-0971-9

[36] S. Frandsen, R. Barthelmie, S. Pryor, O. Rathmann, S. Larsen, J. Højstrup, and M. Thøgersen, "Analytical modelling of wind speed deficit in large offshore wind farms," *Wind Energy*, vol. 9, no. 1-2, pp. 39–53, 2006. doi: 10.1002/we.189

[37] P. M. O. Gebraad, F. W. Teeuwisse, J. W. Van Wingerden, P. a. Fleming, S. D. Ruben, J. R. Marden, and L. Y. Pao, "A data-driven model for wind plant power optimization by yaw control," *Proceedings of the American Control Conference*, pp. 3128–3134, 2014. doi: 10.1109/ACC.2014.6859118

[38] A. Rott, B. Doekemeijer, J. K. Seifert, J.-W. van Wingerden, and M. Kühn, "Robust active wake control in consideration of wind direction variability and uncertainty," *Wind Energy Science*, vol. 3, no. 2, pp. 869–882, nov 2018. [Online]. Available: https://wes.copernicus.org/articles/3/869/2018/. doi: 10.5194/wes-3-869-2018

[39] B. M. Doekemeijer and R. Storm, "Florisse m," 2018. [Online]. Available: https://github.com/TUDelft-DataDrivenControl/FLORISSE_M/tree/f0653ef3e8e56e284cdfa0a188aba0a7e42fce5c

[40] J. Schreiber, C. L. Bottasso, B. Salbert, and F. Campagnolo, "Improving wind farm flow models by learning from operational data," *Wind Energy Science*, vol. 5, no. 2, pp. 647–673, may 2020. [Online]. Available: https://wes.copernicus.org/articles/5/647/2020/. doi: 10.5194/wes-5-647-2020

[41] A. Betz, "Das maximum der theoretisch möglichen ausnützung deswindes durch windmotoren," *Zeitschrift für das gesamte Turbinenwesen*, vol. 26, pp. 307–309, 1920.

[42] N. Joukowsky, "Windmill of the nej type," *Transactions of the central institute for aero-hydrodynamics of moscow*, 1920.

[43] H. Glauert, "Airplane propellers," p. 169–360, 1935. doi: https://doi.org/10.1007/978-3-642-91487-4_3

[44] L. E. Lignarolo, D. Ragni, C. Krishnaswami, Q. Chen, C. J. Simão Ferreira, and G. J. van Bussel, "Experimental analysis of the wake of a horizontal-axis wind-turbine model," *Renewable Energy*, vol. 70, pp. 31–46, oct 2014. doi: 10.1016/j.renene.2014.01.020

[45] H. Lu and F. Porté-Agel, "Large-eddy simulation of a very large wind farm in a stable atmospheric boundary layer," *Physics of Fluids*, vol. 23, no. 6, p. 065101, jun 2011. [Online]. Available: http://aip.scitation.org/doi/10.1063/1.3589857. doi: 10.1063/1.3589857

[46] L. P. Chamorro, D. R. Troolin, S. J. Lee, R. E. Arndt, and F. Sotiropoulos, "Three-dimensional flow visualization in the wake of a miniature axial-flow hydrokinetic turbine," *Experiments in Fluids*, vol. 54, no. 2, pp. 1–12, feb 2013. [Online]. Available: https://link.springer.com/article/10.1007/s00348-013-1459-9. doi: 10.1007/s00348-013-1459-9

[47] L. E. Lignarolo, D. Mehta, R. J. Stevens, A. E. Yilmaz, G. van Kuik, S. J. Andersen, C. Meneveau, C. J. Ferreira, D. Ragni, J. Meyers, G. J. van Bussel, and J. Holierhoek, "Validation of four LES and a vortex model against stereo-PIV measurements in the near wake of an actuator disc and a wind turbine," *Renewable Energy*, vol. 94, pp. 510–523, aug 2016. doi: 10.1016/j.renene.2016.03.070

[48] M. Sherry, J. Sheridan, and D. L. Jacono, "Characterisation of a horizontal axis wind turbine's tip and root vortices," *Experiments in Fluids*, vol. 54, no. 3, pp. 1–19, mar 2013. [Online]. Available: https://link.springer.com/article/10.1007/s00348-012-1417-y. doi: 10.1007/s00348-012-1417-y

[49] M. Sherry, A. Nemes, D. Lo Jacono, H. M. Blackburn, and J. Sheridan, "The interaction of helical tip and root vortices in a wind turbine wake," *Physics of Fluids*, vol. 25, no. 11, p. 117102, aug 2013. [Online]. Available: http://aip.scitation.org/doi/10.1063/1.4824734. doi: 10.1063/1.4824734

[50] H. Hu, Z. Yang, and P. Sarkar, "Dynamic wind loads and wake characteristics of a wind turbine model in an atmospheric boundary layer wind," *Experiments in Fluids*, vol. 52, no. 5, pp. 1277–1294, may 2012. [Online]. Available: https://link.springer.com/article/10.1007/s00348-011-1253-5. doi: 10.1007/s00348-011-1253-5

[51] G. V. Iungo, F. Viola, S. Camarri, F. Porté-Agel, and F. Gallaire, "Linear stability analysis of wind turbine wakes performed on wind tunnel measurements," *Journal of Fluid Mechanics*, vol. 737, pp. 499–526, dec 2013. [Online]. Available: https://www.cambridge.org/core/journals/journal-of-fluid-mechanics/article/abs/linear-stability-analysis-of-wind-turbine-wakes-performed-on-wind-tunnel-measurements/9B607E1A9D005870B30ECDBEC77516FE. doi: 10.1017/jfm.2013.569

[52] F. Viola, G. V. Iungo, S. Camarri, F. Porté-Agel, and F. Gallaire, "Prediction of the hub vortex instability in a wind turbine wake: Stability analysis with eddy-viscosity models calibrated on wind tunnel data," *Journal of Fluid Mechanics*, vol. 750, p. R1, jul 2014. [Online]. Available: https://www.cambridge.org/core/journals/journal-of-fluid-mechanics/article/abs/prediction-of-the-hub-vortex-instability-in-a-wind-turbine-wake-stability-analysis-with-eddyviscosity-models-
8924A9CAEB0AD82531C606F406416009. doi: 10.1017/jfm.2014.263

[53] G. V. Iungo, "Experimental characterization of wind turbine wakes: Wind tunnel tests and wind LiDAR measurements," *Journal of Wind Engineering and Industrial Aerodynamics*, vol. 149, pp. 35–39, 2016. doi: 10.1016/j.jweia.2015.11.009

[54] R. Barthelmie, G. Larsen, S. Pryor, H. Jørgensen, H. Bergström, W. Schlez, K. Rados, B. Lange, P. Vølund, S. Neckelmann, S. Mogensen, G. Schepers, T. Hegberg, L. Folkerts, and M. Magnusson, "ENDOW(efficient development of offshore wind farms): modelling wake and boundary layer interactions," *Wind Energy*, vol. 7, no. 3, pp. 225–245, jul 2004. [Online]. Available: http://doi.wiley.com/10.1002/we.121. doi: 10.1002/we.121

[55] M. Bastankhah and F. Porté-Agel, "Wind tunnel study of the wind turbine interaction with a boundary-layer flow: Upwind region, turbine performance, and wake region," *Physics of Fluids*, vol. 29, 2017. doi: 10.1063/1.4984078

[56] Y. T. Wu and F. Porté-Agel, "Large-Eddy Simulation of Wind-Turbine Wakes: Evaluation of Turbine Parametrisations," *Boundary-Layer Meteorology*, vol. 138, no. 3, pp. 345–366, dec 2011. [Online]. Available: https://link.springer.com/article/10.1007/s10546-010-9569-x. doi: 10.1007/s10546-010-9569-x

[57] A. Englberger and A. Dörnbrack, "Impact of Neutral Boundary-Layer Turbulence on Wind-Turbine Wakes: A Numerical Modelling Study," *Boundary-Layer Meteorology*, vol. 162, no. 3, pp. 427–449, mar 2017. [Online]. Available: https://link.springer.com/article/10.1007/s10546-016-0208-z. doi: 10.1007/s10546-016-0208-z

[58] V. L. Okulov, I. V. Naumov, R. F. Mikkelsen, and J. N. Sørensen, "Wake effect on a uniform flow behind wind-turbine model," in *Journal of Physics: Conference Series*, vol. 625, no. 1. Institute of Physics Publishing, jun 2015, p. 012011. [Online]. Available: https://iopscience.iop.org/article/10.1088/1742-6596/625/1/012011https://iopscience.iop.org/article/10.1088/1742-6596/625/1/012011/meta. doi: 10.1088/1742-6596/625/1/012011

[59] P. B. Johnson, C. Jonsson, S. Achilleos, and I. Eames, "On the spread and decay of wind turbine wakes in ambient turbulence," *Journal of Physics: Conference Series*, vol. 555, p. 012055, 2014. doi: 10.1088/1742-6596/555/1/012055

[60] A. Crespo and J. Hernández, "Turbulence characteristics in wind-turbine wakes," *Journal of Wind Engineering and Industrial Aerodynamics*, vol. 61, no. 1, pp. 71–85, 1996. doi: 10.1016/0167-6105(95)00033-X

[61] G.-W. Qian and T. Ishihara, "A New Analytical Wake Model for Yawed Wind Turbines," *Energies*, vol. 11, no. 3, p. 665, mar 2018. doi: 10.3390/en11030665

[62] S. Xie and C. Archer, "Self-similarity and turbulence characteristics of wind turbine wakes via large-eddy simulation," *Wind Energy*, vol. 18, no. 10, pp. 1815–1838, oct 2015. doi: 10.1002/we.1792

[63] D. Medici and P. H. Alfredsson, "Measurements on a wind turbine wake: 3d effects and bluff body vortex shedding," *Wind Energy*, vol. 9, no. 3, pp. 219–236, 2006. doi: 10.1002/we.156

[64] P. A. Fleming, P. M. Gebraad, S. Lee, J. van Wingerden, K. Johnson, M. Churchfield, J. Michalakes, P. Spalart, and P. Moriarty, "Evaluating techniques for redirecting turbine wakes using sowfa," *Renewable Energy*, vol. 70, pp. 211–218, 2014. doi: 10.1016/j.renene.2014.02.015

[65] M. Bastankhah and F. Porté-Agel, "Experimental and theoretical study of wind turbine wakes in yawed conditions," *Journal of Fluid Mechanics*, vol. 806, pp. 506–541, 2016. doi: 10.1017/jfm.2016.595

[66] M. F. Howland, J. Bossuyt, L. A. Martínez-Tossas, J. Meyers, and C. Meneveau, "Wake structure in actuator disk models of wind turbines in yaw under uniform inflow conditions," *Journal of Renewable and Sustainable Energy*, vol. 8, no. 4, p. 043301, 2016. doi: 10.1063/1.4955091

[67] M. J. Churchfield, S. Lee, P. J. Moriarty, L. A. Martinez, S. Leonardi, G. Vijayakumar, and J. G. Brasseur, "A large-eddy simulation of wind plant aerodynamics," *AIAA Scitech 2012 Forum*, 2012. doi: 10.2514/6.2012-537

[68] J. Wang, S. Foley, E. M. Nanos, T. Yu, F. Campagnolo, C. L. Bottasso, A. Zanotti, and A. Croce, "Numerical and experimental study of wake redirection techniques in a boundary layer wind tunnel," *Journal of Physics: Conference Series*, vol. 854, 2017. doi: 10.1088/1742-6596/854/1/012048

[69] F. Porté-Agel, M. Bastankhah, and S. Shamsoddin, *Wind-Turbine and Wind-Farm Flows: A Review*. Springer Netherlands, 2020, vol. 174, no. 1. ISBN 1054601900473. [Online]. Available: https://doi.org/10.1007/s10546-019-00473-0

[70] L. P. Chamorro and F. Porté-Agel, "Effects of thermal stability and incoming boundary-layer flow characteristics on wind-turbine wakes: A wind-tunnel study," *Boundary-Layer Meteorology*, vol. 136, no. 1, pp. 515–533, 2010. doi: 10.1007/s10546-010-9512-1

[71] K. Howard, L. Hu, and L. P. Chamorro, "Characterizing the response of a wind turbine model under complex inflow conditions," *Wind Energy*, vol. 18, no. 4, pp. 729–743, 2015. doi: 10.1002/we.1724

[72] Z. Yang, P. Sarkar, and H. Hu, "An experimental investigation on the aeromechanic performance and wake characteristics of a wind turbine model subjected to pitch motions," *29th AIAA Applied Aerodynamics Conference*, no. 4, 2016.

[73] J. Bartl, F. Mühle, and L. Sætran, "Wind tunnel study on power output and yaw moments for two yaw-controlled model wind turbines," *Wind Energy Science*, vol. 3, no. 2, pp. 489–502, 2018. doi: 10.5194/wes-3-489-2018

[74] J. Schottler, A. Holling, J. Peinke, and M. Holling, "Design and implementation of a controllable model wind turbine for experimental studies," *Journal of Physics: Conference Series*, vol. 753, pp. 506–541, 2016. doi: 10.1088/1742-6596/753/7/072030

[75] C. L. Bottasso, F. Campagnolo, and V. Petrović, "Wind tunnel testing of scaled wind turbine models: Beyond aerodynamics," *Journal of Wind Engineering and Industrial Aerodynamics*, vol. 127, pp. 11–28, 2014. doi: 10.1016/j.jweia.2014.01.009

[76] H. Mendez Reyes, S. Kanev, B. Doekemeijer, and J.-W. van Wingerden, "Validation of a lookup-table approach to modeling turbine fatigue loads in wind farms under active wake control," *Wind Energy Science Discussions*, pp. 1–19, 2019. doi: 10.5194/wes-2019-34

[77] M. Bastankhah and F. Porté-Agel, "A new miniature wind turbine for wind tunnel experiments. part i: Design and performance," *Energies*, vol. 10, no. 7, p. 908, 2017. doi: 10.3390/en10070908

[78] R. Lanfazame, S. Mauro, and M. Messina, "Numerical and experimental analysis of micro hawts designed for wind tunnel applications," *Int J Energy Environ Eng*, vol. 7, p. 199–210, 2016. doi: 10.1007/s40095-016-0202-8

[79] H. Canet, P. Bortolotti, and C. L. Bottasso, "On the scaling of wind turbine rotors," *Wind Energ. Sci. Discuss.*, 2020. doi: 10.5194/wes-2020-66

[80] C. L. Kelley, D. C. Maniaci, and B. R. Resor, "Scaled aerodynamic wind turbine design for wake similarity," *34th Wind Energy Symposium, AIAA SciTech Forum, American Institute of Aeronautics and Astronautics*, 2016. [Online]. Available: http://arc.aiaa.org/doi/10.2514/6.2016-1521

[81] C. L. Bottasso and C. Riboldi, "Estimation of wind misalignment and vertical shear from blade loads," *Renewable Energy*, vol. 62, pp. 293–302, 2014. doi: 10.1016/j.renene.2013.07.021

[82] O. Hyunseok and K. Bumsuk, "Comparison and verification of the deviation between guaranteed and measured wind turbine power performance in complex terrain," *Energy*, vol. 85, pp. 23–29, 2015.

[83] J. Lange, J. Mann, J. Berg, D. Parvu, R. Kilpatrick, A. Costache, J. Chowdhury, K. Siddiqui, and H. Hangan, "For wind turbines in complex terrain, the devil is in the detail," *Environmental Research Letters*, vol. 12, no. 9, p. 094020, sep 2017. doi: 10.1088/1748-9326/aa81db

[84] J. Kuo, D. Rehman, D. A. Romero, and C. H. Amon, "A novel wake model for wind farm design on complex terrains," *Journal of Wind Engineering and Industrial Aerodynamics*, vol. 174, pp. 94–102, mar 2018. [Online]. Available: https://www.sciencedirect.com/science/article/pii/S0167610517305093?{_}rdoc=1{&}{_}fmt=high{&}{_}origin=gateway{&}{_}docanchor={&}md5=b8429449ccfc9c30159a5f9aeaa92ffb{&}dgcid=raven{_}sd{_}recommender{_}email. doi: 10.1016/J.JWEIA.2017.12.016

[85] C. Sacre, "An experimental study of the airflow over a hill in the atmospheric boundary layer," *Boundary-Layer Meteorology*, vol. 17, no. 3, pp. 381–401, nov 1979. doi: 10.1007/BF00117926

[86] H. Teunissen, "Wind-tunnel and full-scale comparisons of mean wind flow over an isolated low hill," *Journal of Wind Engineering and Industrial Aerodynamics*, vol. 15, no. 1-3, pp. 271–286, dec 1983. doi: 10.1016/0167-6105(83)90197-6

[87] P. Taylor, P. Mason, and E. Bradley, "Boundary-layer flow over low hills," *Boundary-Layer Meteorology*, vol. 39, no. 1-2, 1987. doi: 10.1007/BF00121870

[88] Y. Han, M. Stoellinger, and J. Naughton, "Large eddy simulation for atmospheric boundary layer flow over flat and complex terrains," *Journal of Physics: Conference Series*, vol. 753, no. 3, p. 032044, sep 2016. doi: 10.1088/1742-6596/753/3/032044

[89] K. W. Ayotte, "Observations of boundary-layer wind tunnel flow over isolated ridges of varying steepness and roughness," *Boundary-Layer Meteorology*, pp. 525–556, 2003.

[90] E. Politis, J. Prospathopoulos, D. Cabezon, K. Hansen, P. Chaviaropoulos, and R. Barthelmie, "Modeling wake effects in large wind farms in complex terrain: The problem, the methods and the issues," *Wind Energy*, 2011. doi: 10.1002/we.481

[91] J. Berg, N. Troldborg, N. Sørensen, E. G. Patton, and P. P. Sullivan, "Large-Eddy Simulation of turbine wake in complex terrain," *Journal of Physics: Conference Series*, vol. 854, no. 1, p. 012003, may 2017. doi: 10.1088/1742-6596/854/1/012003

[92] C. Schulz, P. Letzgus, P. Weihing, T. Lutz, and E. Krämer, "Numerical simulation of the impact of atmospheric turbulence on a wind turbine in complex terrain," in *Journal of Physics: Conference Series*, vol. 1037, no. 7. Institute of Physics Publishing, jun 2018, p. 072016. doi: 10.1088/1742-6596/1037/7/072016

[93] B. Conan, A. Chaudhari, S. Aubrun, J. Van Beeck, J. Hämäläinen, and A. Hellsten, "Experimental and Numerical Modelling of Flow over Complex Terrain: The Bolund Hill," *Boundary-Layer Meteorology*, vol. 158, pp. 183–208, 2016. doi: 10.1007/s10546-015-0082-0

[94] Y. Li, P. Hu, X. Xu, and J. Qiu, "Wind characteristics at bridge site in a deep-cutting gorge by wind tunnel test," *Journal of Wind Engineering and Industrial Aerodynamics*, vol. 160, pp. 30–46, jan 2017. doi: 10.1016/j.jweia.2016.11.002

[95] C. M. Jubayer and H. Hangan, "A hybrid approach for evaluating wind flow over a complex terrain," *Journal of Wind Engineering and Industrial Aerodynamics*, vol. 175, pp. 65–76, apr 2018. doi: 10.1016/j.jweia.2018.01.037

[96] A. Hyvärinen and A. Segalini, "Effects From Complex Terrain on Wind-Turbine Performance," *Journal of Energy Resources Technology*, vol. 139, no. 5, p. 051205, mar 2017. doi: 10.1115/1.4036048

[97] W. Tian, A. Ozbay, W. Yuan, P. Sarakar, and H. Hu, "An experimental study on the performances of wind turbines over complex terrain," *51st AIAA Aerospace Sciences Meeting including the New Horizons Forum and Aerospace Exposition 2013*, no. January, pp. 1–14, 2013. doi: 10.2514/6.2013-612

[98] B. Subramanian, N. Chokani, and R. Abhari, "Aerodynamics of wind turbine wakes in flat and complex terrains," *Renewable Energy*, vol. 85, no. 1-3, pp. 454–463, 2016. doi: 10.1016/J.RENENE.2015.06.060

[99] Francesco Castellani1, "Investigation of terrain and wake effects on the performance of wind farms in complex terrain using numerical and experimental data."

[100] E. Gonzalez, E. M. Nanos, H. Seyr, L. Valldecabres, N. Y. Yürüşen, U. Smolka, M. Muskulus, and J. J. Melero, "Key performance indicators for wind farm operation and maintenance," *Energy Procedia*, vol. 137, pp. 559 – 570, 2017. doi: https://doi.org/10.1016/j.egypro.2017.10.385

[101] F. Campagnolo, V. Petrović, J. Schreiber, E. M. Nanos, A. Croce, and C. L. Bottasso, "Wind tunnel testing of a closed-loop wake deflection controller for wind farm power maximization," *Journal of Physics: Conference Series*, vol. 753, p. 032006, 2016. doi: 10.1088/1742-6596/753/3/032006

[102] J. Schreiber, E. M. Nanos, F. Campagnolo, and C. L. Bottasso, "Verification and calibration of a reduced order wind farm model by wind tunnel experiments," *Journal of Physics: Conference Series*, vol. 854, p. 012041, 2017. doi: 10.1088/1742-6596/854/1/012041

[103] E. M. Nanos, C. L. Bottasso, F. Campagnolo, S. Letizia, G. V. Iungo, and M. A. Rotea, "Design, performance and wake characterization of a scaled wind turbine with closed-loop controls," *Wind Energ. Sci. Discuss.*, 2021. doi: 10.5194/wes-2021-66

[104] E. M. Nanos, J. Robke, F. Heckmeier, M. Cerny, K. Jones, V. Iungo, and C. L. Bottasso, "Wake characterization of a multipurpose scaled wind turbine model," *AIAA Scitech 2019 Forum*, 2019. doi: 10.2514/6.2019-2082

[105] E. Nanos, K. Yilmazlar, A. Zanotti, A. Croce, and C. Bottasso, "Wind tunnel testing of a wind turbine in complex terrain," *Journal of Physics: Conference Series*, vol. 1618, 2020. doi: 10.1088/1742-6596/1618/3/032041

[106] E. M. Nanos, C. L. Bottasso, D. I. Manolas, and V. A. Riziotis, "Vertical wake deflection for floating wind turbines by differential ballast control," *Wind Energ. Sci. Discuss.*, 2021. doi: 10.5194/wes-2021-79

[107] C. L. Bottasso and F. Campagnolo, "Wind tunnel testing of wind turbines and farms," in *Handbook of Wind Energy Aerodynamics*, B. Stoevesandt, G. Schepers, P. Fuglsang, and Y. Sun, Eds. Springer Nature, to appear, 2020. ISBN 978-3-030-31308-1

[108] M. Raffel, C. Willert, F. Scarano, C. Kähler, S. Wereley, and J. Kompenhans, *Particle Image Velocimetry*. Springer, 2011. ISBN 978-3-319-68851-0. [Online]. Available: http://www.springer.com/gb/BLDSS

[109] Bachmann Company Web Site. [Online]. Available: http://www.bachmann.info

[110] E. A. Bossanyi, "The design of closed loop controllers for wind turbines," *Wind Energy*, vol. 3, pp. 149–163, 2000.

[111] S. Guntur, J. J. M., J. B., W. Q., Sprague, M. A., R. Sievers, and S. J. Schrek, "Fast v8 verification and validation for a mw-scale wind turbine with aeroelastically tailored blades," *Wind Energy Symp.*, 2016.

[112] N. Troldborg, J. N. Sørensen, and R. Mikkelsen, "Actuator line simulation of wake of wind turbine operating in turbulent inflow," *J. Phys.: Conf. Ser.*, vol. 75, 2007. doi: 10.1088/1742-6596/75/1/012063

[113] M. J. Churchfield, S. Schreck, L. A. Martínez-Tossas, C. Meneveau, and P. R. Spalart, "An advanced actuator line method for wind energy applications and beyond," 2017. doi: 10.2514/6.2012-537

[114] M. J. Churchfield and S. Lee, "Nwtc design codes-sowfa," *Tech. rep., National Renewable Energy Laboratory (NREL), Golden, CO*, 2012.

[115] M.-C. Lai and C. S. Peskin, "An immersed boundary method with formal second-order accuracy and reduced numerical viscosity," *J. Comput. Phys.*, vol. 160, p. 705–719, 2011.

[116] H. Jasak and D. Rigler, "Finite volume immersed boundary method for turbulent flow simulations," *OpenFOAM Workshop, 9th International OpenFOAM Workshop, Zagreb, Croatia*, 2014.

[117] M. Drela, "Xfoil: An analysis and design system for low reynolds number airfoils," in *Low Reynolds Number Aerodynamics*, T. Mueller, Ed. Springer, Berlin, Heidelberg, 1989.

[118] C. L. Bottasso, S. Cacciola, and I. X, "Calibration of wind turbine lifting line models from rotor loads," *J. Wind Eng. Ind. Aerodyn.*, vol. 124, no. 1, pp. 29–45, 2014. doi: 10.1016/j.jweia.2013.11.003

[119] J. Smagorinsky, "General circulation experiments with the primitive equations," *Monthly Weather Review*, vol. 91, no. 3, p. 99–164, 1963. doi: 1:10.1175/1520-0493(1963)09

[120] F. Porté-Agel, Y. T. Wu, H. Lu, and R. J. Conzemius, "Large-eddy simulation of atmospheric boundary layer flow through wind turbines and wind farms," *J. Wind Eng. Ind. Aerod.*, vol. 99, p. 154–168, 2011. doi: 10.2514/6.2012-537

[121] H. Jasak, "OpenFOAM: open source CFD in research and industry," *Int. J. Nav. Arch. Ocean*, vol. 1, pp. 89–94, 2009. doi: 10.2478/IJNAOE-2013-0011

[122] H. Jasak, H. Weller, and A. Gosman, " High resolution NVD differencing scheme for arbitrarily unstructured meshes," *Int. J. Numer. Meth. Fluids*, vol. 31, p. 431–449, 1999. doi: 10.1002/(SICI)1097-0363

[123] J. Schreiber, E. M. Nanos, F. Campagnolo, and C. L. Bottasso, "Verification and calibration of a reduced order wind farm model by wind tunnel experiments," *Journal of Physics: Conference Series*, vol. 854, no. 1, p. 012041, 2017. [Online]. Available: http://stacks.iop.org/1742-6596/854/i=1/a=012041

[124] S. E. Commission, " Key performance indicators for the european wind industrial initiative," 2011. [Online]. Available: https://setis.ec.europa.eu/implementation/eii/eii-key-performance-indicators/KPIs_Wind/view

[125] B. S. Institute, " BS EN 15341:2007 Maintenance - Maintenance Key Performance Indicators," 2007.

[126] R. Scott, J. Bossuyt, and R. Cal, "Characterizing tilt effects on wind plants," *Journal of Renewable and Sustainable Energy*, vol. 12, pp. 2135—-2143, 2020. doi: 10.1063/5.0009853

Available online at www.sciencedirect.com

ScienceDirect

Energy Procedia 137 (2017) 559–570

Energy Procedia

www.elsevier.com/locate/procedia

14th Deep Sea Offshore Wind R&D Conference, EERA DeepWind'2017, 18-20 January 2017, Trondheim, Norway

# Key Performance Indicators for Wind Farm Operation and Maintenance

Elena Gonzalez[a,f], Emmanouil M. Nanos[b,f], Helene Seyr[c,f,*], Laura Valldecabres[d,f], Nurseda Y. Yürüşen[a,f], Ursula Smolka[e], Michael Muskulus[c], Julio J. Melero[a]

[a] *CIRCE-Universidad de Zaragoza, C/Mariano Esquillor Gómez 15, 50018 Zaragoza, Spain*
[b] *Wind Energy Institute, Technische Universität München, 85748 Garching bei München, Germany*
[c] *Department of Civil and Environmental Engineering, Norwegian University of Science and Technology, NTNU, 7491 Trondheim, Norway*
[d] *ForWind - University of Oldenburg, Institute of Physics, Ammerländer Heerstraße 136, 26129 Oldenburg, Germany*
[e] *Ramboll Wind, Stadtdeich 7, 20097 Hamburg, Germany*
[f] *Shared first authorship, these authors contributed to the work equally.*

**Abstract**

Key performance indicators (KPI) are tools for measuring the progress of a business towards its goals. Although wind energy is now a mature technology, there is a lack of well-defined best practices to asses the performance of a wind farm (WF) during the operation and maintenance (O&M) phase; processes and tools of asset management, such as KPIs, are not yet well-established. This paper presents a review of the major existing indicators used in the O&M of wind farms (WFs), as such information is not available in the literature so far. The different stakeholders involved in the O&M phase are identified and analysed together with their interests, grouped into five categories. A suggestion is made for the properties that KPIs should exhibit. For each category, major indicators that are currently in use are reviewed, discussed and verified against the properties defined. Finally, we propose a list of suitable KPIs that will allow stakeholders to have a better knowledge of an operating asset and make informed decisions. It is concluded that more detailed studies of specific KPIs and the issues of their implementation are probably needed.


Peer-review under responsibility of SINTEF Energi AS.

*Keywords:* Wind Energy, Performance, Operation and Maintenance, Key Performance Indicator, Review

## 1. Introduction

Wind energy has become a mature and cost-competitive source of electricity in Europe [1]. Although new offshore wind projects still show remarkable growth rates [2], changes in regulations amplify the interest in optimising the performance of existing installations. Consequently, in the last years much effort is put into improving operation and maintenance (O&M).

* Corresponding author. Tel.: +47-40086761
*E-mail address:* helene.seyr@ntnu.no

1876-6102 
Peer-review under responsibility of SINTEF Energi AS.
10.1016/j.egypro.2017.10.385

A key perfomance indicator (KPI) is "a metric, measuring how well an organisation or an individual performs an operational, tactical or strategic activity that is critical for the current and future success of the organisation" [3]. Using key performance indicators (KPIs) allows stakeholders to measure the progress towards a stated goal. Many industries use KPIs, like the nuclear industry [4], the financial sector [5] and health care [6]. During the O&M phase of a wind farm (WF), KPIs can influence the decision-making process by providing the stakeholders with valuable information assessing the status of the operational asset. Indeed they reflect changes in the O&M strategy.
Although many indicators have been defined, there is still no consensus within the wind industry and no agreement on the calculation or even the definition of KPIs during the O&M phase of a WF yet. The literature on this topic is limited; A study from 2011 only investigated four KPIs for the wind industry initiative [7]. The existing European standards for maintenance [8,9] provide a guideline for terminology and 71 maintenance indicators. We present a complimentary study, focused on the wind industry, by filtering the existing ones. Additionally, this review covers operational and financial indicators.
The Advanced Wind Energy System Operation and Maintenance Expertise (AWESOME) project organized a joint industry workshop (JIW), gathering both industrial and academic partners. The present authors addressed the need for KPIs for the O&M phase of a WF that was stated by the partners during the JIW. This paper presents a condensed and updated version of the results of the report [10] and intends to shed light on the definition of KPI properties, classification of KPIs and assessment of their value to wind farm O&M activities.
This paper is organized as follows. Section 2 describes the methodology of the workshop and of the paper. In Section 3, the different stakeholders are identified and analysed together with their interests resulting in five different categories; major indicators are reviewed and discussed. A proposed list of KPIs is given in Section 4; their properties and suitability are discussed. The study is concluded in Section 5 with further research suggestions.

## 2. Methodology

Based on the goal of defining KPIs for the O&M phase of a WF we conducted the analysis of the KPIs in five main steps. We used the well-established brainstorming technique [11] that is also applied in other fields [12], since it was suitable for the format of the JIW. First, we addressed the definition of the term KPI. In the context of the O&M phase of a WF, KPIs have to support informed decisions and reduce uncertainty by managing risks. Defining KPIs helps the stakeholders to address different concepts of the WF project by using the same metrics, leading to a common understanding of the important aspects and the success of a WF project. KPIs should answer the question: Which information should be monitored by the different stakeholders during the O&M phase of a WF?
Having defined the purpose of the KPIs, we identified the different stakeholders involved in the O&M phase of a wind power project. Once the stakeholders were identified, we discussed, collected and assembled their needs. Some of them are overlapping, so the main requirements were grouped into five categories. This has been addressed in Section 3.1. Next, we investigated the main properties that KPIs should fulfil, leading to a set of recommended properties that is presented in Section 3.2. For each defined category we conducted a review of the state-of-art, followed by a discussion, in Section 3.3. Our study initiated from the BS EN 15341:2007 [8] standards which offer maintenance related KPIs. These standards deal with all industrial and supporting facilities, introducing 71 KPIs, while they focus only on the maintenance. Finally, we present a comprehensive set of KPIs for the O&M industry that fulfil all the properties we previously defined.

## 3. Results

### *3.1. Stakeholders and their requirements*

Various stakeholders are involved in the O&M phase of a wind power project. Their strategic decisions rely on the information they have about the current status of the operating asset, referring to different aspects, i.e. regulatory, economical, technical and safety aspects. The different stakeholders are identified and presented here, together with their main needs for information.
***Wind Farm Operator***
The WF operators' main interest is to maximise the revenue of the WF and hence the energy production throughout

the lifetime of the project. The operator needs information about the energy production, the efficiency of the WF, the production losses and might also request information about future expectations of energy production and remaining lifetime, as well as the current value of the asset, profits, costs and debt.

***The Investor***

Investors and banks can partially or completely own the WF. They are mainly interested in the economic and financial aspects of the wind power project development, including information about production, efficiency, future expectations, costs, debt, profits and current value of the asset.

***The Maintenance Service Provider***

Maintenance services are commonly outsourced to a maintenance service provider (MSP), who is often the original equipment manufacturer (OEM). The most important aspect of a standard O&M contract is the wind turbine availability warranty. This warranty states a certain percentage of time that the WFs operation shall not be affected by maintenance actions from the MSP. Otherwise, the MSP shall pay the WF operator compensations. The main interest of the MSP lies in reducing the time and cost of the maintenance operations through a good understanding of the health status together with the failure history and the component cost. From a safety and efficiency perspective of the maintenance tasks, the MSP also seeks information about health, safety and environmental (HSE) issues, like safety indicators and environmental restrictions.

***The Insurance Provider***

Insurance companies provide services to cover the costs of various incidents that might occur during the operational phase of the WF. This can include [13] damage to the WTs and associated equipment due to storms, thefts, malicious actions, or fires, costs of spare parts, loss of revenue, damage to third party property or environmental damage. Consequently, the insurance provider is mainly interested in the health status, failure history and the HSE aspects.

***Utility and Grid Operator***

According to the European grid codes, all the energy produced from wind has to be bought by an electrical companies, i.e a utility. This stakeholder is usually interested in the energy production of the WF, the future expectations of production and the electricity price. In addition to the utility, the integration of energy produced from wind into the grid is a challenge for the Grid Operator [14–16] . This stakeholder is interested in performance, stoppages and energy production, power quality and other quantities that can affect grid stability.

***Government, Public and End Users***

Here we identify and group together stakeholders that are not technically involved in a WF's operation. First, the governments regulate the activities of the wind industry through regulatory bodies. Non-compliance with these laws and regulations can result in penalties and subsequent withdrawal of operating license. The public expects protection of the environment and minimum interference of the plant with adjacent living communities. Finally, the end users expect competitive prices of energy in comparison to other sources. Consequently, public opinion and political decisions may affect the profitability of a wind power project, since their support of wind energy can have an economic impact on the project, e.g. in terms of subsidies. In summary, this group of stakeholders is mainly interested in the efficiency of the WF, the electricity price and the environmental impact of the project.

An obvious conclusion that can be derived from the above listing of the most important stakeholders, is that their needs are frequently overlapping. This characteristic, along with the fact that it will facilitate our study of the most important KPIs, guided us when categorizing the stakeholders' requirements. The five chosen categories, as well as the corresponding requirements, are shown in Table 1.

### *3.2. Definition of the properties*

One of the main requests that the industry representatives expressed during the discussion at the JIW was the need to identify the properties of the indicators. In this regard, safety indicators have already been developed for the Offshore wind industry [17], which have guided us to define the necessary properties.

As the most important property, KPIs need to be **relevant**, i.e. they have to carry information valuable to stakeholders. Since they have to allow the stakeholder to take informed decisions, the indicators have to be such that they can trigger changes. Another property is that KPIs must be **specific**, meaning that the observed value needs to be well defined, so that it is clear what exactly is being observed and how. In order to have an easily observable value, indicators should be **measurable**, either in a qualitative or in a quantitative way. The measurement can be a numerical value,

Table 1. Categorisation of the stakeholder requirements

| **Performance** | **Reliability** | **Maintenance** | **Finances** | **Safety** |
|---|---|---|---|---|
| Efficiency | Failure history | Component cost | Component cost | Environmental issues |
| Future expectations | Fatigue | Failure history | Current asset value | Health & Safety environment |
| Production | Health status | Logistics | Debts & Profits | |
| Production losses | Loads | Maintenance hours | Electricity price | Safety indicators |
| | Remaining lifetime | Maintenance restrictions | Risks and insurance | |
| | | | Subsidies | |
| | | | Unnecessary cost | |

like hours of operation, or a categorical statement, like "WF is running ok". Stakeholders should be able to use KPIs to compare different assets without much effort; therefore, **comparability** is another necessary property for the KPIs. In this way, WFs with different layout, size and location can be compared to each other, by only looking at the KPIs. To track the wind power project development over time, it is necessary for the KPIs to be **traceable on different timescales**. For some indicators it might be sensible to provide hourly data, whereas for others a yearly summary is more beneficial to the stakeholder. To leave no room for individual interpretations, a standard should be implemented, giving exact definition of all terms and indicators used. With the **standard**, different stakeholders can use the same indicators without worrying about the scope of interpretation. Standardised KPIs enable the comparison of different assets through benchmarking, comparing the performance of a WF to the best performances recorded in the industry [18]. Defining properties for the individual indicators is not enough, since there will be a set of them. This set needs to be able to give a complete picture of the whole WF, both in onshore and offshore cases, with the fewest possible KPIs. Therefore, we are looking for a **minimal set** of KPIs, which are clear and easy to understand. The indicators do not necessarily need to be disjoint, so two or more of them are allowed to present overlapping observations. Sets of KPIs that are disjoint however, should be preferred over non-disjoint sets. For disjoint KPIs, changes in one KPI cannot imply changes in any other KPIs. This means that changes in the observed WF only influence one specific KPI, which makes interpretation of the KPIs easier for the stakeholders. To sum up, effective KPIs need to be **relevant, specific, measurable, comparable, traceable in time, standardised and form a minimal complete set**.

### *3.3. Review of the existing KPIs and their properties*

For each category defined in 3.1, we performed an extensive review of the indicators used in the industry and the ones covered in the literature. The identified metrics are reported here and then assessed with respect to the necessary properties defined in 3.2.

#### *3.3.1. Performance*

One of the most important operator's interests is the performance of the asset. The word performance is very broad and can embrace many aspects of the WF operation, from annual energy production (AEP) to generated revenue. We would like to read here WF performance as its efficiency. Indicators should then answer the following question: *is the WF producing as much energy as it could?* The most commonly used indicators are presented subsequently.

***Wind / Energy Index*** [19–22]

First developed in Denmark in 1979, the concept was later copied by other northern countries. It is based on the production of a number of reference WTs over a wide geographic area. It establishes a statistically "normal" period of yearly wind energy content, expressed as 100%, so that the operator can distinguish between WT under-performance and wind strengths below expected levels; it allows for comparison of the production of a WF with the available wind resource. Although it fulfils many of the properties stated in 3.2, it does not provide the operator with sufficient information so that informed decisions can be solely based on the index.

***Capacity Factor*** [23,24]

Defined as the energy generated during a period of time divided by the WF rated power multiplied by the number of

hours in the same period. Since the denominator is a constant, it does not represent the theoretical energy production according to real on-site wind conditions. Although it is a valuable indicator during feasibility and wind project development stages, we believe it is not an effective indicator for evaluating WF operational efficiency.

***$P_{50}$ deviation*** [25]

During the process of wind resource assessment, the $P_{50}$ energy yield gives the level of AEP that is expected to be exceeded with a probability of 50%. Many operators currently look at the deviation of the actual AEP from the calculated $P_{50}$, especially when looking into deviations of planned budget. From our experience, the $P_{50}$ is subject to important uncertainty. Furthermore, there is no standard procedure to obtain this figure.

***Time-based availability*** [26]

Defined as the accumulated time that the WT is operational divided by the total period of time. This indicator is specific, since the observed value is clearly defined and is the time that a WT is operational; measurable and easy to understand, it is relatively easy to distinguish periods of power production from periods of inactivity; strategies to reduce the downtime result in an increase of this metric. Despite existing technical specifications for its calculation, no international standard exists. Furthermore, it does not provide information about WF efficiency or power losses due to unavailability. The existing standard [8] defines four technical indicators, namely T1 T6, T7 and T15 which relate the total operating time with downtimes due to maintenance activities. TBA comprises the information included in these three technical indicators but it does not consider that the operating time of the wind turbine is influenced by the wind conditions.

***Energy-based availability*** [27,28]

Defined as the ratio between the real energy production and the actual energy available. In our opinion, it illustrates the ”real” efficiency of a WT or WF since it reveals the percentage captured from the available energy. It is a more objective indicator for comparison between different assets, but difficult to implement. Although it is very easy to measure the produced energy over a certain period of time, it is quite difficult to precisely define the actual available energy for the same period. Therefore it is very challenging to define a standard procedure. Current approaches rely on theoretical production calculation from an operational power curve based on SCADA data.

### *3.3.2. Reliability*

Reliability is defined as the “ability of an item to perform a required function under given conditions for a given time interval” [9]. Applied to a WT, its reliability can be defined as its ability to perform properly, without failures, during specified site wind conditions for the whole lifetime (defined to be at least 20 years) or in a specific time window. WT reliability is compromised by component failures, leading to downtime. For that reason, the industry currently uses different metrics to assess WT reliability [29] by answering questions like: *How often does a WT fail?* and *Which WT downtimes are associated with which failure?* [9]. The indicators are summarised below.

***Mean Time between Failures (MTBF) & Failure rate*** [9,30]

The MTBF expresses the total operational hours divided by the number of failures for a specific component or for the whole WT. The term MTBF is frequently used to describe reliability, as well as its reciprocal value, the failure rate. Both indicators satisfy the majority of the identified properties for KPIs. However, an effective comparison between WTs or WFs will not be possible until a standard WT taxonomy is defined. Even though some recent approaches have been published, like RDS-PP [31] and ReliaWind [32], there is still no agreement on a unique and standard designation. This issue has been discussed in detail by Reder et al. [33]. MTBF is defined in the standard [8] as the technical indicator T17.

***Mean Time to Repair (MTTR) & Repair rate*** [9,30]

The MTTR is the average time to return a WT to its functional state [9]. This can imply either a repair or a full replacement of the faulty component, leading to the term of restoration, as defined in [8]. This indicator can be assessed by dividing the total time of restoration by the number of failures. Given the definition in the maintenance standards [9] this term should rather be referred to as mean time to restoration. Nevertheless, we stick here to the designation as mean time to repair due its widespread used in the industry. The reciprocal of the MTTR is the repair rate. As well as the previous indicators, they meet all the desired properties and their definition is specific and standardized within the industry. But again, comparison is limited due to the lack of a standard WT taxonomy and the inconsistency of intervention specific failure definitions. MTTR is defined in the standard [8] as the technical indicator T21.

***Mean Time to Failure (MTTF)*** [30]

The MTTF is similar to MTBF but it is used to describe reliability of non-repairable systems. Non-repairable refers

to systems that are replaced after a failure because there is no possible maintenance action that can make them work properly. Hence, over the lifetime of a non-repairable system, this fails once and the MTTF measures the average time until this unique failure occurs.

***Availability*** [34]

The time-based availability (3.3.1) is the amount of time that a system or component is available for use divided by the total amount of time in the period of operation. From the previous metrics, it can be defined as the ratio between the MTTF and the sum of MTTF and MTTR. In our opinion, availability is most closely related to energy production. Thus, the previous metrics seem to be more adequate to assess WT reliability.

The identified indicators satisfy most of the necessary properties for KPIs. Nonetheless, we believe that it is difficult to make them comparable due to the lack of a standard WT taxonomy and due to potentially different component behaviour in different WTs, especially with regard to differences in turbine size and technology [33]. Moreover, data collection on wind turbine failures is not standardised and there is an important lack of failure data, contributing to a high level of uncertainty related to the indicators. We would also like to mention the importance of initiatives for standardisation of data and reliability analyses like [35] and [36].

### *3.3.3. Maintenance*

Maintenance activities are crucial to keep a system in good condition. In general, these activities can be divided into corrective and preventive actions, including both time-based and opportunity-based maintenance. While preventive maintenance intends to avoid failure, corrective actions are implemented once a component has already failed. Maintenance indicators assess the quality of the maintenance, in terms of time consumed for different interventions and related costs. The reported indicators are presented in the following.

***Response time*** [37–41]

Defined as the time between failure occurrence and maintenance intervention, it informs about the efficiency in maintenance planning. Since it is often difficult to detect the failure starting time, it can be redefined as the time between failure detection and intervention. This new indicator is then specific and measurable. However, since the sensors and alarm systems vary between different WT types [42], this indicator is not comparable.

***Number of interventions*** [37–41]

An intervention is the fieldwork conducted to keep a WT in good condition; it implies a displacement of the maintenance crew. Monitoring the number of interventions, both scheduled and unplanned, can show the results after an optimisation of the O&M strategies. In case of higher WT reliability, less interventions should be needed; this would result in lower O&M costs, especially in offshore cases where the number of interventions is related to the necessary vessel transfers. Nevertheless, there is no agreement on the definition of intervention; during a maintenance work one intervention could be accounted for the entire WF or per WT intervened. Even though this indicator could easily fulfil most of the necessary properties with a consensual definition, the comparability between assets remains difficult. This is not only due to possible differences in terms of size of the WFs, but also to the duration of the interventions, and their related costs. Comparability could be improved by normalising the number of interventions by the number of turbines in a WF, but their duration should be definitely included. Further research would be needed on this issue.

***Corrective maintenance (%)*** [37–41]

Defined as the ratio of the purely corrective interventions over the total number of interventions, this indicator meets all the properties and defining a standard is possible. Since corrective interventions are generally more costly than preventive actions, it also allows the assessment of the success of new O&M strategies. Indeed, some operators are experiencing a decrease of this percentage after the introduction of condition-based strategies. The existing standard [8] includes two organizational indicators (O16, O18) which describe the corrective maintenance activities and the immediate corrective maintenance activities, respectively. Our indicator does not distinguish between immediate and non-immediate activities. These two indicators are expressed in man hours instead of number of interventions.

***Schedule compliance (%)*** [37–41]

It is defined as the ratio between the scheduled maintenance tasks completed on time and the total number of tasks. This indicator fulfils most of the properties and a standard can be easily defined. Furthermore, it can be used to assess the efficiency of maintenance execution or accuracy in maintenance planning. The organizational indicator O22 in [8] also describes this.

***Overtime jobs (%)*** [37–41]

Defined as the ratio between the overtime working hours and the planned working hours (working hours per worker and per size of the workforce), this metric can be measured on different time-scales. It is comparable and a standard can be defined. It informs about effectiveness of maintenance planning, worker health or ideal work force size. The organizational indicator O21 in [8] describes this in terms of internal man hours. We do not distinguish between internal and external man hours.

***Total Downtime*** [37–41]

Since downtime is affecting the WT availability, we presented this in the Sections 3.3.1 and 3.3.2.

***Equipment reliability*** [37–41]

We also do not show the equipment reliability here, since it was already presented in section 3.3.2.

***Backlog*** [37–41]

It can be defined as the list of maintenance work that still needs to be completed. Hence, its size might sound like a very intuitive way to measure the effectiveness of maintenance execution. However, there is no specific definition for this effectiveness and it cannot therefore be measured. Indeed, it is possible to sum the time for the expected scheduled interventions but it might not correspond to the exact time that will be finally needed. Furthermore, a big backlog can be due to very different reasons, among them poor planning, poor execution or too small workforce.

***Labour costs versus total maintenance costs (TMC) (%)*** [37–41]

The labour costs, expressed as a percentage of the total maintenance costs (TMC), inform about the effectiveness of maintenance execution; most operators agree on the importance of having qualified maintenance staff to ensure an ideal percentage of labour costs. It fulfils most of the properties defined and can be easily standardized. The standard [8] defines two economic indicators (E8 and E9) describing the total internal and external personnel cost, respectively. Again, we do not make a distinction between internal and external personnel cost.

***Cost of spare parts versus total maintenance costs (TMC) (%)*** [37–41]

The cost of spare parts, expressed as a percentage of the TMC, is directly related to the number of failures followed by replacements. Moreover, historical values might help in the budget planning. This indicator provides information about the proportion of cost of spare part cost of the TMC. Other factors to the TMS include equipment hire, consumables and labour costs. Moreover the indicator fulfils many of the desired properties for KPIs. However, its specificity and standardisation depends on the costs included in the definition.

***Total annual maintenance cost versus annual maintenance budget (%)*** [37–41]

Setting the TMC in relation to the annual maintenance budget (AMB) can give insight into the quality of maintenance planning and is therefore relevant to stakeholders. Defining the indicator as three categories ($TMC<AMB \equiv green$, $TMC \approx AMB \equiv yellow$, $TMC>AMB \equiv red$) is specific and measurable. It can further be compared between WFs, is traceable in time and can be defined in a standard. The stakeholders can use this indicator to know, whether they are spending as much as anticipated or more on the maintenance of their asset. Using three different colours is intuitive and very demonstrative.

The standard [8] includes many more indicators concerned with the cost of maintenance and materials, e.g. T16, E11. However, the indicators presented here are a comprehensive overview of the most important aspects of the maintenance phase of a WF.

### *3.3.4. Finance*

The financial status of the wind power project is a general concern throughout its entire lifetime. Financial KPIs are fundamental tools for making an asset status summary or for comparing different investment options. Consequently, they can be used as a feedback mechanism for management decisions evaluation. Some might be more useful during the feasibility phase, as they can influence the decision of undertaking the project [43,44]. As the investment is already made in the O&M phase, the main interest is to know about the financial status of the operating asset; any decision-making process seeks to maximise the return on the investment. The most widely used indicators are summarised in the following.

***Operational Expenditures (OPEX)*** [43]

The OPEX include the cost of operating the site, planned O&M and unscheduled maintenance. These costs can be grouped into two different categories: the O&M costs, which represent approximately 60% of the OPEX and tend to increase as the WF reaches the end of its lifetime [45]; the other category covers other operating costs like rent, taxes and insurance. In order to be comparable, this metric should be normalised by WF installed capacity.

***Earnings Before Interest, Taxes, Depreciation, and Amortisation (EBITDA) margin*** [46,47]
The EBITDA margin is a financial metric used to assess profitability by comparing revenues with earnings. It is defined as the percentage of the revenue remaining after covering the OPEX. This indicator meets all the desired properties and is used to track changes due to new O&M strategies. Its drawback is the omission of the capital expenditures (CAPEX). Even if a negative margin undoubtedly indicates profitability problems, a positive margin does not necessarily indicate that the WF generates cash. Indeed, this metric cannot track changes in working capital, CAPEX, taxes, and interest rate. In our opinion, CAPEX should be included when evaluating the profitability of a WT or WF project. Hence, the EBITDA margin could be considered as a good KPI allowing the comparison between different WFs profitability, but it should be presented in conjunction with another KPI which includes the CAPEX.
***Loan Life Coverage Ratio (LLCR)*** [46,48]
Defined as the ratio between Net Present Value (NPV) of the cash and the amount of debt, it informs about loan repayments. Financial modelling of LLCR is now a standard metric calculated in a project finance model and has been standardised. Apart from other properties that this metric clearly fulfils, it has a special relevance since it provides the WF Operator with information about the ability to repay the debt over the whole lifetime of the asset.
***Debt-Service Coverage Ratio (DSCR)*** [46,49]
The DSCR is the ratio between the available cash for debt payment and the sum of interest, principal and lease. It is an accepted financial KPI in industry for the measurement of an entity's ability to balance debt payments with produced cash. The main difference with the LLCR is that it measures the ability to pay the debt in a specific year. Similar to the LLCR it meets all the desired properties for KPIs.
***Free Cash Flow to Equity (FCFE)*** [46,50]
The FCFE is a measure of how much cash can be paid to the equity shareholders of a company after all expenses, reinvestment and debt repayment. FCFE takes into account the net income, the depreciation of amortisation, the change in working capital and the net borrowing. A standard definition can be found in [46,50]. Although it provides the investor with relevant financial information, this indicator cannot be used for benchmarking since it is not comparable between assets.
***Levelised Cost of Energy (LCOE)*** [7,51]
The LCOE is probably the most popular financial KPI in the wind industry and particularly useful for investors seeking to compare different generation sources. It allows to compare different WFs in terms of financial status. The LCOE takes into account the CAPEX, the installed capacity, the capital recovery factor, the discount rate, the WF lifetime, the OPEX and the annualised energy production. A complete definition can be found in [7,51]. A standard methodology was proposed, discussed and approved in [7]. This KPI is now a standard and specific indicator and includes both CAPEX and OPEX. However, the suggested methodology was criticized, since the normalisation for benchmarking is done in terms of installed capacity (MW); indeed, the LCOE could be better described in terms of $€/m^2$ of rotor swept area since it would be directly related to the WT energy production. Unfortunately this would require a much more complex model and further data uncertainties. In any case, this KPI remains as a very effective indicator to evaluate the financial performance of an operating asset. As an example, many recent studies are mostly focused on improving the LCOE [51].
***Other indicators***
Some other more complex indicators might be found as the wind speed dependent cash flow, semi-elasticity (function of averaged weighted payment duration and interest rate) and relative convexity (ratio between convexity of cash flow and semi-elasticity) [52]. The break-even price of energy (BEPE) for renewable energy projects, defined in [53], tries to overcome the omission of the legal framework in the LCOE by taking into account parameters such as inflation and tax rate. Given that the renewable energy sector is highly influenced by local conditioning factors, the suggested metric seems to be an interesting alternative to the LCOE.

### *3.3.5. Safety*

In the RAMS literature [54], KPIs for the system performance are often distinguished from indicators monitoring the safety of a system (safety indicators). KPIs are more focused on system performance and output in terms of financial gain. Safety indicators on the other hand help to monitor the safety of both the system and the workers. We want to refer to an analysis by Scottish Power [55] concerned with major hazard risks, as an example for system safety indicators. For the worker health and safety, we want to refer to a publication on safety indicators for offshore WFs

[17]. Safety indicators enable the operator to track changes in the worker health and safety for different maintenance strategies, legal regulations and specific procedures.

## 4. Discussion

The review of the indicators showed some of the shortcomings of the potential KPIs in terms of fulfilling all properties. For the KPIs describing **performance**, the energy-based availability allows to have a better tracking of variations in the WF energy efficiency. However, theoretical production cannot be measured accurately and neither indicator is standardized. Although time-based availability does not inform about power losses, it can be helpful for illustrating downtime reduction. All of the indicators concerned with **reliability** fulfil all properties except for being standardised, due to the lack of a common WT taxonomy. Since there is a common understanding in RAMS literature, defining a standard seems feasible and much effort is currently devoted to nomenclature standardisation. In any case, the suggested KPIs allow to track the progress towards increased WT reliability. Also the KPIs for the **maintenance** category lack the definition of a standard. This should be a common goal of the wind energy industry and academia for the future. All discussed **financial** KPIs fulfil the necessary properties and can be used as they are, allowing to reveal variations in the financial status of the asset. An overview over the proposed indicators and their properties can be found in Table 2.

Table 2. Proposed list of indicators and their properties, as listed in section 3.2. The property of a minimal set of indicators is not included in the table. A checkmark indicates that the indicator fulfils the properties, a crossmark that the indicator does not fulfil a property and the asterisk indicates indicators that are not yet fulfilling the property in question but can be modified to do so.

| | Relevant | Specific | Measurable | Comparable | Traceable in time | Standard |
|---|---|---|---|---|---|---|
| **Performance** | | | | | | |
| Time-based availability (%) | ✓ | ✓ | ✓ | ✓ | ✓ | ✗ |
| Energy-based availability (%) | ✓ | ✓ | - | ✓ | ✓ | ✗ |
| **Reliability** | | | | | | |
| MTBF & Failure rate (%) | ✓ | ✓ | ✓ | ✓ | ✓ | ✓* |
| MTTR & Repair rate (%) | ✓ | ✓ | ✓ | ✓ | ✓ | ✓* |
| MTTF | ✓ | ✓ | ✓ | ✓ | ✓ | ✓* |
| **Maintenance** | | | | | | |
| Interventions per WT | ✓ | ✓ | ✓ | ✓* | ✓ | ✓* |
| Corrective maintenance (%) | ✓ | ✓ | ✓ | ✓ | ✓ | ✓* |
| Schedule compliance (%) | ✓ | ✓ | ✓ | ✓ | ✓ | ✓* |
| Overtime jobs (%) | ✓ | ✓ | ✓ | ✓ | ✓ | ✓* |
| Labour costs vs. TMC (%) | ✓ | ✓ | ✓ | ✓ | ✓ | ✓* |
| TMC vs. AMB (%) | ✓ | ✓ | ✓ | ✓ | ✓ | ✓* |
| **Finance** | | | | | | |
| OPEX | ✓ | ✓ | ✓ | ✓ | ✓ | ✓ |
| EBIDTA margin | ✓ | ✓ | ✓ | ✓ | ✓ | ✓ |
| LLCR | ✓ | ✓ | ✓ | ✓ | ✓ | ✓ |
| DSCR (historical & expected) | ✓ | ✓ | ✓ | ✓ | ✓ | ✓ |
| LCOE | ✓ | ✓ | ✓ | ✓ | ✓ | ✓ |

## 5. Conclusions and further work

In this paper the topic of key performance indicators for the wind industry has been discussed. After defining properties and a thorough review of existing indicators, we propose a list of possible key performance indicators that fulfil these properties or can be modified to do so. The work was based on discussions with representatives from industry. However further numerical validation with real WF data is highly recommended to make a quantitative evaluation among different KPIs both for onshore and offshore cases.

## Acknowledgements

This paper was written as a result of the 1st Joint Industry Workshop (JIW) in the AWESOME project, organised by Ramboll Germany. The AWESOME project has received funding from the European Union's Horizon 2020 research and innovation programme under the Marie Skłodowska-Curie grant agreement No 642108.
The authors would like to thank the industry representatives who participated in the JIW as well as other O&M experts consulted subsequently. The following companies/associations actively participated in the workshop: Airwerk GmbH, CUBE Engineering GmbH, EWE Offshore Service & Solution GmbH, Fraunhofer IWES, IK4-Ikerlan, Siemens AG, Simis AS, Wölfel Engineering GmbH.

## References

[1] EWEA, Wind in power 2015 European Statistics , Tech. rep., Brussels, 2016.
URL https://windeurope.org/wp-content/uploads/files/about-wind/statistics/EWEA-Annual-Statistics-2015.pdf
[2] Global Wind Energy Council, Offshore wind power , online, (2015) Accessed 05/01/2017.
URL http://www.gwec.net/global-figures/global-offshore/
[3] H. Kerzner, *Project management metrics, KPIs, and dashboards*, John Wiley & Sons, Inc., Hoboken, New Jersey, 2011.
[4] SETIS European Commission, Key performance indicators for the European sustainable nuclear industrial initiative , online, accessed 11/01/2017 (2012).
URL https://setis.ec.europa.eu/system/files/Key_Performance_Indicators_Nuclear.pdf
[5] PricewaterhouseCoopers, Guide to key performance indicators, online, (2007) Accessed 11/01/2017.
URL https://www.pwc.com/gx/en/audit-services/corporate-reporting/assets/pdfs/uk_kpi_guide.pdf
[6] S. Rozner, Developing key performance indicators a tool kit for health sector managers , Tech. rep., Bethesda, MD: Health Finance & Governance Project, Abt Associates Inc., (2013) Accessed 11/01/2017.
URL https://www.hfgproject.org/developing-key-performance-indicators-toolkit-health-sector-managers/
[7] SETIS European Commission, Key performance indicators for the european wind industrial initiative , online, accessed 21/12/2016 (2011).
URL https://setis.ec.europa.eu/system/files/Key_Performance_Indicators_Wind.pdf
[8] "BS EN 15341:2007 Maintenance Maintenance Key Performance Indicators", BRITISH STANDARDS INSTITUTE, London (2007).
[9] "BS EN 13306:2010 Maintenance - Maintenance Terminology", BRITISH STANDARDS INSTITUTE, London (2010).
[10] E. Gonzalez, E. M. Nanos, H. Seyr, L. Valldecabres, N. Y. Yurusen, Key performance indicators for wind farm operation and maintenance, Tech. rep., aWESOME 1st Joint Industry Workshop Report, J.J. Melero, M. Muskulus, U. Smolka (Eds.), Zaragoza, Spain, 2016.
URL http://awesome-h2020.eu/1st-joint-industry-workshop-scientific-report/
[11] A. F. Osborn, *Applied imagination. principles and procedures of creative problem-solving*, Charles Scribeners Sons, New York, 1953.
[12] Y. Luo, M. van den Brand, Metrics design for safety assessment, *Information and Software Technology* 73 (2016) 151–163.
[13] Northern Alliance LTD, Wind turbine insurance – Wind farm insurance, online, (2016) Accessed 21/12/2016.
URL http://www.northernalliance.co.uk/wind-turbine-insurance/
[14] "IEC 61400-21: Wind turbine generator systems - Part 21: Measurement and assessment of power quality characteristics of grid connected wind turbines", International Electrotechnical Comission, Geneva (2001).
[15] S. W. Mohod, M. V. Aware, *Power quality and grid code issues in wind energy conversion system*, INTECH, Open Access Publisher, (2013) Accessed 21/12/2016.
URL http://www.intechopen.com/books/howtoreference/an-update-on-power-quality/power-quality-and-grid-code-issues-in-wind-energy-conversion-system
[16] W. L. Kling, L. Söder, I. Erlich, et al., Wind power grid integration: the european experience, in: *17th Power Systems Computation Conference (PSCC), Stockholm, Sweden*, 2011.
[17] H. Seyr, M. Muskulus, Safety indicators for the marine operations in the installation and operating phase of an offshore wind farm, *Energy Procedia* 94 (2016) 72–81.
[18] V. Peters, A. Ogilvie, C. Bond, Continuous reliability enhancement for wind (CREW) database: wind plant reliability benchmark, Tech. rep., Sandia National Laboratories, Energy, Climate, & Infrastructure Security. energy. sandia. gov, (2012) Accessed 21/12/2016.
URL http://energy.sandia.gov/wp-content/gallery/uploads/CREW2012Benchmark-Report-SAND12-7328.pdf

[19] D. Rimpl, A. Westerhellweg, Development of a wind index concept for brazil, Tech. rep., DEWI, (2013) Accessed 21/12/2016.
URL https://energypedia.info/images/7/76/Development_of_a_Wind_Index_Concept_for_Brazil.pdf
[20] A. Broe, P. Hoebeke, R. Donnelly, A. Kyriazis, Validated wind power plant modelling for accurate kpi benchmarks, in: *European Wind Energy Conference & Exhibition 2012*, 2012.
[21] Eoltech, IREC Index: the multisource energy index, online, (2015) Accessed 21/12/2016.
URL http://www.eoltech.fr/wind-energy-index/
[22] M. Ritter, Z. Shen, B. López Cabrera, M. Odening, L. Deckert, Designing an index for assessing wind energy potential, *Renewable Energy* 83 (2015) 416–424.
[23] T. Burton, D. Sharpe, N. Jenkins, E. Bossanyi, *Wind energy handbook*, John Wiley & Sons, Chichester, UK., 2001.
[24] H.-J. Wagner, J. Mathur, *Introduction to wind energy systems: basics, technology and operation*, Springer, Berlin, Heidelberg, 2013.
[25] H. Klug, What does exceedance probabilities P-90-P75, P50 mean?, online, *DEWI Magazin*, vol 28, (2006) Accessed 21/12/2016.
URL http://www.dewi.de/dewi/fileadmin/pdf/publications/Magazin_28/07.pdf
[26] "IEC TS 61400-26-1: Wind turbines - Part 26-1: Time-based availability for wind turbine generating systems", International Electrotechnical Comission, Geneva (2011).
[27] "IEC TS 61400-26-2: Wind turbines - Part 26-2: Production-based availability for wind turbines", International Electrotechnical Comission, Geneva (2014).
[28] H. J. Krokoszinski, Efficiency and effectiveness of wind farms-keys to cost optimized operation and maintenance, *Renewable Energy* 28 (14) (2003) 2165–2178.
[29] R. R. Hill, J. A. Stinebaugh, D. Briand, A. Benjamin, J. Linsday, Wind turbine reliability: a database and analysis approach, Tech. rep., Sandia National Laboratories, Albuquerque, New Mexico, (2008) Accessed 21/12/2016.
URL http://windpower.sandia.gov/other/080983.pdf
[30] L. Steffens, *Reliability, Maintenance and Logistic Support: - A Life Cycle Approach, Chapter: Reliability Measures*, Springer US, Boston, MA, 2000, pp. 51–95.
[31] VGB-PowerTech, VGB-Standard RDS-PP Application specification Part 32: Wind energy, Tech. rep., VGB-PowerTech, Essen, Germany (2014).
[32] M. Wilkinson, K. Harman, B. Hendriks, F. Spinato, T. van Delft, Measuring wind turbine reliability-results of the reliawind project, in: EWEA Conference, Brussels, 2011, pp. 1–8.
[33] M. D. Reder, E. Gonzalez, J. J. Melero, Wind turbine failures - tackling current problems in failure data analysis, *Journal of Physics: Conference Series* 753 (2016) 072027.
[34] J. Swift, *Reliability, Maintenance and Logistic Support: - A Life Cycle Approach, Chapter: Availability*, Springer US, Boston, MA, 2000, pp. 377–388.
[35] IEA Wind, Task 33 - Reliability Data: standardization of data collection for wind turbine reliability and maintenance analyses, online, (2014) Accessed 04/01/2017.
URL https://www.ieawind.org/summary{_}page{_}33.html
[36] N. Simpson, SPARTA project system performance, availability and reliability trend analysis, online, All-Energy Exhibition & Conference, Aberdeen, UK, (2014) Accessed 21/12/2016.
URL http://www.all-energy.co.uk/__novadocuments/54083?v=635375640923370000
[37] M. Sondalini, Useful key performance indicators for maintenance , online, (2016) Accessed 21/12/2016.
URL http://www.lifetime-reliability.com/cms/
[38] T. Wireman, *Developing performance indicators for managing maintenance*, Industrial Press Inc., New York, USA, 2005.
[39] A. Weber, R. Thomas, Key performance indicators, online, Ivara, (2005) Accessed 21/12/2016.
URL http://www.plant-maintenance.com/articles/KPIs.pdf
[40] P. Muchiri, L. Pintelon, L. Gelders, H. Martin, Development of maintenance function performance measurement framework and indicators, *International Journal of Production Economics* 131 (1) (2011) 295–302.
[41] P. Wheelhouse, Maintenance key performance indicators , online, (2013) Accessed 21/12/2016.
URL http://www.maintenanceonline.co.uk/article.asp?id=7569
[42] E. Gonzalez, M. Reder, J. J. Melero, SCADA alarms processing for wind turbine component failure detection, *Journal of Physics: Conference Series* 753 (2016) 072019.
[43] Deloitte, Establishing the investment case wind power , online, (2014) Accessed 21/12/2016.
URL https://www2.deloitte.com/content/dam/Deloitte/global/Documents/Energy-and-Resources/gx-er-deloitte-establishing-the-wind-investment-case-2014.pdf
[44] Leonardo ENERGY, Application note - Economic analysis of wind projects , online, (2013) Accessed 21/12/2016.
URL http://www.leonardo-energy.org/resources/230/economic-analysis-of-wind-projects-57f3cbf1f27c4
[45] EWEA, The economics of wind energy, Tech. rep., Brussels, (2009) Accessed 21/12/2016.
URL http://pineenergy.com/files/pdf/Economics_of_Wind_Main_Report_FINAL_lr.pdf
[46] J. D. Stowe, T. R. Robinson, J. E. Pinto, D. W. McLeavy, *Equity asset valuation*, John Wiley & Sons, Hoboken, New Jersey, 2007.
[47] M. Samonas, *Financial forecasting, analysis and modelling: a framework for long-term forecasting*, John Wiley & Sons, Chichester, UK, 2015.
[48] F. Pretorius, B.-F. Chung-Hsu, A. McInnes, P. Lejot, D. Arner, *Project finance for construction and infrastructure: principles and case studies*, Blackwell Publishing, Oxford, UK, 2008.
[49] K. F. Seidman, *Economic development finance*, Sage, California, USA, 2005.
[50] G. Chacko, C. L. Evans, *Valuation: methods and models in applied corporate finance*, Pearson Education, New Jersey, USA, 2014.

[51] P. K. Chaviaropoulos, A. Natarajan, P. H. Jensen, Key performance indicators and target values for multi-megawatt offshore turbines, in: *European Wind Energy Conference & Exhibition 2014*, Barcelona, Spain, 2014.

[52] G. D'Amico, F. Petroni, F. Prattico, Performance indicators of wind energy production, online, (2015) Accessed 21/12/2016.
URL https://arxiv.org/abs/1502.03205

[53] J. Garcia-Barberena, A. Monreal, M. Sánchez, The bepe–break-even price of energy: a financial figure of merit for renewable energy projects, *Renewable Energy* 71 (2014) 584–588.

[54] A. Hopkins, A. Hale, B. Kontic, Process safety indicators / SRAE 2006, *Safety Science* 47, 459–568.

[55] M. Sedgwick, A. Wands, The implementation of effective key performance indicators to manage major hazard risks , online, (2012) Accessed 21/12/2016.
URL http://www.csb.gov/UserFiles/file/Implementing%20Effective%20Key%20Performance%20Indictors%20To%20Manage%20Major%20Hazard%20Risks.pdf

# Wind tunnel testing of a closed-loop wake deflection controller for wind farm power maximization



The Science of Making Torque from Wind (TORQUE 2016) IOP Publishing
Journal of Physics: Conference Series **753** (2016) 032006 doi:10.1088/1742-6596/753/3/032006

# Wind tunnel testing of a closed-loop wake deflection controller for wind farm power maximization

**Filippo Campagnolo[1], Vlaho Petrović[1], Johannes Schreiber[1], Emmanouil M. Nanos[1], Alessandro Croce[2] and Carlo L. Bottasso[1,2]**

[1] Wind Energy Institute, Technische Universität München, Boltzmannstraße 15, D-85748 Garching bei München, Germany
[2] Dipartimento di Scienze e Tecnologie Aerospaziali, Politecnico di Milano, Via La Masa 34, I-20156 Milano, Italy

E-mail: `filippo.campagnolo@tum.de`

**Abstract.** This paper presents results from wind tunnel tests aimed at evaluating a closed-loop wind farm controller for wind farm power maximization by wake deflection. Experiments are conducted in a large boundary layer wind tunnel, using three servo-actuated and sensorized wind turbine scaled models. First, we characterize the impact on steady-state power output of wake deflection, achieved by yawing the upstream wind turbines. Next, we illustrate the capability of the proposed wind farm controller to dynamically driving the upstream wind turbines to the optimal yaw misalignment setting.

## 1. Introduction

Wind energy production is often organized in wind power plants rather than single isolated wind turbines, because of lower construction, maintenance and commissioning costs. However, the design of a wind farm requires taking into account the complex interactions that take place within the wind power plant itself, since the wakes of upwind wind turbines have a strong impact on the power and loading of downstream machines. In recent years, interest has grown in the area of cooperative control of wind turbines, with the goal of maximizing the total wind farm power output, of achieving a given power setpoint while minimizing fatigue loading, or others that require some form of coordination among the wind turbines.

Among the several approaches investigated so far [7], controlling the direction of the wake by yawing the upwind wind turbines seems to be the most promising one [6]. In fact, by redirecting the wake, one may reduce or eliminate altogether the exposure of downwind wind turbines to the wakes shed upstream. In this paper, we present results obtained by testing a closed-loop wind farm control algorithm in a large boundary layer wind tunnel [3] using servo-actuated and sensorized wind turbine models, described in §2. The model-free controller, which optimizes online the yaw misalignment of the upstream wind turbines to increase the total wind farm power output, is discussed in §3, while results are reported in §4.

## 2. Experimental setup

Tests were conducted with a scaled wind farm (see Fig. 1) composed of three identical scaled wind turbine models with a rotor diameter of 1.1 m (in the following named G1s). The undisturbed

The Science of Making Torque from Wind (TORQUE 2016) IOP Publishing
Journal of Physics: Conference Series **753** (2016) 032006 doi:10.1088/1742-6596/753/3/032006

wind speed was measured by means of a Pitot tube, also shown in the figure, placed at hub height and 3 diameters in front of the upstream model.

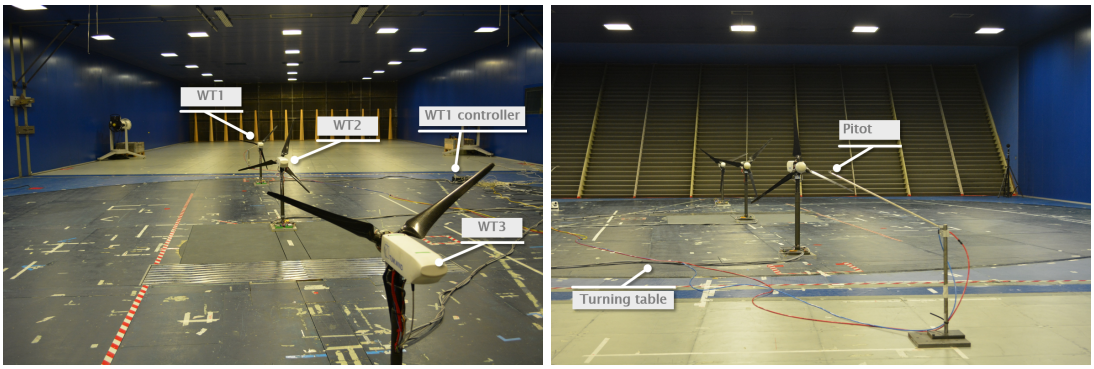


Figure 1: Wind farm layout in the wind tunnel

Each `G1` (see Fig. 2), whose rated rotor speed is 850 rpm, is equipped with three blades, which are composed by a layer of unidirectional carbon fiber covering a machined Rohacell core, mounted on the hub with two bearings in order to enable pitch actuation while limiting free-play. The individual pitch angle of each blade can be varied by means of a small brushed motor equipped with a gearhead and built-in relative encoder, used to measure the blade pitch. The three motors are housed within the blades hollow root, and their position is monitored and adjusted by dedicated electronic control boards housed in the hub spinner.

The shaft is held by two bearings, in turn housed in the rectangular carrying box that constitutes the main frame of the nacelle. The shaft also exhibits four small bridges on which strain gages are glued, to provide measurements of the torsional and bending loads. Three miniaturized electronic boards, fixed to the hub, provide for the power supply and conditioning of the shaft strain gages. The transmission of the electrical signals from the rotating system to the fixed one, and vice versa, is guaranteed by a through-bore 12-channels slip ring.

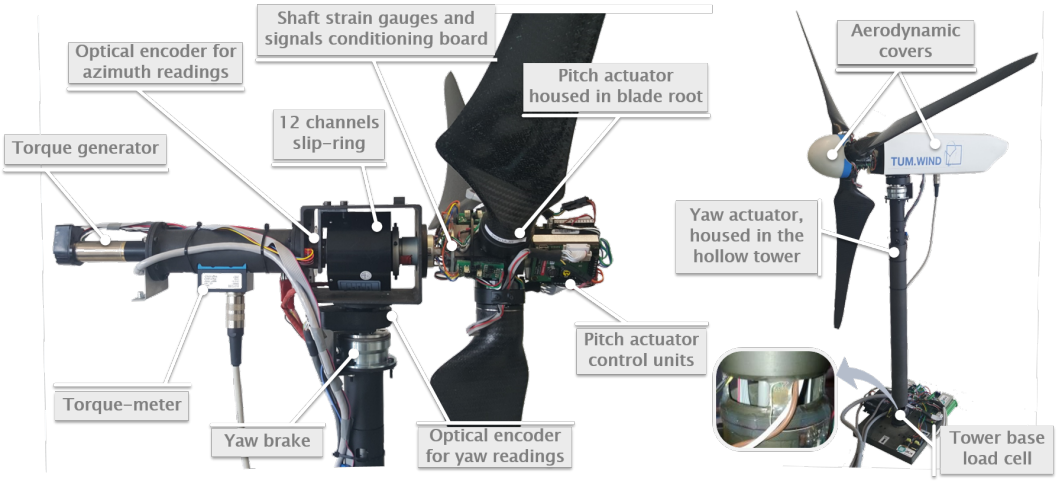


Figure 2: Layout of G1 model

A torque-meter, located after the two shaft bearings, allows for the measurement of the torque provided by a brushless motor equipped with a gearhead and a tachometer. The motor, located

The Science of Making Torque from Wind (TORQUE 2016) IOP Publishing
Journal of Physics: Conference Series **753** (2016) 032006 doi:10.1088/1742-6596/753/3/032006

in the rear part of the nacelle, is operated as a generator by using a servocontroller. An optical encoder, located between the slip ring and the rear shaft bearing, allows for the measurement of the rotor azimuth.

The entire nacelle can be yawed by means of a brushed motor, housed within the hollow tower, equipped with a gearhead. This latter element is connected by a multi-beam coupling to a shaft rigidly joined to the rectangular carrying box, and hold in place by two bearings located within the upper portion of the tower. An optical encoder provides feedback to an electronic device that controls both the yaw actuator and a magnetic brake.

The tower, whose stiffness was designed so that the first fore-aft and side-side natural frequencies of the nacelle-tower group are properly placed with respect to the harmonic per-rev excitations, is softened at its base by machining four small bridges, on which strain gages are glued. Bridges were sized so as to have sufficiently large strains to achieve the necessary level of accuracy for the strain gages. Two electronic boards provide for the power supply and adequate conditioning of this custom-made load cell.

Aerodynamic covers of the nacelle and hub ensure a satisfactory quality of the flow in the central rotor area

Due to the small dimensions of the scaled wind turbine, low Reynolds numbers are expected. Therefore, the low-Reynolds airfoil RG14 [8] was chosen for the model wind turbine blades. The aerodynamic performance of the rotor was measured for different values of the airfoil Reynolds by operating the models at several combinations of tip speed ratio (TSR) and collective pitch settings. The measured maximum power coefficients are approximately 0.42 at $\lambda \in [7, 8]$ and $\beta \in [-2°, 0°]$.

## 3. Control system

The control system of the wind turbine models is organized in three different levels, as shown in Fig. 3. The low level control operates the wind turbine actuators, while the communication with sensors, actuators, and control algorithms are implemented on the industrial real-time controller Bachmann M1 (http://www.bachmann.info). Wind farm control algorithms, as well as supervisory control for each model, are implemented on a standard PC, which communicates with each wind turbine controller over an Ethernet network.

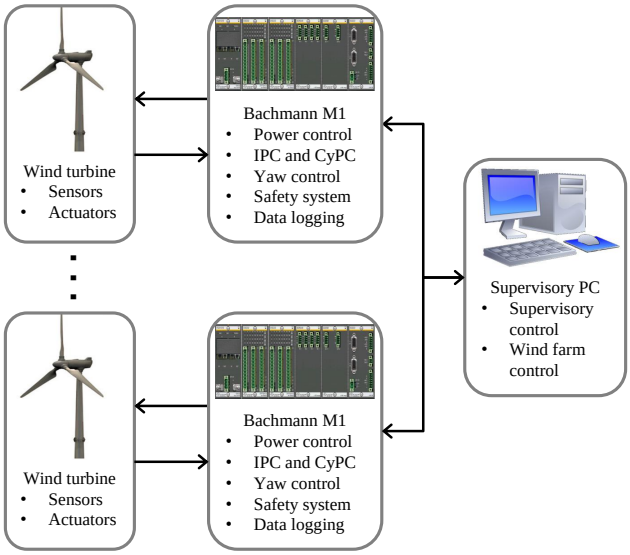


Figure 3: Control structure of the wind turbine models.

The Science of Making Torque from Wind (TORQUE 2016) IOP Publishing
Journal of Physics: Conference Series **753** (2016) 032006 doi:10.1088/1742-6596/753/3/032006

*3.1. Wind turbine control system*

The Bachmann M1 system used for wind turbine control is a modular real-time controller with a CPU module for running control algorithms, a counter module for acquiring rotor speed and azimuth from the digital encoder, a communication module for communication with actuators through a CAN network and two analogue input-output modules for acquiring measurements and sending commands to the torque motor and the yaw break. The Bachmann M1 system is capable of acquiring data with a sample rate of 2.5 kHz, which is used for acquiring aerodynamic torque, shaft bending moments and rotor azimuth position. All other measurements are acquired with a sample rate of 250 Hz.

Each wind turbine model is controlled by a separate Bachmann M1 system with a sampling time of 4 ms. Besides data-logging and safety systems (such as shutdown in case of overspeed), the following control algorithms are implemented on each M1 system:

- **Power control, i.e. torque and collective pitch control (CPC).** A standard power control is implemented based on [1], with two distinct control regions. In the region below rated wind speed, blade pitch angles are kept constant, while the generator torque reference follows a quadratic function of rotor speed in order to maximize energy extraction. Above rated wind speed, the generator torque is kept constant, while a PI controller is used to collectively pitch the rotor blades in order to keep the generated power at the desired level. Additionally, for the purpose of wind farm control, the wind turbine power output can be lowered to an arbitrary percentage of the available power below rated wind speed and of the nominal power above rated wind speed. Since power reduction can be achieved in different ways, it is possible to easily modify the control trajectories while the models are idling.
- **Individual and cyclic pitch control (IPC and CyPC).** Besides collective pitch control, the models are also capable of individually pitching each blade, enabling additional control actions for influencing loading or wakes. To this aim, the reference of each blade follows a harmonic function of the blade azimuth position with adjustable amplitude and phase angle. This leads to continuous blade pitching with frequency 1P, whose maximal amplitude has to be constrained according to the pitch actuator capabilities. This kind of pitch activity has a strong impact on loads, while the generated power remains unaffected above rated wind speed. On the other hand a slight power loss can be observed below rated wind speed, depending on the pitch amplitude [2, 11]. The amplitude and the phase angle of the blade pitch can be determined either in close loop by two decoupled PI controllers trying to reduce 1P oscillations of the shaft bending moments (IPC, for more details see [10]), or in open loop (CyPC).
- **Yaw control.** The misalignment angle of a wind turbine model with respect to the wind can be set by changing the yaw angle. A PI controller is used for controlling the yaw motor, and the yaw reference value is provided from the supervisory controller. An additional control logic is implemented that enables the yaw brake once the nacelle gets in the desired position. Whenever the yaw reference is changed, the brake is released and the PI controller ensures that the nacelle is yawed to the new position. Besides constant yaw references, the yaw controller is also capable of continuous yaw motion, such as a harmonic function with adjustable amplitude and frequency. Such a motion can be useful for wind farm control algorithms or for the generation of wake meandering in the wind tunnel.

*3.2. Wind farm control system*

High level control is implemented on a standard PC, and communication with the wind turbine Bachmann M1 controllers is established over an Ethernet network. Through a dedicated graphic interface, the supervisory controller allows for the user to monitor the wind turbine conditions, change their operating state, control algorithms and reference values, and to set up and initialize

The Science of Making Torque from Wind (TORQUE 2016) IOP Publishing
Journal of Physics: Conference Series **753** (2016) 032006 doi:10.1088/1742-6596/753/3/032006

the data acquisition process. Additionally, a wind farm control algorithm collects measurements from the Bachmann M1 controllers, and can send the following control actions back to them:

- a command to reduce produced power,
- a yaw angle reference,
- CyPC settings.

The wind turbine controller described in §3.1 is in charge of following the references sent by the wind farm controller.

At present, a gradient-based extremum seeking control algorithm is implemented with the goal of increasing energy capture. Gradients are computed by first-order finite differencing the energy capture, properly averaged over a time horizon, at two different wind turbine operating points. The control algorithm is based on [5], where yaw misalignment optimization is performed rather than axial induction. The algorithm uses the simplified assumption that control actions of a wind turbine affect only the closest downstream wind turbine. Therefore, instead of solving a single optimization problem for the entire wind farm, a series of smaller optimization problems (one for each wind turbine) is being solved:

$$\gamma_i^* = \arg\max_{\gamma} P_i + P_{i+1}. \tag{1}$$

The optimal yaw angle $\gamma_i^*$ is therefore determined based on the power output of the $i^{th}$ wind turbine $P_i$ and its closest downwind neighbor, $P_{i+1}$. The optimization problems are suitably synchronized by waiting for the propagation of the wakes only to the neighboring wind turbines, thus significantly reducing the convergence time of the algorithm. The time required for the wake to propagate is computed online using Jensen's model to estimate the speed in the wake. The average wind speed measured by the Pitot tube described earlier is used as input to the Jensen's model. The axial induction factor is computed by properly non-dimensionalizing the rotor thrust, in turn derived from the fore-aft bending moment measured at tower base, using the well-known relationship

$$C_T = 4a(1-a). \tag{2}$$

The wake decay coefficient is obtained by best-fitting experimental data from previous wind tunnel tests [4].

Although such an approach changes the original objective (power maximization in the entire wind farm), and therefore could result in suboptimal performance, it can also lead to significantly faster convergence.

## 4. Results

Tests were conducted by simulating the atmospheric boundary layer by means of spires placed at the inlet of the wind tunnel, in order to generate a wind speed vertical profile and turbulence intensity typical of offshore applications.

The machines were arranged with a flow-wise longitudinal spacing of 4 diameters and a laterally shift of half a diameter, as depicted in Fig. 1. The average wind speed measured by the Pitot tube described earlier is used to derive the wind turbine and wind farm power coefficients, the latter being defined as the sum of the wind turbine ones.

At first, different combinations of yaw misalignment for the upstream ($WT1$) and second ($WT2$) wind turbine model were tested within the wind tunnel, with the aim of experimentally identifying the operating condition maximizing wind farm power output. Figure 4 shows that, for the tested wind farm layout and wind condition, wind farm power can be substantially increased (up to 15%) by misaligning $WT1$ and $WT2$ of approximately 20 deg and 16 deg, respectively.

The Science of Making Torque from Wind (TORQUE 2016) IOP Publishing
Journal of Physics: Conference Series **753** (2016) 032006 doi:10.1088/1742-6596/753/3/032006

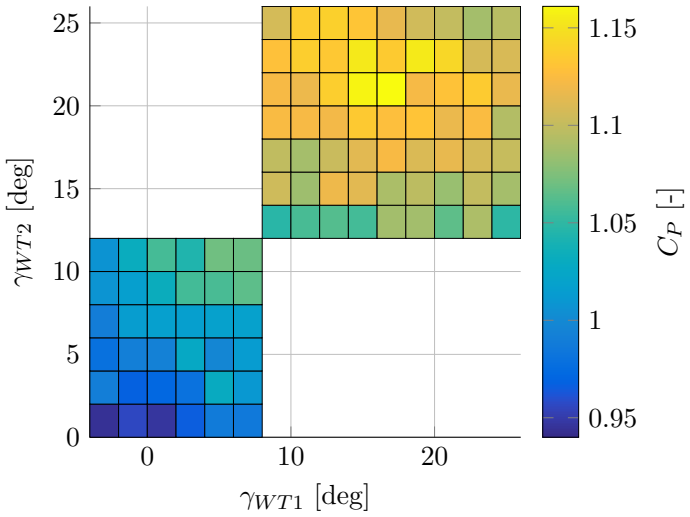


Figure 4: Measured wind farm power coefficient $C_P$ as function of upstream WT yaw misalignment ($\gamma_{WT1}$) WT yaw misalignment ($\gamma_{WT1}$).

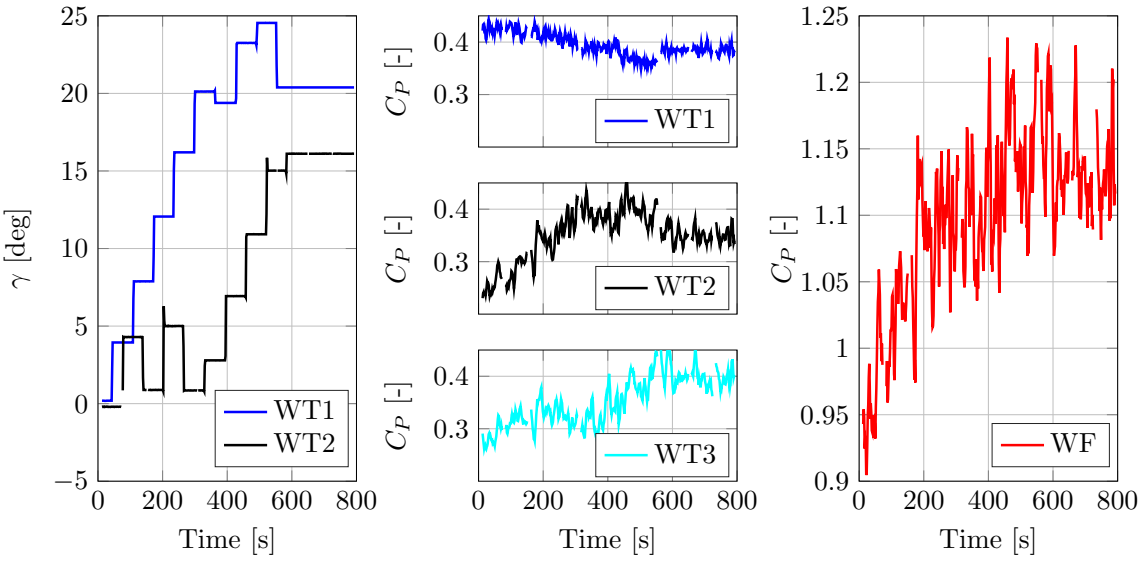


Figure 5: WTs yaw misalignment (on left), WTs power coefficient (center) and wind farm power coefficient as function of time (right)

.

Figure 5 shows the time evolution of the upstream WT yaw misalignments, as well as the evolution of the power coeffient for the three wind turbines and the whole wind farm, after the activation of the proposed wind farm controller. The data reported in Fig. 5 clearly highlights that the wind farm controller is capable of dynamically driving the wind turbines to yaw misalignment settings that, based on the results shown in Fig. 4, maximize the wind farm power output. This leads to an increase of power in excess of 15%, a result which is in line with what reported by other authors using simulations [6] and wind tunnel testing [9].

The Science of Making Torque from Wind (TORQUE 2016) IOP Publishing
Journal of Physics: Conference Series **753** (2016) 032006 doi:10.1088/1742-6596/753/3/032006

## 5. Conclusions

A closed-loop model-free controller has been developed and tested in a large boundary layer wind tunnel, where one can simulate wind conditions typical of offshore applications. Thanks to the use of sophisticated wind turbine models, extensively instrumented and equipped with individual pitch, torque and yaw control, it has been experimentally demonstrated that wake redirection by means of yaw misalignment can lead to substantial increase in wind farm power output. Moreover, it was shown for the first time that a closed-loop wind farm controller is capable of dynamically driving the upstream wind turbines to the optimal operational conditions.

## Acknowledgments

This work was financially supported by the German Federal Ministry for Economic Affairs and Energy (BMWi) within the CompactWind project (FKZ 0325492D).

## References

[1] Bossanyi E 2000 *Wind Energy* **3** 149–163
[2] Bossanyi E 2005 *Wind Energy* **8** 481–485
[3] Bottasso C L, Campagnolo, F and Petrović V 2014 *Journal of Wind Engineering and Industrial Aerodynamics* **127** 11–28
[4] Campagnolo F, Petrović V, Bottasso C L and Croce A 2016 *American Control Conference (ACC)* 513–518
[5] Gebraad P M Om van Wingerden J W, 2015 *Wind Energy* **18** 429–447
[6] Gebraad P M O, Teeuwisse FM, van Wingerden JW, Fleming PA, Ruben SD, Marden JR and Pao LY 2014 *Wind Energy* **19** 95–114
[7] Knudsen T, Bak T and Svenstrup M 2015 *Wind Energy* **18** 1333-1351
[8] Lyon C A, Broeren A P, Gigure P, Gopalarathnam A, Selig M S 1998 *SoarTech Publications* **3**
[9] Park J, Law K 2016 *IEEE Transactions on Control Systems Technology* **24** 1655-1668.
[10] Petrović V and Campagnolo F 2013 *European Control Conference 2013*, Zurich
[11] Petrović V, Jelavić M and Baotić M 2015 *Renewable Energy* **76** 418–431

# Numerical and Experimental Study of Wake Redirection Techniques in a Boundary Layer Wind Tunnel

Wake Conference 2017 IOP Publishing
IOP Conf. Series: Journal of Physics: Conf. Series **854** (2017) 012048 doi:10.1088/1742-6596/854/1/012048

# Numerical and Experimental Study of Wake Redirection Techniques in a Boundary Layer Wind Tunnel

**J Wang[1], S Foley[1], E M Nanos[1], T Yu[1], F Campagnolo[1], C L Bottasso[1,2], A Zanotti[2] and A Croce[2]**

[1] Wind Energy Institute, Technische Universität München, Boltzmannstraße 15, D-85748 Garching bei München, Germany
[2] Dipartimento di Scienze e Tecnologie Aerospaziali, Politecnico di Milano, Via La Masa 34, I-20156 Milano, Italy

E-mail: jesse.wang@tum.de

**Abstract.**
The aim of the present paper is to validate a wind farm LES framework in the context of two distinct wake redirection techniques: yaw misalignment and individual cyclic pitch control. A test campaign was conducted using scaled wind turbine models in a boundary layer wind tunnel, where both particle image velocimetry and hot-wire thermo anemometers were used to obtain high quality measurements of the downstream flow. A LiDAR system was also employed to determine the non-uniformity of the inflow velocity field. A high-fidelity large-eddy simulation lifting-line model was used to simulate the aerodynamic behavior of the system, including the geometry of the wind turbine nacelle and tower. A tuning-free Lagrangian scale-dependent dynamic approach was adopted to improve the sub-grid scale modeling. Comparisons with experimental measurements are used to systematically validate the simulations. The LES results are in good agreement with the PIV and hot-wire data in terms of time-averaged wake profiles, turbulence intensity and Reynolds shear stresses. Discrepancies are also highlighted, to guide future improvements.

## 1. Introduction

Wake redirection is currently one of the most promising wind farm control methodologies, which may lead to the improved power capture and reduced structural loading. The current research on wake redirection is very active, covering high-fidelity numerical simulations [14], scaled experiments in the wind tunnel [10], direct measurements in the field [1], reduced order models [2] and control methods [9]. In a previous paper [27], we used a three-pronged approach based on the combination of an analytical formulation, a LES-lifting-line CFD method [26] and wind tunnel scaled models to investigate two wake redirection methods, yaw misalignment (noted YM in this paper) and cyclic pitch control (noted CyPC). The analysis showed that, as already noticed by other authors, YM is more effective than CyPC in displacing the wake laterally. CyPC, however, was shown to have some effect on the speed of recovery of the wake, although the practical use of this concept is put in serious doubt by the large loads that are generated on the wind turbine.

Wake Conference 2017 IOP Publishing
IOP Conf. Series: Journal of Physics: Conf. Series **854** (2017) 012048 doi:10.1088/1742-6596/854/1/012048

In the present paper, we use additional wind tunnel measurements to further characterize the behavior of the CFD approach in the context of these two wake redirection techniques. Our long term goal is to develop the ability to accurately simulate our wind tunnel experiments by a validated numerical environment, and to upscale the validation to full scale. The present paper considers both integral rotor quantities such as power and thrust, as well as local flow measurements obtained by particle image velocimetry (PIV) and hot-wire probes. Scanning LiDARs are used to create a map of the wind tunnel inlet, to account for some spatial variability of the generated flow conditions, which is useful for a more accurate verification of the numerical results. The analysis highlights the general good qualitative agreement between experiments and simulations. The results also show that some local improvements are still necessary, highlighting some weakness of the numerical approach that motivate further refinements.

## 2. Simulation model

### *2.1. CFD formulation*

The simulation model is implemented in the SOWFA code [12], a CFD simulation tool based on an incompressible solver within the OpenFOAM repository, employing the Boussinesq approximation to include buoyancy-driven flow. Large scale transient simulations are conducted using the PIMPLE time marching algorithm. The grid-collocated formulation computes quantities at cell centers. The interpolation of Rhie and Chow [24] is employed to remove numerical oscillations caused by pressure-velocity decoupling induced by grid collocation. The time marching scheme uses a second order backward implicit discretization. The momentum and potential temperature equations use a diagonal incomplete preconditioned bi-conjugate gradient linear solver, while pressure is solved using a geometric agglomerated algebraic multi-grid solver. Parallel computing is based on the Message Passing Interface (MPI) [13]. In addition, SOWFA uses the lifting-line method embedded in a large-eddy simulation (LES) environment, coupled with the aeroservoelastic simulator FAST [13].

Apart from the numerical methods used for wind farm simulations, other techniques are employed to perform more robust and accurate large-eddy simulations of the scaled wind farm facility. The immersed boundary formulation is used for the modeling of geometries, like nacelle and tower, within the control volume. The convection vector-field scheme uses a deferred correction Gamma-bounded interpolation method, which belongs to the family of categorized normalized variable diagram (NVD) schemes [18]. This Gamma scheme contains a pre-specified constant, $\beta_m$, which allows one to limit the numerical diffusion and to minimize numerical dispersion. In general, a larger value of $\beta_m$ implies a lower dispersion and a higher diffusion, vice versa. Therefore, $\beta_m$=0.35 is employed within the near wake to stabilize the simulations, since actuator line body forces and immersed boundary possibly increment the numerical stability issues, while $\beta_m$=0.05 is used for the far wake to minimize numerical diffusion. This algorithm represents an important improvement with respect to normal unbounded and non-flux-limited central differencing schemes. In fact, it is capable of minimizing the numerical dispersion otherwise often observed at large yaw misalignment angles, where the wake is oblique to the grid. Moreover, this approach performs better than other low diffusive schemes such as the one of Vanleer in terms of limiting the numerical diffusion in the wake region, where small-scale eddies are dissipated due to such flux limiters [16]. A tuning-free Lagrangian scale-dependent dynamic approach is used for the Smagorinsky sub-grid scale modeling [23]. This approach improves the modeling of inhomogeneous flow fields such as in the case of wind turbine wakes, where first and second-order flow quantities vary significantly within the domain.

### *2.2. Actuator line method*

The LES formulation is augmented with an actuator line method. The complete geometry of the blades is not resolved in the present LES formulation, due to its excessive computational costs.

Wake Conference 2017 IOP Publishing
IOP Conf. Series: Journal of Physics: Conf. Series **854** (2017) 012048 doi:10.1088/1742-6596/854/1/012048

Instead, blades are represented by a given number of points on an actuator line. Aerodynamic forces are calculated based on the local angle of attack by means of look-up tables storing the local airfoil lift and drag coefficients. The resulting forces acting at each blade section are then smoothly mapped to a body force field by a Gaussian projection characterized by a width parameter $\varepsilon$. The determination of the $\varepsilon$ parameters is dependent on several factors. According to Ref. [13], $\varepsilon$ should account for cell size, chord width and other geometrical parameters, but cannot be lower than a minimum value to avoid spurious oscillations of the velocity field. A comprehensive study of the effect of the projection width on the simulation quality is reported in Ref. [20].

### *2.3. Immersed boundary method*

An immersed boundary (IB) formulation [17] is used to model the wind turbine nacelle and tower. The IB method is employed to avoid the use of surface conforming meshes to resolve the shape of the body [22]. The present IB approach, based on a discrete forcing method, uses a direct imposition of the boundary conditions. This way, the sharpness of the body shape is preserved and no extra stability constraints are introduced. In fact, with this approach boundary conditions and wall models can be directly imposed on the IB surfaces, yielding a significant improved solution quality for higher Reynolds number viscous flows [3], such as the present case of wind turbines operating in an atmospheric boundary layer. Details of the formulation are described in Ref. [28].

## 3. Experimental methods

Experiments were conducted in a 36 m $\times$ 16.7 m $\times$ 3.84 m boundary layer wind tunnel at Politecnico di Milano (POLIMI) [7]. Tests were performed with a scaled wind turbine model, shown in figure 1, together with the reference frame adopted to express the flow velocity components, which has a rotor diameter (D) of 1.1 m and a rated rotor speed of 850 RPM, and which has already been used within other research projects [9–11].

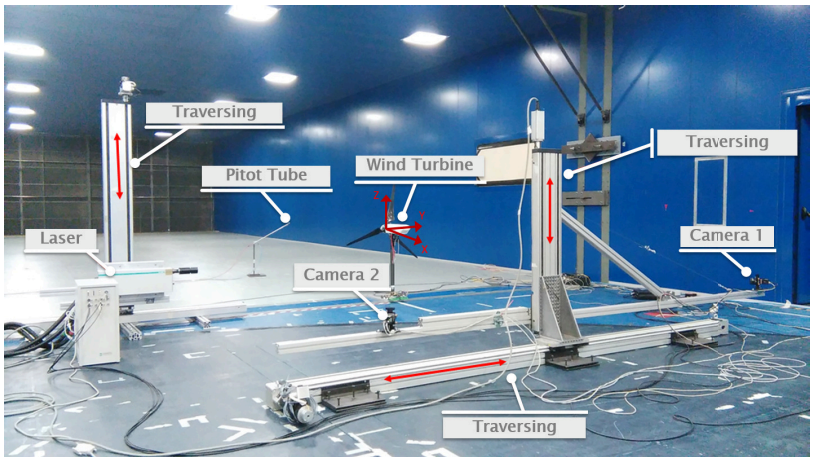


Figure 1: Experimental setup within the boundary layer wind tunnel at Politecnico di Milano.

The model is characterized by a realistic aerodynamic performance, both at the airfoil and rotor levels, and its wake is characterized by shape, deficit and recovery that are in good accordance with those of full-scale machines. Moreover, the model features active individual pitch, torque and yaw control that, together with a comprehensive onboard sensorization of the

Wake Conference 2017 IOP Publishing
IOP Conf. Series: Journal of Physics: Conf. Series **854** (2017) 012048 doi:10.1088/1742-6596/854/1/012048

machine (including measures of shaft and tower loads), enables the testing of modern control strategies similar to the ones described in [5] and references therein.

The wind tunnel can be operated with different configuration of spires and pyramids at the inlet of the test section, to realize varying vertical shear and turbulence intensity conditions. Hot-wire probes, LiDAR (Light Detection And Ranging) and PIV (Particle Image Velocimetry) are used to perform high quality measurements of aerodynamic quantities, which will then be used for the validation of the LES-lifting-line model.

### *3.1. Inflow measurements*

Previous experimental testing in the POLIMI facility has revealed that the inflow generated by the wind tunnel is non-uniformly distributed, with variations in flow velocity of up to 6%. The inhomogeneity of the flow is non-negligible, and it will influence the operation of the wind turbine models and of the associated flow-field. To address this problem, instead of imposing a uniform inflow for the inlet boundary condition, a non-uniform inflow was used to more accurately represent the incoming flow generated in the wind tunnel. Properly capturing the inflow velocity requires the full cross-sectional wind map to be recorded upstream of the wind turbines, rather than sampling a single point (or several scattered points in space) at hub height. The measured experimental wind map can then be implemented as the inlet boundary condition to the CFD simulation.

In order to obtain a reliable high resolution wind map, two synchronized scanning LiDARs were employed. LiDARs are instruments equipped with a steering laser beam that fires rapid pulses and, by measuring the frequency shift of the backscattered light from the aerosols present in the air, are able to record the line-of-sight component of the wind speed. In this work, LiDAR data was obtained from the collaborative efforts of ForWind-Oldenburg, TUM, Technical University of Denmark and POLIMI [25]. Figure 2 shows the time-averaged velocity scanned inflow map. The figure clearly shows the lack of uniformity of the inflow, probably due to the presence of a discrete number of fans and of the structural arrangement of the tunnel just upstream of the test section. The black circle indicates the location of the rotor, which appears to be placed in correspondence with a local peak of the flow velocity.

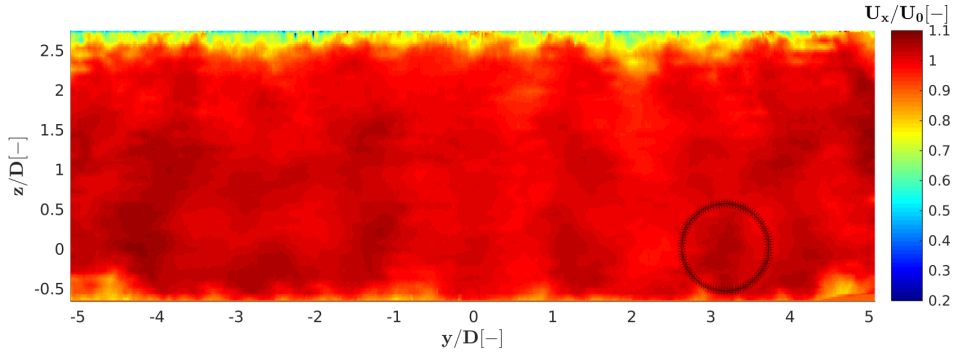


Figure 2: Inflow velocity profile (facing upstream) as measured by two scanning LiDARs at a 3D distance upstream of the wind turbine model.

### *3.2. Wake measurement*

The stereo PIV instrumentation, shown in figure 1, was used to measure the three velocity components at cross-flow planes located at two different positions at 0.56D and 6D downstream from the rotor. The measurement planes cover quite a broad fraction of the wind turbine

Wake Conference 2017 IOP Publishing
IOP Conf. Series: Journal of Physics: Conf. Series **854** (2017) 012048 doi:10.1088/1742-6596/854/1/012048

wake. In order to achieve a higher spatial resolution of the velocity field, the measurement area was divided into several smaller windows with slight overlapping areas between them. A rapid scanning of the entire measurement area was achieved by the use of an automated traversing system, moving both the laser and the cameras. In particular, the two cameras, equipped with a 1952 × 1112 pixel array, were connected to a metallic arm and mounted on a 4 m × 2 m double axis traversing system. The Nd:Yag double pulsed laser, with a 200 mJ output energy, was also mounted on a traversing system to move the laser sheet simultaneously with the measurement window. The measuring windows were divided into 32 × 32 pixel interpolation areas, which resulted in an approximately 15 mm spatial resolution. For each measuring window, 200 pairs of images were acquired (per camera) without any phase lock (time-averaged flow field). Additional details concerning the PIV instrumentation are given in [29]

## 4. Computational setup

The computational domain, as shown in figure 3, has a height of 3.84 m height, equal to the height of the wind tunnel test section. The inlet is located 3.3 m upstream of the wind turbine, in the same plane where the LiDAR inflow map is measured. The streamwise length is 10D. The lateral dimension is reduced to 4 m, to limit the domain size and hence the computational cost. Multiple simulation tests have shown that the reduction of the lateral dimension has no noticeable effect on the results. After determining the size of the computational domain, grid resolution requirements are investigated through a mesh independence study. Three levels of refinement are used: zone 1 defines a cube-shaped background mesh ($\Delta x = \Delta y = \Delta z$) with a cell size of 0.08 m, zone 2 is the first level of refinement with a cell size of 0.04 m, followed by zone 3 that uses a size of 0.01 m.

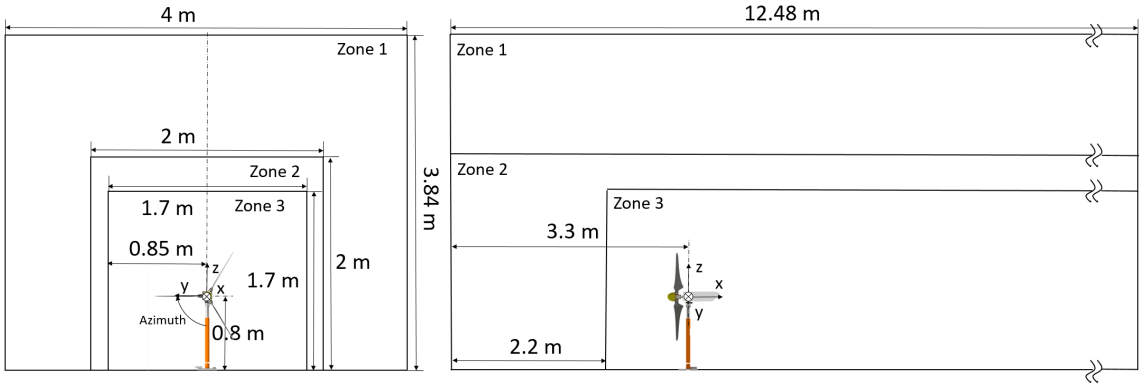


Figure 3: Views of the computational domain. Left: cross-section. Right: lateral view.

The inflow velocity measured by LiDARs is used at the domain inlet, to capture the lack of uniformity of the wind tunnel generated flow. Apart from this, the inflow of the numerical simulation is steady and non-turbulent. This creates a difference between the numerical and experimental flow conditions, because the latter has a turbulence intensity equal to about 2%. This should be kept in mind when comparing numerical and experimental results, because the different ambient turbulence conditions may have some effects.

Slip boundary condition is applied at the left and right walls, while a wall model equivalent to a no-slip condition is used for the floor and ceiling of the tunnel. A wall model is also used for the immersed boundary surface that models the nacelle and tower. Neumann type boundary condition for the pressure at all walls is also imposed. A modified version of the mesh partitioning algorithm was developed, which tries to allocate the same number of cells to all processors without cutting the mesh at the immersed boundary surfaces.

Wake Conference 2017 IOP Publishing
IOP Conf. Series: Journal of Physics: Conf. Series **854** (2017) 012048 doi:10.1088/1742-6596/854/1/012048

A fixed time-step of 0.0002 s is used for baseline and two CyPC setups, while 0.0003 s is used for YM setup. The time-step equates to a maximum Courant number $C_{max}$ of 0.17 and a displacement of 0.99 cells per time-step at the tip of the blades for the baseline case. In all cases, the machines are operating in the partial load region at an averaged wind speed of 5.83 m/sec across the rotor, while the rotating speed varies from 780 to 840 RPM due to different redirection control methods. The Initial blade pitch were kept to be constant for all 4 setups. The ratio $\frac{\varepsilon}{\Delta x}$ between the Gaussian width and the cell size has been kept equal to 2.2 for the baseline and two CyPC simulations, while it has increased to 3.4 for 20 deg yaw misalignment case. Most simulations were performed on an Intel Haswell-EP computing cluster. With these computational resources, 5.2 s of physical time (≈26,000 time steps) require about 13,440 cpu hours. The solution converges to steady state after about 4 s of physical time.

## 5. Results and analysis

### *5.1. Power and thrust*

Four operating conditions are considered: a baseline condition (constant pitch setting, no misalignment), cyclic pitching with two different phase angles, and a yaw misalignment of 20 deg. For CyPC, the blade is pitched according to $\theta_i = \theta_0 + \theta_c \cos(\psi_i + \gamma)$, where $\theta_0$ is the collective pitch constant, $\theta_c$ the 1P pitch amplitude, $\psi_i$ the blade azimuth angle (counter-clockwise looking upstream, and null when the blade is pointing vertically up along the tower), and $\gamma$ is the phase angle (clockwise looking upstream). Two values for $\gamma$ are considered: 52 and 270 deg. The wind tunnel was operated without spires at the test chamber inlet, resulting in low-turbulence (≈2%) flow conditions.

Table 1 shows the wind turbine power and thrust at the four operating conditions. A good agreement between the simulations and experiments is observed for the baseline case, with differences of 3% and 6% for power and thrust, respectively. The match is less accurate for the CyPC cases. For both cases, power is underestimated by the numerical simulations, while thrust is underestimated in one case and overestimated in the other.

Table 1: Comparison of rotor power and thrust between simulation and experiment for the baseline case, cyclic pitch amplitude of 5.3 deg with phase shifts of 52 and 270 deg, and yaw misalignment $\varphi$=20 deg.

| | Type | Baseline | CyPC $\gamma$=52 [deg] | CyPC $\gamma$=270 [deg] | YM $\varphi$=20 [deg] |
|---|---|---|---|---|---|
| Power | Exp. $[W]$ | 44.55 | 35.19 | 35.04 | 40.98 |
| | Sim. $[W]$ | 43.29 | 32.24 | 31.63 | 40.63 |
| | $\Delta P$ % | -2.82 | -8.39 | -9.74 | -0.85 |
| Thrust | Exp. $[N]$ | 15.93 | 14.03 | 15.42 | 13.69 |
| | Sim. $[N]$ | 16.85 | 14.78 | 14.53 | 13.59 |
| | $\Delta T$ % | 5.76 | 5.34 | -5.79 | -0.73 |

Several possible effects may help explain the larger errors in the CyPC cases. First, unsteady airfoil aerodynamic effects (including dynamic stall) are completely neglected, as the present lifting-line formulation only uses look-up-tables of steady lift and drag coefficients. This could be improved by using the suitable unsteady aerodynamics model for the airfoils. Some of these models, such as the Beddoes-Leishman [21], are available within the current LES framework. However, this model requires the definition of several airfoil-dependent governing parameters that were unknown to us at the time when simulations were performed, and would need to be specifically calibrated. Second, the CyPC experiments were conducted at a lower RPM than the

Wake Conference 2017 IOP Publishing
IOP Conf. Series: Journal of Physics: Conf. Series **854** (2017) 012048 doi:10.1088/1742-6596/854/1/012048

baseline (780 RPM instead of 840 RPM, corresponding to a reduction of about 7%, due to the shift of operating point under cyclic pitch control), which induces a reduction in the operating Reynolds of the airfoils. The airfoil lift and drag coefficients, obtained during previous research activities [10], are tabulated for two values of the Reynolds number (namely, Re=90000 and Re=75000), and they are interpolated during the simulation based on the local instantaneous conditions [21]. However, the lower Reynolds coefficients may be less accurate than the higher ones, which might induce a larger discrepancy in the results in this case. This might be improved by tuning the aerodynamic coefficients, as suggested in Ref. [6].

The same table shows also good results for the misalignment case. However, various numerical experiments showed a significant sensitivity of the results to the Gaussian width parameter $\varepsilon$. In fact, the results of the table were obtained with a parameter $\varepsilon$ 54% higher than the one used for the baseline case, as addressed in section 4. This problem deserves further careful investigation. Here again, a possible reason might be the lack of modeling of unsteady aerodynamic effects at the level of the airfoils, effects that increase for increasing misalignment. Clearly, finding a specific value of the Gaussian width parameter to correct for this deficiency of the method is not a sensible option, and it is certainly not suggested as a general solution.

*5.2. Wake properties*

*5.2.1. Cyclic pitch case* Normalized time-averaged velocity plots are shown in figure 4 and 5. The figures report results just behind the rotor ($x/D$=0.56) and in the far wake ($x/D$=6), for the baseline and the two considered CyPC cases.

The analysis of the $U_x$ component at 0.56D downstream of the rotor is particularly interesting, as this is a position where few results have been previously reported. The images show that the use of CyPC has a strong effect on the wake structure, leading to marked unsymmetrical shapes. Measurements are missing from two areas left and right of the rotor disk, where, due to the close proximity of the measuring plane with the wind turbine, part of the nacelle (which is of a white color) was on the background, leading to bad correlation between the images. A comparison between experimental and numerical results shows that there is in general a good qualitative agreement, and that the main distortion effects caused by CyPC are reasonably captured. The difference $\mathbf{\Delta U_i}$ between experiment and simulation velocities was evaluated at several locations within the rotor swept area (black dot circles in figure 4). Based on these quantities, the average velocity difference $\overline{\mathbf{\Delta U}}$ and its root mean square $\mathbf{\Delta U}_{\mathrm{RMS}}$ were calculated. $\overline{\mathbf{\Delta U}}$ is equal to -1.36%, 2.69% and 5.05% for the baseline, CyPC $\gamma$=52 and 270 deg cases, respectively, while $\mathbf{\Delta U}_{\mathrm{RMS}}$ is 0.43 m/sec, 0.79 m/sec and 0.72 m/sec for the same three cases. Positive value of $\overline{\mathbf{\Delta U}}$ means that the average simulated velocity is higher.

Figure 5 shows the wake plots in the far wake region at 6D. $\overline{\mathbf{\Delta U}}$ in this case is 4.9%, 9.4% and 4.9% for the baseline, CyPC $\gamma$=52 and 270 deg cases, respectively. $\mathbf{\Delta U}_{\mathrm{RMS}}$ is 0.33 m/sec, 0.46 m/sec and 0.44 m/sec for the same three cases. $\mathbf{\Delta U}_{\mathrm{RMS}}$ are slightly improved at 6D compared to the near wake for all three cases, while $\overline{\mathbf{\Delta U}}$ at 6D show in general higher wake recovery. Lower $\mathbf{\Delta U}_{\mathrm{RMS}}$ implies a higher correlation between LES and PIV wake profile. In fact, compared with the near wake region, the flow in the far wake is further mixed and less structured, exhibiting a velocity profile that is typically well approximated by a single Gaussian. Lastly, it should be remarked that CyPC leads to a faster recovery of the wake than in the baseline case, as already noticed in Ref. [27]. In principle, this could be of interest for wind farm control, although the very large loads exerted on the rotor by the use of CyPC severely limits the possible applicability of this control concept.

Next, the hub-height velocity profile is considered. Figure 6 reports the time-averaged streamwise velocity profiles at hub height for the three considered operating conditions. In the near wake (0.56D), matching for the baseline case is reasonable, except the region close to the hub. Here, the effects of the nacelle and tower are not captured accurately. A visualization

Wake Conference 2017 IOP Publishing
IOP Conf. Series: Journal of Physics: Conf. Series **854** (2017) 012048 doi:10.1088/1742-6596/854/1/012048

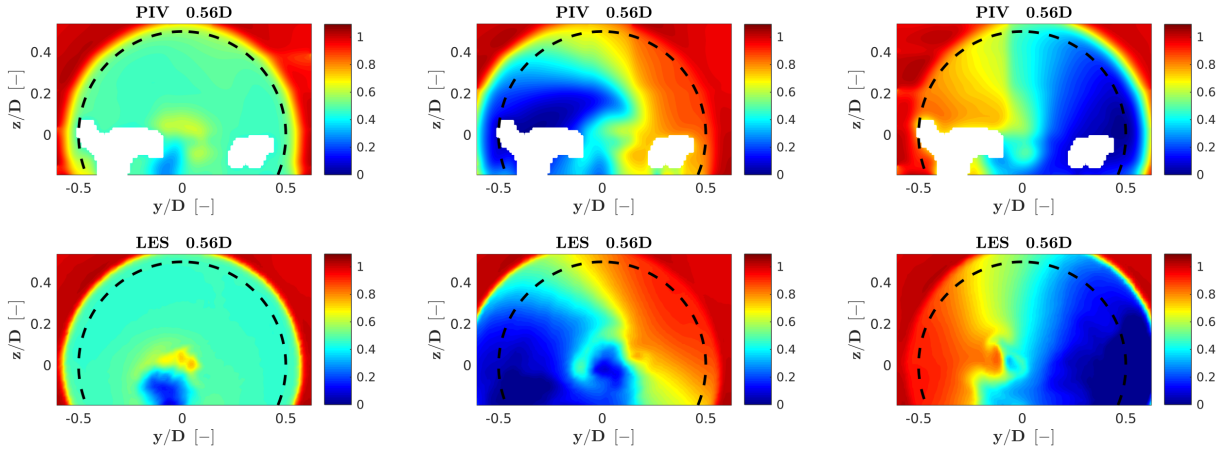


Figure 4: Normalized time-averaged streamwise velocity on the yz-plane at 0.56D downstream of the wind turbine (facing upstream). From left to right, baseline condition and cyclic pitch amplitude of 5.3 deg with phase shift $\gamma$ of 52 and 270 deg. Top: PIV experimental measurements; bottom: simulation results.

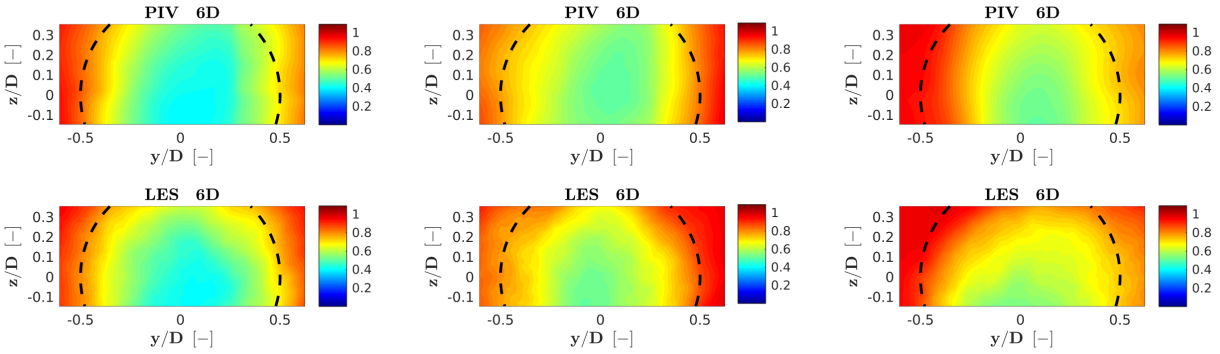


Figure 5: Normalized time-averaged streamwise velocity on the yz-plane at 6D downstream of the wind turbine (facing upstream). From left to right, baseline condition and cyclic pitch amplitude of 5.3 deg with phase shift $\gamma$ of 52 and 270 deg. Top: PIV experimental measurements; bottom: simulation results.

of the numerical results seems to indicate a strong tower shedding. Accuracy might be affected by a lack of background turbulence in the simulations. In fact, as previously explained, the wind tunnel flow is characterized by a turbulence intensity of 2%, while the numerical simulations are conducted in uniform non-turbulent inlet conditions. For the CyPC case, matching is much poorer, with significant differences both close to the hub and especially at the tip of the low speed region. As previously noted, differences might be due to limits of the lifting-line formulation, and/or because of a lack of grid resolution.

The situation is improved for the 6D case, as expected. Here good results are obtained for the baseline case, while small discrepancies are visible for the CyPC conditions. Note that the wind speed velocities at the left and right ends of the rotor are not identical, which, as previously explained, is a phenomenon due to the non-uniform inflow conditions of the wind tunnel.

Wake Conference 2017 IOP Publishing
IOP Conf. Series: Journal of Physics: Conf. Series **854** (2017) 012048 doi:10.1088/1742-6596/854/1/012048

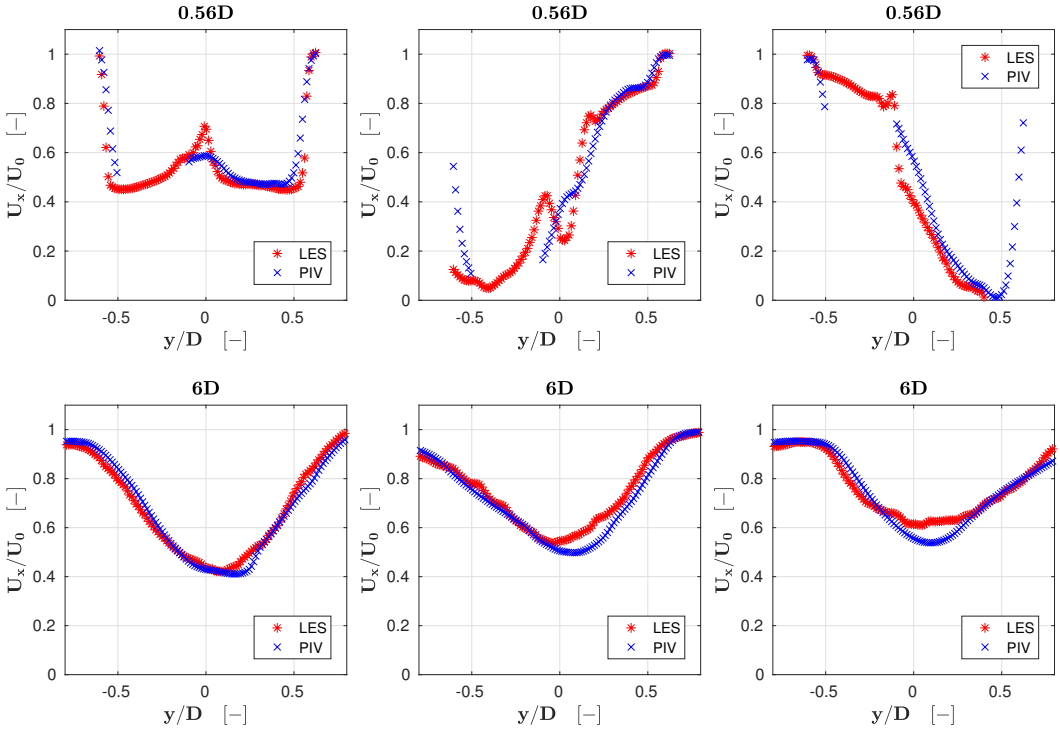


Figure 6: Normalized time-averaged streamwise velocity along a hub-height horizontal line at 0.56D (top) and 6D (bottom) downstream of the wind turbine. From left to right, baseline condition and cyclic pitch amplitude of 5.3 deg with phase shift $\gamma$ of 52 and 270 deg.

*5.2.2. Active yaw control* Next, we consider the wake velocity profiles for the 20 deg YM case. As previously mentioned, the $\varepsilon$ parameter was adjusted to better approximate the experimental results, while the other parameters remained identical to the baseline case. Figure 7 shows the numerically computed time-averaged streamwise velocity at three downstream locations; no PIV measurements are available in this case. The wake structure exhibits a characteristic 'kidney' shape, in accordance with the observations of other authors [4, 15].

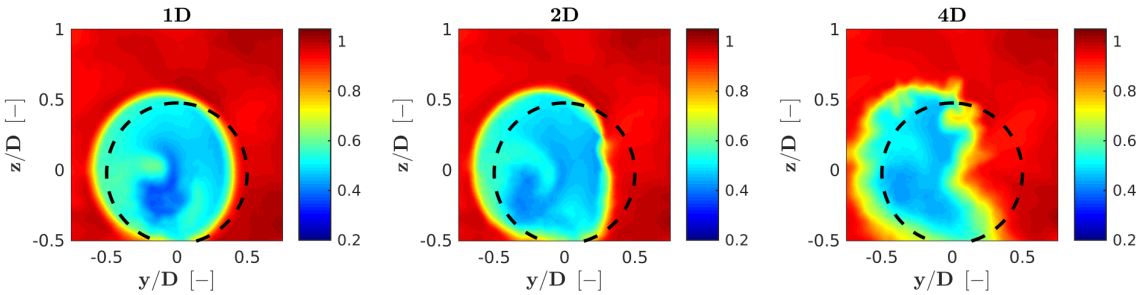


Figure 7: Simulated normalized time-averaged streamwise velocity (facing upstream) at 1D, 4D, and 7D downstream of a wind turbine with 20 deg yaw misalignment.

Wake Conference 2017 IOP Publishing
IOP Conf. Series: Journal of Physics: Conf. Series **854** (2017) 012048 doi:10.1088/1742-6596/854/1/012048

Figure 8 reports the first order (velocity profile) and second order (turbulence intensity TI and Reynolds shear stress $\overline{u'v'}$) flow quantities at 4D for the baseline case (top row of plots) and YM case (bottom row of plots). Experimental measurements were obtained with triple hot-wire probes [25], while simulations are reported with and without the presence of nacelle and tower. The baseline wake profile with nacelle and tower included correlates well with the measurement data. It appears that the presence of the nacelle and tower in the model is indispensable for an accurate solution ($\overline{\mathbf{\Delta U}} = 2\%$ in this case), as already noticed by other authors [8]. Although the situation is not as good for the YM case, matching with the experimental measurements is still quite reasonable ($\overline{\mathbf{\Delta U}} = 4\%$). In addition, the prediction of the displacement of the wake center, computed as the location of the minimum of the Gauss fit to the wake, appears to be highly accurate and essentially identical to -0.26D for both the simulation and experiment.

Similar effects can be observed for the two second order quantities, TI and $\overline{u'v'}$. Regarding the former quantity, the plots show that ambient TI, as seen at the end of the scan line, is nearly 0% for the simulation case and 2% for the experiments, as previously noted. Although there is more scatter for TI than for $\overline{u'v'}$, the plots show once again the importance of including tower and nacelle in the model to improve accuracy.

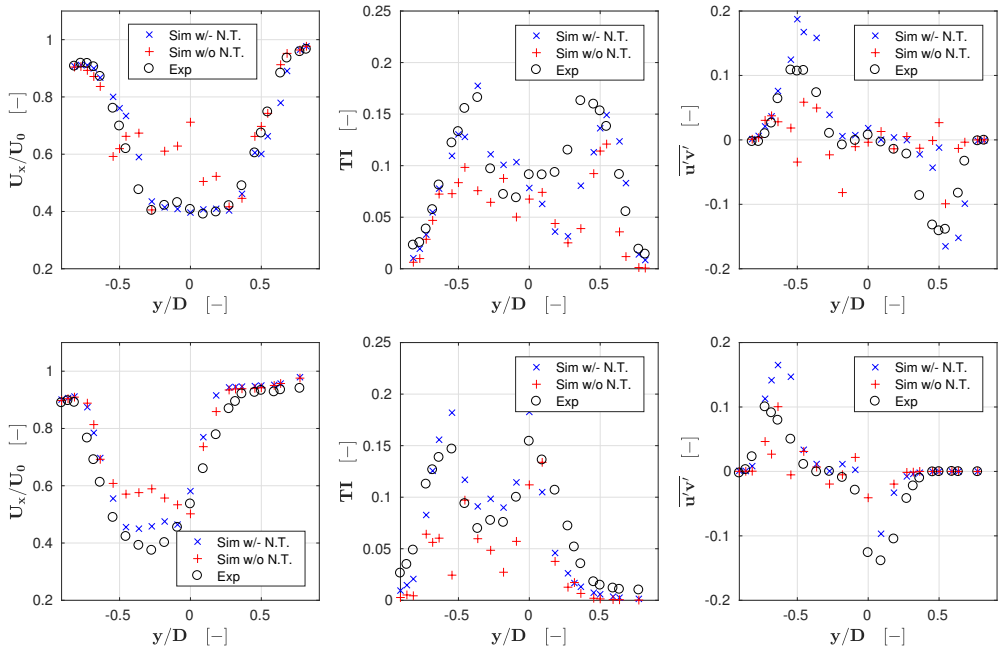


Figure 8: From left to right, hub-height horizontal line time-averaged streamwise velocity, turbulence intensity and Reynolds stress component $\overline{u'v'}$ at 4D. Top: baseline case; bottom: YM case with $\varphi$=20 deg. Black circles: experimental values; blue x's: simulations with nacelle and tower; red crosses: simulations without nacelle and tower.

## 6. Conclusion and outlook

This paper has presented the comparison of the results of a LES-lifting-line solver with wind tunnel measurements obtained with scaled wind turbine models. The analysis has considered a baseline flow-aligned case, the use of cyclic pitching to affect the wake, and the misalignment of the wind turbine with the incoming wind. Comparisons included integral rotor quantities as power and thrust, and local flow quantities measured by PIV and hot-wire probes. Measurements

were performed in the near wake region, and after vortex breakdown in the far wake. Two scanning LiDARs were used to generate a map of the velocity at the inlet of the test section, to account for the non-uniformity of the wind tunnel generated flow.

Based on the results shown in the paper, it appears that the CFD formulation is able to capture both the integral and local quantities with reasonable accuracy. In general, the baseline case exhibits the best results, while both CyPC and YM are qualitatively acceptable but not always very precise.

Overall, results appear to be very encouraging, although there are several effects that may potentially further improve the level of accuracy of the current numerical model. The LES framework can be improved on three fronts: using more accurate airfoil polars, which may be achieved with the existing polar-identification procedures, and introducing unsteady effects in the airfoil model. Results presented herein showed in a very clear manner the importance of including the nacelle and tower in the CFD model. However, the same results also show that the accuracy of such components is still not sufficient, and improvements may be obtained by the use of denser grids and possibly an improved formulation. Finally, the present simulation did not match the ambient turbulence of the experiment, which might be the source of additional discrepancies. For higher turbulence cases (which are closer to full scale operating conditions), eddies in the wind tunnel flow are generated by the use of spires at the inlet. For such conditions we have already developed a CFD model that can be used as a precursor of the lifting-line simulations. In the future, we will work on expanding that method to also account for the non-uniformity of the mean velocity, a problem that was considered here using a LiDAR-measured inflow map.

## Acknowledgments

This project was partly funded by the EU Horizon 2020 research and innovation programme under the Marie Skłodowska-Curie grant agreement No. 642108. The authors wish to thank G. Campanardi and D. Grassi from the Politecnico di Milano for their contribution to the PIV measurements.

## References

[1] Aitken M L, Banta R M, Pichugina Y L and Lundquist J K 2014 Quantifying wind turbine wake characteristics from scanning remote sensor data *Journal of Atmospheric and Oceanic Technology* **31** 765-87
[2] Annoni J, Gebraad P, and Seiler P 2016 Wind farm flow modeling using an input-output reduced-order model *American Control Conference* 506-12
[3] Bandringa H 2010 *Immersed boundary methods* (Netherlands: University of Groningen)
[4] Bastankhah M and Porté-Agel F 2016 Experimental and theoretical study of wind turbine wakes in yawed conditions *Journal of Fluid Mechanics* **806** 506-41
[5] Bossanyi E 2000 The design of closed loop controllers for wind turbines *Wind Energy*, **3** 149-63
[6] Bottasso C L, Cacciola S, and Iriarte X 2014 Calibration of wind turbine lifting line models from rotor loads *Journal of Wind Engineering and Industrial Aerodynamics*, **124** 29-45
[7] Bottasso C L, Campagnolo F and Petrović V 2014 Wind tunnel testing of scaled wind turbine models: Beyond aerodynamics *Journal of wind engineering and industrial aerodynamics* **127** 11-28
[8] Santoni C, Carrasquillo K, Arenas-Navarro I, Leonardi S 2017 Effect of tower and nacelle on the flow past a wind turbine *Wind Energy, preprint (under review)*
[9] Campagnolo F, Croce A, Manos E, Petrović V, Schreiber J and Bottasso C L 2016 Wind tunnel testing of a. closed-loop wake deflection controller for wind farm power maximization *Journal of Physics: Conference Series* **753**
[10] Campagnolo F, Petrović V, Bottasso C L and Croce A 2016 Wind tunnel testing of wake control strategies *Proceedings of the American Control Conference* 513-18
[11] Campagnolo F, Petrović V, Nanos E, Tan C, Bottasso C L, Paek I, Kim H, and Kim K 2016 Wind tunnel testing of power maximization control strategies applied to a multi-turbine floating wind power platform *Proceedings of the International Offshore and Polar Engineering Conference* 309-16
[12] Churchfield M and Lee S 2012 *NWTC design codes-sowfa* (USA: http://wind. nrel. gov/designcodes/simulator S./SOWFA)

[13] Churchfield M, Lee S, Moriarty P, Martinez L A, Leonardi S, Vijayakumar G, and Brasseur J 2012 large-eddy simulation of wind-plant aerodynamics *AIAA paper* **537** 2012

[14] Fleming P, Gebraad P, Lee S, van Wingerden J W, Johnson K, Churchfield M, Michalakes J, Spalart P and Moriarty P 2014 Evaluating techniques for redirecting turbine wakes using sowfa *Renewable Energy* **70** 211-18

[15] Howland M F, Bossuyt J, Martinez-Tossas L A, Meyers J and Meneveau C 2016 Wake structure of wind turbines in yaw under uniform inflow conditions *arXiv* (*preprint* arXiv:1603.06632)

[16] Jasak H, 1996 *Error analysis and estimation for finite volume method with applications to fluid flow* (UK: Imperial College London)

[17] Jasak H and Rigler D 2014 Finite volume immersed boundary method for turbulent flow simulations *9th OpenFOAM Workshop*

[18] Jasak H, Weller H and Gosman A 1999 High resolution nvd differencing scheme for arbitrarily unstructured meshes *International journal for numerical methods in fluids* **31(2)** 431-49

[19] Jonkman J and Buhl M L 2004 *Fast user guide* (USA: Technical report, EL-500-29798, National Renewable Energy Laboratory, Golden, CO)

[20] Martinez L A, Leonardi S, Churchfield M, and Moriarty P 2012 comparison of actuator disk and actuator line wind turbine models and best practices for their use. *AIAA Paper* **1** 2012-0900

[21] Moriarty P L and Craig H 2005 *Aerodyn user's guide* (USA: National Renewable Energy Laboratory)

[22] Mittal R and Iaccarino G 2005 Immersed boundary methods *Annu. Rev. Fluid Mech.* **37** 239-61

[23] Porté-Agel F, Wu Y T, Lu H and Conzemius R J 2011 Large-eddy simulation of atmospheric boundary layer flow through wind turbines and wind farms *Journal of Wind Engineering and Industrial Aerodynamics* **99(4)** 154-68

[24] Rhie C and Chow W 1983 Numerical study of the turbulent flow past an airfoil with trailing edge separation *AIAA journal* **21(11)** 1525-32

[25] Van Dooren M, Khn M, Petrović V, Bottasso C, Campagnolo F, Sjholm M, Angelou N, Mikkelsen T, Croce A and Zasso A 2016 Demonstration of synchronised scanning lidar measurements of 2d velocity fields in a boundary-layer wind tunnel *Journal of Physics: Conference Series* **753**

[26] Wang J, Bottasso C L and Campagnolo F 2016a Les modeling of a scaled wind farm facility in a boundary layer wind tunnel *4th Symposium on OpenFOAM in Wind Energy*

[27] Wang J, Bottasso C L and Campagnolo F 2016b Wake redirection: comparison of analytical, numerical and experimental models *Journal of Physics: Conference Series* **753**

[28] Wang J, Mclean D, Campagnolo F, Yu T and Bottasso C L 2017 Large-eddy simulation of waked turbines in a scaled wind farm facility *Journal of Physics: Conference Series, preprint (under review)*

[29] Zanotti A, Ermacora M, Campanardi G and Gibertini G 2014 Stereo particle image velocimetry measurements of perpendicular bladevortex interaction over an oscillating airfoil *Experiments in Fluids* **55** 1-13

# Verification and Calibration of a Reduced Order Wind Farm Model by Wind Tunnel Experiments



Wake Conference 2017 IOP Publishing
IOP Conf. Series: Journal of Physics: Conf. Series **854** (2017) 012041 doi:10.1088/1742-6596/854/1/012041

# Verification and Calibration of a Reduced Order Wind Farm Model by Wind Tunnel Experiments

**J Schreiber[1], E M Nanos[1], F Campagnolo[1], C L Bottasso[1,2]**

[1] Wind Energy Institute, Technische Universität München, Boltzmannstraße 15, D-85748 Garching bei München, Germany
[2] Dipartimento di Scienze e Tecnologie Aerospaziali, Politecnico di Milano, Via La Masa 34, I-20156 Milano, Italy

E-mail: {johannes.schreiber, em.nanos, filippo.campagnolo, carlo.bottasso}@tum.de

**Abstract.** In this paper an adaptation of the FLORIS approach is considered that models the wind flow and power production within a wind farm. In preparation to the use of this model for wind farm control, this paper considers the problem of its calibration and validation with the use of experimental observations. The model parameters are first identified based on measurements performed on an isolated scaled wind turbine operated in a boundary layer wind tunnel in various wind-misalignment conditions. Next, the wind farm model is verified with results of experimental tests conducted on three interacting scaled wind turbines. Although some differences in the estimated absolute power are observed, the model appears to be capable of identifying with good accuracy the wind turbine misalignment angles that, by deflecting the wake, lead to maximum power for the investigated layouts.

## 1. Introduction

In a wind farm environment wind turbine wakes, which are characterized by a lower wind speed and higher turbulence intensity than the free steam, can adversely affect other turbines. This in turn may lead to higher fatigue loads and a significantly reduced power output on affected turbines.

To increase total wind farm power and/or reduce fatigue loads, several techniques have been proposed [1, 2]. At present, one of the most promising approaches seems to be a technique where the wake is deflected by operating the wind turbine in yaw-misalignment condition with respect to the incoming wind [3]. In fact, as the wind turbine is yawed out of the wind, its wake is laterally deflected, which may reduce its interaction with downstream machines. Wind farm control strategies based on wake deflection have been proposed to increase the total energy capture and/or decrease fatigue loading [3, 4]. In this context, reduced order wind farm models as the FLORIS (FLOw Redirection and Induction in Steady-state) approach [4] may be used to enable model-based wind farm control.

This paper describes first a FLORIS-like wind farm model. Next, its parameters are calibrated based on wake measurements of a scaled wind turbine in a wind tunnel environment. Finally, the tuned model is used to estimate the wind farm power output for several different wind farm layouts comprising three scaled interacting wind turbines. For each layout, a variety of different yaw-misalignment combinations are tested and the turbine power is compared to the model-predicted one. Results and the causes for the observed mismatches are discussed.

Wake Conference 2017 IOP Publishing
IOP Conf. Series: Journal of Physics: Conf. Series **854** (2017) 012041 doi:10.1088/1742-6596/854/1/012041

## 2. Wind farm model

In this section a reduced order wind farm model is presented, following the work of Gebraad et al. [4]. In the present study, the model has been re-implemented with some modifications. First, the model describing expansion, reduction and deflection of a single wind turbine wake is presented. Next, the models that describe wind turbine power extraction and multiple wake interactions are presented. Finally, the process of calculating wind farm flow and power is summarized.

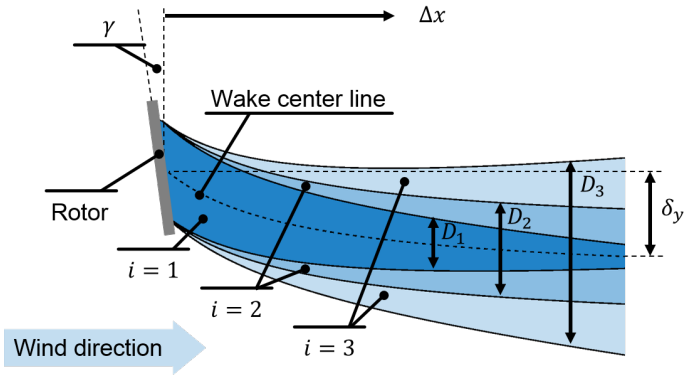


**Figure 1.** Wake model with three zones.

It is assumed that every wind turbine wake consists of three wake zones, as depicted in figure 1. In the generic wake zone $i$, the Jensen model [5] is used to describe wake expansion in terms of coefficient $k_{e,i}$. Experimental results suggest that the wake diameter of a turbine operated in a misaligned condition with respect to the wind direction is reduced (see the results section later on in this work). Taking this effect into account, the wake zone outer diameter is defined as

$$D_i(\Delta x, \gamma) = \max\left(0, (D + 2\Delta x k_{e,i})\cos(\gamma)^{k_{e,\gamma}}\right), \tag{1}$$

where $\Delta x$ is the distance downstream of the wind turbine, $D$ the rotor diameter, $\gamma$ the wind turbine yaw-misalignment angle and $k_{e,\gamma}$ a parameter that describes the reduced wake expansion due to wind turbine yaw-misalignment. As the wake zones can have a negative expansion coefficient, the wake diameter has to be limited to positive values.

The wake velocity in each wake zone is described by the Jensen wake model as

$$U_i(\Delta x) = U_\infty\Big(1 - r_i(\Delta x)\Big), \tag{2}$$

where $U_\infty$ is the ambient free stream velocity and $r_i$ the reduction factor defined as

$$r_i(\Delta x) = 2a\left(\frac{D}{D + 2\Delta x k_{r,i}}\right)^2, \tag{3}$$

where $a$ is the wind turbine induction and $k_{r,i}$ the wake reduction parameter of wake zone $i$.

The wake center line deflection due to yaw-misalignment is taken into account as described in [4], leading to

$$\delta_y(\Delta x, \gamma) = \frac{C_T(\gamma)\left(15(2k_d\frac{\Delta x}{D} + 1)^4 + C_T(\gamma)^2\right)}{30\frac{k_d}{D}(2k_d\frac{\Delta x}{D} + 1)^5} - \frac{C_T(\gamma)D\left(15 + C_T(\gamma)^2\right)}{30k_d}, \tag{4}$$

Wake Conference 2017 IOP Publishing
IOP Conf. Series: Journal of Physics: Conf. Series **854** (2017) 012041 doi:10.1088/1742-6596/854/1/012041

where $k_{\mathrm{d}}$ is the single parameter describing the recovery of the wake flow direction and $C_{\mathrm{T}}$ the turbine thrust coefficient, which in turn is defined as a function of the rotor induction $a$ and the yaw-misalignment as

$$C_T(\gamma) = \frac{1}{2}\cos(\gamma)^2 \sin(\gamma)\Big(4a(1-a)\Big). \tag{5}$$

For calculating the power extracted by a wind turbine, its rotor disk is split into $m$ discrete elements $e$. The turbine power is obtained by summing up the power extracted in each element

$$P = \sum_{e=1}^{m} \frac{1}{2}\rho A_e C_{\mathrm{P}}(\gamma) V_e^3, \tag{6}$$

where $\rho$ is the air density, $A_e$ the element area, $V_e$ the wind velocity at the discrete element and $C_{\mathrm{P}}(\gamma)$ the power coefficient expressed as a function of yaw-misalignment as

$$C_{\mathrm{P}}(\gamma) = C_{\mathrm{P},\gamma=0}\cos(\gamma)^{k_{\mathrm{P}}}. \tag{7}$$

Furthermore, $C_{\mathrm{P},\gamma=0}$ is the power coefficient of the turbine operating aligned with the wind, while $k_{\mathrm{p}}$ is the parameter taking into account power reduction due to yaw-misalignment. Speed $V_e$ is calculated based on the wake deficits of all upstream turbines

$$V_e = U_\infty\left(1 - \left(\sum_{w=1}^{n} r_w^2\right)^{\frac{1}{2}}\right), \tag{8}$$

where $n$ is the number of wake zones overlapping with the turbine rotor, while $r_w$ the reduction factor of a wake zone impinging the element. In case $n = 0$, no wake is impinging on the element and therefore $V_e = V_\infty$.

The implemented algorithm is organized as follows. First, the power and wake characteristics of the first upwind turbine is calculated. In a second step, the next wind turbine is considered and the wake position, reduction, and expansion of all upwind turbines are interpolated at the given downwind position. Based on this, the turbine power can readily be computed by equation (6) and (8). Finally, the turbine wake is also computed, using equations (1,2) and (4), and the second step is repeated until the last turbine is reached.

## 3. Results

### *3.1. Experimental setup*

The experiments described in this section were conducted with a scaled wind farm (see figure 2) composed of three identical scaled wind turbine models, longitudinally spaced 4 diameters (D) apart, whose rotor diameter is equal to 1.1 m (in the following named G1s for Generic 1 m diameter rotor), which were already used in other research projects [3, 6, 7]. The models were operated in the boundary-layer test section of the wind tunnel of the Politecnico di Milano, which has a cross-sectional area of 13.84 m by 3.84 m and a length of 36 m. Atmospheric boundary-layer conditions were simulated by the use of spires placed at the chamber inlet. The vertical profile of the longitudinal wind speed was measured prior to testing, resulting in the following best-fitted exponential law

$$U(z) = U_H\left(\frac{z}{z_H}\right)^{0.088}, \tag{9}$$

where $U_H \approx 5.7$ m/s and $z_H = 0.825$ m are the free-stream wind speed at hub height and the elevation of the rotor axis from the ground, respectively. The turbulence intensity (TI) at hub

Wake Conference 2017 IOP Publishing
IOP Conf. Series: Journal of Physics: Conf. Series **854** (2017) 012041 doi:10.1088/1742-6596/854/1/012041

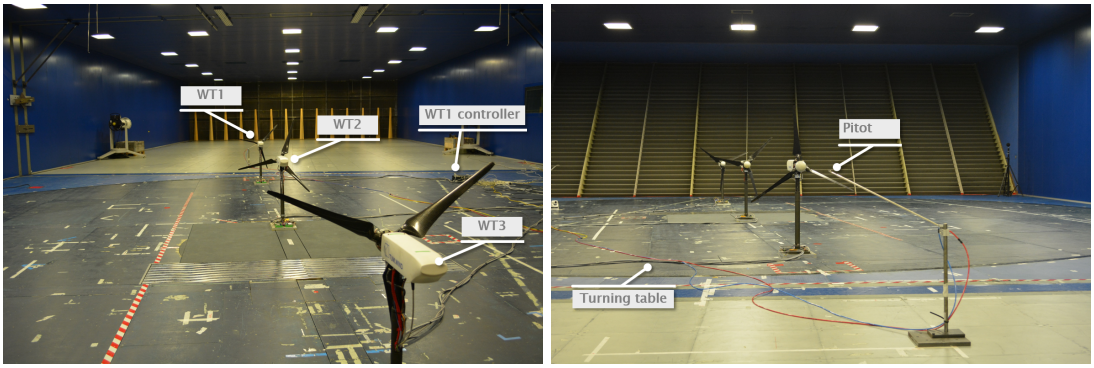


**Figure 2.** Wind farm layout in the wind tunnel.

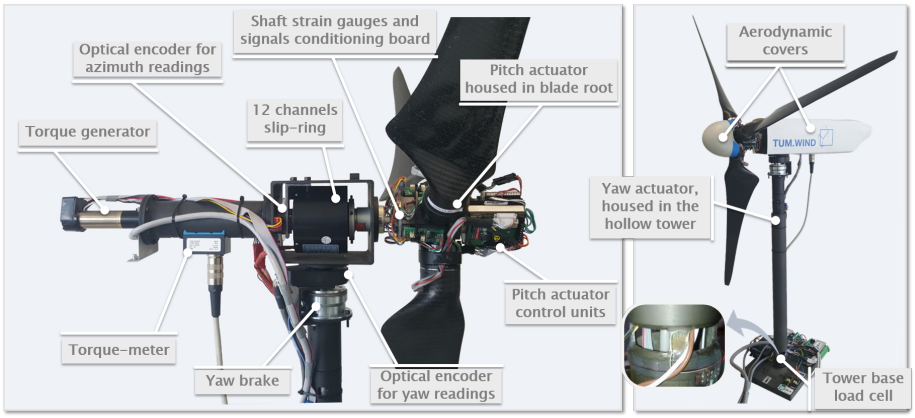


**Figure 3.** `G1` rotor-nacelle assembly (left) and overall model layout (right).

height was circa 5%. The undisturbed wind speed was measured by means of a pitot tube, also shown in figure 2, placed at hub height and 3D in front of the upstream model.

The dimensions of the model (see figure 3) are a compromise among the need for miniaturization, wind tunnel blockage, Reynolds effects and the need to realize multiple wind turbine interference conditions typical of wind farm operations. The scaled wind turbine is characterized by realistic aerodynamic performance, both at the airfoil and rotor levels, and generates a wake with shape, deficit and recovery that match closely the ones of a full scale machine. Moreover, the model features active individual pitch, torque and yaw control that, together with a comprehensive onboard sensorization of the machine (including measures of shaft and tower loads), enables the testing of modern control strategies.

Each model is controlled by a `M1 Bachmann` module that hard-real-time executes, similarly to what is done on real wind turbines, control laws similar to the ones described in [8] and references therein. In the present study, only operation below rated wind speed was considered. Therefore, the turbines were torque controlled according to a precomputed quadratic relation between rotor speed and torque.

### *3.2. Model parameter identification*

For the identification of the model parameters, the wake velocity of an isolated G1 wind turbine was measured with hot wire probes and compared to model-predicted velocities. In the wind

Wake Conference 2017 IOP Publishing
IOP Conf. Series: Journal of Physics: Conf. Series **854** (2017) 012041 doi:10.1088/1742-6596/854/1/012041

conditions described above (TI of circa 5%), wake measurements were available at hub height at several downwind distances (3D, 4D, 6D, 9D). In this first set of experiments, no wake measurements in yawed condition had been conducted ($\gamma = 0$). Therefore, a second set of experiments had to be used for identifying the parameters that influence the wake in case of yaw-misalignment ($k_{e,\gamma}$ and $k_d$). In this second set of experiments, TI was much lower (TI of circa 1%), but the wind turbine was operated with yaw-misalignments between $-20° < \gamma < +20°$. The wake velocity was measured at a distance of 4D downwind of the wind turbine, again at hub height.

For the parameter identification, the hot wire velocity measurements $V_{HW}$ were utilized to solve the minimization problem

$$\min_p \int (V_{HW}(x) - V_M(x,p))^2 \, dx, \tag{10}$$

where $x$ is the lateral position of the measurement, $V_M$ the model-predicted wake velocity for a set of model parameters $p$. The problem is solved by the Nelder-Mead simplex direct search algorithm implemented in the MATLAB function `fminsearch`. The wind turbine induction was obtained from a G1 blade element momentum simulation and set to $a = 0.35$ for operation below rated wind speed.

For the first set of experiments, the model parameters to be identified are defined as

$$p_1 = \{k_{e,1}, k_{e,2}, k_{e,3}, k_{r,1}, k_{r,2}, k_{r,3}\}. \tag{11}$$

Figure 4 shows the hot wire measurements $V_{HW}(x)$ (red dashed line) and the model-predicted wake velocity $V_M(x,p)$ (blue solid line) for the identified set of parameters. Only measurements at 4D were utilized for the identification (red solid line). The good quality matching of the profiles at 3D, 6D and 9D, since they were not used for calibrating the model, demonstrate its good generality.

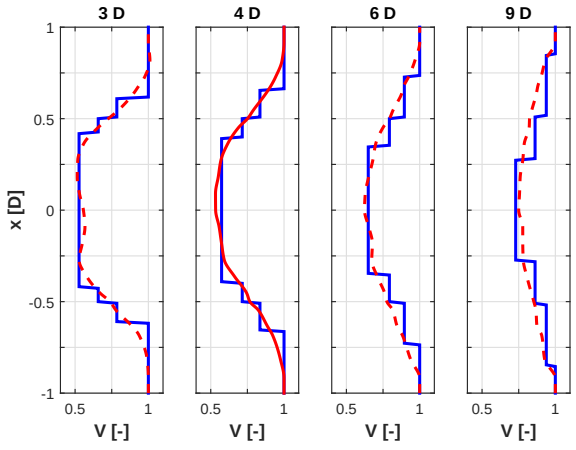


**Figure 4.** First measurement set (TI circa 5%), modeled (blue solid line) and measured (red solid and dashed lines) wake deficit for different distances behind the wind turbine.

To identify the wake parameters that play a role in turbine yaw-misalignment, the second set of experiments was used and the parameters to be identified by equation (10) were set to be

$$p_2 = \{k_{e,\gamma}, k_d\}. \tag{12}$$

Wake Conference 2017 IOP Publishing
IOP Conf. Series: Journal of Physics: Conf. Series **854** (2017) 012041 doi:10.1088/1742-6596/854/1/012041

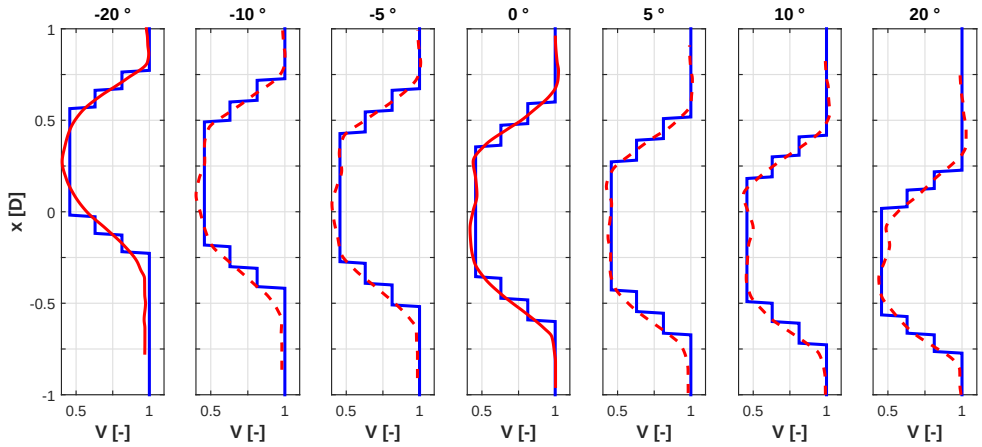


**Figure 5.** Second measurement set (TI circa 1%), modeled (blue solid line) and measured (red solid and dashed lines) wake deficit for different yaw-misalignments.

The parameters $p_1$ were re-identified for the low TI case to take the slower wake recovery of this different flow condition into account. Figure 5 shows the hot wire measurements $V_{\mathrm{HW}}(x)$ and the model-predicted wake velocity $V_{\mathrm{M}}(x, p)$ for the identified set of parameters. Again, the generality of the wake model is demonstrated by only taking the measurements of $\gamma = -20°$ and $\gamma = 0°$ into account during the identification. Note the wake diameter reduction in the cases characterized by larger yaw-misalignment. The modeled maximum wake diameter for $\gamma = 0°$ is 1.2D, whereas for $\gamma = \pm 20°$ the wake diameter is only 1D, giving a good fit with the wake measurements.

It is assumed that the parameters $k_{\mathrm{e},\gamma}$ and $k_{\mathrm{d}}$ are independent of TI. Therefore, they can be used to describe the wake also for the higher TI cases used in the wind farm experiments.

Parameter $k_{\mathrm{p}}$ was identified based on a subset of the wind farm experiments in which the first turbine yaw-misalignment was $-36° < \gamma < 0°$. In this subset, the first wind turbine experimental power coefficient $C_{\mathrm{P,Exp}}(\gamma)$ was calculated based on turbine power measurements and pitot tube measurements 3D in front of the hub, as shown in figure 6 (red circles). The squared error between the measured and modeled power coefficients, given by equation (7), was minimized with respect to the free parameters $k_{\mathrm{p}}$ and $C_{\mathrm{P},\gamma=0}$, yielding the modeled power coefficient shown in figure 6 (blue solid line). Coefficient $C_{\mathrm{P},\gamma=0}$ was included in the free parameters to account for a low precision in the pitot tube measurements.

The full set of identified model parameters is reported in Table 1. For the sake of completeness, Table 1 also reports the identified parameters for low TI, which correspond to Figure 5.

**Table 1.** Identified model parameters.

| | $k_{\mathrm{e},1}$ | $k_{\mathrm{e},2}$ | $k_{\mathrm{e},3}$ | $k_{\mathrm{r},1}$ | $k_{\mathrm{r},2}$ | $k_{\mathrm{r},3}$ | $k_{\mathrm{e},\gamma}$ | $k_{\mathrm{d}}$ | $k_{\mathrm{p}}$ |
|---|---|---|---|---|---|---|---|---|---|
| high TI | -0.0251 | 0.0011 | 0.0386 | 0.0320 | 0.0669 | 0.2130 | 2.8808 | 0.1219 | 1.7870 |
| low TI | -0.0363 | -0.0062 | 0.0236 | 0.0140 | 0.0433 | 0.1864 | 2.8808 | 0.1219 | 1.7870 |

Wake Conference 2017 IOP Publishing
IOP Conf. Series: Journal of Physics: Conf. Series **854** (2017) 012041 doi:10.1088/1742-6596/854/1/012041

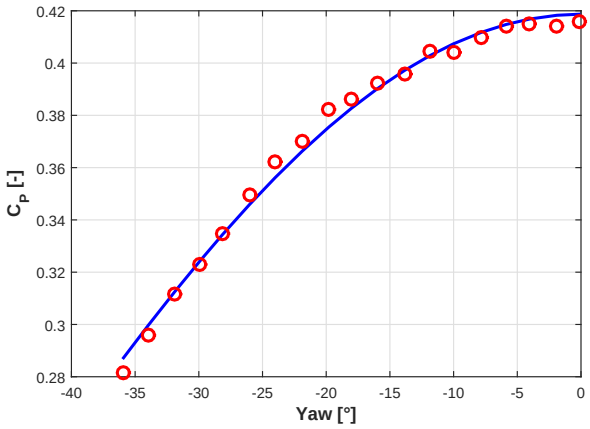


**Figure 6.** Measured (red circles) and modeled (blue solid line) power coefficients plotted as functions of wind turbine yaw-misalignment.

*3.3. Wind farm experiments*

In the wind farm experiments, three G1s were operated in the wind tunnel in three different layouts (noted A, B and C) as shown in figure 7. In each layout, the most upwind wind turbine is labeled WT1, the middle turbine is noted WT2, while the most downwind wind turbine is termed WT3. The turbines were torque controlled below rated wind speed, and the reduced order model assumed a constant operation of all turbines with $C_{\mathrm{P},\gamma=0} = 0.419$ and $a = 0.35$.

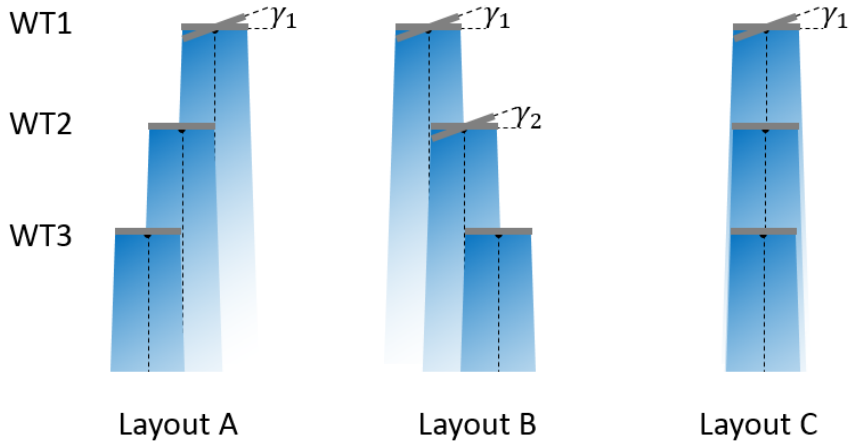


**Figure 7.** Wind farm layouts A, B, C with lateral displacements of ±0.5D and 0D. The longitudinal displacement is approximately 4D. Note that the sketch is not to scale.

First, for every layout several experiments were conducted with different yaw-misalignments of WT1 ($\gamma_1$), in order to deflect the wake away from the downstream turbines. For these experiments, figure 8 shows the power coefficient of all three wind turbines and the total wind farm in layouts A, B and C, as indicated by the column title. The red circles indicate the measured and the blue solid line the modeled power coefficient, respectively.

Wake Conference 2017 IOP Publishing
IOP Conf. Series: Journal of Physics: Conf. Series **854** (2017) 012041 doi:10.1088/1742-6596/854/1/012041

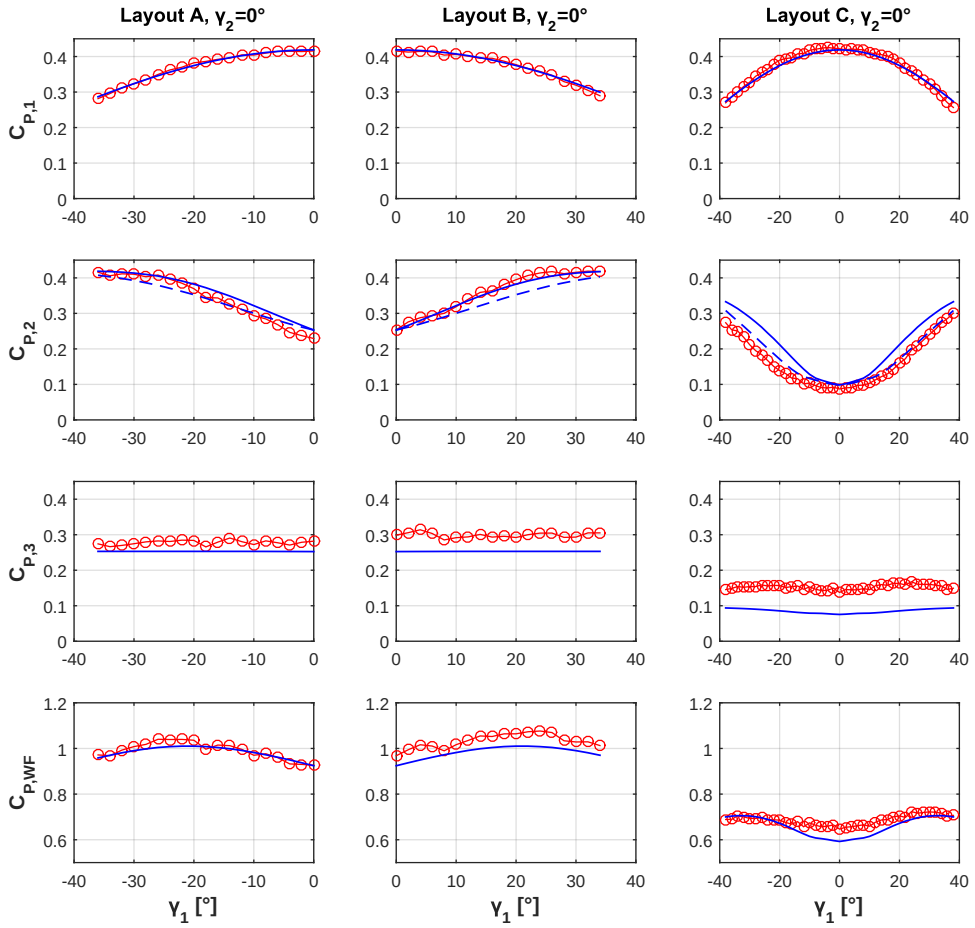


**Figure 8.** Measured (red circles) and modeled (blue solid line) power coefficient for WT1, WT2, WT3 and the total wind farm, for layouts A, B and C.

The first row of subplots shows the power coefficient of WT1 ($C_{\mathrm{P},1}$) in each layout. As expected from the identification of parameter $k_{\mathrm{p}}$, the model-predicted and measured results correlate very well.

The second row of subplots shows the power coefficient of WT2 ($C_{\mathrm{P},2}$). For $\gamma_1 = 0°$, the model predicts well the downwind turbine power for all layouts. However, a small asymmetric behavior in the measurements can be observed between the symmetric layouts A and B — perhaps due to asymmetric wake behavior or due to a small horizontal variation in the wind tunnel inflow speed. In the experiments of layout B, maximum power is reached already at $\gamma_1 \approx 25°$ and further upwind turbine yawing does not influence the second wind turbine power anymore. In the full wake case of layout C, the model significantly over-predicts power for $|\gamma_1| > 10°$. A first hypothesis that could explain this behavior is that the model predicts a slightly inaccurate wake location in the yawed cases (which is possible, given that the corresponding parameter was identified at a much lower TI). Indeed, simulations with a larger wake deflection parameter ($k_{\mathrm{d}} = 0.28$, see blue dashed line) show improved results for layout C, but the new parameter

Wake Conference 2017 IOP Publishing
IOP Conf. Series: Journal of Physics: Conf. Series **854** (2017) 012041 doi:10.1088/1742-6596/854/1/012041

affects also the results in layouts A and B, where now the modeled power coefficient exhibits an increased error. Results in layout C might improve by adjusting the model in such a way that in yaw-misalignment conditions the wake speed decreases or the wake diameter reduces further than currently predicted, but this would worsen the results in layouts A and B. The previously mentioned slight lateral variation in the inflow speed, which cannot be captured by the use of a single pitot tube, could also be a partial cause of the mismatch seen here. It is also possible that the wake deflection position is affected by the downwind turbine position. Understanding the reasons causing these discrepancies will be part of further studies, involving additional wind farm flow measurements.

The third row of subplots shows the power coefficient of WT3 ($C_{\mathrm{P},3}$). In layout A and B, no significant $\gamma_1$-dependency can be observed in the experiments as well as in the model. Nevertheless, the power is constantly under-predicted. The cause might be a faster wake recovery of the wake of WT2 that, operating within the wake of WT1, experiences a higher turbulence intensity, leading to a faster wake mixing. Conversely, a strongly deflected wake (i.e. $|\gamma_1| > 25°$) should in that case also lead to lower power at WT3 — an effect that however is not observed in the experiments. Again, further studies and measurements are necessary to better explain this contradiction. For layout C, the power of WT3 is clearly affected by $\gamma_1$. The model correctly predicts an increase of power for increased $\gamma_1$. However, above $|\gamma_1| > 20°$ the experimental results show a decrease of power, which might be caused by a slower wake recovery of the WT2 wake compared to the full wake case ($\gamma_1 = 0$).

The total power coefficient of all three wind turbines ($C_{\mathrm{P,WF}} = C_{\mathrm{P},1} + C_{\mathrm{P},2} + C_{\mathrm{P},3}$) is shown in the last row of figure 8. Taking into account the discrepancies noted above, the overall correlation is rather good. In layouts A and B the predicted power achieves a maximum for $|\gamma_1| = 20°$, which correlates well with the experimental data. In the full wake case, the predicted power is maximum at $|\gamma_1| = 34°$, which again correlates well with the experimental data.

For layout B, experiments were also conducted in which WT2 is operating in yaw-misalignment ($\gamma_2$). Figure 9 shows experiments in which WT2 is yawed by $\gamma_2 = 8°$ (first column), $\gamma_2 = 18°$ (second column) and $\gamma_2 = 28°$ (third column). The power of WT1 is again well predicted. For WT2 the modeled and measured power decreases for increased $\gamma_2$, even though the model under-predicts this effect slightly at higher $\gamma_2$. The power of WT3 increases as expected with increased $\gamma_2$. Surprisingly, for $\gamma_2 = 28°$ the WT3 power exceeds the maximum power coefficient in four experiments — possibly due to a flow acceleration just outside of the wakes of WT1 and WT2. The total power of all three turbines follows the trend of the experiments, but the previously observed power over-prediction becomes smaller for increased $\gamma_2$, mainly due to the under estimation at WT2 and the smaller error at WT3.

The full set of experiments, not shown here for brevity, includes all combinations of $\gamma_1$ and $\gamma_2$ in steps of 2° around the point of maximum power. By using this data, the experimental optimum yaw configuration could be readily identified and was found to be at $\gamma_1 = 20°$ and $\gamma_2 = 16°$. The model-predicted point of maximum wind farm power was on the other hand found to be located at $\gamma_1 = 20°$ and $\gamma_2 = 22°$.

## 4. Conclusions and outlook

In this paper, the parameters of a reduced order wind farm model were identified with the help of wake measurements along a hub-height horizontal line for an isolated wind turbine. The modeled wakes are in good agreement with the measurements, even though only a small subset of the measurements were taken into account for the model identification procedure.

For three different wind farm layouts, including a variety of yaw angles of the two upstream wind turbines, the model-predicted wind turbine power coefficient was compared with experimental measurements. The comparison shows a good correlation in the overall trends, but the absolute values are not always well predicted especially for the last downstream wind turbine.

Wake Conference 2017 IOP Publishing
IOP Conf. Series: Journal of Physics: Conf. Series **854** (2017) 012041 doi:10.1088/1742-6596/854/1/012041

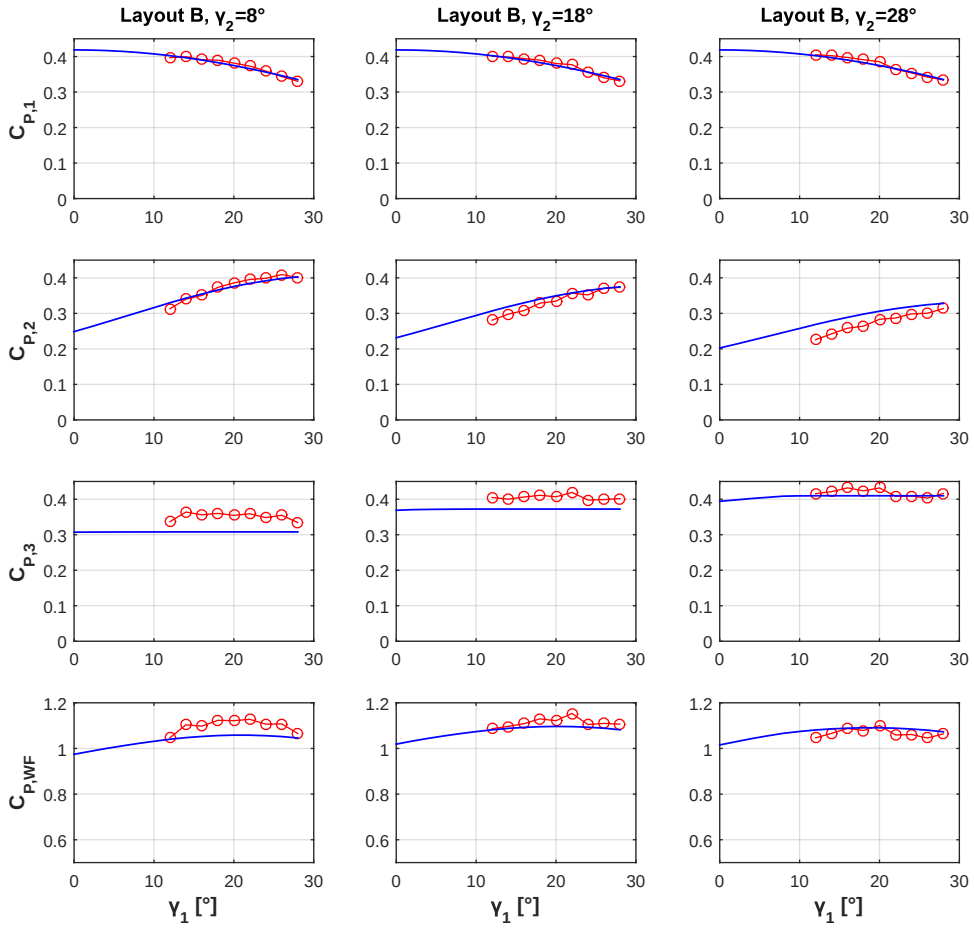


**Figure 9.** Measured (red circles) and modeled (blue solid line) power coefficient for WT1, WT2, WT3 and the total wind farm, for layout B for different $\gamma_2$ values.

The causes are believed to be a combination of various effects, including a faster recovery of wakes shed by waked turbines, flow acceleration outside the wakes, lateral flow speed variations in the wind tunnel, Reynolds number effects in the experiments, the assumption of a uniform power coefficient on each rotor, the assumption of axisymmetric wakes and certainly additional not modeled and fully understood effects like the influence of the downwind turbines on the upstream wake development.

Regardless of these open questions, it is important to note that the employed rather simplistic wind farm model, after a tuning by wake measurements, predicts well the operating point of maximum wind farm power. This is a promising result in view of the use of the model for wind farm control. It is also worth noting that the power gradient is very small around the optimum yaw angles for all studied layouts, implying that for wind farm control purposes a rough estimation of the optimum yaw configuration should be enough to harvest most of its potential.

Future work will try to clarify the open points and improve the model, taking into account

the various deficiencies stated above. In addition, rotor load-based wind estimation and wake detection techniques [9] will be coupled with the model for the development of robust model-based closed-loop wind farm control.

**Acknowledgments**
The authors wish to thank Dr. Vlaho Petrović for his help in the preparation and realization of the experiments, and Mr. Amr Balbaa for the assistance with the parameter identification.

This research was partially supported by the European Union Horizon 2020 research and innovation program under the Marie Skłodowska-Curie grant agreement No. 642108, and it was also partially supported by the German Federal Ministry for Economic Affairs and Energy (BMWi) within the CompactWind project (FKZ: 0325492D).

**References**

[1] Wang J, Bottasso C L and Campagnolo F 2016 Wake redirection: comparison of analytical, numerical and experimental models *Journal of Physics: Conference Series* **753** 32064
[2] Fleming P A, Gebraad P M O, Lee S, van Wingerden J-W, Johnson K, Churchfield M, Michalakes J, Spalart P and Moriarty P 2014 Evaluating techniques for redirecting turbine wakes using SOWFA *Renewable Energy* **70** 211-8
[3] Campagnolo F, Petrović V, Schreiber J, Nanos E M, Croce A and Bottasso C L 2016 Wind tunnel testing of a closed-loop wake deflection controller for wind farm power maximization *Journal of Physics: Conference Series* **753** 32006
[4] Gebraad P M, Teeuwisse F W, Van Wingerden J W, Fleming P A, Ruben S D, Marden J R and Pao L Y 2016 *Wind Energy* **19** 95–114 ISSN 10954244
[5] Jensen N O 1983 A note on wind generator interaction (Roskilde, Denmark: Risø National Laboratory)
[6] Campagnolo F, Petrović V, Bottasso, C L and Croce A 2016 Wind tunnel testing of wake control strategies *Proceedings of the American Control Conference* 513–518
[7] Campagnolo F, Petrović V, Nanos E M, Tan C W, Bottasso C L, Paek I, Kim H and Kim K 2016 Wind tunnel testing of power maximization control strategies applied to a multi-turbine floating wind power platform *Proceedings of the International Offshore and Polar Engineering Conference* 309–316
[8] Bossanyi, E 2000 The design of closed loop controllers for wind turbines *Wind Energy*, **3** 149–163.
[9] Schreiber J, Cacciola S, Campagnolo F, Petrović V, Mourembles D and Bottasso C L 2016 Wind shear estimation and wake detection by rotor loads - First wind tunnel verification *Journal of Physics: Conference Series* **753** 32027

https://doi.org/10.5194/wes-2021-66
Preprint. Discussion started: 6 July 2021


eawe european academy of wind energy
Open Access WIND ENERGY SCIENCE DISCUSSIONS

# Design, performance and wake characterization of a scaled wind turbine with closed-loop controls

Emmanouil M. Nanos[1], Carlo L. Bottasso[1], Filippo Campagnolo[1], Stefano Letizia[2], G. Valerio Iungo[2], and Mario A. Rotea[2]

[1]Wind Energy Institute, Technische Universität München, Garching bei München, D-85748, Germany
[2]Center for Wind Energy, Mechanical Engineering, University of Texas at Dallas, 800 W. Campbell Road, Richardson, TX 75080-3021, USA

**Correspondence:** C.L. Bottasso (carlo.bottasso@tum.de)

**Abstract.** This paper describes the design and characterization of a scaled wind turbine model, conceived to support wake and wind farm control experiments in a boundary layer wind tunnel. The turbine has a rotor diameter of 0.6 meters, and was designed to match the circulation distribution of a target conceptual full-scale turbine at its design tip speed ratio. In order to enable the testing of plant-level control strategies, the model is equipped with closed-loop pitch, torque and yaw control, and is sensorized with integrated load cells, as well as with rotor azimuth and blade pitch encoders.

After describing the design of the turbine, its performance and wake characteristics are assessed by conducting experiments in two different wind tunnels, in laminar and turbulent conditions, collecting wake data with different measurement techniques. A large-eddy simulator coupled to an actuator-line model is used to develop a digital replica of the turbine and of the wind tunnel. For increased accuracy, the polars of the low-Reynolds airfoil used in the numerical model are tuned directly from measurements obtained from the rotor in operation in the wind tunnel. Results indicate that the scaled turbine performs as expected, measurements are repeatable and consistent, and the wake appears to have a realistic behavior in line with expectations and with a similar slightly larger scaled model turbine. Furthermore, the predictions of the numerical model are well in line with experimental observations.

## 1 Introduction

Over the last decade, wind tunnel tests conducted with miniature wind turbine models have gained an increase attention from the research community (Bottasso and Campagnolo, 2020). The main focus of recent studies conducted with scaled turbines has been on wakes, including the characterization of the effects of the turbine operating conditions, of inflow profiles, and of thermal stability, and the testing of plant control strategies, as reported by —among many others— Chamorro and Porté-Agel (2009, 2010); Hu et al. (2012); Iungo et al. (2013); Bottasso et al. (2014b); Viola et al. (2014); Bastankhah and Porté-Agel (2015); Howard et al. (2015); Yang et al. (2016); Campagnolo et al. (2016b); Bastankhah and Porté-Agel (2016, 2017c); Wang et al. (2017); Schreiber et al. (2017a); Campagnolo et al. (2020). Even though far from exhaustive, this list of references clearly illustrates the diversity of topics where scaled wind turbine models have been profitably used for wind energy research. Indeed, today scaled experiments in the known, controllable and repeatable conditions of the wind tunnel play a significant role in the

https://doi.org/10.5194/wes-2021-66
Preprint. Discussion started: 6 July 2021


eawe european academy of wind energy
Open Access WIND ENERGY SCIENCE DISCUSSIONS

understanding of the physics, they support the development of mathematical models and the validation of simulation tools, and enable the testing of new ideas and technologies in preparation for full-scale demonstration.

The vast majority of the literature focuses on the results of the experiments, but the wind turbine models are typically only superficially described. There is only a handful of articles that address the methodology behind the design of scaled models and/or provide some assessment of their characteristics. Trying to fill this gap is one of the goals of this work, which provides a detailed description of the design and characterization of a new miniature wind turbine.

In Canet et al. (2021), the authors consider the laws that govern steady and transient gravo-aeroelastic scaling of wind turbine rotors, resulting in probably the most comprehensive analysis of the problem of scaling to the present date. A similar analysis is also developed in Bottasso and Campagnolo (2020), and forms the basis for a description of the design of scaled wind turbines for wind tunnel testing. Scaling analysis forms also the theoretical backbone of the study presented in Wang et al. (2020a), aimed at understanding the realism of the wakes generated by scaled models with respect to full-scale reality.

The aeroelastically scaled turbine of Bottasso et al. (2014b) and Campagnolo et al. (2014) is one of the first models described in some detail in the literature. With a rotor diameter of 2 meters, this turbine is relatively large in size. Accordingly, it has been primarily used in the large boundary layer test section of the wind tunnel at Politecnico di Milano, which features a 3.84 m (height) by 13.84 m (width) by 36 m (length) test section. The authors matched the relative placement of the lowest natural frequencies of rotor, drivetrain and tower with respect to the rotor rotating frequency, and equipped the blades with low-Reynold airfoils to guarantee a sufficiently high efficiency notwithstanding the small chord length. In addition, the model is equipped with active individual pitch and torque control; a second-generation version of the model is also capable of active yaw control. Strain gages measure loads on the blades, shaft and tower. Bottasso et al. (2014b) present applications related to wind turbine controls, including emergency shutdown maneuvers, individual pitch control for load alleviation in waked conditions, and the demonstration of an observer of the rotor inflow based on blade load harmonics (see Bertelé et al. (2021) and references therein).

Most other models described in the literature are comparatively smaller in size. The development of a scaled model with a rotor diameter of 0.58 m is presented in Schottler et al. (2016). The rotor aerodynamics are designed with a blade element momentum (BEM) formulation, and the model is equipped with closed-loop active pitch and torque control. BEM is used also in Lanfazame et al. (2016) to evaluate the effects caused on miniature wind turbine blades by the low chord-based Reynolds flow conditions (Winslow et al., 2018). The authors designed, manufactured and tested two rotors, one of 0.45 m and one of 0.225 m of diameter. The performance of the two rotors measured in wind tunnel tests was compared against BEM and 3D CFD simulations. Kelley et al. (2016) present a methodology for designing scaled wind turbine rotors for wake similarity.

Bastankhah and Porté-Agel (2017b) give a quite comprehensive description of a scaled wind turbine with a rotor diameter of 0.15 m and fixed pitch. The model blades employ a cambered plate because of the low chord-based Reynolds, resulting in a maximum power coefficient of 0.4 for a fairly low tip speed ratio (TSR) equal to 4, which probably limits the realism of the wake immediately downstream of the rotor disk when compared to current full-scale designs. The wake of the model is extensively characterized in Bastankhah and Porté-Agel (2017c), which report speed deficits, turbulence intensity, momentum turbulent fluxes, meandering motions and loads on downstream machines.

https://doi.org/10.5194/wes-2021-66
Preprint. Discussion started: 6 July 2021


eawe european academy of wind energy
Open Access WIND ENERGY SCIENCE DISCUSSIONS

A larger model is the G1 scaled turbine (Campagnolo et al., 2016b; Bottasso and Campagnolo, 2020), which has a 1.1 m diameter rotor, a power coefficient of 0.42 at a TSR of 7.5, and features closed-loop individual pitch, torque and yaw control. The rotor matches the circulation distribution of a conceptual full-scale reference at the design TSR, resulting in a realistic wake even relatively close to the rotor disk —except for the effects of the nacelle, which is comparatively larger than the one of the reference (Wang et al., 2020a). This turbine has been extensively used for wind farm control experiments and for the validation of wake models and CFD simulations (Campagnolo et al., 2016b; Schreiber et al., 2017b; Wang et al., 2019, 2020a; Bottasso and Campagnolo, 2020), here again exploiting the large dimensions of the wind tunnel in Milano to accommodate small clusters of wake-interacting turbines.

One of the principal design choices for a scaled wind turbine is its size. The literature shows that this choice implies crucial tradeoffs. In fact, smaller models alleviate the problem of blockage (Barlow et al., 1999), i.e. the effects on the flow —and hence also on the tested object— caused by the finite size of the test section. Smaller models can be tested in relatively small-size wind tunnels or, in larger facilities, allow for more numerous clusters of models to be simulated, for example in support of the study of multiple-wake interactions (Campagnolo et al., 2016b, 2020) or deep-array effects. A small size, however, limits the complexity of the model because of miniaturization and power density constraints (Bottasso and Campagnolo, 2020); additionally, a small size leads also to very low chord-based Reynolds numbers, which may limit the aerodynamic characteristics of the model. On the other hand, larger sizes enable advanced features —as for example closed-loop controls, aeroelastic scaling, and a more comprehensive sensorization—, and therefore more sophisticated applications. While a larger size relaxes somewhat the constraints due to Reynolds and miniaturization, on the other hand it also fundamentally limits the use of the models because of blockage.

Against this background, the aim of the present study is the design of a scaled turbine with similar characteristics to the G1, but with a smaller size. The main design requirements for this new turbine are the following:

- The turbine should be smaller than the G1 to expand the range of usable wind tunnels, to allow deeper array configurations than the three G1s in a row that can be tested in Milano, and it should be usable for complex terrain studies as the one described in Nanos et al. (2020).
- Despite its smaller size, the rotor should generate realistic wakes, even in the near-wake region (Wang et al., 2020a) to support the study of closely-spaced configurations.
- The model should feature closed-loop controls, to enable wind farm control studies, and should install sensors to measure loads.

It is another goal of this work to contribute to the literature, by providing a detailed description of the design, manufacturing and characterization of this new scaled wind turbine.

The material is organized as follows. Section 2 describes the design methodology and gives an overview of the model characteristics. Then, Sect. 3 presents the main performance characteristics of the turbine and its wake. Finally, Sect. 4 summarizes the main findings and gives an outlook towards future work.

https://doi.org/10.5194/wes-2021-66
Preprint. Discussion started: 6 July 2021


eawe european academy of wind energy
Open Access WIND ENERGY SCIENCE DISCUSSIONS

## 2 Model description and design methodology

### 2.1 General description

Figure 1 shows the model with its principal components, while the main turbine characteristics are reported in Table 1. The model features a 0.6 m three-bladed clockwise rotating rotor, and a hub height of 0.64 m. It is equipped with load sensors on the shaft and at tower base. Collective pitch control is realized by an actuator and bevel gear system integrated in the hub, while active yaw control is achieved with a standalone turning base. In the nacelle, two ball bearings support the shaft, which carries a slip ring to serve the pitch actuator and shaft load sensors; an optical encoder placed immediately behind the slip ring provides the rotor azimuthal position. A torque-meter is placed behind the aft shaft bearing, while the torque actuator is placed at the very end of the drive train. More details on the various model sub-systems are given in the following sections.

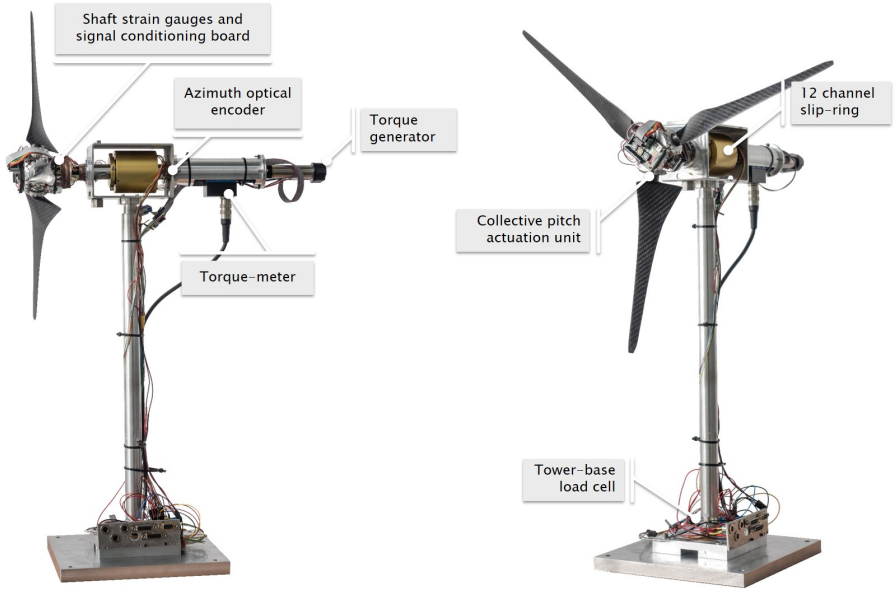


**Figure 1.** The G06 turbine with its main components.

### 2.2 Sizing of the model

As previously argued, one of the principal design choices requires the determination of the general model size, and in particular of the rotor diameter upon which many other dimensions eventually depend. Since a compact size is a basic requirement for this new model, the aim is to reduce the rotor diameter as much as possible. However, other design requirements impose constraints on how small the rotor can be:

https://doi.org/10.5194/wes-2021-66
Preprint. Discussion started: 6 July 2021


eawe european academy of wind energy
Open Access WIND ENERGY SCIENCE DISCUSSIONS

**Table 1.** Basic characteristics of the G06 scaled turbine.

| | |
|---|---|
| Nr. of blades | 3 |
| Rotation | Clockwise |
| Airfoil | RG-14 |
| Rotor diameter | 0.6 m |
| Hub height | 0.64 m |
| Rated wind speed | 10 $ms^{-1}$ |
| Rated power | 65 W |
| Active pitch control | Yes (collective) |
| Active torque control | Yes |
| Active yaw control | Yes (separate mechanism) |

– The model should be usable for simulating wake effects, including wake-induced loads, and for supporting wind farm control applications. These usage scenarios imply that:

  1. Load-induced strains should be high enough to guarantee a sufficient precision of the measurements obtained from the installed transducers, notwithstanding the small aerodynamic loads. In the present case, this requirement was one of the main drivers of the geometric scaling factor.

  2. The actuators and control hardware and software should be fast enough, accounting for the fact that down-scaling implies an acceleration of time with respect to the full-scale case (Bottasso et al., 2014b). This has also a strong effect on power density, which grows rapidly with time scaling (Bottasso and Campagnolo, 2020).

– Very small sizes increase the influence of manufacturing imperfections on blade aerodynamics, leading to performance deterioration and/or discrepancies among different blades (which cause rotor imbalances and differences of behavior among different models). More importantly, very small blades operate in low chord-based Reynolds conditions, which negatively influence aerodynamic performance. Wiring and miniaturization become also increasingly difficult with smaller sizes.

Other Reynolds-related conditions have an effect only for extremely small models, which however are not suitable for the present controls-oriented applications. In fact, wake behaviour is independent from the rotor-based Reynolds number when this parameter is larger than circa $10^5$ (Chamorro et al., 2012). Similarly, Reynolds-independent flows over complex terrains are obtained for terrain-height-based Reynolds numbers above $10^4$ (McAuliffe and Larose, 2012). Unless extremely small scale factors are considered, these conditions are readily met when testing in air in tunnels that produce wind speeds of the same order of magnitude of full-scale flows.

Considering these various requirements and constraints, the rotor diameter was finally chosen as D$= 0.6$ m.

https://doi.org/10.5194/wes-2021-66
Preprint. Discussion started: 6 July 2021


eawe european academy of wind energy
Open Access WIND ENERGY SCIENCE DISCUSSIONS

### 2.3 Rotor aerodynamic design

#### 2.3.1 General considerations

The DTU 10 MW wind turbine (Bak et al., 2013) is chosen as a baseline full-scale reference for the scaling of the G06. This machine has a rotor diameter of 178.3 m, an optimum TSR $\lambda_{\text{opt}} = 8$ and a rated wind speed of 11.4 ms$^{-1}$.

The detailed aerodynamic design of the rotor aims at defining the geometry of the blade (airfoil profile(s), twist and chord distributions) that fulfills the requirements. Ideally, one would like to achieve an exact kinematic and dynamic flow similarity between scaled and reference wind turbine rotors. Kinematic similarity translates into flow streamlines that are geometrically similar, and it is directly connected to the matching of TSR. Dynamic similarity implies that the ratio of the forces acting on the model and full-scale airfoils is matched; this is a more difficult condition to achieve, as it would require matching the chord-based Mach and Reynolds numbers (for a more in-depth discussion on the topic of scaling, see Anderson (2001) and Bottasso and Campagnolo (2020)).

For the Mach number it is sufficient to guarantee that an upper bound is not exceeded, in order to ensure the absence of compressibility effects (Bottasso and Campagnolo, 2020). The situation is, however, quite different for the Reynolds number. In fact, when testing in air, Reynolds scales as $\text{Re}_M/\text{Re}_F = n^2/n_t = nn_v$ (Canet et al., 2021; Bottasso and Campagnolo, 2020), where $\text{Re}_M$ is the Reynolds number of the scaled model and $\text{Re}_F$ the one at full scale, $n$ is the geometric scaling factor, $n_t$ is the time scaling, and $n_v = n/n_t$ is the scaling of speed. Bottasso and Campagnolo (2020) present a detailed analysis of the effects of scaling on chord-based Reynolds, including those caused by changes of chord solidity (see Fig. 1.1 of that paper). However, even a rough order-of-magnitude calculation shows the nature of the problem. In fact, scaling down the 10 MW DTU rotor to the 0.6 m diameter of the G06, implies that $n \approx 3.3 \cdot 10^{-3}$. Additionally, typical testing speeds in the boundary layer wind tunnel in Milano are around 5 ms$^{-1}$; such a value, assuming experiments conducted around the full-scale rated wind speed, leads to $n_v \approx 1/2$. In these conditions the Reynolds mismatch is $\mathcal{O}(10^{-3})$, which is a substantial difference. Incidentally, notice that this implies $n_t = \mathcal{O}(10^{-2})$, which means that time flows about two orders of magnitude faster in the experiment than in reality. While this is a benefit in terms of data collection time (one day at full scale reduces to about 15 minutes in the tunnel), it is also a drawback in terms of real-time control, actuation rate, and sampling requirements.

Aerodynamic efficiency is defined as $E = C_L/C_D$, where $C_L$ and $C_D$ are the lift and drag coefficients, respectively. In general, typical airfoils suffer from a drastic drop in aerodynamic efficiency below a Reynolds number of about 70,000 (Selig et al., 1995) because of the formation of a laminar separation bubble. In addition, as shown in Fig. 2, at these low Reynolds a standard wind turbine airfoil as S-806 (Tangler, 1987) suffers from multiple stall-reattachment cycles even at small angles of attack. An improved behavior is obtained by ad hoc low-Reynolds airfoils, such as the RG-14 profile (Selig et al., 1995). Notice however that the efficiency of these special airfoils is lower than the one of typical wind energy airfoils when operating at full-scale; for example, the RG-14 has an efficiency of 33.3 for a Reynolds of $5 \cdot 10^4$, while the efficiency of S-806 is about 120 for a Reynolds of $10^6$. In the end, this limits the achievable maximum power coefficient of scaled rotors. Based on these considerations, the G06 blade uses the RG-14 over its entire span, with the exception of the root region in close proximity of

https://doi.org/10.5194/wes-2021-66
Preprint. Discussion started: 6 July 2021


eawe european academy of wind energy
Open Access WIND ENERGY SCIENCE DISCUSSIONS

the pitch bearing. Tripping, which can be employed for triggering the boundary layer transition and eliminate or reduce the laminar bubble (Selig and McGranahan, 2004), is not used on the G06 blades because it is not effective on low-camber airfoils.

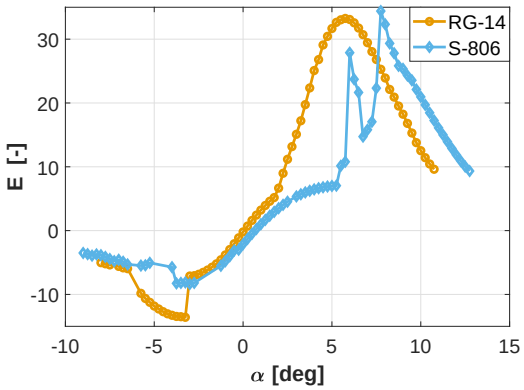


**Figure 2.** Airfoil efficiency $E$ vs. angle of attack $\alpha$ for the high Reynolds S-806 airfoil (blue line and $+$ symbols) and the low Reynolds RG-14 airfoil (red line and $\circ$ symbols). The characteristics of both airfoils are evaluated at Re$= 50,000$ using Xfoil (Drela).

Wake similarity is obtained by matching the geometry and strength of the vortex filaments released by the blades (Canet et al., 2021; Bottasso and Campagnolo, 2020).

The correct vortex geometry is obtained by ensuring kinematic similarity, i.e. matching the TSR $\lambda = \Omega R/U$, where $\Omega$ is the rotor speed, $R = D/2$ the rotor radius, and $U$ the ambient wind speed.

On the other hand, the correct strength of the vortex filaments is obtained by matching the spanwise circulation distribution. According to Prandtl lifting line theory (Anderson, 2001), a blade can be represented as a superposition of vortices of strength $\Gamma$ (circulation). Due to Helmholtz's theorem, each vortex extends as two free vortices trailing downstream all the way to infinity. Biot-Savart law states that each filament induces a velocity $w = \Gamma/4\pi h$ at an arbitrary point located at a filament-orthogonal distance $h$ away. Eventually, the velocity at any point in the flowfield is the combination of the free-stream velocity and the velocities induced by all vortex filaments at that point. The lift per unit span $\mathrm{d}L$ at a blade segment of span $\mathrm{d}r$ is related to the circulation $\Gamma$ of this segment by the Kutta-Joukowski theorem:

$$\mathrm{d}L = \rho W \Gamma \mathrm{d}r, \tag{1}$$

where $\rho$ is air density, $W$ is the relative flow velocity, lift is $\mathrm{d}L = 1/2\rho W^2 c C_L \mathrm{d}r$, where $c$ is the chord length. Inserting the expression for lift into Eq. (1) and nondimensionalizing by the free stream velocity and the rotor radius yields:

$$\Gamma' = \frac{C_L}{2}\frac{W}{U}\frac{c}{R}. \tag{2}$$

Wake similarity is obtained by matching the circulation distribution, as expressed by Eq. (2), along the span of the scaled and reference turbines.

https://doi.org/10.5194/wes-2021-66
Preprint. Discussion started: 6 July 2021


eawe european academy of wind energy
Open Access WIND ENERGY SCIENCE DISCUSSIONS

### 2.3.2 Rotor design methodology

The rotor design problem is formulated as the following constrained optimization:

$$C_P^* = \max_{\theta,c} C_P\left(\theta, c, D, \lambda_{\text{opt}}, \Omega_{\text{scaled,rated}}\right), \tag{3a}$$

$$\text{s.t.:} \quad \Gamma_i' = \Gamma_i'^{\text{ref}}, \quad i = [1, N], \tag{3b}$$

$$\text{Re}_{av.} \geq 70,000, \tag{3c}$$

where the power coefficient is $C_P = P/(0.5\rho U^3 \pi R^2)$, $P$ indicates power, and subscript $i$ stands for a generic spanwise control section along the blade.

The optimization problem seeks the blade twist $\theta$ and chord $c$ distributions that maximize the rotor power coefficient $C_P$. The power coefficient is estimated by using BEM (Burton et al., 2001), and chord and twist distributions are discretized using splines. The optimal design problem is solved using the Interior Point Method, as implemented in Matlab (Mathworks, 2019).

The optimization is constrained by the matching of the nondimensional circulation at a number $N$ of spanwise control stations. A second constraint condition sets a lower limit for the average Reynolds number along the blade, which can be met by the optimizer by locally increasing the chord with respect to the one of the reference turbine. Since there is no explicit constraint on solidity, it should be noted that the maximum power coefficient of the scaled rotor is not necessarily coincident with the optimum TSR $\lambda_{\text{opt}}$ of the reference rotor (Bottasso and Campagnolo, 2020), which is however not a concern in this case.

The rated rotor speed of the scaled model, $\Omega_{\text{scaled,rated}} = 2,250$ rpm, was primarily determined by the requirement to avoid compressible effects over the blade, as expressed by the condition $\Omega_{\text{scaled,rated}} R/c_s \leq 0.3$, $c_s$ being the speed of sound.

### 2.3.3 Blade shape and fabrication

The methodology described in the previous section resulted in the blade geometry shown in Fig. 3 in terms of chord and twist distributions.

Criteria for the choice of the blade material and of the manufacturing technology were rigidity (to avoid deformations in operation), high precision and consistency (to ensure similar blades), and lifetime (on account of the high rotor speed and hence large expected number of cycles).

The blade comprises of three parts: the carbon fiber skin, which determines the external shape of the blade and carries the loads, a foam filler in Rohacell, and an aluminum root used to connect with the pinion gear.

The manufacturing process uses a high-precision aluminum female mold in two halves. Each mold half is laminated with carbon fiber sheets of 0.25 mm of thickness, using two plies close to the root and one from mid-span onwards towards the tip. The metal root is then inserted into position. The Rohacell foam filler is placed on the molds, which are then joined together and placed in the oven for the curing process. The Rohacell foam expands during curing, pushing the carbon fiber sheets onto the molds, thereby ensuring a smooth external surface.

https://doi.org/10.5194/wes-2021-66
Preprint. Discussion started: 6 July 2021


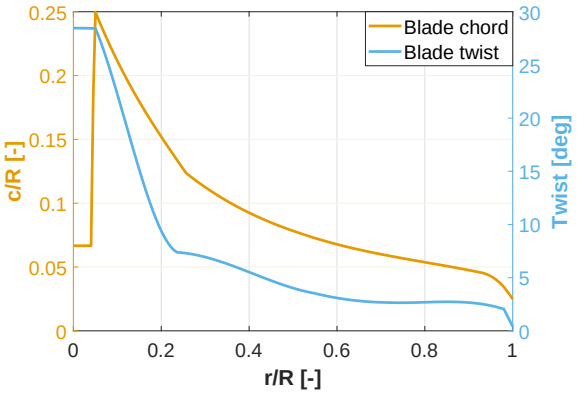


**Figure 3.** Chord and twist distributions along the blade.

### 2.4 Actuators

#### 2.4.1 Pitch actuation mechanism

Given the relatively small size of the G06, an individual pitch control system would increase cost and complexity. Considering also its typical use cases, a collective pitch control system was chosen for this model.

The pitch mechanism is realized through a bevel gear system, featuring a crown and three pinions (see Fig. 4). The crown is connected through a flexible coupling with a Maxon gearhead, and each pinion is connected with its own respective blade. The gearhead has a 84:1 ratio, and it is driven by a Maxon 30 W DC motor. According to the manufacturer, a $1.3°$ backlash is to be expected for the gearhead. Given that the bevel gear ratio is 27:15, this gearhead backlash translates into a $2°$ play at the blade pitch angle, which is unacceptable. To eliminate this backlash, each blade is attached to a torsional spring. The spring constant and its position ensure that the spring is always under tension within the pitch angle operational range, and that the applied torque is always higher than the aerodynamic pitching moment on the blade. Consequently, the loading direction on the gearhead is always the same, resulting in a solution that presents no backlash of the blade pitch motion.

The pitch motor is controlled through a two-channel encoder, thus only relative angular displacements are possible. The absolute pitch rotation of the blade is obtained by Hall sensors, as described later in Sect. 2.5.2.

To verify the suitability of the actuator, the pitch actuation system dynamics were modeled in Simulink. The maximum continuous pitch rate is $550°s^{-1}$. Considering that the time scale factor between the G06 and the full-scale reference is $n_t \approx 1/240$, this corresponds to a full-scale pitch rate of approximately $2.3°s^{-1}$. This value is smaller than the typical maximum operational pitch rate of full-scale turbines, which is approximately in the range $[6-9]°s^{-1}$. Aeroelastic simulations of the DTU 10 MW turbine were conducted in the full-load regime (region III) with a turbulence intensity of $10\%$. The analysis of these simulations indicates that the pitch actuation exceeds $2.3°s^{-1}$ for only $5\%$ of the time. Based on these results, the speed of the pitch actuator was deemed acceptable.

https://doi.org/10.5194/wes-2021-66
Preprint. Discussion started: 6 July 2021


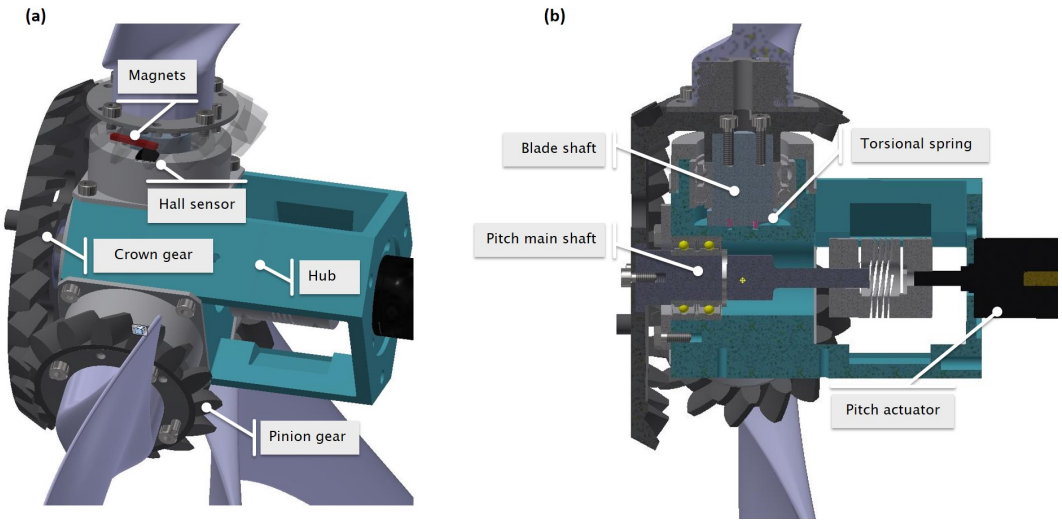


**Figure 4.** Different views of the hub assembly. View with one transparent blade gear, to show the magnets and Hall sensor **(a)**. View where the assembly has been cut to reveal hidden elements **(b)**.

With this pitch rate, the G06 actuation system is suitable also for other non-standard applications, such as dynamic induction wind farm control (Frederik et al., 2020; Munters and Meyers, 2018). For example, a high (above the optimal) Strouhal frequency $\mathrm{St} = fD/U = 0.6$ and a pitch amplitude of $6^\circ$ are well within the limits of the present system.

### 2.4.2 Torque actuator

The torque actuator provides either a torque or a speed operation mode, depending on the application. In torque mode, the actuator plays the same role of the generator in a real wind turbine, whereas in speed mode it provides the torque that is necessary to spin the rotor at a desired angular velocity. The actuator is a Maxon DC 120 W motor, equipped with a gearhead with a 4.4:1 gear ratio, produced by the same manufacturer. The motor is controlled through an analog Maxon ESCON Module 50/5 controller, which allows for the user to select between the two modes (torque or speed) of operation.

When the motor works as a generator, current flows from the motor to the controller and from there to the power supply. To dissipate this flow of current, the motor controller is connected in parallel with an 8 Ohm resistor capable of dissipating up to 100 W of power.

### 2.4.3 Yaw actuation system

Due to the small size of the G06 model, integrating the yaw mechanism into the tower —as done for the G1 and G2 turbines— would increase the tower diameter. An excessively out-of-scale tower creates a wider wake and has a mismatched vortex

https://doi.org/10.5194/wes-2021-66
Preprint. Discussion started: 6 July 2021


eawe european academy of wind energy
Open Access WIND ENERGY SCIENCE DISCUSSIONS

shedding (Wang et al., 2020a), in turn affecting the turbine wake. To avoid this problem, the yaw actuation mechanism is realized through a separate turning base on which the G06 is mounted.

This solution not only enables the design of a thinner tower, but also decouples the yaw mechanism from the turbine itself, making the assembly process easier and faster. Despite the physical decoupling, the yaw actuation mechanism is controlled through the same control hardware and software as the other models of the TUM family of scaled wind turbines.

## 2.5 Sensorization of the model

### 2.5.1 Force and torque sensors

The G06 is equipped with strain sensors to measure bending and torsional moments on its shaft. To this end, three full-strain gauge bridges are located immediately in front of the first bearing (Fig. 5a); two bridges are sensitive to shaft bending, whereas the third is sensitive to torsion. Bending information is used for assessing the loading on the turbine, optionally after transforming the rotating signals into a fixed frame of reference. Torsional loads are used for the evaluation of the rotor performance by measuring the aerodynamic torque. Each bridge is connected to a conditioning board mounted on the hub. Signals and power to/from the conditioning boards are transferred to the control unit through a 12-channel slip ring. In addition to the strain gauges, a high-precision commercial torque-meter (Lorenz Messtechnik GmbH) is placed between the aft bearing and the generator. The torque-meter has a higher precision and sampling frequency than the strain gauges, but its readings are affected by the friction in the bearings and the slip ring. This friction, which depends on various factors and may change over time because of temperature and wear, can be estimated by the difference between the readings of the strain gauges and the torque-meter.

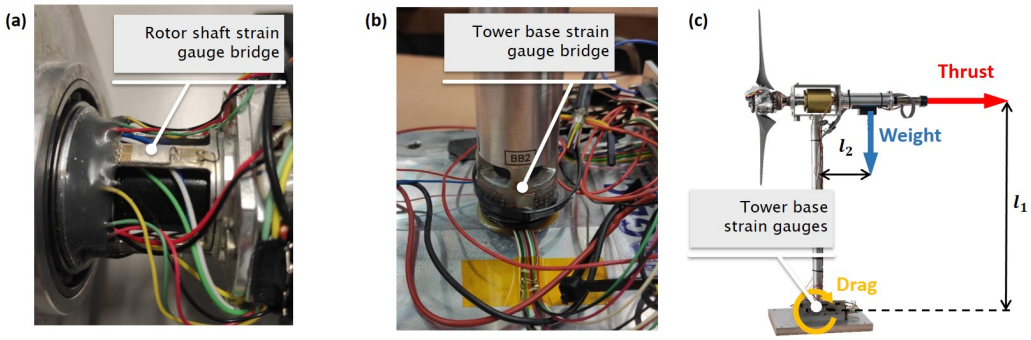


**Figure 5.** The rotor shaft, with its strain gauge bridge **(a)**; tower base, with its own integrated load cell **(b)**; schematic representation of the forces acting in the fore-aft direction on the model, and the respective moments induced at the strain gauge position **(c)**.

Two additional full bridges are placed at the base of the tower to measure fore-aft and side-side bending (Fig. 5b). The thrust generated by the rotor can be estimated from the former bending moment. In fact, as shown in Fig. 5c, the total fore-aft moment $M_o$ measured by the strain gauges is the sum of the moments due to the rotor thrust $M_T$, the tower and nacelle drag $M_D$, and

https://doi.org/10.5194/wes-2021-66
Preprint. Discussion started: 6 July 2021


eawe european academy of wind energy
Open Access WIND ENERGY SCIENCE DISCUSSIONS

the nacelle weight $M_G$, i.e.

$$M_o = M_T + M_D + M_G, \tag{4}$$

where $M_T = T l_1$, $l_1$ being the moment arm of thrust $T$, which is assumed to be applied at the rotor center. The values of $M_D$ and $M_G$ are determined off-line with dedicated measurements. For calculating $M_D$, the blades are removed and the model is placed in thewind tunnel, where measurements at various wind speeds are taken. For calculating $M_G$, a single measurement without wind is sufficient.

The shaft and tower bridges are calibrated prior to each experiment by the use of known loads, measuring the voltage and correlating loads and output via a linear regression.

### 2.5.2 Position sensors

Two kinds of position sensors are used in the model: Hall sensors and rotary optical encoders. Both the torque and pitch motors have their own internal optical encoders, which are used by the respective internal controllers.

The pitch motor is used to rotate the blades to a specific angular position, but can only be commanded through a relative angular displacement. The absolute orientation of the blades is obtained by a Hall sensor. As shown in Fig. 4a, the Hall sensor is stationary and placed on the casing of the blade bearings, while magnets are placed on the bevel gear and rotate together with the blades. The relationship between Hall sensor output and blade pitch angle is determined by a calibration procedure. Using an adapter, an inclinometer is mounted on the blade. The blade is then rotated at several different pitch angles, and the readings of the Hall sensor output and the inclinometer are recorded. Before the model can be used, a “homing procedure” is performed where the blades are moved to a predefined known position, thereby providing the desired reference.

A third optical encoder is placed on the main shaft for measuring the rotating speed of the rotor and its azimuthal position, which is necessary for interpreting shaft loads and for performing phase-locked flow measurements. Instead of using a Hall sensor, in this case the calibration is performed manually by placing the rotor at a known azimuthal position.

### 2.5.3 Measurement uncertainty

For every experimental activity it is necessary to estimate the error of the results that it generates. For the tower and shaft loads, given the sensitivity of the strain gauges and the expected strain within the operational regime, the uncertainty is estimated to be $1\%$. Similarly, the uncertainty of the torque measurement obtained from strain gauges is estimated to range between $2\%$ and $3\%$, depending on the operating point. The manufacturer gives a value of $0.05\%$ for the torque-meter, and below $1\%$ for the Hall sensor. Given the very small dimensions of the collective pitch mechanism assembly and all the uncertainties that this implies, a tolerance of $\pm 0.3^\circ$ can be estimated for the blade pitch angle. Uncertainties in the dimensions of the model (blade length, tower height etc.) and in the measurement of the rotor angular velocity are considered to be negligible.

https://doi.org/10.5194/wes-2021-66
Preprint. Discussion started: 6 July 2021


eawe european academy of wind energy
Open Access WIND ENERGY SCIENCE DISCUSSIONS

### 2.6 Control software

The G06 is operated by a Bachmann M1 (Bachmann, 2020) programmable logic controller (PLC), which runs in real time the supervisory logic and the pitch-torque-yaw controllers.

Two analog acquisition modules and one counter module are used for acquiring the sensor readings (strain gauges, encoder), as well as the wind speed. All signals are gathered at a frequency of 250 Hz, except for the torque-meter and shaft bending moments that are sampled at 2.5 kHz. All sensors readings are provided as inputs to the supervisory controller, which is real-time executed by the M1-CPU unit with a clock time of 4 ms; the control pitch, torque and yaw demands are sent to the actuator control boards via a M1-CAN module or by analog output. The real-time controller is organized into several applications written in the C programming language, each handling specialized tasks such as communicating with the actuators, recording data, or calculating actuator demands according to a control algorithm and the state of the machine (idle, power generation etc.).

The control hardware and software is the same for all models of the TUM scaled wind turbine family. Each individual model is uniquely identified by its own ID, which allows the software to select the appropriate model-specific parameters, such as friction tables, controller gains etc. This unified framework simplifies software maintenance and development, and shortens the preparation time for the experimental setup.

## 3 Model characterization

This section presents the basic characteristics of the G06 in terms of its rotor aerodynamic performance, comparing design predictions with measurements obtained in two different wind tunnels. Additionally, the wake is characterized in terms of velocity deficit and wake center deflection in misaligned conditions, and compared to the G1 scaled model and to an engineering wake model. Further results are presented for turbulence intensity (TI), turbulent momentum fluxes and turbulence dissipation rate.

### 3.1 Experimental test conditions

The model was tested in two different atmospheric boundary layer wind tunnels: the BLAST facility at the University of Texas at Dallas (UTD), shown in Fig. 6a, and the tunnel at the Institute of Aerodynamics of the Technical University of Munich (TUM), shown in Fig. 6b.

The UTD BLAST wind tunnel test section has a height of 2.1 m, a width of 2.8 m and a length of 30 m. In this wind tunnel, measurements were taken using Stereo Particle Image Velocimetry (S-PIV) with a LaVision system. The S-PIV equipment comprises of two sCMOS 5.5 Mp cameras mounted on Scheimpflug adapters and equipped with 50 mm Nikon AF 1.8D lenses. A Quantel Evergreen HP laser was used with 380 mJ/pulse, and the cameras were calibrated with a 300 mm by 300 mm dual-plane target. The wake was measured in planes perpendicular to the flow at several downstream distances. All planes

https://doi.org/10.5194/wes-2021-66
Preprint. Discussion started: 6 July 2021


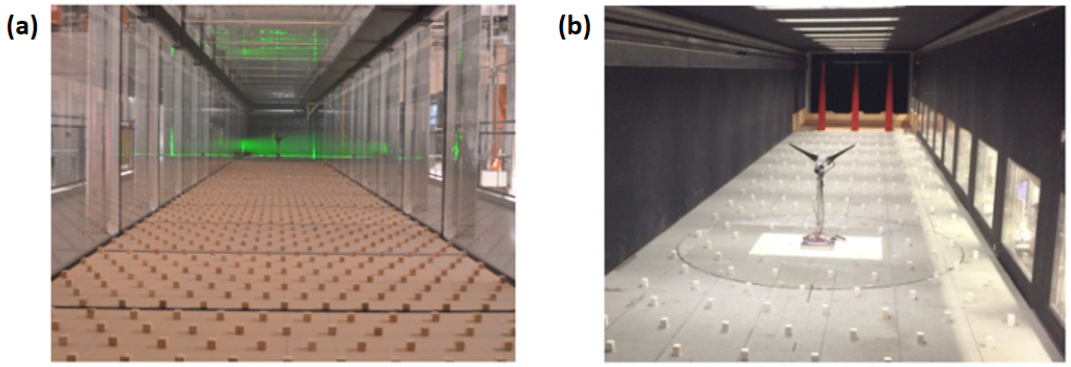


**Figure 6.** The UTD BLAST atmospheric boundary layer test section looking downstream towards the model **(a)**, and the TUM atmospheric boundary layer test section looking upstream **(b)**.

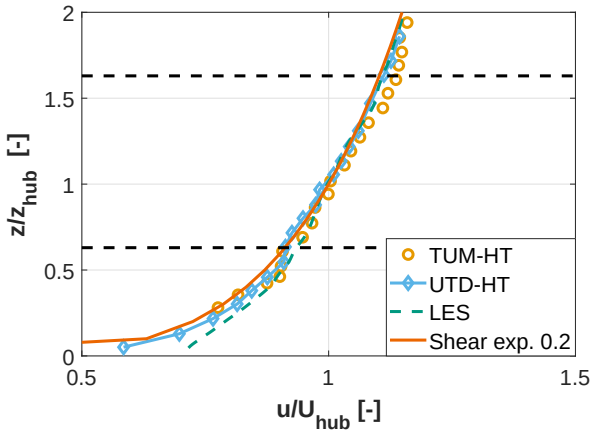


**Figure 7.** Inflow velocity profiles for TUM-HT and UTD-HT inflow conditions; black dashed lines denote the rotor tips.

https://doi.org/10.5194/wes-2021-66
Preprint. Discussion started: 6 July 2021


eawe european academy of wind energy
Open Access WIND ENERGY SCIENCE DISCUSSIONS

had a spatial resolution of approximately 0.015 D. The mean flow field for each plane was calculated by averaging 2,000 instantaneous flow fields, which were captured at 10 Hz frequency.

The TUM wind tunnel has a height of 1.8 m, a width of 2.7 m and a length of 27 m. In this wind tunnel the wake was measured using a triple-wire device based on a DISA 55P91 probe and manufactured in-house at TUM (Heckmeier et al., 2019). The three gold-plated tungsten wires have a diameter of 5 $\mu$m with a length of 1.25 mm. The characteristic temperature coefficient of the sensor is $\alpha_{20} = 0.0036$ K$^{-1}$. Based on calibration, the overheat ratio, gain, and offset were set to $a_{ov} = 1:8$, $G = 2$ and $O = 2$, respectively (Perry and Morrison, 1971).

In both wind tunnels, two different inflow conditions were generated: the first is characterized by a low turbulence and uniform velocity profile, as obtained by the natural development of the flow in the clean wind tunnel; the second was obtained by the use of spires located at the test section inlet and by roughness elements placed on the floor, leading to a higher turbulence and a sheared velocity profile. The resulting conditions are labelled UTD- or TUM- (depending on the tunnel) LT (for low turbulence) and HT (for high turbulence), and are reported in Table 2, together with the testing conditions in terms of TSR $\lambda$ and thrust coefficient $C_T = T/0.5\rho U^3 \pi R^2$. Figure 7 shows the vertical profile of the normalized streamwise inflow speed $u/U_{\text{hub}}$ for TUM-HT and UTD-HT.

**Table 2.** Summary of test conditions in the UTD and TUM boundary layer wind tunnels.

| | UTD-HT | UTD-LT | TUM-HT | TUM-LT |
|---|---|---|---|---|
| Cross-section | 2.8 m × 2.1 m | | 2.7 m × 1.8 m | |
| Blockage ratio | 4.8 % | | 5 % | |
| $U_{\text{hub}}$ (wake) | 10.2 ms$^{-1}$ | 10.1 ms$^{-1}$ | 8 ms$^{-1}$ | 10 ms$^{-1}$ |
| $U_{\text{hub}}$ (performance) | – | 5 – 11 ms$^{-1}$ | – | – |
| TI at hub height $I_{\text{hub}}$ | 8.5 % | 0.15 % | 12 % | 0.3 % |
| Shear exponent | 0.2 | 0 | 0.21 | 0 |
| Downstream position ($x$/D) | 2, 3.5, 5, 6.5, 8.5 | | 1, 3, 6 | |
| Wake measurement method | S-PIV | | Hot-Wire | |
| TSRs | $\lambda = 3.5,\ \lambda = 5.35,\ \lambda = 7.2$ | | $\lambda = 7.1$ | |
| Thrust coefficients | $C_T = 0.38, C_T = 0.54, C_T = 0.72$ | | $C_T = 0.71$ | |

### 3.2 Aerodynamic performance characterization

#### 3.2.1 Wind tunnel tests

The aerodynamic performance characterization was performed in the BLAST wind tunnel in UTD-LT conditions (see Table 2). Since blockage is below 5%, no correction was deemed necessary.

Figures 8a-c report the power, thrust and torque coefficients as functions of TSR for several pitch angles. The maximum measured power coefficient is $C_{P_{\text{max}}} \approx 0.41$, which is a good result for such a small rotor, yet 20% lower than the one of the

https://doi.org/10.5194/wes-2021-66
Preprint. Discussion started: 6 July 2021


eawe european academy of wind energy
Open Access WIND ENERGY SCIENCE DISCUSSIONS

full-scale reference. The maximum power coefficient is achieved at $\lambda = 7.5$, which is close to the value of 8 of the reference model. However, the difference in performance between $\lambda = 7.5$ and 8 is insignificant due to the flat shape of the curve. At the optimum pitch and TSR, the thrust coefficient is $C_T \approx 0.75$, which is in line with expectations for a full-scale turbine.

Figures 8d-f show the variation of the power $C_P$, thrust $C_T$ and torque $C_Q = C_P/\lambda$ coefficients with respect to TSR for different inflow speeds at a fixed (optimum) pitch angle. The observed dependency of performance on wind speed is relevant because the G06 turbine is intended for use in waked conditions, where the impinging flow is slower than the free stream. Even though utility scale wind turbines performance coefficients are essentially insensitive to wind speed (except for deformation-induced effects, which however are not present here since the model is rigid), this is not the case for scaled models. Indeed, as seen in the figure, there is an evident performance deterioration as the inflow speed is reduced. This can be explained by the rapid increase in the airfoil drag with decreasing Reynolds number, as shown in Fig. 9. The resulting drop in efficiency affects primarily the $C_P$ coefficient, as expected, whereas it generates only modest changes in $C_T$, which is mostly driven by lift and not drag. It should be noted that, notwithstanding the reduced and condition-dependent $C_P$, a rotor designed with the criteria adopted here still results in a very realistic wake behavior, as shown later on and more in detailed discussed in Wang et al. (2020a). Additionally, for a wake management application, these characteristics of the power coefficient are not really an issue if the control solution demonstrates improvement over a baseline case. This is in fact one of the roles of scaled models: although not all physics can always be matched at scale, and therefore absolute values cannot be accurately captured, these models can still typically show trends and changes with respect to a reference (Canet et al., 2021).

Figure 10a shows the variation of power with respect to the yaw misalignment angle $\gamma$, at the optimum pitch angle and tip speed ratio. Fitting the cosine power loss model to the experimental data yields:

$$P = P_{\gamma=0} \left(\cos\gamma\right)^{2.01}. \tag{5}$$

The power loss exponent for the G1 scaled wind turbine is 2.17 (Campagnolo et al., 2020), while Pedersen (2004) reported 2, Schepers (2001) 1.8, and Damiani et al. (2018) found 1.9. Other studies have found values closer to the theoretical limit of 3 (Bastankhah and Porté-Agel, 2015; Bartl et al., 2018).

Figure 10b shows the $C_P$-$\lambda$ curves of two different G06 rotors for the same TUM-HT inflow conditions and a blade pitch angle $\beta = 0°$. Results indicate that the two rotors have an almost identical performance, which validates the repeatability of the manufacturing, calibration and data acquisition processes.

### 3.2.2 Numerical simulations: polar identification

One of the intended uses of the G06 turbine is the validation of simulation tools. Most numerical models of rotor aerodynamics depend on the airfoil lift and drag coefficients (polars). Especially for scaled models, the determination of the airfoil polars involves considerable uncertainties. In fact, manufacturing imprecisions, in combination with the small dimensions of the blade, can have significant effects on the airfoil shape and, consequently, on its polars. As a result, the nominal polars used for designing the rotor might not be completely accurate.

https://doi.org/10.5194/wes-2021-66
Preprint. Discussion started: 6 July 2021


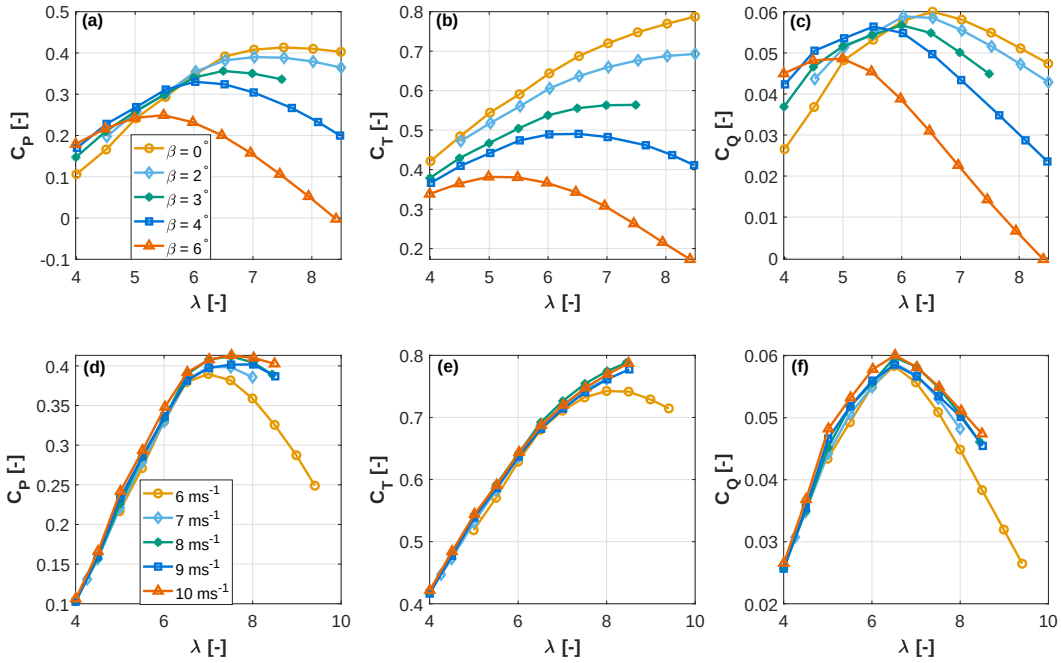


**Figure 8.** Power $C_P$ **(a,d)**, thrust $C_T$ **(b,e)** and torque $C_Q$ **(c,f)** coefficients as functions of TSR $\lambda$ for different pitch angles $\beta$ at 10 ms$^{-1}$ **(a,b,c)**, and for different wind speeds at the optimum pitch angle **(d,e,f)**.

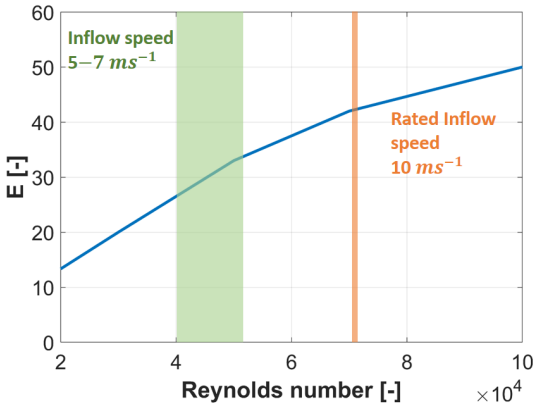


**Figure 9.** Efficiency of the RG-14 airfoil as a function of Reynolds numbers, as computed with Xfoil (Drela). The orange line indicates the G06 Reynolds operating regime at rated speed. The green area indicates the approximate Reynolds number of waked wind turbines that are further downstream in a column configuration.

https://doi.org/10.5194/wes-2021-66
Preprint. Discussion started: 6 July 2021


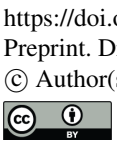

eawe european academy of wind energy
Open Access WIND ENERGY SCIENCE DISCUSSIONS

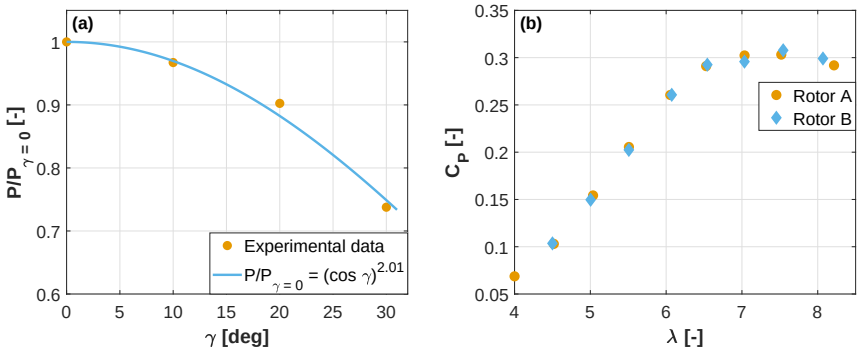


**Figure 10.** Power output as a function of the wind misalignment angle $\gamma$, normalized with respect to the $\gamma = 0^\circ$ case **(a)**. $C_P$ vs. $\lambda$ for two G06 rotors in the same inflow conditions (TUM-HT) and same pitch angle $\beta = 0^\circ$ **(b)**.

To address this problem, Bottasso et al. (2014a) developed a method for identifying the airfoil aerodynamic characteristics directly from measurements of the power and thrust produced by the rotor. By this method, the nominal polars are corrected, resulting in tuned aerodynamic characteristics that better reflect the actual conditions on the manufactured rotor. This maximum-likelihood calibration procedure was further improved in Wang et al. (2020b), to better account for measurement errors.

This method was used here to tune the polars, using 160 different operating conditions measured in the UTD wind tunnel in UTD-LT inflow. Figure 11a shows the airfoil efficiency as a function of angle of attack for the nominal and tuned polars. Results show that, although not identical, the difference between the two sets of polars is small, which seems to indicate a good overall manufacturing precision of the blades. This small difference has also a relatively small effect on the circulation distribution, as shown in Fig. 11b. This same figure also reports the normalized circulation distribution of the reference model obtained with FAST (Jonkman and Jonkman, 2018). Results show that, outboard of $r/R = 0.3$, the circulation of the G06 blade is almost identical to the reference one when using the nominal polars; this is expected, as this condition is explicitly enforced in the rotor design problem (see Eq. (3)). When considering the identified polars, the circulation matching error is less than $2\%$, which is a more than satisfactory result given the small size of the rotor. The difference between the G06 and reference circulations in the innermost $30\%$ of blade span is due to the rather long extent of the cylindrical root of the scaled blade, due to manufacturing reasons.

### 3.3 Wake characterization

#### 3.3.1 Velocity deficit, recovery and wake deflection

This section aims at characterizing the wake of the G06 turbine in terms of velocity deficit, recovery rate, and path deflection as a function of misalignment angle.

https://doi.org/10.5194/wes-2021-66
Preprint. Discussion started: 6 July 2021


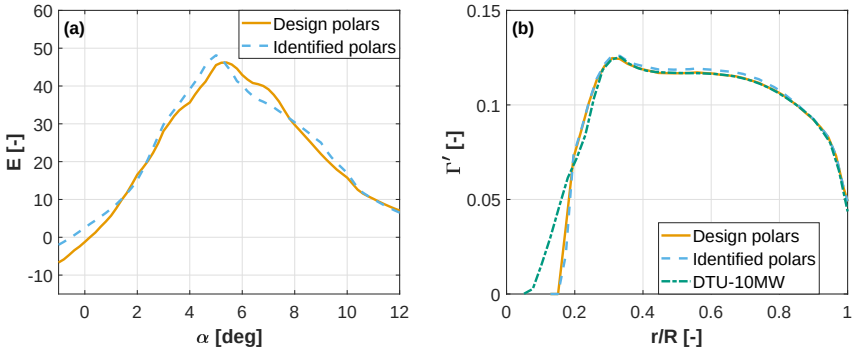


**Figure 11.** Comparison between airfoil efficiency $E$ calculated with the nominal polars and the identified ones, for a chord-based Reynolds equal to 70,000 **(a)**. Nondimensional circulation distribution $\Gamma'$ along the blade span $r/R$ for the G06 using the nominal design and the identified polars, and for the reference turbine **(b)**.

Considering the number of parameters that can affect the results, the repeatability of wake measurements was verified in different wind tunnels and with different measurement techniques. To this end, the turbine wake was measured at different downstream distances in the UTD wind tunnel in UTD-LT conditions using S-PIV, and in the TUM wind tunnel in the comparable TUM-LT inflow using hot-wire probes. Figure 12 shows an excerpt from this data set, reporting both the lateral (panel a) and vertical (panel b) wake profiles obtained at $x/D = 3.5$. Results show a very good agreement between the two measurements, with an average error of 1.5% and a standard deviation of 1%. Similar results, not shown here for brevity, were obtained at other downstream distances. The good match between these two sets of measurements serves as an additional validation of the calibration, measurement and postprocessing procedures.

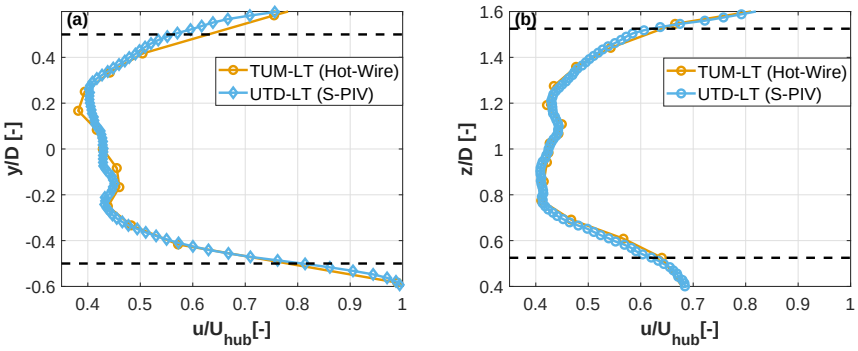


**Figure 12.** Comparison of wake measurements at $x/D = 3.5$ in two different wind tunnels and with two different measurement techniques. The comparison is made for laminar and uniform inflow (UTD-LT, TUM-LT). Black dashed lines indicate the rotor tips. Horizontal profile **(a)**; vertical profile **(b)**.

https://doi.org/10.5194/wes-2021-66
Preprint. Discussion started: 6 July 2021


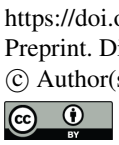

eawe european academy of wind energy
Open Access WIND ENERGY SCIENCE DISCUSSIONS

Figure 13 reports horizontal and vertical profiles of normalized velocity deficit for the laminar and uniform TUM-LT and sheared and turbulent TUM-HT conditions. Results for the TUM-LT inflow conditions reveal, especially for the horizontal scan, the typical double-Gaussian profile in the near wake (Schreiber et al., 2020a). As expected, in the TUM-HT case the higher TI accelerates the dissipation of the nacelle wake, resulting in a single-Gaussian profile (Bastankhah and Porté-Agel, 2017a; Vermeer et al., 2003). The vertical profile is distorted by the presence of the boundary layer in the TUM-HT inflow case. The profiles of the two different inflow conditions are similar immediately behind the rotor at $x/D = 1$, where recovery has not yet initiated and the deficit is mainly driven by the extraction of kinetic energy from the flow performed by the wind turbine. On the other hand, the evolution further downstream is markedly different, on account of the different TI.

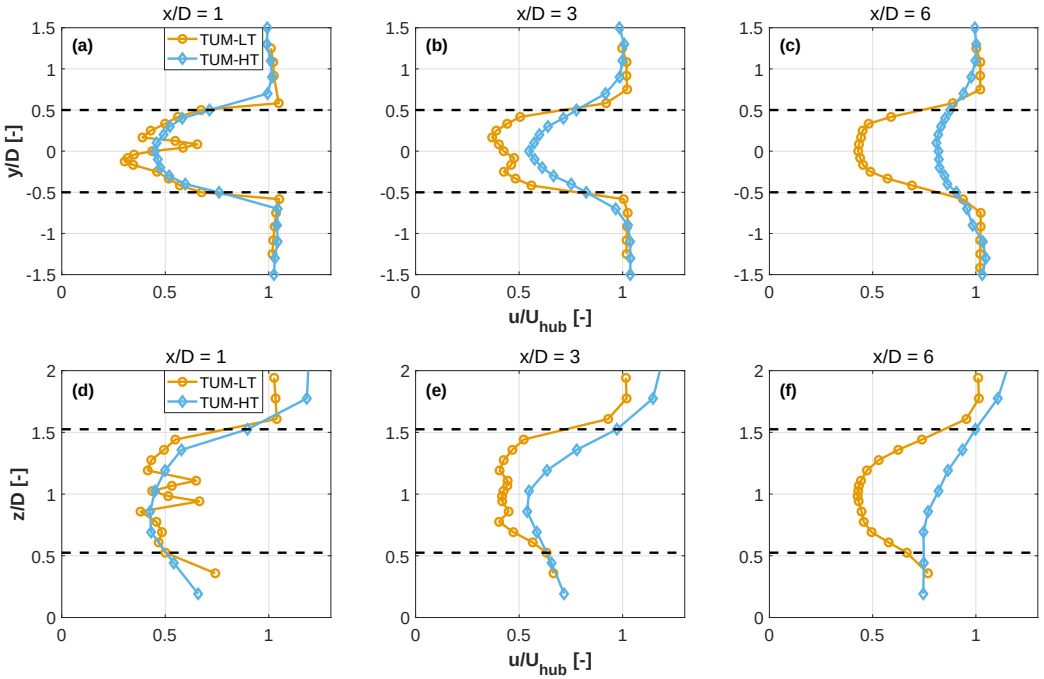


**Figure 13.** Horizontal **(a-c)** and vertical **(d-f)** profiles of the normalized streamwise velocity at several downstream distances, for sheared turbulent (TUM-HT), and uniform laminar (TUM-LT) inflow conditions. Black dashed lines indicate the rotor tips.

Figure 14 shows the downstream evolution of the velocity deficit at wake center for different thrust coefficients in UTD-HT inflow. The experimental data is plotted together with the predictions of the model of Bastankhah and Porté-Agel (2014). The model depends on the thrust coefficient and a wake growth parameter, which was calculated according to Cheng and Porté-Agel (2018). Results show that experimental data and model predictions are in good agreement, with the exception of the low-thrust cases ($C_T = 0.38$, $C_T = 0.54$) closer to the rotor disk (up to $x/D = 3.5$), where the model overpredicts the wake velocity. This is probably due to the wake of the nacelle still being a contributing factor at this distance and position. The figure also clearly

https://doi.org/10.5194/wes-2021-66
Preprint. Discussion started: 6 July 2021


eawe european academy of wind energy
Open Access WIND ENERGY SCIENCE DISCUSSIONS

shows that lower thrust coefficients are associated with slower recovery rates, which partially explain why static derating wind farm control strategies lead to only limited power gains (Annoni et al., 2016; Campagnolo et al., 2016a).

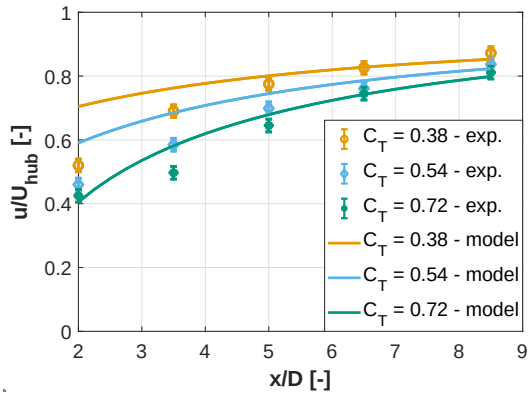


**Figure 14.** Velocity deficit evolution in UTD-HT inflow, for several values of $C_T$, against the wake model of Bastankhah and Porté-Agel (2014).

The wake of the G06 was also compared to the one of the G1 model, a scaled turbine designed using similar criteria and already extensively used for wake and wind farm control studies (Campagnolo et al., 2016b; Schreiber et al., 2017b; Wang et al., 2019, 2020a; Bottasso and Campagnolo, 2020; Campagnolo et al., 2020). Figure 15 shows lateral profiles of normalized streamwise velocity at hub height 5D downstream of the two turbines. The profiles are compared in the wind-aligned condition $\gamma = 0°$, and for a high misalignment angle of $\gamma = 30°$. The G06 model operates in the UTD tunnel in HT conditions at a thrust coefficient $C_T = 0.72$, and the speed profile was obtained from S-PIV measurements. The G1 was tested in the wind tunnel at Politecnico di Milano in a condition characterized by a vertical shear of 0.2, a TI of 10% and $C_T = 0.75$, and the wake profile was measured with triple hot-wire probes. Notwithstanding the different models, wind tunnels and measurement techniques, the wake profiles both in aligned and misaligned conditions are in good agreement with each other.

Finally, following Wang et al. (2020a), the wake of the G06 was compared to the one of its reference, to verify to what extent the scaled wake represents the characteristics of its full-scale counterpart. To this end, simulations were conducted with the large-eddy simulation (LES) actuator-line method (ALM) implemented in the flow solver described by Wang et al. (2019), and already validated in previous work. To ensure a meaningful comparison, the scaled and full-scale models were simulated with the same code, using exactly the same numerical methods and algorithmic parameters. Specifically, the fluid grid and the ALM discretization were scaled up according to the geometric scaling factor, whereas all other numerical and algorithmic parameters of the solver were kept exactly the same for the scaled and full-scale simulations. The two wind turbine models were also exposed to the same identical ambient turbulent inflows at their respective scales. To achieve this result, first the G06 inflow was obtained by simulating the UTD wind tunnel test section to match the UTD-HT conditions (see Fig. 7); next,

https://doi.org/10.5194/wes-2021-66
Preprint. Discussion started: 6 July 2021


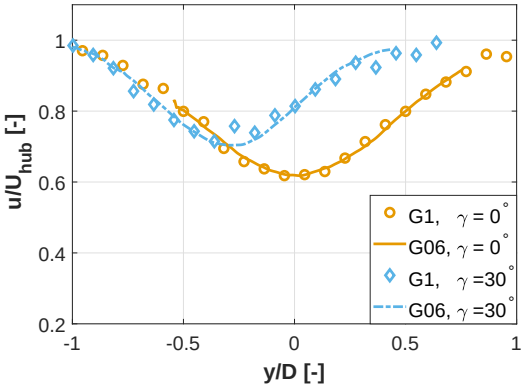


**Figure 15.** Velocity deficit for the G06 and G1 turbines 5D downstream of the rotor, for both a wind-aligned and a high misalignment angle of $\gamma = 30°$. Measurements were taken at similar thrust coefficients; $C_T = 0.72$ for G06 and $C_T = 0.75$ for G1, in similar turbulent inflows in different wind tunnels.

the DTU 10 MW inflow was generated by scaling up the G06 one based on the time and length scaling factors, following the approach described in Wang et al. (2020a).

Figure 16 shows contours (looking upstream) of the normalized streamwise velocity difference in the wakes of the G06 and of the DTU 10 MW reference, computed as

$$\frac{(u/U_{\text{hub}})_{\text{G06}} - (u/U_{\text{hub}})_{\text{DTU}}}{(u/U_{\text{hub}})_{\text{DTU}}}, \tag{6}$$

where the subscripts $(\cdot)_{\text{G06}}$ and $(\cdot)_{\text{DTU}}$ stand for the respective turbines; in the same figure, the arrows indicate the difference in the normalized in-plane velocity components. The comparison is made at two downstream distances, namely immediately behind the rotor disk at $x/D = 1$ (panel a) and at $x/D = 5$ (panel b).

To isolate the effects due to the rotor, the turbine tower and nacelle were not included in the simulations. The models were operating at their respective optimum pitch angle and at TSR $\lambda = 8$. In these conditions the G06 has a $C_P = 0.41$ and a $C_T = 0.75$, whereas the full-scale turbine has a $C_P = 0.47$ and a $C_T = 0.81$.

The figure indicates that at $x/D = 1$ the G06 wake speed is faster on a ring that covers approximately 50% of the blade span, on account of the lower $C_T$. There is also a difference at the center of the wake because of the larger hub diameter of the G06 (see Fig. 11b). The counterclockwise rotation of the in-plane velocity difference indicates a stronger swirl of the DTU 10 MW wake, because of its higher $C_Q$. Notwithstanding these differences immediately behind the rotor, at $x/D = 5$ the wakes appear to be very similar, with errors in the longitudinal speed component around $1-2\%$ for most of the domain, reaching a maximum of $3\%$ in the center of the wake. At this distance the wake rotation has dissipated almost completely, and the in-plane velocity vectors have been removed from the figure.

https://doi.org/10.5194/wes-2021-66
Preprint. Discussion started: 6 July 2021


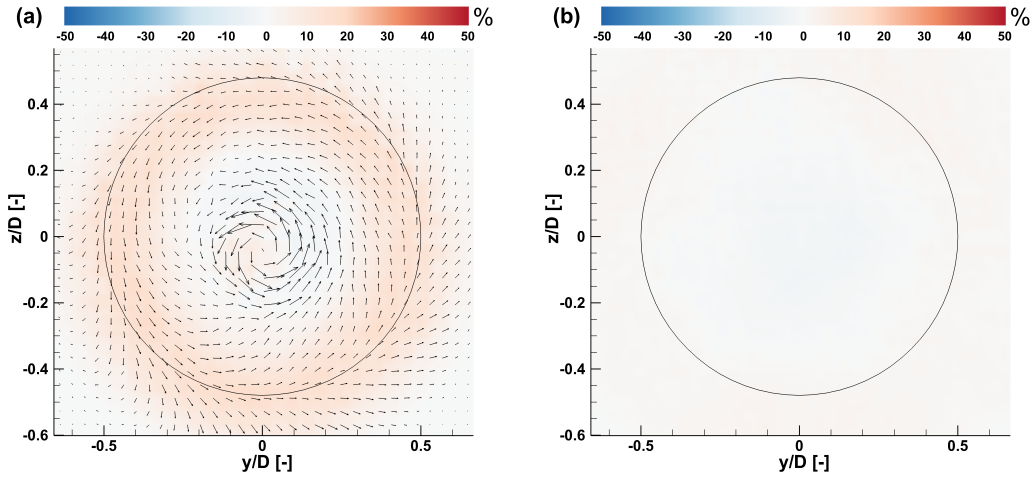


**Figure 16.** Normalized streamwise velocity difference in the wakes of the G06 of the DTU 10 MW at $x/D = 1$ **(a)** and at $x/D = 5$ **(b)**. The black circle denotes the rotor circumference, while arrows indicate the difference between in plane velocities.

Wang et al. (2020a) presents a more comprehensive discussion on the comparison of full-scaled and scaled wakes, considering the G1 turbine. That study shows that a scaled rotor —designed according to the principles followed also here for the G06— generates wakes that are in very good agreement with full-scale ones with respect to a number of different metrics.

### 3.3.2 Turbulence intensity

Within the wake of a wind turbine, the TI level is typically different than the ambient one. In fact, additional turbulence is produced by the boundary layers forming on the rotor blades, by the flow that separates from the tower and the nacelle, and by the velocity shear within the wake (Quarton and Ainslie, 1990). The so-called "added" TI (Ainslie, 1986) is used to quantify the change in turbulence with respect to the ambient conditions, and it is defined as

$$I_{\text{add}} = +\sqrt{I^2 - {I_{\text{hub}}}^2}, \qquad I \geq I_{\text{hub}}, \tag{7a}$$

$$I_{\text{add}} = -\sqrt{{I_{\text{hub}}}^2 - I^2}, \qquad I < I_{\text{hub}}, \tag{7b}$$

where $I$ is the TI at a generic point, while $I_{\text{hub}}$ is the TI at hub height.

Figure 17 shows contour lines of $I_{\text{add}}$ in UTD-HT inflow at several downstream distances in aligned conditions for $C_T = 0.72$, as obtained from the post-processing of S-PIV measurements in the UTD tunnel. The figures show that the influence of the rotor on the flow is highly nonuniform. In fact, the added TI has a horseshoe shape with a maximum at the top of the rotor; this region of higher TI is sharp and highly localized immediately behind the rotor and diffuses moving downstream. The lower-center part of the wake is characterized by an added TI that is either negligible or slightly negative, i.e. lower than the ambient one. This effect could have the following exegesis: due to the presence of the boundary layer, the velocity deficit

https://doi.org/10.5194/wes-2021-66
Preprint. Discussion started: 6 July 2021


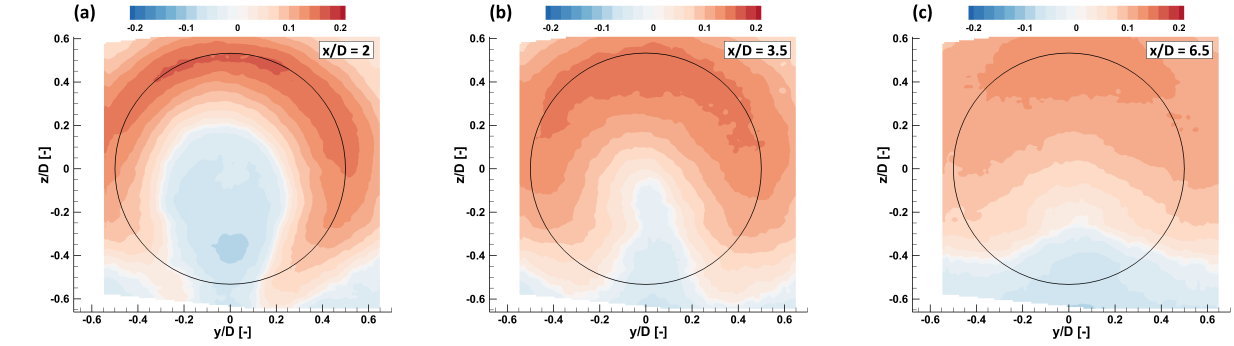


**Figure 17.** Added turbulence intensity $I_{\text{add}}$ for UTD-HT inflow at several downstream distances. The black circle denotes the rotor circumference.

Figure 18 shows vertical and lateral profiles of added TI in high turbulence sheared inflow (TUM-HT) and laminar uniform inflow (TUM-LT), for a wind aligned condition at $C_T = 0.72$. These results are coherent with the ones of the previous figures, and show that for the sheared inflow the maximum added TI is found at the top of the rotor disk, whereas at the center and bottom the values are slightly negative and reduce in magnitude while moving downstream. For the uniform inflow case, the profiles are nearly symmetrical, with a markedly slower evolution on account of the weak mixing; the nacelle wake effects are also clearly visible in the immediate vicinity of the rotor.

Several studies have considered the modelling of added TI, because of its importance in wake recovery and in the loading experienced by downstream machines. Figure 19 shows a comparison between experimental data for the G06 in UTD-HT inflow and the empirical model for the maximum added TI proposed by Crespo and Hernández (1996). This empirical model is applicable beyond 5D downstream of the rotor, and it writes:

$$I_{\text{add}_{\text{max}}} = 0.73 a^{0.8325} I_{\text{hub}}^{0.0325} (x/D), \tag{8}$$

where $a$ is the axial induction factor. The figure shows that there is a very good agreement between the estimated and the measured maximum added TI. This provides an additional confirmation of the realistic behavior of the wake even from this point of view, since this model has been verified against numerical simulations and field data at full scale (Crespo and Hernández, 1996; Niayifar and Porté-Agel, 2015).

https://doi.org/10.5194/wes-2021-66
Preprint. Discussion started: 6 July 2021


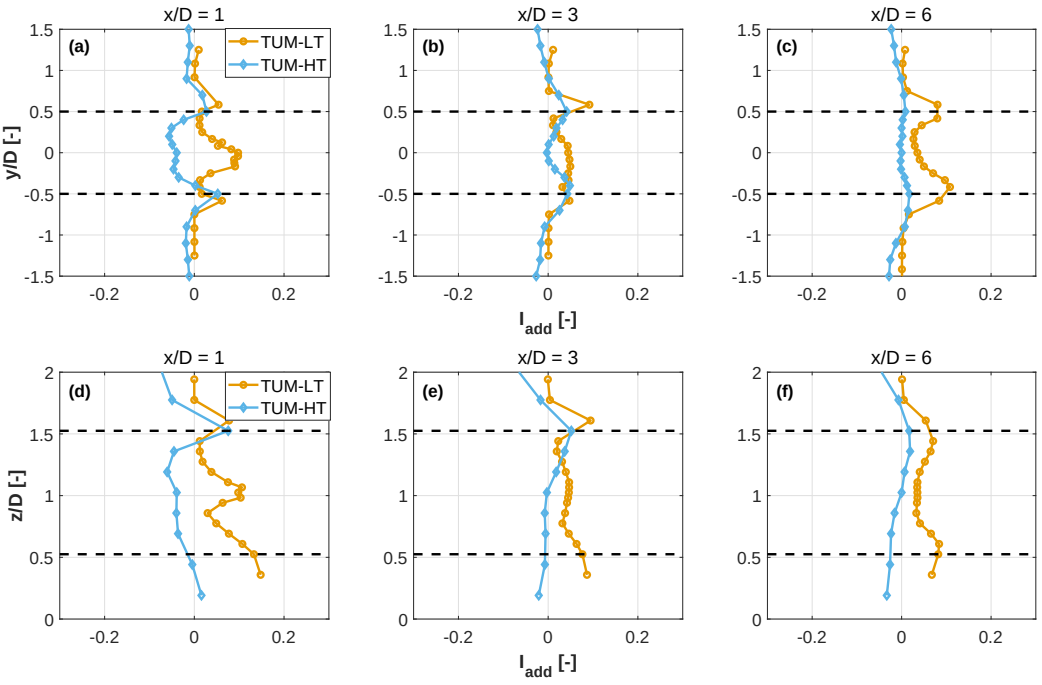


**Figure 18.** Horizontal **(a-c)** and vertical **(d-f)** profiles of added TI at several downstream distances and different inflow conditions. Black dashed lines indicate the rotor tips.

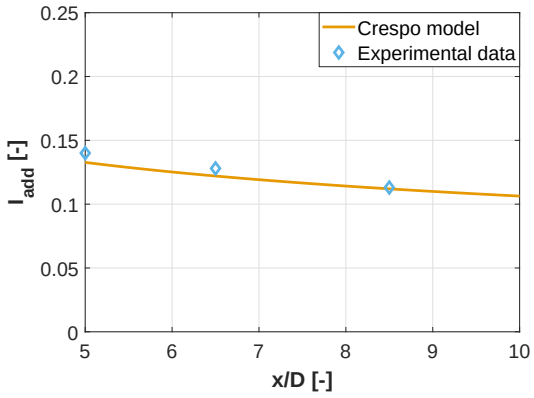


**Figure 19.** Maximum added TI vs. downstream distance, for the G06 in UTD-HT inflow and the the empirical model of Crespo and Hernández (1996).

https://doi.org/10.5194/wes-2021-66
Preprint. Discussion started: 6 July 2021


eawe european academy of wind energy
Open Access WIND ENERGY SCIENCE DISCUSSIONS

### 3.3.3 Turbulent momentum fluxes

After Reynolds decomposition and time averaging (Durst, 2008), the momentum equation reads:

$$\overline{\rho u}_i \frac{\partial \overline{u}_j}{\partial x_i} = -\frac{\partial \overline{p}}{\partial x_j} + \frac{\partial}{\partial x_i} \underbrace{\left( \mu \frac{\partial \overline{u_j}}{\partial x_i} - \overline{\rho u_i' u_j'} \right)}_{\tau_{ij}} + \overline{\rho} g_j, \tag{9}$$

where $u$ is velocity, $t$ is time, $x$ is a spatial coordinate, $p$ is pressure and $\mu$ is kinematic viscosity. The subscript $(\cdot)_i$ refers to a component in a Cartesian coordinate system, while $(\cdot)'$ and $\overline{(\cdot)}$ denote the fluctuating and time-averaged values of the relevant quantities, respectively. The Reynolds decomposition introduces additional terms to the molecular momentum transport equation, which represent turbulent velocity fluctuations $\rho \overline{u_i' u_j'}$ for $i \neq j$ and are called turbulent momentum fluxes (or Reynolds stresses). These terms express the main mechanism of re-energization of the wake, as they are responsible for entraining ambient high-momentum flow into it.

Figure 20 shows contours of the normalized lateral turbulent momentum flux $\overline{u'w'}/U_{hub}^2$, while Fig. 21 shows contours of the normalized vertical flux component $\overline{v'w'}/U_{hub}^2$. Measurements were obtained with sPIV in UTD-HT inflow conditions at a thrust coefficient $C_T = 0.72$. Qualitatively, the figures show that the exchange of momentum due to turbulent velocity fluctuations increases moving downstream (compare the figures at $x/D = 2$ and $x/D = 3.5$), reaching deeper into the wake core. This is in agreement with previous studies (Bastankhah and Porté-Agel, 2017a) and in line with the observation that the breakdown of the tip vortices, which occurs at approximately $x/D = 4$, removes a separation layer between the wake and the ambient flow, thereby facilitating the exchange of momentum (Medici, 2006).

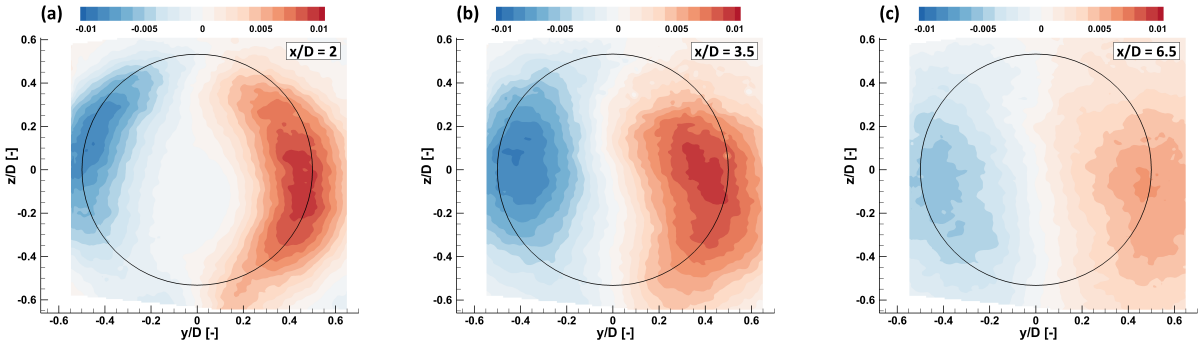


**Figure 20.** Normalized lateral turbulent flux $-\overline{v'u'}/U_{hub}^2$ for UTD-HT inflow at several downstream distances. The black circle denotes the rotor circumference.

Figure 22 shows profiles of lateral and vertical turbulent momentum fluxes at different downstream positions and for different thrust coefficients, in the same UTD-HT inflow. The figure shows that a higher thrust coefficient leads to stronger turbulent momentum fluxes. The figure also allows one to appreciate how the vertical momentum flux dissipates quickly in the lower part of the rotor disk, a result of the reduced shear shown in Fig. 13d-f. The lack of symmetry for both the lateral and vertical

https://doi.org/10.5194/wes-2021-66
Preprint. Discussion started: 6 July 2021


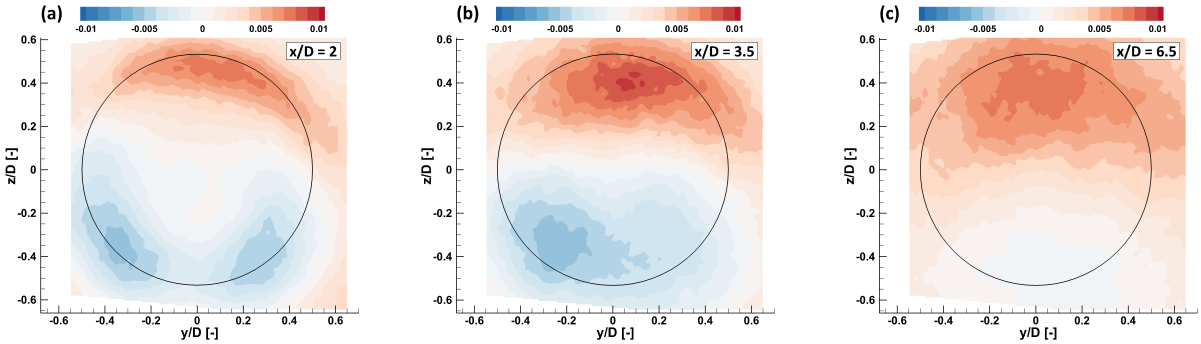


**Figure 21.** Normalized vertical turbulent flux $-\overline{w'u'}/U_{hub}^2$ for UTD-HT inflow at several downstream distances. The black circle denotes the rotor circumference.

turbulent fluxes is probably related to the rotating motion of the wake (Chamorro and Porté-Agel, 2009). Furthermore, it appears that the lateral momentum flux maximum value is higher than the vertical one at any position, similarly to the results obtained in wind tunnel tests by Bastankhah and Porté-Agel (2017c) and by CFD simulations by Shamsoddin and Porté-Agel (2016), on account of the more pronounced lateral than vertical meandering (Bastankhah and Porté-Agel, 2017a).

### 3.3.4 Dissipation rate

The analysis of the turbulent energy budget provides further insight into wake behavior. The kinetic energy equation for the turbulent flow is derived from the momentum equation after averaging over time and subtracting the energy equation of the mean flow, which results into the expression

$$\underbrace{\overline{\rho u_i}\frac{\partial}{\partial x_i}\left(\frac{1}{2}\overline{u_j'^1}\right)}_{\frac{\partial k}{\partial x_i}} = \underbrace{-\frac{\partial}{\partial x_j}\left(\overline{p'u_j'}\right)+\frac{\partial}{\partial x_j}\left(\mu\overline{u_j'\frac{\partial u_j'}{\partial x_i}}\right)-\frac{\overline{\rho}}{2}\frac{\partial}{\partial x_i}\left(u_i'u_j'^2\right)}_{\frac{\partial D_{kj}}{\partial x_j}} \underbrace{-\overline{\rho u_i'u_j'}\frac{\partial \overline{u}_j}{\partial x_i}}_{P_\kappa} \underbrace{-\mu\overline{\frac{\partial u_j'}{\partial x_i}\frac{\partial u_j'}{\partial x_i}}}_{\epsilon_\kappa}, \tag{10}$$

where $k$ is the turbulent kinetic energy and $D_k$, $P_\kappa$ and $\epsilon_\kappa$ are the turbulent kinetic energy diffusion, production, and dissipation, respectively. This last term represents the rate at which turbulent kinetic energy is transformed into heat, and it is an important parameter for the evolution of the wake.

Despite its relevance, only a few studies report an analysis of the dissipation rate of wind turbine wakes: Smalikho et al. (2013) and Lundquist and Bariteau (2015) analyzed data from field experiments, while Hamilton et al. (2012) calculated the dissipation rate in a scaled wind farm employing hot wire anemometry with a high sampling frequency of 40 kHz. In fact, the dissipation rate of turbulent kinetic energy can be directly calculated from experimental data, provided that the sampling frequency is sufficiently high to capture the smallest eddies in the flow. If this requirement is not fulfilled, the inertial dissipation approach can be employed (Champagne, 1978). This method is based on the inertial subrange theory, which suggests that the rate of energy transfer from bigger eddies to medium size eddies is equal to the dissipation rate of the smallest eddies in the

https://doi.org/10.5194/wes-2021-66
Preprint. Discussion started: 6 July 2021


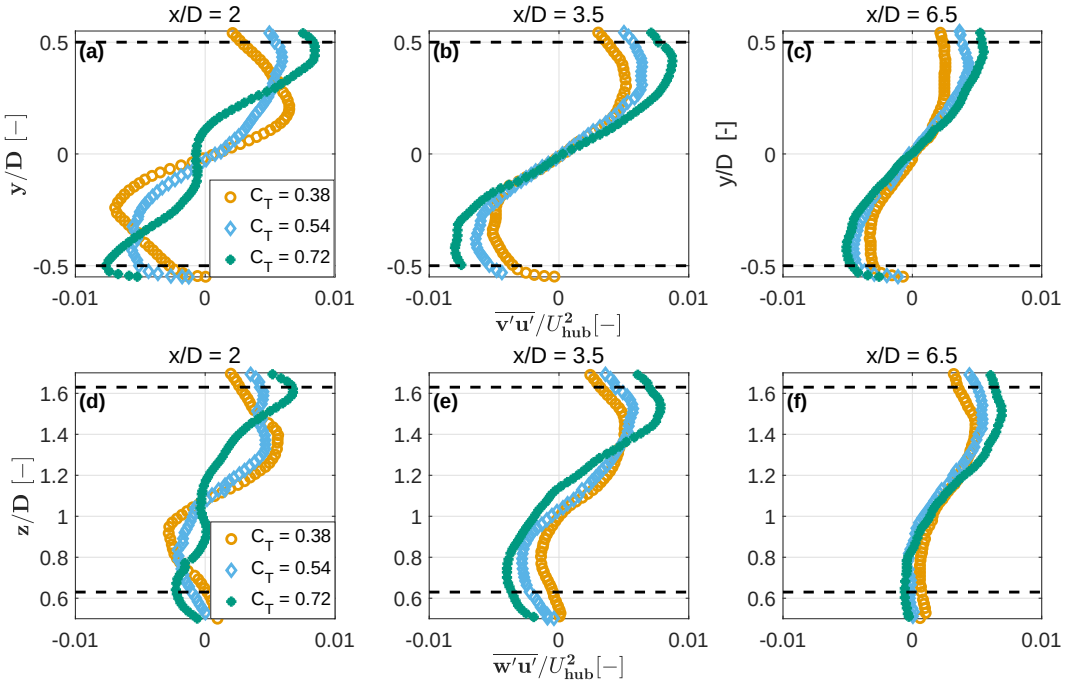


**Figure 22.** Horizontal **(a-c)** and vertical **(d-f)** profiles of the normalized lateral and vertical turbulent fluxes at several downstream distances and for different thrust coefficients, in the sheared turbulent UTD-HT inflow. Black dashed lines indicate the rotor tips.

energy cascade. Therefore, a sensor that is capable of capturing the inertial subrange of the energy cascade is also adequate for calculating the dissipation rate according to the following formula:

$$\epsilon_\kappa = \left(\frac{2\pi}{U}\right)\left(\frac{f^{5/3}S_u(f)}{k}\right)^{3/2}, \tag{11}$$

where $S_u(f)$ is the power spectrum of the velocity $u$ in the inertial subrange, while $f$ is frequency and $k = 0.52$ is the Kolmogorov constant (Fairall and Larsen, 1986; Lundquist and Bariteau, 2015). The inertial subrange can be estimated from the fast Fourier transform of the $u$ velocity. Next, the average value of $f^{5/3}S_u(f)$ can be computed over this frequency band. This same approach was used here.

Figures 23a and 23b show, respectively, the horizontal and vertical profiles of the dissipation rate at different downstream distances, for TUM-HT inflow conditions. A qualitative analysis of the results shows that the dissipation rate inside the wake is almost two orders of magnitude higher than in the ambient flow, which agrees with the observations of Lundquist and Bariteau (2015). Moreover, the dissipation rate profiles have a similar shape to the added TI ones (see Fig. 18). Even though the sampling frequency requirements suggested in the literature are met here, the accurate quantification of the dissipation rate was a rather tedious procedure with a considerable degree of uncertainty, similarly to what reported in Bluteau et al. (2011). The

https://doi.org/10.5194/wes-2021-66
Preprint. Discussion started: 6 July 2021




eawe european academy of wind energy
Open Access WIND ENERGY SCIENCE DISCUSSIONS

main sources of uncertainty are the estimation of the inertial subrange frequency band and the assumption of the Kolmogorov constant, in addition to important factors in the calculation of the dissipation rate —such as flow characteristics (anisotropy, shear etc.) and instrumentation limitations (signal to noise ratio, sampling frequency).

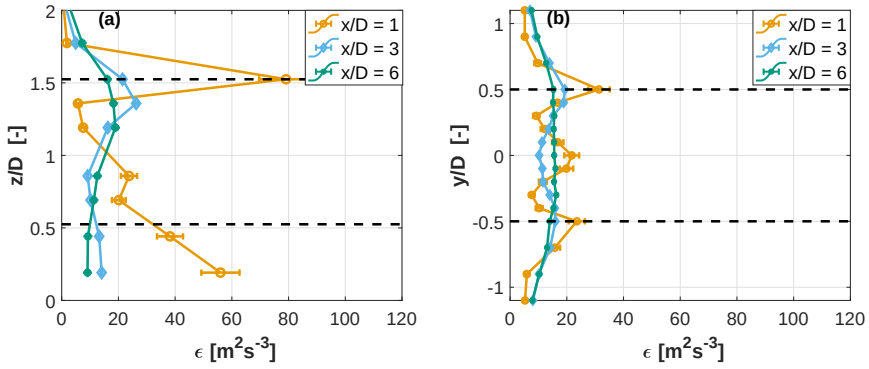


**Figure 23.** Horizontal **(a)** and vertical **(b)** profiles of the dissipation rate $\epsilon_\kappa$ at several downstream distances, for TUM-HT inflow conditions. Black dashed lines indicate the rotor tips.

The uncertainty in the inertial subrange was estimated following Piper (2001), and reported in Figs. 23 in the form of error bars. Results indicate that the error in $\epsilon_\kappa$ is around $10\%$ at $x/D = 1$, which however diminishes considerably when moving further downstream. Sreenivasan (1995) reviewed hundreds of experiments, considering different flows and different applications, and concluded that approximately the same value of the Kolmogorov constant applies to all those conditions. More specifically, for isotropic flows, the constant was found to have a mean value of 0.53 with a standard deviation of $10\%$. Given that the Kolmogorov constant appears in Eq. (11) to the power of $3/2$, a $10\%$ deviation in the constant leads to a $15\%$ deviation in the dissipation rate.

## 4 Conclusions

This paper has presented the design and characterization of the new scaled multipurpose wind turbine model G06. The need to design the G06 arose from an increased interest in the understanding of plant and complex-terrain flows, including improved operation by wind farm control. In fact, given the challenges posed by full-scale field measurements, experiments conducted in boundary layer wind tunnels with sophisticated small-scale wind turbines are attracting an increased attention from the research community and are providing additional opportunities for the collection of high-quality data sets. The characterization of the model served the purposes of verifying that the turbine operates as intended, and represented an opportunity to generate reference measurements to support future studies.

The foreseen use cases demand close-loop controls and sensorization in a compact size, yet with realistic aerodynamic characteristics, including at the rotor and in the near- and far-wake regions. The blade was designed to match the circulation

https://doi.org/10.5194/wes-2021-66
Preprint. Discussion started: 6 July 2021


eawe european academy of wind energy
Open Access WIND ENERGY SCIENCE DISCUSSIONS

distribution of a full-scale reference at the same optimum TSR. Effects caused by the unmatched chord-based Reynolds number were mitigated by the use of an ad hoc airfoil. To evaluate the as-manufactured performance of the blades, the airfoil polars were identified directly from rotor power and thrust measurements using a dedicated estimation procedure. The identified polars are only marginally different from the nominal ones, resulting in a very good quality match of the circulation distribution over the outboard $75\%$ of the blade span. High fidelity LES-ALM simulations of the G06 and its full-scale reference showed a very good agreement between the two wakes, resulting in errors of a few percent points in the streamwise velocity component of the developed far wake; additionally, the two turbines have an almost identical thrust coefficients at the design TSR. Lastly, the comparison between two different G06 rotors achieved extremely similar characteristics, demonstrating the repeatability and consistency of the manufacturing, calibration and measuring procedures.

The G06 wake was extensively tested in two different boundary layer wind tunnels and two different inflows, a laminar one and a sheared turbulent one. The measurements in both wind tunnels revealed the expected strong influence of inflow conditions on the wake profiles and recovery rate. Comparisons with the G1 turbine and with an engineering wake model showed very good agreement, both in terms of velocity deficit within the wake and wake deflection in yaw misaligned conditions.

The wind tunnel data was also used to analyze high-order flow statistics, including added TI, turbulent momentum fluxes and turbulence dissipation rate. Contour plots of the added TI revealed a horseshoe shape, with a maximum in the upper wake region and small or negative values in the center-lower region. Comparison of the measured maximum added TI with the Crespo and Hernandez empirical model showed a very good agreement.

Profiles of the turbulent momentum fluxes showed that higher thrust coefficients lead to a higher transfer of momentum flux from the ambient flow inside the wake, leading to a faster wake recovery. The turbulent momentum fluxes reach a maximum at $x/D = 3.5$, where also the fastest speed recovery is found, probably on account of the vortex breakdown taking place in this region of the wake.

The turbulence dissipation rate was also characterized in this work, for the first time directly from wind tunnel measurements. It was found that the inertial dissipation method poses challenges in the accurate estimation of the inertial subrange frequency band and the Kolmogorov constant. Nevertheless, the resulting shape of the profiles were found to be rather insensitive to the uncertainties, and were also in line with similar field measurements at full scale.

The characterization conducted so far seems to indicate that the new scaled G06 turbine satisfies the initial requirements, works reliably without any evident weakness, and is ready for supporting future wind tunnel test campaigns. Undoubtedly, the turbine can be further improved and several of the topics addressed in this paper can be analyzed in greater depth. On the hardware side, a second generation of the turbine could include individual pitch control, for example by using a swashplate, and simplifications in the wiring, for example eliminating the slip ring in favour of wireless technology. Faster, simpler and even more precise manufacturing of the blades could be obtained by 3D printing. Regarding capabilities, the wind observation technology of Schreiber et al. (2018, 2020b) has still to be demonstrated and validated on the G06, in support of advanced wind farm control strategies. Finally, the fidelity of the wake of the G06 with respect to the full-scale reference should be more extensively verified, following the approach of Wang et al. (2020a) and even using higher fidelity CFD simulations. In fact, a

https://doi.org/10.5194/wes-2021-66
Preprint. Discussion started: 6 July 2021


eawe european academy of wind energy
Open Access WIND ENERGY SCIENCE DISCUSSIONS

thorough understanding of the fidelity and limits of this —and in general of all— scaled models is of crucial importance, for a correct interpretation of the results and their scientific credibility.

*Data availability.* Data from the experiments is available upon request.

*Author contributions.* EMN designed, assembled and operated the G06 turbine, performed the wind tunnel experiments at TUM and analyzed the results; CLB defined the design requirements, defined the design methods, contributed to the interpretation of the results and supervised the whole work; EMN and CLB wrote the manuscript; FC contributed to the design of the G06, developed the rotor design code, and performed the wind tunnel measurements with the G1 turbine. EMN and SL conducted the experiments at UTD; VGI supervised the experiments at UTD, and contributed to the interpretation of the results; MAR facilitated and supported the experiments at UTD. All authors provided important input to this research work through discussions, feedback and by improving the manuscript.

*Competing interests.* The authors declare that they have no conflict of interest.

*Acknowledgements.* The authors would like to thank several persons who contributed to this work. Chengyu Wang (TUM) and Daniel Barreiro Clemente (TUM) supported the work on the CFD simulations and polar identification. Moreover, Nady Kheirallah (TUM) contributed to the rotor design, and Johanne Robke (TUM) assisted in the wake analysis. Last but not least, Christian Breitsamter, Florian Heckmeier and Kyle Jones supported the wind tunnel measurements at TUM and UTD, respectively.

https://doi.org/10.5194/wes-2021-66
Preprint. Discussion started: 6 July 2021


eawe european academy of wind energy
Open Access WIND ENERGY SCIENCE DISCUSSIONS

## References

Ainslie, J. F.: Wake modelling and the prediction of turbulence properties, Proceedings of the BWEA Wind Energy Conference, pp. 115–120, 1986.

Anderson, J. D.: Fundamentals of aerodynamics, [McGraw - Hill], [S.l.], 2001.

Annoni, J., Gebraad, P. M. O., Scholbrock, A. K., Fleming, P. A., and van Wingerden, J.-W.: Analysis of axial-induction-based wind plant control using an engineering and a high-order wind plant model, Wind Energy, 19, 1135–1150, https://doi.org/10.1002/we.1891, 2016.

Bachmann: Bachmann website , http://www.bachmann.info, 2020.

Bak, C., Zahle, F., Bitsche, R., Kim, T., Yde, A., Henriksen, L. C., Hansen, M. H., Blasques, J. P., Gaunaa, M., and Natarajan, A.: The DTU 10-MW Reference Wind Turbine, Danish Wind Power Research 2013, Technical University of Denmark, DTU Wind Energy, 2013.

Barlow, J. B., Rae, W. H., and Pope, A.: Low-speed wind tunnel testing, 3rd Edition, Wiley, 1999.

Bartl, J., Mühle, F., and Saetran, L.: Wind tunnel study on power output and yaw moments for two yaw-controlled model wind turbines, Wind Energy Science, 3, 489–502, https://doi.org/10.5194/wes-3-489-2018, 2018.

Bastankhah, M. and Porté-Agel, F.: A new analytical model for wind-turbine wakes, Renewable Energy, 70, 116–123, https://doi.org/10.1016/j.renene.2014.01.002, 2014.

Bastankhah, M. and Porté-Agel, F.: A wind-tunnel investigation of wind-turbine wakes in yawed conditions, Journal of Physics: Conference Series, 625, https://doi.org/10.1088/1742-6596/625/1/012014, 2015.

Bastankhah, M. and Porté-Agel, F.: Experimental and theoretical study of wind turbine wakes in yawed conditions, Journal of Fluid Mechanics, 806, 506–541, https://doi.org/10.1017/jfm.2016.595, 2016.

Bastankhah, M. and Porté-Agel, F.: A new miniature wind turbine for wind tunnel experiments. Part II: wake structure and flow dynamics, Energies, 10, 923, https://doi.org/10.3390/en10070923, 2017a.

Bastankhah, M. and Porté-Agel, F.: A New Miniature Wind Turbine for Wind Tunnel Experiments. Part I: Design and Performance, Energies, 10, 908, https://doi.org/10.3390/en10070908, 2017b.

Bastankhah, M. and Porté-Agel, F.: Wind tunnel study of the wind turbine interaction with a boundary-layer flow: Upwind region, turbine performance, and wake region, Physics of Fluids, 29, https://doi.org/10.1063/1.4984078, 2017c.

Bertelé, M., Bottasso, C., and Schreiber, J.: Wind observation from load harmonics — Initial steps towards a field validation, Wind Energy Science, 6, 759–775, 2021.

Bluteau, C. E., Jones, N. L., and Ivey, G. N.: Estimating turbulent kinetic energy dissipation using the inertial subrange method in environmental flows, Limnology and Oceanography Methods, 9, 302–321, https://doi.org/10.4319/lom.2011.9.302, 2011.

Bottasso, C. L. and Campagnolo, F.: Wind tunnel testing of wind turbines and farms, in: Handbook of Wind Energy Aerodynamics, edited by Stoevesandt, B., Schepers, G., Fuglsang, P., and Sun, Y., Springer Nature, to appear, 2020.

Bottasso, C. L., Cacciola, S., and X, I.: Calibration of wind turbine lifting line models from rotor loads, J. Wind Eng. Ind. Aerodyn., 124, 29–45, https://doi.org/10.1016/j.jweia.2013.11.003, 2014a.

Bottasso, C. L., Campagnolo, F., and Petrović, V.: Wind tunnel testing of scaled wind turbine models: Beyond aerodynamics, Journal of Wind Engineering and Industrial Aerodynamics, 127, 11–28, https://doi.org/10.1016/j.jweia.2014.01.009, 2014b.

Burton, T., Sharpe, D., Jenkins, N., and Bossanyi, E.: Wind energy handbook, John Wiley & Sons, 2001.

Campagnolo, F., Bottasso, C. L., and Bettini, P.: Design, manufacturing and characterization of aero-elastically scaled wind turbine blades for testing active and passive load alleviation techniques within a ABL wind tunnel, Journal of Physics: Conference Series, 524, 2014.

https://doi.org/10.5194/wes-2021-66
Preprint. Discussion started: 6 July 2021


Campagnolo, F., Petrović, V., Bottasso, C. L., and Croce, A.: Wind tunnel testing of wake control strategies, in: Proceedings of the American Control Conference, vol. 2016-July, pp. 513–518, Institute of Electrical and Electronics Engineers Inc., https://doi.org/10.1109/ACC.2016.7524965, 2016a.

Campagnolo, F., Petrović, V., Schreiber, J., Nanos, E. M., Croce, A., and Bottasso, C. L.: Wind tunnel testing of a closed-loop wake deflection controller for wind farm power maximization, Journal of Physics: Conference Series, 753, 032 006, https://doi.org/10.1088/1742-6596/753/3/032006, 2016b.

Campagnolo, F., Weber, R., Schreiber, J., and Bottasso, C. L.: Wind tunnel testing of wake steering with dynamic wind direction changes, Wind Energy Science, 5, 1273–1295, https://doi.org/10.5194/wes-5-1273-2020, 2020.

Canet, H., Bortolotti, P., and Bottasso, C. L.: On the scaling of wind turbine rotors, Wind Energ. Sci., 6, 601–626, https://doi.org/10.5194/wes-6-601-2021, 2021.

Chamorro, L. P. and Porté-Agel, F.: A Wind-Tunnel Investigation of Wind-Turbine Wakes: Boundary-Layer Turbulence Effects, Boundary-Layer Meteorology, 132, 129–149, https://doi.org/10.1007/s10546-009-9380-8, 2009.

Chamorro, L. P. and Porté-Agel, F.: Effects of Thermal Stability and Incoming Boundary-Layer Flow Characteristics on Wind-Turbine Wakes: A Wind-Tunnel Study, Boundary-Layer Meteorology, 136, 515–533, https://doi.org/10.1007/s10546-010-9512-1, 2010.

Chamorro, L. P., Arndt, R., and Sotiropoulos, F.: Reynolds number dependence of turbulence statistics in the wake of wind turbines, Wind Energy, 15, 733–742, https://doi.org/10.1002/we.501, 2012.

Champagne, F. H.: The fine-scale structure of the turbulent velocity field, Journal of Fluid Mechanics, 86, 67–108, https://doi.org/10.1017/S0022112078001019, 1978.

Cheng, W. C. and Porté-Agel, F.: A simple physically-based model for wind-turbine wake growth in a turbulent boundary layer, Boundary-Layer Meteorol, 169, https://doi.org/10.1007/s10546-018-0366-2, 2018.

Crespo, A. and Hernández, J.: Turbulence characteristics in wind-turbine wakes, Journal of Wind Engineering and Industrial Aerodynamics, 61, 71–85, https://doi.org/10.1016/0167-6105(95)00033-X, 1996.

Damiani, R., Dana, S., Annoni, J., Fleming, P., Roadman, J., van Dam, J., and Dykes, K.: Assesment of wind turbine component loads under yaw-offset conditions, Wind Energy Sci., 3, 173–189, 2018.

Drela, M.: https://web.mit.edu/drela/Public/web/xfoil/, MIT Aero & Astro, Boston, Massachusetts.

Durst, F.: Fluid mechanics - An introduction to the theory of fluid flows, [Springer], [S.l.], 2008.

Fairall, C. and Larsen, S. E.: Inertial-dissipation methods and turbulent fluxes at the air-ocean interface, Boundary-Layer Meteorology, 34, 287–301, https://doi.org/10.1007/BF00122383, 1986.

Frederik, J. A., Weber, R., Cacciola, S., Campagnolo, F., Croce, A., Bottasso, C., and van Wingerden, J.-W.: Periodic dynamic induction control of wind farms: proving the potential in simulations and wind tunnel experiments, Wind Energy Science, 5, 245–257, https://doi.org/10.5194/wes-5-245-2020, https://wes.copernicus.org/articles/5/245/2020/, 2020.

Hamilton, N., Kang, H., Meneveau, C. C., and B., R.: Statistical analysis of kinetic energy entrainment in a model wind turbine array boundary layer, Journal of Renewable and Sustainable Energy, 4, https://doi.org/10.1007/978-3-030-25253-3_61, 2012.

Heckmeier, F. M., Iglesias, D., and C., B.: Unsteady multi-hole probe measurements of the near wake of a circular cylinder at sub-critical Reynolds numbers, Notes on Numerical Fluid Mechanics and Multidisciplinary Design, 142, 643–652, https://doi.org/10.1007/978-3-030-25253-3_61, 2019.

Howard, K., Hu, L., and Chamorro, L. P.: Characterizing the response of a wind turbine model under complex inflow conditions, Wind Energy, 18, 729–743, https://doi.org/10.1002/we.1724, 2015.

https://doi.org/10.5194/wes-2021-66
Preprint. Discussion started: 6 July 2021


Hu, H., Yang, Z., and Sarkar, P.: Dynamic wind loads and wake characteristics of a wind turbine model in an atmospheric boundary layer wind, Exp Fluids, 52, 1277–1294, https://doi.org/10.1007/s00348-011-1253-5, 2012.

Iungo, G. V., Viola, F., Camarri, S., Porté-Agel, F., and Gallaire, F.: Linear stability analysis of wind turbine wakes performed on wind tunnel measurements, Journal of Fluid Mechanics, 737, 499–526, https://doi.org/10.1017/jfm.2013.569, 2013.

Jonkman, J. and Jonkman, B.: FAST 8, Tech. rep., NREL, https://nwtc.nrel.gov/FAST8, 2018.

Kelley, C. L., Maniaci, D. C., and Resor, B. R.: Scaled Aerodynamic Wind Turbine Design for Wake Similarity, 34th Wind Energy Symposium, AIAA SciTech Forum, American Institute of Aeronautics and Astronautics, http://arc.aiaa.org/doi/10.2514/6.2016-1521, 2016.

Lanfazame, R., Mauro, S., and Messina, M.: Numerical and experimental analysis of micro HAWTs designed for wind tunnel applications, Int J Energy Environ Eng, 7, 199–210, https://doi.org/10.1007/s40095-016-0202-8, 2016.

Lundquist, J. K. and Bariteau, L.: Dissipation of turbulence in the wake of a wind turbine, Boundary-Layer Meteorology, 154, 229–241, https://doi.org/10.1007/s10546-014-9978-3, 2015.

Mathworks: MATLAB version 9.7.0.1216025 (R2019b) Update 1, The Mathworks, Inc., Natick, Massachusetts, 2019.

McAuliffe, B. and Larose, G.: Reynolds-number and surface-modeling sensitivities for experimental simulation of flow over complex topography, Journal of Wind Engineering and Industrial Aerodynamics, 104-106, 603–613, https://doi.org/10.1016/j.jweia.2012.03.016, 2012.

Medici, D.: Experimental studies of wind turbine wakes - power optimization and meandering, mechanics, Royal Institute of Technology (KTH), Stockholm, 2006.

Munters, W. and Meyers, J.: Towards practical dynamic induction control of wind farms: analysis of optimally controlled wind-farm boundary layers and sinusoidal induction control of first-row turbines, Wind Energy Science, 3, 409–425, https://doi.org/10.5194/wes-3-409-2018, 2018.

Nanos, E., Yilmazlar, K., Zanotti, A., Croce, A., and Bottasso, C.: Wind tunnel testing of a wind turbine in complex terrain, Journal of Physics: Conference Series, p. 032041, https://doi.org/10.1088/1742-6596/1618/3/032041, 2020.

Niayifar, A. and Porté-Agel, F.: A new analytical model for wind farm power prediction, Journal of Physics: Conference Series, 625, https://doi.org/10.1088/1742-6596/625/1/012039, 2015.

Pedersen, T. F.: On wind turbine power performance measurements at inclined airflow, Wind Energy, 7, 163–176, https://doi.org/10.1002/we.112, 2004.

Perry, A. E. and Morrison, G. L.: A study of the constant-temperature hot-wire anemometer, Journal of Fluid Mechanics, 47, 577–599, https://doi.org/10.1017/S0022112071001241, 1971.

Piper, M. D.: The effects of a frontal passage on fine-scale nocturnal boundary layer turbulence, Ph.D. thesis, University of Colorado at Boulder, 2001.

Quarton, D. and Ainslie, J. F.: Turbulence in wind turbine wakes, Wind Engineering, 14, 15–23, 1990.

Schepers, J. G.: EU projects in German Dutch Wind Tunnel, DNW, Netherlands Energy Research Foundation, 2001.

Schottler, J., Holling, A., Peinke, J., and Holling, M.: Design and implementation of a controllable model wind turbine for experimental studies, Journal of Physics: Conference Series, 753, 506–541, https://doi.org/10.1088/1742-6596/753/7/072030, 2016.

Schreiber, J., Nanos, E. M., Campagnolo, F., and Bottasso, C. L.: Verification and Calibration of a Reduced Order Wind Farm Model by Wind Tunnel Experiments, Journal of Physics: Conference Series, 854, 012 041, https://doi.org/10.1088/1742-6596/854/1/012041, 2017a.

Schreiber, J., Nanos, E. M., Campagnolo, F., and Bottasso, C. L.: Verification and Calibration of a Reduced Order Wind Farm Model by Wind Tunnel Experiments, Journal of Physics: Conference Series, 854, 012 041, http://stacks.iop.org/1742-6596/854/i=1/a=012041, 2017b.

https://doi.org/10.5194/wes-2021-66
Preprint. Discussion started: 6 July 2021


Schreiber, J., Cacciola, S., and Bottasso, C.: Local wind speed estimation, with application to wake impingement detection, Renewable Energy, 116, 155–168, 2018.

Schreiber, J., Balbaa, A., and Bottasso, C.: Brief communication: A double-Gaussian wake model, Wind Energy Science, 5, 237–244, https://doi.org/10.5194/wes-5-237-2020, 2020a.

Schreiber, J., Bertelé, M., and Bottasso, C.: Field testing of a local wind inflow estimator and wake detector, Wind Energy Science, 5, 2020b.

Selig, M. S. and McGranahan, B. D.: Wind tunnel aerodynamic tests of six airfoils for use on small wind turbines, Journal of solar energy engineering, 126, 2004.

Selig, M. S., Guglielmo, J. J., Broeren, A. P., and Giguere, P.: Summary of Low-Speed Airfoil Data, SoarTech Publications, 1995.

Shamsoddin, S. and Porté-Agel, F.: A large-eddy simulation study of vertical axis wind turbine wakes in the atmospheric boundary layer, Energies, 9, 366, 2016.

Smalikho, I. N., Banakh, V. A., Pichugina, Y. L., Brewer, W., Banta, R. M., Lundquist, J., and Kelley, N.: Lidar investigation of atmosphere effect on a wind turbine wake, J Atmos Ocean Technol, 30, 2554–2570, https://doi.org/10.1175/JTECH-D-12-00108.1, 2013.

Sreenivasan, K.: On the universality of Kolomogorov constant, Physics of Fluids, 7, https://doi.org/10.1063/1.868656, 1995.

Tangler, J. L.: Status of the special-purpose airfoil families, Tech. Rep. SERI/TP-217 -3264, Solar Energy Research Institute, 1987.

Vermeer, L. J., Sørensen, J. N., and Crespo, A.: Wind turbine wake aerodynamics, Progress in Aerospace Sciences, 39, 467–510, https://doi.org/10.1016/S0376-0421(03)00078-2, 2003.

Viola, F., Iungo, G. V., Camarri, S., Porté-Agel, F., and Gallaire, F.: Prediction of the hub vortex instability in a wind turbine wake: Stability analysis with eddy-viscosity models calibrated on wind tunnel data, Journal of Fluid Mechanics, p. R1, https://doi.org/10.1017/jfm.2014.263, 2014.

Wang, C., Campagnolo, F., Canet, H., Barreiro, D., and L., B. C.: How realistic are turbine wakes in wind tunnel tests?, Wind Energy Sci. Discuss, https://doi.org/https://doi.org/10.5194/wes-2020-115, 2020a.

Wang, C., Campagnolo, F., and L., B. C.: Identification of airfoil polars from uncertain experimental measurements, Wind Energ. Sci. Discuss., https://doi.org/in review, 2020b.

Wang, J., Foley, S., Nanos, E. M., Yu, T., Campagnolo, F., Bottasso, C. L., Zanotti, A., and Croce, A.: Numerical and Experimental Study of Wake Redirection Techniques in a Boundary Layer Wind Tunnel, Journal of Physics: Conference Series, 854, 012 048, https://doi.org/10.1088/1742-6596/854/1/012048, 2017.

Wang, J., Wang, C., Campagnolo, F., and L., B. C.: Wake behavior and control: comparison of LES simulations and wind tunnel measurements, Wind Energy Sci., 4, 71–88, 2019.

Winslow, J., Otsuka, H., Govidarajan, B., and Chopra, I.: Basic understanding of airfoil characteristics at low Reynolds numbers ($10^4 - 10^5$), Journal of Aircraft, 55, https://doi.org/10.2514/1.C034415, 2018.

Yang, Z., Sarkar, P., and Hu, H.: An Experimental Investigation on the Aeromechanic Performance and Wake Characteristics of a Wind Turbine Model Subjected to Pitch Motions, 29th AIAA Applied Aerodynamics Conference, 2016.

## Nomenclature

| | |
|---|---|
| $a$ | Axial induction factor |
| $c$ | Chord length |
| $c_s$ | Speed of sound |

https://doi.org/10.5194/wes-2021-66
Preprint. Discussion started: 6 July 2021


eawe european academy of wind energy
Open Access WIND ENERGY SCIENCE DISCUSSIONS

| | | |
|---|---|---|
| | $C_L$ | Lift coefficient |
| | $C_D$ | Drag coefficient |
| | $C_P$ | Power coefficient |
| 765 | $C_Q$ | Torque coefficient |
| | $C_T$ | Thrust coefficient |
| | $D$ | Rotor diameter |
| | $I$ | Turbulence intensity |
| | $I_{\text{add}}$ | Added turbulence intensity |
| 770 | $k$ | Kolmogorov constant |
| | $M$ | Mach number |
| | $R$ | Rotor radius |
| | Re | Reynolds number |
| | $U$ | Ambient wind speed (time averaged) |
| 775 | $u$ | Streamwise velocity component (time averaged) |
| | $v$ | Lateral velocity component (time averaged) |
| | $w$ | Vertical velocity component (time averaged) |
| | $\alpha$ | Angle of attack |
| | $\beta$ | Pitch angle |
| 780 | $\theta$ | Twist angle |
| | $\gamma$ | Wind misalignment angle |
| | $\epsilon_k$ | Dissipation rate |
| | $\phi$ | Flow angle |
| | $\rho$ | Air density |
| 785 | $\Gamma$ | Circulation |
| | $\Omega$ | Rotor angular speed |
| | ALM | Actuator-line method |
| | BEM | Blade element momentum |
| | CFD | Computational fluid dynamics |
| 790 | LES | Large-eddy simulation |
| | S-PIV | Stereo-Particle image velocimetry |

# Wake Characterization of a Multipurpose Scaled Wind Turbine Model

Emmanouil M. Nanos* , Johanne Robke† , Florian M. Heckmeier‡ , Michael Cerny§ and Carlo L. Bottasso¶

*Technische Universität München, Germany*

Kyle L. Jones‖ and G. Valerio Iungo **

*University of Texas at Dallas, USA*

**The increasing need for validation of reduced-order wind-farm models over the last years requires even more sophisticated scaled wind turbines for wind tunnel testing. In this article, the wake behavior of the recently developed G06 scaled wind turbine model is presented. This model is designed for complex terrain experiments as well as wind farm control studies. Therefore, it combines compact design, realistic aerodynamic performance and sufficient instrumentation. The wake characteristics are studied in two different wind tunnels under similar inflow conditions with the results showing that the effect of the wind tunnel on the wake is negligible. Furthermore, wake measurements were made under two basic inflow conditions and they are evaluated in terms of velocity deficit, wake deflection and recovery rate. Results confirmed that all quantities are greatly affected by the inflow conditions.**

## I. Introduction

It is common practice to install wind energy power plants in the form of wind farms, where multiple wind turbines are placed close to each other in order to reduce the cost of energy by minimizing installation and maintenance costs.[1] However, this practice results in some wind turbines impinging with the wake of upstream ones leading to reduction in the power yield and increased fatigue loads on these machines.[2,3] To mitigate these effects, careful decision of the wind farm site and design of the wind farm layout are essential.[4–6] However, most often than not, wind farm designers are highly constrained on these aspects by other factors. Besides, wind turbine interaction with the wake of neighboring machines is unavoidable within a wind farm, even after careful planning. Therefore, in addition to the aforementioned ways to passively mitigate the effects of wake turbine-wake interaction, a lot of attention has been given lately on dynamically optimizing wind farm power output and/or wind turbine fatigue through active wind farm control.[7] Indeed, several studies have proven the potential of this strategy.[8] The main requirement for the aforementioned mitigation actions is good understanding of the physics that govern the wake behavior. Consequently, it is not a surprise that wake physics has always been, and still is, in the front line of research within the wind energy community[9,10] with many studies that approach the topic theoretically, numerically or experimentally. More specifically about the experimental studies, they range from wake measurements of propellers[11] or even porous discs to sophisticated wind turbine scaled models.[12–15] The latter ones are gaining a lot more attention over the last decade with the capabilities of these scaled models extending beyond wake measurements.[16]

*Ph.D. candidate, em.nanos@tum.de, Wind Energy Institute, Boltzmannstraße 15, 85748 Garching bei München.

†M.Sc. candidate, johanne.robke@tum.de, Wind Energy Institute, Boltzmannstraße 15, 85748 Garching bei München.

‡Ph.D. candidate, florian.heckmeier@aer.mw.tum.de, Chair of Aerodynamics and Fluid Mechanics, Boltzmannstraße 15, 85748 Garching bei München.

§Ph.D. candidate, michael.cerny@tum.de, Chair of Aerodynamics and Fluid Mechanics, Boltzmannstraße 15, 85748 Garching bei München.

¶Chair of Wind Energy, carlo.bottasso@tum.de, Wind Energy Institute, Boltzmannstraße 15, 85748 Garching bei München.

‖Wind tunnel engineer, Kyle.Jones1@utdallas.edu, Mechanical Department, 800 West Campbell Rd., 75080, Richardson.

**Assistant Professor, Valerio.Iungo@utdallas.edu, Mechanical Department, 800 West Campbell Rd., 75080, Richardson.

In this paper we present an initial characterization of the wake of a new scaled wind turbine model (G06). The idea behind the development of this model is to use it for wake as well as wind farm control studies in complex wind farm configurations and/or in complex terrain. This implies bringing together compact size and sufficient instrumentation while ensuring a realistic aerodynamic performance and wake behavior. For this initial characterization three different wind tunnel studies were performed. Two of them were performed at the wind tunnel facilities of the Chair of Aerodynamics and Fluid Mechanics of the Technical University of Munich (TUM-AER) employing hot wire measurements under two different inflow conditions, and one study was done at the University of Texas at Dallas (UTD) using Stereo Particle Image Velocimetry (S-PIV) under the same inflow conditions as in one of the TUM studies. The paper is organized as follows: in section II, a brief description of the model is given, then section III presents the experimental set-up, followed by section IV that gives an initial discussion of the wake behavior; finally, section V summarizes the most important conclusions and gives an outlook of the future activities.

## II. Wind Turbine Model Description

The G06 is a multi-purpose three bladed scaled wind turbine model. Its basic characteristics are presented in the following table:

| | |
|---|---|
| Rotor diameter | 600 mm |
| Hub diameter | 55 mm |
| Hub height | 610 mm |
| Rated wind speed | 10.5 $ms^{-1}$ |
| Airfoil profile | RG-14 |
| Controllability | Pitch (collective), yaw and torque |
| Sensors | Torque, shaft and tower loads |

Table 1: G06 basic characteristics

As mentioned above, the G06 was designed with the aim of using it primarily for wake and wind farm control studies in complex wind farm configurations and complex terrain. This desired use of the model dictated the following design requirements:

1. Its rotor diameter should allow for several columns of at least 5 models in a 4 m by 14 m atmospheric boundary layer wind tunnel. In addition, the complex topography that is intended to be used is a scaled model of real test site in southwest Germany, where research wind turbines will be installed for (among others) field studies of complex terrain and wind turbine interaction.[17] Consequently, turbine and terrain model scaled up together should result in a realistic scenario close to the one of typical onshore applications in complex terrain.

2. G06 should be sufficiently instrumented and controllable in order for it to be suitable for wind farm control studies as well as for testing wind observation algorithms.

3. The aerodynamic design of the rotor should result in a realistic performance and, consequently, in a similar to utility scale wind turbine wake behavior.

Clearly, the requirements listed above are mutually contradictory: the smaller the rotor gets, the more challenging it is to ensure good aerodynamic performance, wake characteristics and instrumentation of the model.

To ensure good aerodynamic performance a low Reynolds airfoil profile was chosen (RG - 14). With the polar data of this airfoil as input, and using the Blade Element Momentum formulation, we optimized the chord and twist distribution along the blade. The goal of the optimization was maximizing the power coefficient while constraining the solution so that the normalized circulation distribution along the blade is matching the one of a reference scale model, as proposed in the work of Kelley[18] in order to achieve wake similarity. In our case, the reference model was the DTU 10-MW wind turbine.[19]

The G06 is equipped with active pitch and torque control. Active yaw control will be realized with a custom made portable turntable. From the sensor point of view, G06 has strain gauges on the shaft measuring the bending loads and aerodynamic torque. The latter can be measured also with a commercial torque meter. Pitch angle is determined with the use of hall sensors while the rotating speed of the rotor and its azimuthal position can be measured by means of an optical encoder. Finally, the bending moments on the tower are measured with strain gauges placed at the root of the tower. Power and signal transmissions from the rotating frame are transferred to the stationary frame through a brushed slip ring. More details about the design of the rotor and the instrumentation of the model can be found in the work of Nanos et al.[20] The configuration of the drive train is presented in Fig. 1 .

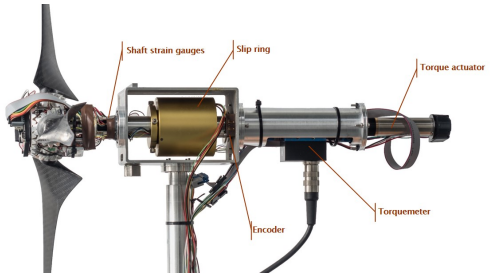


Figure 1: G06 nacelle. The main components of the nacelle are marked in the figure.

Due to the high complexity of the model and in order to decrease the possibility of damaging expensive and time consuming equipment, a simplified version has been designed and used in test campaigns that do not require active pitch control and shaft load sensors. The simplified version is identical to the one described above, except for the active pitch control capability and the shaft strain gauges. Nevertheless, it is possible to adjust manually the pitch angle of the blades.

## III. Experimental Setup

### A. Hot-wire measurements at TUM-AER

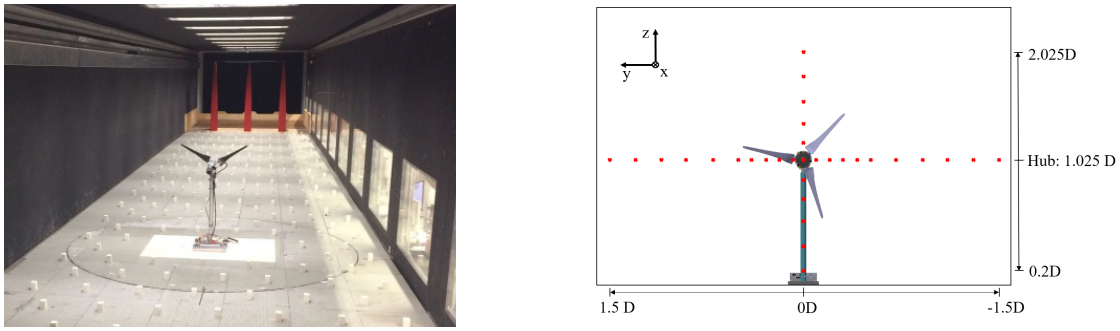


Figure 2: G06 mounted in the test section of the TUM-AER atmospheric boundary layer wind tunnel (*left*) and measuring points along the vertical and the spanwise line (front view), repeated at downstream locations of 1 D, 3 D, 3.5 D and 6 D (*right*).

The hot-wire measurements were performed in the atmospheric boundary layer wind tunnel at TUM-AER, which has a maximal velocity of $U_\infty = 30\ ms^{-1}$. The wind tunnel, which was operated in a closed circuit mode (Göttingen type), has a cross section of $h \cdot b = 1.80\ m \cdot 2.70\ m$ where h is the height and b the width, and a test section length of 21 $m$. The boundary layer profile is achieved with the help of vortex generators and roughness elements (Lego bricks). More details about the wind tunnel can be found in the work of Kozmar.[21]

Two sets of measurements were made in this wind tunnel. First, measurements were conducted under a high turbulence sheared inflow. The mean incoming velocity and turbulence intensity at hub height were kept constant at $\overline{u_h} = 8.22\ ms^{-1}$ and $I_{u,inflow} = 12\ \%$, respectively. The model was operating at a rotational speed $\omega = 2050\ rpm$ which gives a power and thrust coefficient of $Cp \approx 0.25$ and $Ct \approx 0.65$. The second set of measurements was performed under low turbulence uniform inflow. The wind speed in this case was $\overline{u_h} = 10\ ms^{-1}$ and turbulence intensity $I_{u,inflow} = 0.3\ \%$. The model's rotational speed was $\omega = 2250\ rpm$

which resulted in a power and thrust coefficient of $Cp \approx 0.4$ and $Ct \approx 0.7$. In both sets of measurements the pitch angle and the tip speed ration were kept at $\beta \approx 0$ and $\lambda = 7.1$, respectively. For both inflow conditions measurements were done for yaw angle $\gamma = 0^o$ and $\gamma = -30^o$ which corresponds to a clockwise rotation of the nacelle from a top view. Unsteady velocity measurements are recorded with a triple-wire probe which is based on a DISA 55P91 probe and manufactured in-house at TUM-AER. Measurements are compensated for large changes in temperature using the method introduced by Bearman.[22] The three gold-plated tungsten wires have a diameter of 5 $\mu m$ with a length of 1.25 $mm$. The characteristic sensor temperature coefficient is $\alpha_{20} = 0.0036\ 1/K$. An overheat ratio, a gain and offset of $a = 1.8$, $G = 2$ and $O = 2$, respectively, were set during the calibration process. Moreover, the triple-wire was calibrated for cone angles up to $\pm 35°$. In an interpolation process which uses the calibration data the spatial resolution up to those high angles of attack are guaranteed. The probe is attached to a three-dimensional traversing system which ensures the accurate translation of the probe along one vertical and one spanwise line for each downstream position, as can be seen in Figure 2 (*right*). The hot-wire data is recorded with an A.A.-Lab constant temperature anemometer AN-1003.[23] A temperature probe (PT100) is installed to correct the wire temperature. The sampling frequency is $f_s = 3\ kHz$ and measurements are recorded for a total acquisition time of $t_s = 60\ s$. Analog low-pass filters are applied in order to filter frequencies higher than the Nyquist frequency $f_N = f_s/2$.

### B. PIV measurements at UTD

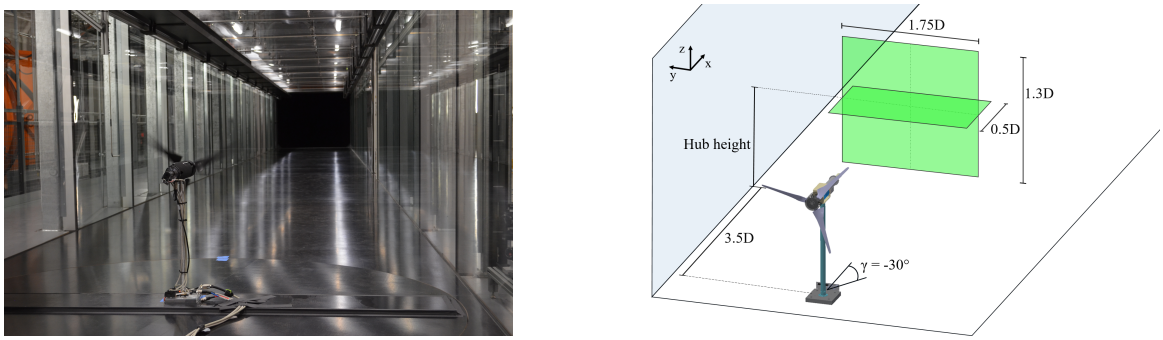


Figure 3: G06 mounted in the test section of the UTD atmospheric boundary layer wind tunnel BLAST (*left*) and the two measuring planes (*right*).

The stereo PIV measurements were conducted in the atmospheric boundary layer wind tunnel (BLAST) at the University of Texas at Dallas (UTD). The boundary layer test section is 2.8 m wide, 2.1 m tall and 30 m long. The incoming wind profile was uniform and laminar ($I_{u,inflow} = 0.03\%$). The mean wind speed during all S-PIV measurements was $\overline{u_h} = 10.1\ ms^{-1}$ while the model was operating at $\omega = 2250\ rpm$ at the same pitch angle and tip speed ratio as in the TUM-AER uniform inflow case described above. Similar to TUM-AER tests, measurements were done for yaw angle $\gamma = 0^o$ and $\gamma = -30^o$ which corresponds to a clockwise rotation of the nacelle from a top view. The thrust and power coefficients at this operating point were $Ct \approx 0.7$ and $Cp \approx 0.4$, respectively. For the S-PIV measurements a complete LaVision system was used which comprised of two sCMOS 5.5 Mp cameras mounted on Scheimpflug adapters and equipped with 50 mm Nikon AF 1.8D lense. A Quantel Evergreen HP laser was used with 380 mJ/pulse. For the calibration of the cameras we used a 300 mm x 300 mm dual - plane calibration target which also determined the dimensions of our field of view (FOV). The flow was measured in two planes as shown in Figure 3 (*right*). The first was horizontal (i.e. xy-plane where x and y stand for streamwise and lateral direction respectively ), at hub height, which consisted of 4 FOVs with 10% overlap and total dimensions 0.5 D x 1.75 D. The second plane was perpendicular to the flow (i.e. yz-plane where y and z stand for lateral and vertical direction respectively) and consisted of 12 FOVs with 10% overlap between them and had final dimensions of 1.75 D x 1.3 D. Both planes had a spatial resolution of approximately 0.015 D. The mean flow field for each FOV

was calculated by averaging 500 instantaneous flow fields which were captured at 10 Hz frequency.

## IV. Results

### A. Basic wake properties

In this paragraph the G06 basic wake properties are presented. From a wake modeling point of view these properties are velocity deficit, wake diameter and wake deflection under yawed conditions. The measurements taken in two different wind tunnels under uniform inflow are compared with the aim of evaluating the effect of the different wind tunnels. What is more, the evolution of the wake under different inflow conditions (in the same wind tunnel) is also evaluated. All velocities and all distances have been normalized with the incoming average wind speed at hub height $\overline{u_h}$ and with the rotor diameter $D$, respectively. The velocity component in the streamwise ($u$), lateral ($v$) and vertical ($w$)direction downstream the turbine are presented in the form of velocity deficits $\Delta\overline{u}/\overline{u_h}$ where ($\Delta\overline{u} = \overline{u_h} - \overline{u}$), $\Delta\overline{w}/\overline{u_h}$ where ($\Delta\overline{w} = \overline{w_h} - \overline{w}$) and $\Delta\overline{v}/\overline{u_h}$ where ($\Delta\overline{v} = \overline{v_h} - \overline{v}$).

#### 1. *Uniform inflow measurements at TUM-AER and UTD*

Figure 4 shows the normalized streamwise velocity deficit profiles in the lateral and vertical direction for yaw $\gamma = 0^o$ while Figure 5 shows the streamwise velocity deficit profile in the lateral direction for yaw $\gamma = -30^o$. Results show that there is a good agreement for both yaw angles. For the $\gamma = 0^o$ the S-PIV predicts a slightly lower maximum velocity deficit which could be attributed to the S-PIV post processing algorithm. For both yaw angles, there is a small discrepancy at the positive y side of the wake between the two measurements. However, the scarcity of the TUM-AER hot-wire measurement points, in the region of strong gradients at $y/D \approx 0.5$, does not allow for further conclusions.

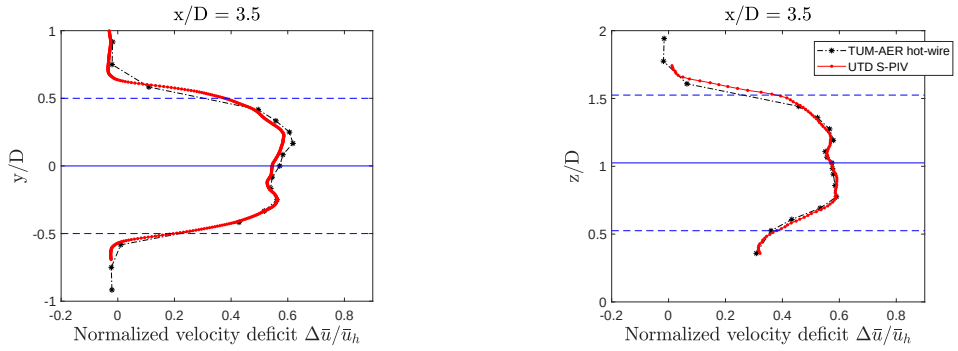


Figure 4: Normalized streamwise velocity deficit profiles in lateral (*left*) and vertical (*right*) direction under uniform inflow for $\gamma = 0^o$.

#### 2. *Uniform and sheared inflow measurements at TUM-AER*

Figure 6 shows the normalized vertical and lateral profiles of the normalized streamwise velocity deficit ($\Delta\overline{u}/\overline{u}_h$) for 1 D, 3 D and 6 D downstream from the rotor under sheared inflow. Figure 7 shows the normalized profiles of the lateral ($\Delta\overline{v}/\overline{u}_h$) and vertical($\Delta\overline{w}/\overline{u}_h$) velocity deficits in the vertical and lateral direction, respectively, at 1 D, 3 D and 6 D downstream from the rotor for the same inflow. Looking at Figure 6, the evolution of the wake expansion as we move downstream is visible. The maximum streamwise velocity deficit is around 0.55 at 1 D downstream and it drops to 0.2 at 6 D downstream for sheared inflow. The distributions of lateral and vertical velocity components shown in Figure 7 reveal the rotation of the wake as a result of the torque that blades exert on the flow. The evolution of the lateral velocity deficit profile shows that the rotation of the wake is dissipated quite fast under the influence of the surrounding turbulence, i.e. at 6 diameters downstream the spanwise component of the lower part of the wake has disappeared completely due to the proximity with the floor and the shear that this proximity introduces.

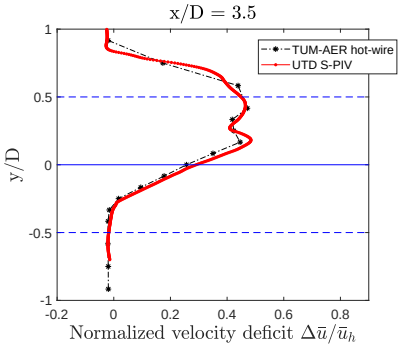


Figure 5: Normalized streamwise velocity deficit profile in the lateral direction under uniform inflow for $\gamma = -30^o$.

The vertical velocity deficit profile shows a similar behavior. In general, the main characteristics of the wake, such as the streamwise velocity deficit, the wake recovery rate and wake diameter agree with those found in previous wind tunnel studies under similar inflow conditions.[8]

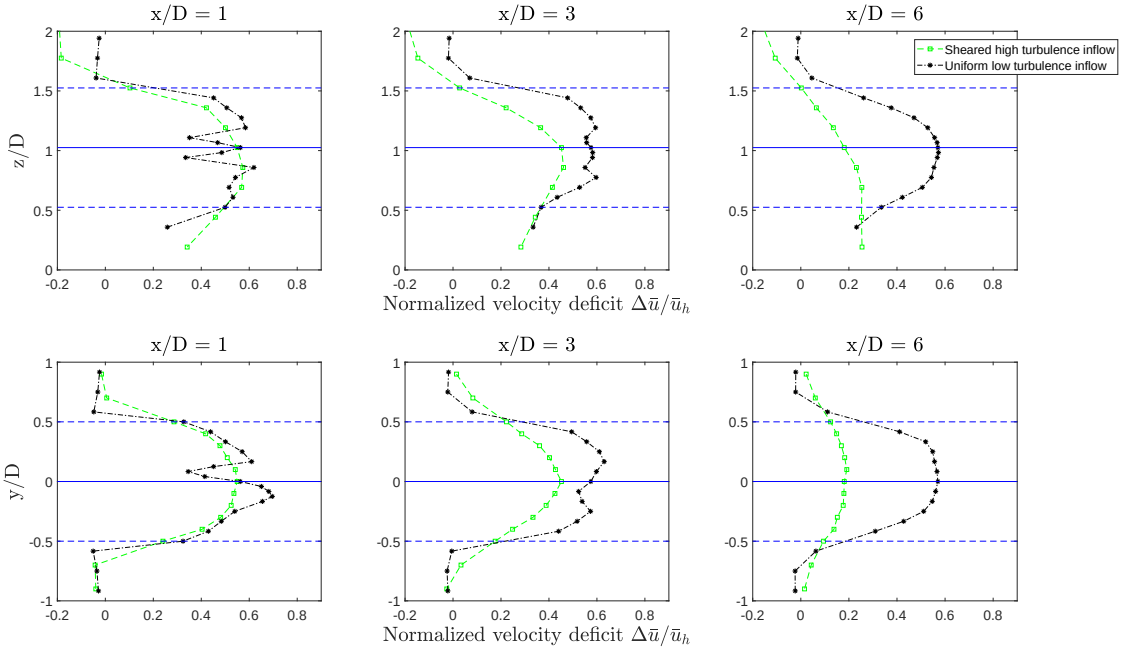


Figure 6: Profiles of the normalized streamwise velocity deficit in vertical (*top*) and lateral (*bottom*) direction for $\gamma = 0^o$. Blue solid line and blue dashed lines stand for rotor axis and blade tip positions, respectively.

In Figure 6 the profiles of the normalized streamwise velocity deficit in lateral and vertical direction for the uniform inflow case are also shown. A first remark is the difference in the shape of the profile at 1 D and 3 D: in the sheared turbulent inflow case the profile has a single Gaussian shape whereas in the uniform inflow case this shape is severely distorted. At 1 D downstream of the rotor disk, the shape is mostly influenced by the geometry of the nacelle and hub together with the rotor while at 3 D the profile is similar to a double Gaussian shape with minima at approximately 50% of the blade span.
The effect of ambient turbulence in the wake recovery is also clear from the evolution of the two profiles. At

1 D, even though the two average velocity deficits have similar magnitude, for the high turbulent ambient inflow case the profile is already smoothed. At 3 D there are differences in both profile shape and velocity deficit and at 6 D the shapes are similar (both Gaussian like profiles) but there is a substantial difference in the velocity deficit. In the non turbulent inflow case the wake recovery is negligible while in the highly turbulent inflow case the velocity deficit is already 1/3 of the initial one.

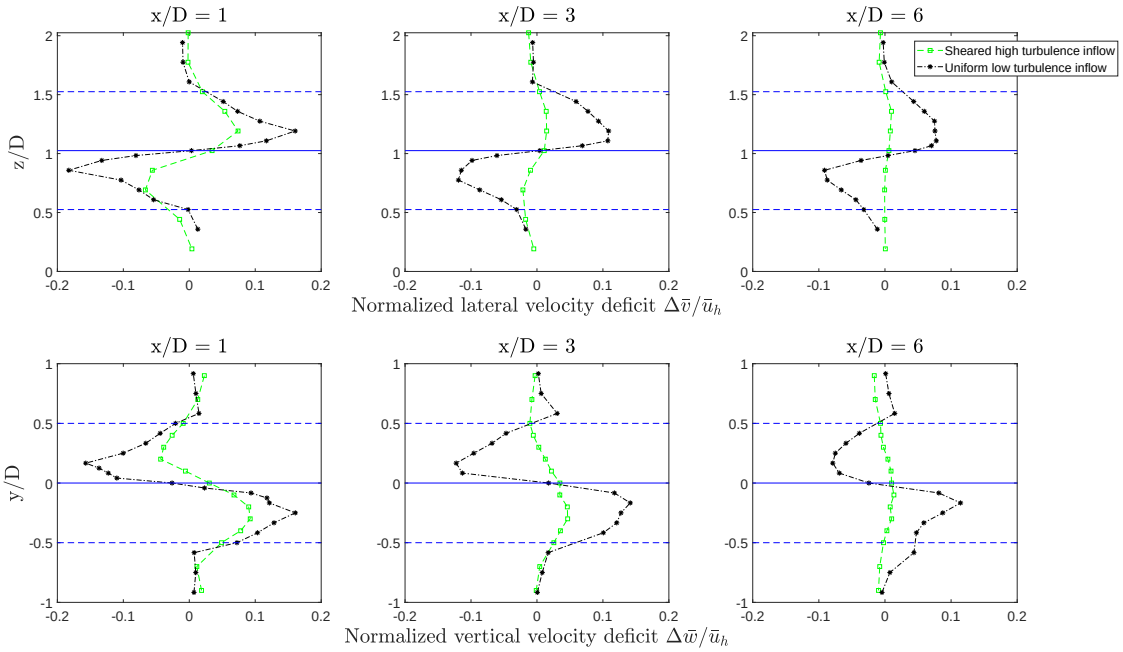


Figure 7: Profiles of the normalized lateral and vertical velocity deficits in the vertical (*top*) and lateral (*bottom*) direction for $\gamma = 0^o$. Blue solid line and blue dashed lines stand for rotor axis and blade tip positions, respectively.

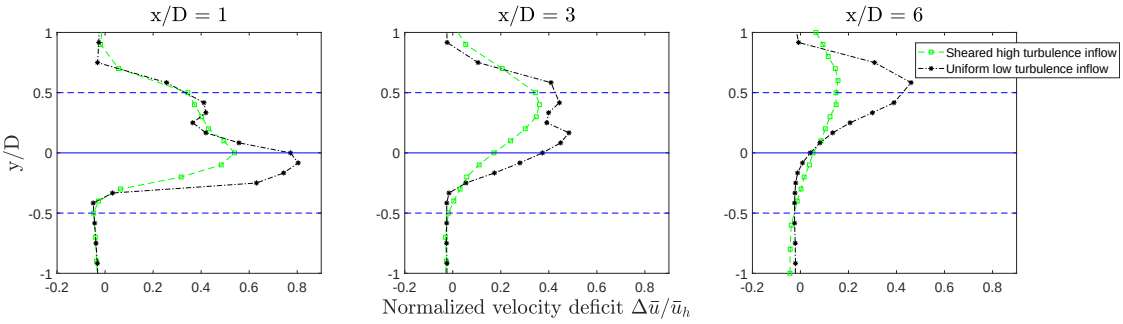


Figure 8: Profiles of the normalized streamwise velocity deficit in the lateral direction for $\gamma = -30^o$. Blue solid line and blue dashed lines stand for rotor axis and blade tip positions, respectively.

In Figure 8 the profile of the streamwise velocity deficit in the lateral direction for yaw angle $\gamma = -30^o$ at three different downstream distances is shown. The wake, due to a lateral component of the thrust that is exerted on the flow when the turbine is yawed, is displaced by approximately 0.6 D at 6 D downstream of the wind turbine which is in line with prior studies.[24] The peculiar profile of the wake at 1 D downstream distance can be explained by the fact that the nacelle is relatively big compared to the rotor diameter and its geometric characteristics are expected to strongly affect the behavior of the near wake.

Another key characteristic of a wind turbine wake is the turbulence intensity, since it directly affects the loads on downstream machines as well as the wake recovery rate. In order to enlighten the turbine's contribution we present the added turbulence intensity which is defined as:

$$I_{u,add} = +\sqrt{{I_u}^2 - {I_{u,inflow}}^2} \qquad I_u \geq I_{u,inflow} \tag{1}$$

$$I_{u,add} = -\sqrt{{I_{u,inflow}}^2 - {I_u}^2} \qquad I_u < I_{u,inflow} \tag{2}$$

where $I_u = \sigma_u / \overline{u_h}$ is the turbulent intensity in the wake and $I_{u,inflow}$ is the ambient turbulence intensity. In Figure 9 the profiles of the added turbulent intensity in the vertical (*top*) and lateral (*bottom*) direction are presented for uniform and sheared inflow. The lateral profile at 1 D for the uniform inflow gives a very clear picture of the effect the turbine has on the flow: the blade tip vortices as well as the nacelle wake are revealed through very well defined peaks in the turbulent intensity.[25] The vertical profile of the same quantity at 1 D reveals also the effect of the tower: the lower blade tip vortex induced turbulence intensity is not clearly defined while it keeps increasing even outside of the rotor area. For the sheared high turbulence inflow case, the profiles are quite different. It can be observed from the profiles in both vertical and lateral direction at 1 D that the wind turbine is reducing the turbulent intensity of flow. As it has been explained in previous studies,[26] in highly sheared flows the presence of wind turbine can actually reduce the intense shear of the flow especially close to the ground.

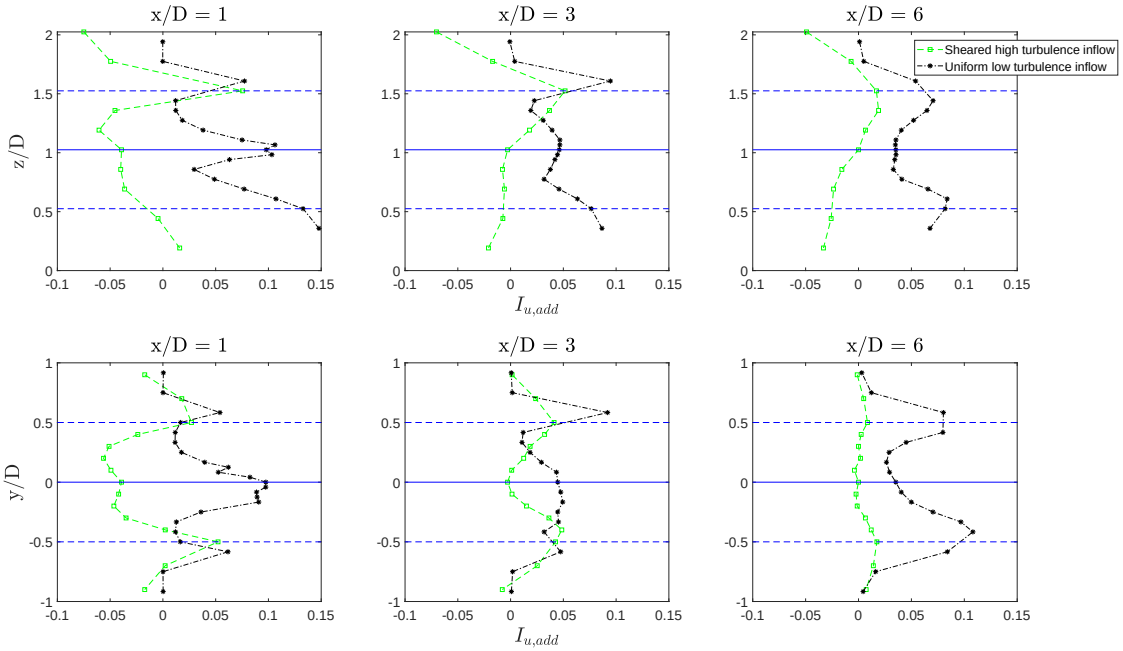


Figure 9: Profiles of the added turbulence intensity in vertical (*top*) and lateral (*bottom*) direction for $\gamma = 0^o$. Blue solid line and blue dashed lines stand for rotor axis and blade tip positions, respectively.

## B. Wake structure

Most of the current reduced wind farm models are two dimensional i.e. they model the wake only at hub height. Similarly, the majority of wind tunnel measurements is constrained to wake profiles at hub height. Nevertheless, the wake is highly anisotropic when it develops within a boundary layer and/or under wind misalignment, conditions that are the rule rather than the exception inside a wind farm. Therefore, knowledge of the complete structure of the wake becomes essential for an adequate fidelity wind farm modeling suitable

for wind farm control.
In this paragraph the structure of the G06 wake is discussed using the data from the S-PIV. Figure 10 (*left*) shows the contour of the velocity deficit normalized with the inflow velocity at 3.5 D downstream for yaw $\gamma = 0^o$ while Figure 10 (*right*) is for $\gamma = -30^o$. The zero yaw case shows a clearly defined isotropic wake, which is to be expected due to the uniform and non turbulent inflow. Another feature, is the area of lower deficit close to the wake center which could be attributed to the relatively high hub to rotor diameter ratio (around 10%) that this model has due to its instrumentation.
The $\gamma = -30^o$ case shows some interesting characteristics. First, it reveals the previously reported[27] kidney shape of the wake and the presence of counter rotating vortex pair that creates that shape. In addition, it is visible that the core of the wake has been pushed upwards quite significantly due to the interaction between the two counter rotating vortices and the wake swirl. This is a phenomenon that has been observed in flows with counter rotating vortex pairs[28] and has also been reported for wind turbine wakes under yawed conditions.[29] The amount of vertical displacement, which can be upward or downward, depending on the sign of the yaw misalignment and rotor rotation, is certainly affected by the inflow conditions. In low turbulence flows, like in our case, the dissipation rate of the vortices is much lower than in high turbulent flows. Hence, they remain active for longer thus pushing the core of the wake further. What is more, the wake swirl, which depends on the torque coefficient, together with the counter rotating vortices induce a complex flow pattern that governs the evolution of the wake shape. Consequently, it is reasonable to believe that the torque coefficient of the wind turbine has an effect on the development of the wake, especially for turbines working under yaw misalignment. This effect should, of course, be quantified with further wake measurements under several model operating points.

Figure 11 shows contours of the normalized streamwise velocity deficit in the horizontal plane of measurement for yaw $\gamma = 0^o$ on the left and $\gamma = -30^o$ on the right. For the yawed turbine case, the streamlines reveal a strong lateral velocity component only at one side of the wake, i.e. as shown in previous studies[30] the lateral component of the velocity has an asymmetric distribution with respect to the wake center.

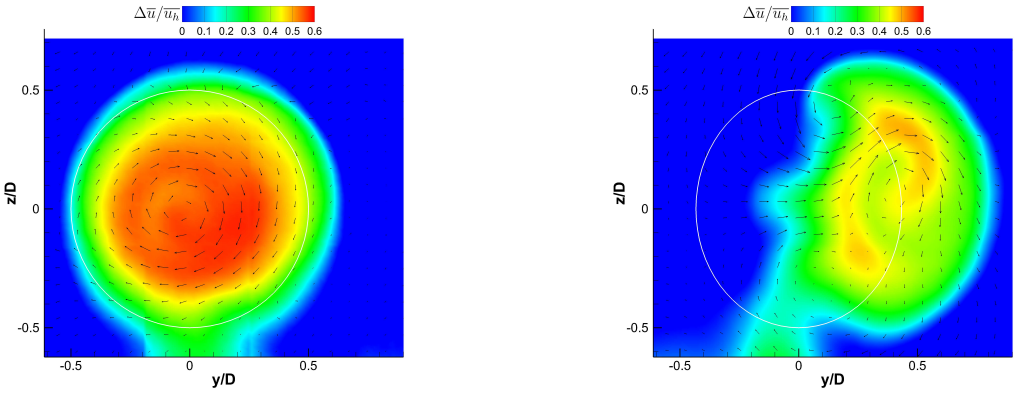


Figure 10: Contours of the normalized streamwise velocity deficit in yz planes 3.5 D downstream of the rotor (looking upstream) for yaw angle $\gamma = 0^o$ (*left*), and $\gamma = -30^o$ (*right*) . The vectors stand for the in-plane velocity components. The white line encloses the rotor area.


Figure 11: Contours of the normalized streamwise velocity deficit in xy planes 3.5 D downstream of the rotor for yaw angle $\gamma = 0^o$ (*left*), and $\gamma = -30^o$ (*right*). In-plane streamlines of the flow are also plotted. The white lines denote rotor edges.

## V. Conclusions

Wind tunnel measurements were conducted with aim of performing an initial characterization of the wake of a novel multipurpose scaled wind turbine model. Two different wind tunnels of similar dimensions were used, under a uniform low turbulent inflow in order to appreciate the effect of the wind tunnel, if any, together with the wake characterization 3.5 D downstream of the model. Results showed a quite good agreement for both tested yaw angles, namely $\gamma = 0^o$ and $\gamma = -30^o$. Regarding the structure of the wake, as obtained from S-PIV measurements, it showed a good agreement with previous studies revealing the most interesting characteristics, like the kidney shape of the wake when the turbine operates in yawed condition with respect to the wind. In addition, measurements were done in the same wind tunnel at 1 D, 3 D and 6 D under two different inflow conditions, namely first under uniform low turbulent and second under sheared high turbulent inflow, in order to evaluate the mean wake statistics for two different inflow conditions. Results confirmed previous findings as the wake characteristics differ substantially for the two inflow cases. Key differences are the recovery rate and added turbulence intensity. Moreover, the wake main characteristics (wind speed deficit, wake center deflection etc.) agree quantitatively with previous wind tunnel studies for both inflow cases. Future steps on the wake characterization of this model include extensive S-PIV measurements for sheared inflow for several yaw angles with a more comprehensive analysis of the wake turbulence statistics and its influence on the dynamics of downstream machines.

## VI. Acknowledgments

This work has been partially supported by the AWESOME project, which receives funding from the European Union Horizon 2020 research and innovation program under grant agreement No. 642108. The authors would also like to thank Professor Christian Breitsamter for his support during the wind tunnel experiments at TUM-AER.

## References

[1]J. G. Schepers and S. P. van der Pijl. Improved modelling of wake aerodynamics and assessment of new farm control strategies. *Journal of Physics: Conference Series*, 75(1):012039, 2007.

[2]R. J. Stevens and C. Meneveau. Flow structure and turbulence in wind farms. *Annual Review of Fluid Mechanics*, 49(1):311–339, 2017.

[3]S. El-Asha, L. Zhan, and G. V. Iungo. Quantification of power losses due to wind turbine wake interactions through

scada, meteorological and wind lidar data. *Wind Energy*, 20(11):1823–1839, 2017.

[4]V. Santhanagopalan, M. Rotea, and G. V. Iungo. Performance optimization of a wind turbine column for different incoming wind turbulence. *Renewable Energy*, 116, 2017.

[5]V. Santhanagopalan, S. Letizia, L. Zhan, L. Al-hamidi, and G. Iungo. Profitability optimization of a wind power plant performed through different optimization algorithms and a data-driven rans solver. *2018 Wind Energy Symposium, AIAA SciTech Forum, American Institute of Aeronautics and Astronautics*, 2018.

[6]G. Iungo, F. Viola, U. Ciri, S. Leonardi, and M. Rotea. Reduced order model for optimization of power production from a wind farm. *34th Wind Energy Symposium, AIAA SciTech Forum, American Institute of Aeronautics and Astronautics*, 2016.

[7]P. M. Gebraad, F. W. Teeuwisse, J. W. van Wingerden, P. A. Fleming, S. D. Ruben, J. R. Marden, and L. Y. Pao. Wind plant power optimization through yaw control using a parametric model for wake effects-a cfd simulation study. *Wind Energy*, 19(1):95–114, 2016.

[8]F. Campagnolo, V. Petrović, J. Schreiber, E. M. Nanos, A. Croce, and C. L. Bottasso. Wind tunnel testing of a closed-loop wake deflection controller for wind farm power maximization. *Journal of Physics: Conference Series*, 753:032006, 2016.

[9]L. J. Vermeer, J. N. Sørensen, and A. Crespo. Wind turbine wake aerodynamics. *Progress in Aerospace Sciences*, 39(6-7):467–510, 2003.

[10]B. Sanderse. Aerodynamics of wind turbine wakes - literature review. Technical report, ECN Wind Energy, 2009.

[11]Coleman, R. P., Feingold, A. M. and Stempin, C. W. Evaluation of the induced-velocity field of an idealized helicoptor rotor. *Technical Report, DTIC Document*, 1945.

[12]I. Grant and P. Parkin. A dpiv study of the trailing vortex elements from the blades of a horizontal axis wind turbine in yaw. *Experiments in Fluids*, 28(4):368–376, 2000.

[13]P. Krogstad and M. S. Adaramola. Performance and near wake measurements of a model horizontal axis wind turbine. *Wind Energy*, 15(5):743–756, 2012.

[14]D. Medici and P. H. Alfredsson. Measurements on a wind turbine wake: 3d effects and bluff body vortex shedding. *Wind Energy*, 9(3):219–236, 2006.

[15]H. Snel, J. G. Schepers, and B. Montgomerie. The mexico project (model experiments in controlled conditions): The database and first results of data processing and interpretation. *Journal of Physics: Conference Series*, 75:012014, 2007.

[16]C. L. Bottasso, F. Campagnolo, and V. Petrović. Wind tunnel testing of scaled wind turbine models: Beyond aerodynamics. *Journal of Wind Engineering and Industrial Aerodynamics*, 127:11–28, 2014.

[17]Cluster WindForS Wind Energy Resarch. A test site for wind energy research. `https://www.windfors.de/en/projects/test-site/`. Accessed: 2018-06-06.

[18]C. L. Kelley, D. C. Maniaci, and B. R. Resor. Scaled aerodynamic wind turbine design for wake similarity. *34th Wind Energy Symposium, AIAA SciTech Forum, American Institute of Aeronautics and Astronautics*, 2016.

[19]C. Bak, F Zahle, R. Bitsche, T. Kim, A. Yde, L. C. Henriksen, M. H. Hansen, J. P. Blasques, M. Gaunaa, and A. Natarajan. The dtu 10-mw reference wind turbine. *Danish Wind Power Research 2013*, Technical University of Denmark, DTU Wind Energy, 2013.

[20]E. M. Nanos, N. Kheirallah, F. Campagnolo, and C. L. Bottasso. Design of a multipurpose scaled wind turbine model. *Journal of Physics: Conference Series*, 1037:052016, 2018.

[21]H. Kozmar. Characteristics of natural wind simulations in the tum boundary layer wind tunnel. *Theoretical and Applied Climatology*, 106(1-2):95–104, 2011.

[22]P.W. Bearman. Corrections for the effect of ambient temperature drift on hot-wire measurements in incompressible flow. *DISA INF.*, 11:25–30, 05 1971.

[23]A.A. Lab Systems. *AN-1003 Hot-Wire & Film Anemometry System - User's Manual*. A.A. Lab Systems LTD, 1999.

[24]J. Schreiber, E. M. Nanos, F. Campagnolo, and C. L. Bottasso. Verification and calibration of a reduced order wind farm model by wind tunnel experiments. *Journal of Physics: Conference Series*, 854:012041, 2017.

[25]T Hahm and S Wuow. Turbulent wakes in wind farm configuration. *European Wind Energy conference and exhibition, Athens, Greece*, pages 1387–1394, 2006.

[26]L. P. Chamorro and F. Porté-Agel. A wind-tunnel investigation of wind-turbine wakes: Boundary-layer turbulence effects. *Boundary-Layer Meteorology*, 132(1):129–149, 2009.

[27]M. F. Howland, J. Bossuyt, L. A. Martínez-Tossas, J. Meyers, and C. Meneveau. Wake structure in actuator disk models of wind turbines in yaw under uniform inflow conditions. *Journal of Renewable and Sustainable Energy*, 8(4):043301, 2016.

[28]R. M. Kelso, T. T. Lim, and A. E. Perry. An experimental study of round jets in cross-flow. *Journal of Fluid Mechanics*, 306(-1):111, 1996.

[29]M. Bastankhah and F. Porté-Agel. A new miniature wind turbine for wind tunnel experiments. part ii: Wake structure and flow dynamics. *Energies*, 10(7):923, 2017.

[30]M. Bastankhah and F. Porté-Agel. Experimental and theoretical study of wind turbine wakes in yawed conditions. *Journal of Fluid Mechanics*, 806:506–541, 2016.

# Wind tunnel testing of a wind turbine in complex terrain



The Science of Making Torque from Wind (TORQUE 2020) IOP Publishing
Journal of Physics: Conference Series **1618** (2020) 032041 doi:10.1088/1742-6596/1618/3/032041

# Wind tunnel testing of a wind turbine in complex terrain

**Emmanouil M Nanos[1], Kutay Yilmazlar[1], Alex Zanotti[2], Alessandro Croce[2] and Carlo L Bottasso[1]**

[1]Wind Energy Institute, Technische Universität München, Garching bei München, Germany.
[2]Dipartimento di Scienze e Tecnologie Aerospaziali, Politecnico di Milano, Milano, Italy.

E-mail: em.nanos@tum.de

**Abstract.** The paper describes the development of a scaled model of complex terrain, suitable for terrain-wind turbine interaction wind tunnel studies, taking into account flow similarity criteria. The size and the geometry of the experimental model of the complex terrain were refined using results of CFD simulations in order to achieve the best possible flow similarity and avoid edge effects arising from the finite (relative to the rotor size) terrain geometry. Moreover, Particle Image Velocimetry was used to survey the flow field on a longitudinal plane along the terrain center line. Flow measurements with and without a wind turbine model enabled to quantitatively evaluate the speed up produced by the terrain in the region of the wind turbine and the effect of the terrain on the wake characteristics of the wind turbine model.

## 1. Introduction

As the share of on-shore wind energy grows rapidly in the global energy mix, turbines are installed on complex sites more and more frequently [1]. It is well known that complex terrain may have considerable effects on the flow within a wind farm, affecting the conditions that a turbine is experiencing. Therefore, accurate micro-siting plays a crucial role for wind farm design and estimation of power production in such landscapes. Studies have shown that even relatively minor errors during the planning phase could lead to considerable losses in annual energy production [2]. Yet, the mathematical models that are commonly used for wind energy systems are not fully validated for complex topographies [3]. Even in the two-dimensional case, it has been shown that linear theories describing the flow over hilly terrains are not sufficiently precise [4]. In a complex terrain with 3D elevation gradients, an erroneous flow prediction might have even higher impact on wind turbine micro-siting. As a consequence, it is necessary to increase the level of understanding of flows over complex terrains so that better flow models can be developed for landscapes where three-dimensional variability of wind characteristics is anticipated [5].

There is a number of studies on flows over complex topographies, typically hills and escarpments, dealing with the topic both from the numerical and experimental points of view [6, 7, 8], while there are some purely numerical studies on wind turbine complex terrain interaction [9, 3, 10, 11]. However, there is a lack of experimental studies that combine complex terrain and wind turbines and can provide benchmark measurements. The studies by Hyvärinen et al. [12] and Tian et al. [13], who used idealized two-dimensional terrain models, are the sole

The Science of Making Torque from Wind (TORQUE 2020) IOP Publishing
Journal of Physics: Conference Series **1618** (2020) 032041 doi:10.1088/1742-6596/1618/3/032041

examples, yet they used simplified geometries with low Reynolds flows. Combining relatively high Reynolds complex terrain and a fully controllable wind turbine requires careful design of the set-up, with the literature lacking relevant examples. This paper aims at filling this gap by presenting the design of a wind tunnel study of a complex terrain coupled with a wind turbine. To this purpose, a scaled model of a real test site is designed and manufactured with the goal of producing an experimental set-up that provides an as-realistic-as-possible flow while satisfying the constraints given by the wind tunnel and the measuring equipment. Following this, PIV measurements are performed as a preliminary analysis of the flow behaviour over the terrain with and without the presence of a scaled wind turbine model. The goal is to validate an experimental set-up that can contribute to a better understanding of turbine-terrain interaction in terms of wake behavior and turbine performance, and to provide data for the validation of numerical codes. The paper is organized as follows: in section 2 the methodology followed for the design of the terrain is described, section 3 presents the wind tunnel measurement results, while section 4 provides the most significant conclusions of this work along with the next steps on this project.

## 2. Terrain design methodology

### *2.1. Design of terrain model*

The terrain model is based on a test site located in Stöttener Berg close to Gieslingen in Baden-Württemberg, in the south-west of Germany. Over the past years, this site has been home to wind energy research projects such as KonTest and WINSENT. Within the scope of these projects, site measurements have been executed involving met masts, Lidars and unmanned aerial vehicles at various locations [14, 15]. Two research wind turbines are planned to be installed close to the escarpment for further wind turbine-terrain interaction studies. The terrain consists of a densely forested steep escarpment, showing a relative elevation of ca. 200 m and slopes up to 30°, and a relatively flat plateau with minor vegetation following the slope. The main wind direction is reported at 295° [14]. A digital elevation of the terrain, aligned with the main wind direction, is shown in Fig. 1. A red frame outlines the portion represented by the wind tunnel model, while a red x symbol reports the turbine position (WT), where the dimensions are given in rotor diameters. In the initial stage of the terrain design, the width of the terrain was chosen to be 7 rotor diameters as a compromise between low blockage (which requires a small width) and effect on the flow (which requires a larger width). In order to ease the manufacturing of the terrain model and the execution of the experiments, the terrain is divided into two parts as labelled in the terrain elevation profile in Fig. 2. The plateau starting from the red dashed line is considered to be completely flat in the present study.

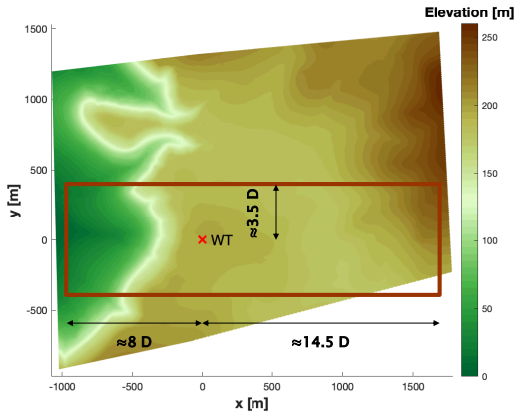


Figure 1: Modelled area on topographic map.

Given the confined space of the wind tunnel, the terrain will have, contrary to the real test field, finite dimensions relative to the size of the turbine. It is therefore necessary to optimize the shape and size of the terrain in a way that edge effects are minimized while blockage is kept as low as possible. To analyse the effects of model boundaries on the flow behaviour, a set of model geometries, which is given in Fig. 3, was simulated via Large Eddy Simulations performed

The Science of Making Torque from Wind (TORQUE 2020) IOP Publishing
Journal of Physics: Conference Series **1618** (2020) 032041 doi:10.1088/1742-6596/1618/3/032041

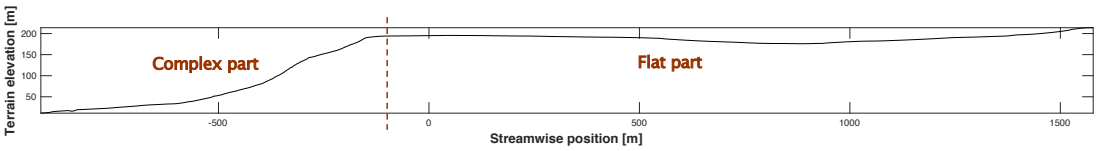


Figure 2: Elevation profile along a plane passing through the center of the wind turbine rotor. The red dashed line indicates the transition point from complex part to flat part.

in *OpenFOAM*. The model geometries are simplified 2D versions of the actual complex model, and were generated by extruding the elevation profile at the edge of the complex part along the lateral direction. This way, the effect of the side boundaries on the flow is isolated from 3D spatial variations of the terrain for a better analysis. Each model holds the same overall dimensions: 6 x 1 x 13.5 m, along width, height and length, respectively. The implemented numerical setup is based on an in-house developed LES framework, which has been validated against wind tunnel measurements [16], [17].

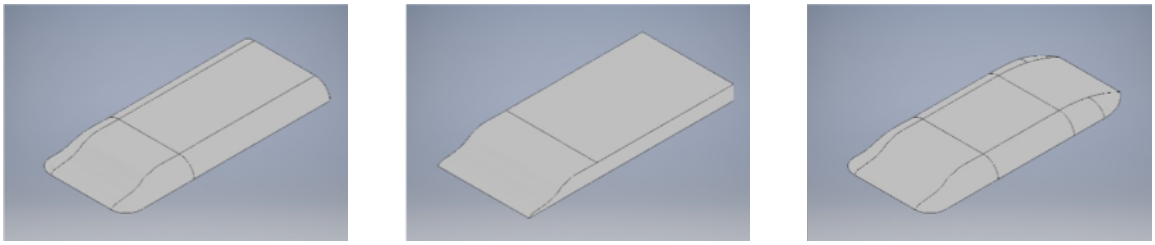

Figure 3: Terrain geometries in comparison: Model A (*left*), Model B (*middle*) and Model C (*right*).

Figure 4 presents a comparison of vorticity magnitudes between Model A and B on the cross-flow plane at the turbine position. As expected, sharp corners induce large vortices at the lateral edges of the model. These vortices are in reality not present in the test field. Since the presence of vortices might influence the flow around the measurement plane and their area of influence is likely to get bigger as they travel downstream, Model A was chosen over Model B.

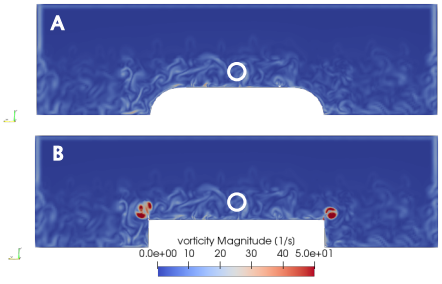


Figure 4: Vorticity comparison: cross-flow plane at rotor position. The white circle indicates the rotor disk.

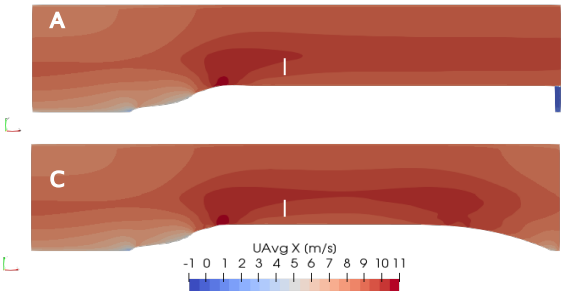


Figure 5: Average velocity comparison: longitudinal plane at rotor center position. The white line indicates the rotor disk.

The Science of Making Torque from Wind (TORQUE 2020) IOP Publishing
Journal of Physics: Conference Series **1618** (2020) 032041 doi:10.1088/1742-6596/1618/3/032041

Another comparative analysis was performed between Model A and C with respect to the back shape of the model. The average velocity fields on the longitudinal plane at the turbine position are presented in Fig. 5. The turbine rotor is indicated with a white line. As shown in the figure, Model C causes a flow acceleration at the beginning of the curved shape at the back of the model. A similar acceleration is reported far downstream of the Bolund Hill plateau before reaching the lee side of the hill in a wind tunnel experiment [18]. Besides, Model A exhibits a more homogeneous flow field behind the turbine, and possible perturbations to the flow caused by the edges of the model and measurement equipment are pushed to the end of the test section by keeping the terrain flat for another 2.5 meters.

*2.2. Flow similarity*

Given that the purpose of the study is to model atmospheric flow in a wind tunnel, it is necessary to assess how the wind tunnel flow is similar to a full scale flow. This was attempted here through a set of dimensionless numbers derived from the Navier-Stokes equations, namely the Reynolds, Richardson, Eckert, Rosby and Prandtl numbers. For the derivation and physical importance of each number the reader can refer to Cermac and Durst [19, 20]. Regarding the Reynolds number, the geometric scaling factor of the terrain is 1:195, which is a relatively large one compared to previous complex-terrain-only studies. In fact, it is well above the minimum scale factor 1:500 for wind modelling over complex terrains recommended by Bowen [21]. Considering an inflow speed of around 8 m/s at hill height, the Reynolds number with respect to hill height $Re_H$ equals ca. $5.14 \times 10^5$, which is the highest $Re_H$ reported in the literature and, according to the findings of McAuliffe and Larose [22], is beyond the threshold for *Re-independent* flow. What is more, with this geometric scaling factor the wind turbine model, which has a D =0.6 m rotor diameter, resembles a typical full-scale on-shore wind turbine.

Since the wind tunnel can produce a neutrally stratified boundary layer, Richardson and Eckert similarity is satisfied. Furthermore, given the fact that the longitudinal length scale of the terrain model (2.6 km at full-scale) is below the maximum limit of 5 km for negligible Coriolis effects [23], Rossby number similarity can be neglected. Finally, the medium of the flow is air, so that Prandtl similarity is also satisfied.

*2.3. Evaluation of blockage effects*

The selected terrain geometry with curved side shapes and a backward facing step has a blockage ratio of 10% in the Atmospheric Boundary Layer (ABL) wind tunnel of Politecnico di Milano, which has a cross section of 13.84 m x 3.84 m. In general, blockage effects can be neglected when the blockage ratio is lower than 5% [24]. Since the present terrain model exceeds this safe limit, the blockage effects should be quantified. At this aim, two CFD analyses have been considered: the first models the correct wind tunnel geometry as implemented for Model A in the previous section, while a second one, with a *blockage-free* configuration, is implemented by extending the wind tunnel domain up to a cross-section of 25 m x 9 m (ca. 1.8 times the actual width and 2.3 times the actual height of the wind tunnel). Hereby, blockage ratio is reduced to 2.5%, which means that blockage effects are negligible. Blockage analysis was performed with steady RANS simulations in *Ansys Fluent* using the standard k-$\epsilon$ turbulence model.

The streamwise velocity component $U_x$ is plotted on longitudinal and lateral planes in Fig. 6. It is clear that the wind tunnel blockage has some influence on the results. A point to point comparison of the results from both models reveals that the turbine rotor is experiencing a 5% higher wind speed in the wind tunnel than it would in an open free-stream environment, a fact that should be taken into account when analysing the experimental data.

The Science of Making Torque from Wind (TORQUE 2020) IOP Publishing
Journal of Physics: Conference Series **1618** (2020) 032041 doi:10.1088/1742-6596/1618/3/032041

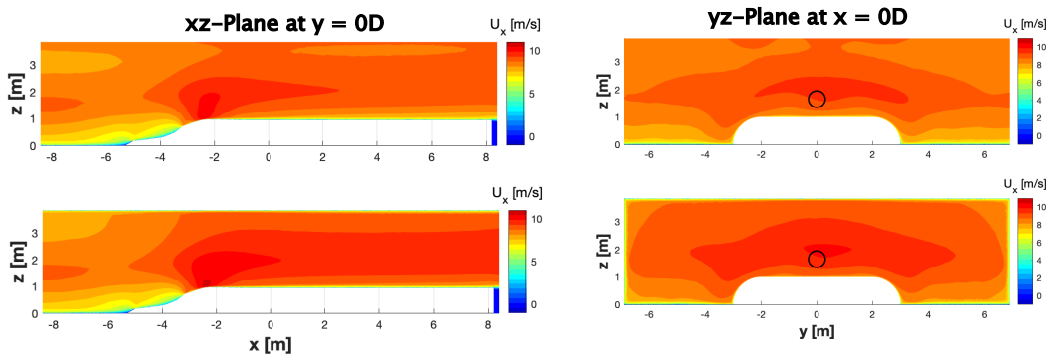


Figure 6: Blockage effects on average velocity field. Top row: results from blockage-free configuration; bottom row: results from model with actual wind tunnel geometry.

*2.4. Manufacturing of the terrain*

The complex terrain model was divided into 9 sub-parts with dimensions around 1.35 m x 1.5 m (width x length), to conform to the CNC machine operational range and for transportability. Polystyrene foam (EPS) with a density of 20 kg/m$^3$ was selected as material based on low cost, low weight and millability. Each part was cut from a block of EPS by a 5-axis-CNC machine starting with a 40 mm diameter spherical cutter to give an initial coarse shape (see Fig. 7), and then refining the surface with an 8 mm diameter spherical cutter. Thanks to the small tolerance range of the CNC machine (+/- 0.15 mm) and the high resolution digital elevation model (grid spacing equal to 5mm), a very precise terrain model was produced. Since $Re_H$ is high enough to ensure a turbulent boundary layer and, consequently, avoid laminar separation issues, the model surface was kept smooth without any additional roughness elements or terraced shapes, which have been used to enhance transition to turbulent boundary layer in previous complex terrain studies [22, 6]. Due to limitations of the minimum thickness that can be produced at the lowest point of the model, an upward offset of 20 mm had to be realized. Furthermore, the upstream parts were glued on a 4 mm thick plywood to prevent the flow to leak under the model. In total, the height of the model is increased by 24 mm to approximately 97 cm.

Figure 7: A complex sub-part cut by CNC machine.

For the rest of the model, a lighter and cheaper EPS with a density of 10 kg/m$^3$ was used. To reduce the costs, these parts were cut by a hot-wire-cutter with a lower precision. For the curved side shapes, 8 cross sections along the length of the complex part were used. Rectangular blocks of foam were used to realise the flat part of the model. Their top surfaces were covered with thin plywood sheets, for ensuring structural integrity and for allowing safe access to the flat surface during experiments. In the middle line of the test section, a thick wooden platform, mounted on an aluminium frame, was constructed to support the model and all the measuring equipment. After mounting all the model components in the wind tunnel, their adjacent edges were taped together in order to block possible flow paths through the terrain model. The final

The Science of Making Torque from Wind (TORQUE 2020) IOP Publishing
Journal of Physics: Conference Series **1618** (2020) 032041 doi:10.1088/1742-6596/1618/3/032041

layout of the experiment can be viewed in Fig. 8.

## 3. Wind tunnel measurements

### *3.1. Experimental set-up*

The experiments were conducted in the ABL test section of the wind tunnel at Politecnico di Milano. The flow field was measured with a PIV system arranged on a vertical plane at the hub height and parallel to the flow, on a rectangular plane of size approximately 4 D x 2 D (see Fig. 9). The PIV equipment included a Nd:Yag double pulsed laser with 200 mJ/pulse and a 2 Mpx double shutter camera mounted on a traversing system to span the entire measurement area. The total investigated domain of about 3 m x 1.2 m is one of the largest areas that have been examined via PIV so far [2]. The total measurement area was composed by twelve windows with

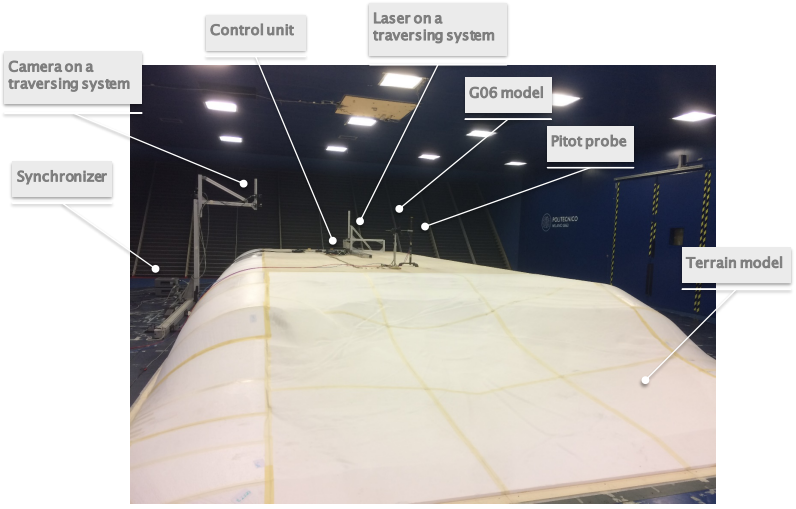


Figure 8: Experimental set-up.

a size of approximately 0.75 m x 0.4 m. For each measurement window, 1000 image pairs were captured. Throughout the measurement campaign, two set of measurements were performed. First, the flow over the terrain was investigated without the turbine. Next, a G06 turbine was installed close to the escarpment (1 D downwind from the edge of the slope), similarly to the position of one of the WINSENT turbines at full-scale. The scaled wind turbine (G06) used in this work is a three bladed model with a 0.6 m rotor designed for studies on wakes and wind farm control. It is equipped with manually pitched low Reynolds (RG-14 airfoil) carbon fibre blades, strain gauges at tower base to measure the tower bending loads and a torque-meter to measure the torque on the main shaft. More details about the design, performance and wake characterization of the model can be found in [25] and [26]. The wind turbine was operated at its optimum tip speed ratio and pitch angle throughout all experiments reported here.

A turbulent inflow was generated with the use of spires at the inlet of the wind tunnel test section and bricks used as roughness elements placed on the tunnel floor upwind of the terrain model for a length of approximately 20 m, about 20 times the hill height. With the given turbulent inlet configuration, the resulting inflow velocity profile is presented in Fig. 10, where the vertical coordinate is normalized by the hill height $H$. Measured velocity values (red stars) were obtained from a Pitot tube 2.5 m upstream of the terrain model, where the ABL is fully developed and the flow is not yet influenced by the terrain. The incoming velocity at hub height ($z_{HH} = 1.58$ m above wind tunnel floor) is 8.7 m/s, while the turbulence intensity is 8.77 % at hub height and 11.54 % at the hill height level. Measured values are fitted with

The Science of Making Torque from Wind (TORQUE 2020) IOP Publishing
Journal of Physics: Conference Series **1618** (2020) 032041 doi:10.1088/1742-6596/1618/3/032041

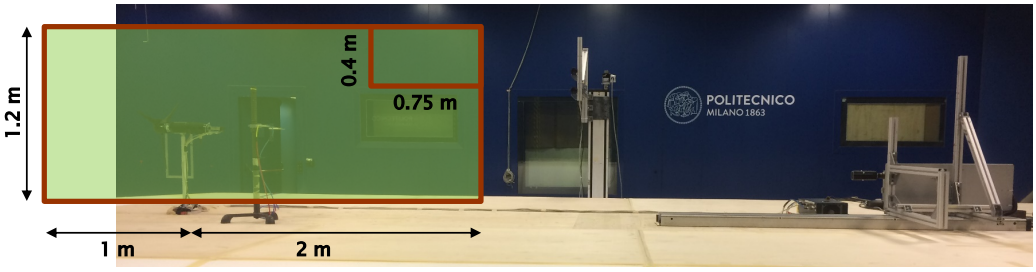


Figure 9: Measurement plane (side view of terrain model).

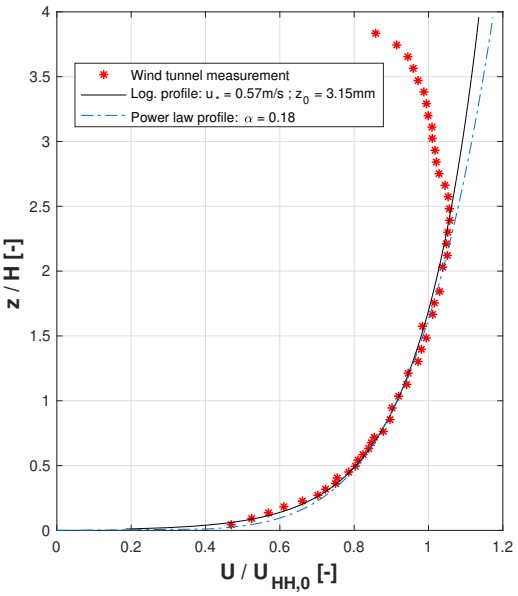


Figure 10: Inflow velocity profile.

a logarithmic wind profile with friction a velocity $u* = 0.57$ m/s and a surface roughness $z_0 = 3.15$ mm. The best match is obtained by power law exponent $\alpha = 0.18$, which is in line with a roughness length classification *moderately rough*, according to VDI guidelines [24]. The ABL profile with this $\alpha$ value builds up above *grassland* terrain, which is, in fact, present in the upwind region of the escarpment. At the light of the wind profile parameters, a high surface Reynolds number $Re_* = u_* \times z_0/\nu = 119$, similar to the one reported by Conan et al. [6], ensures an aerodynamically rough (in other words, fully turbulent) flow.

### *3.2. Results*

Velocity data obtained by PIV for the case without the turbine is visualized in Fig. 11. The origin of the reference system used to report the PIV results is at the rotor hub center. The contour plots of the free-stream velocity component show that the flow reaches its highest speed at the edge of the escarpment, due to the blockage caused by the terrain. At this point, the flow has a low shear, hence a relatively uniform velocity profile. Afterwards, it loses speed along the plateau, where a boundary layer starts developing. The vertical velocity field in Fig. 11 at right reveals that the flow has a vertical component equal to about 20% of the inflow speed, due

The Science of Making Torque from Wind (TORQUE 2020) IOP Publishing
Journal of Physics: Conference Series **1618** (2020) 032041 doi:10.1088/1742-6596/1618/3/032041

to the steep slope of the terrain. However, this vertical component is considerably diminished before reaching the turbine position (x/D = 0).

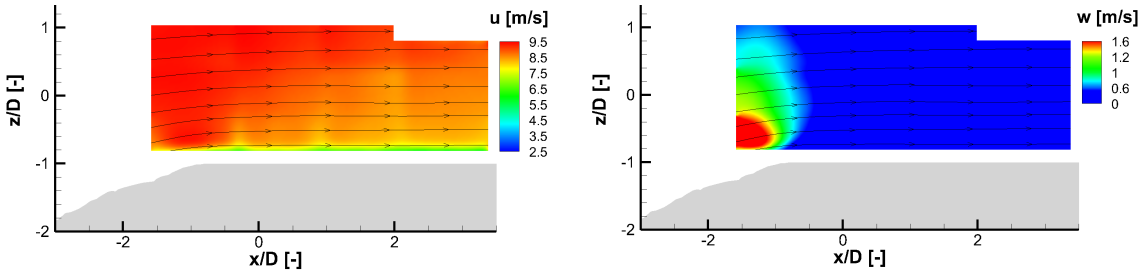


Figure 11: Streamwise (left) and vertical (right) velocity contours without the wind turbine.

Figure 12 shows the contours of the normalized speed-up ratio [27], calculated as the ratio between the free-stream velocity component measured by PIV and the inflow velocity profile measured well upstream of the terrain model (see Fig. 10). Looking at the section in correspondence with the wind turbine rotor disk (x/D = 0), a speed-up of about 25% of the free-stream wind speed with respect to the inlet velocity evaluated without the effect of the terrain is observed at the hub position. Considering the entire region of the rotor disk shown by a black line in Fig. 12, the effect of the terrain results in a consistent increase of the free-stream speed between 18% at the top edge and 37% at the lower edge of the disk.

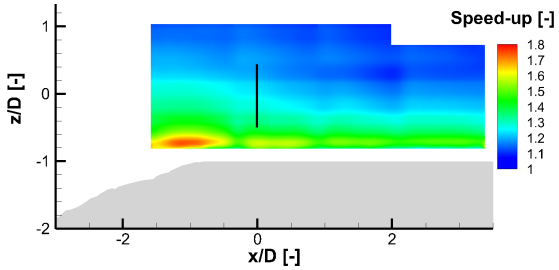


Figure 12: Speed-up ratios at the longitudinal plane; the black line indicates the position of the wind turbine rotor disk.

The flow with the turbine model is illustrated in Fig. 13. The aim here is to analyse the turbine wake behaviour and the impact of the terrain on wake propagation. The velocity deficit behind the turbine along the rotor centerline is clearly seen by looking at the shaded blue contours. The free-stream speed is reduced by ca. 60% at x = 1 D and 50% at x = 3 D at the hub height with respect to the case without the wind turbine. Figure 14 shows vertical profiles of the normalized streamwise velocity $u/U_{hub}$ at x/D = 1 and x/D = 3 downstream of the wind turbine for the complex and flat terrain cases. The flat terrain data are taken from prior measurements in an atmospheric boundary layer at Technical University of Munich with almost identical inflow characteristics ($\alpha = 0.18$, turbulence intensity at hill height 12%) while the complex terrain results have been corrected for blockage effect. Results show a good agreement at x/D = 1 downstream of the rotor for the most part of the wake, except for the lower region where, for the flat terrain case, the velocity is lower. This can be attributed to a reduction in the boundary layer thickness after the escarpment [6], which results in a smaller part of the rotor operating within the boundary layer. At x/D = 3 it can be observed that, apart from the already reported difference close to the terrain, the wake recovers slightly faster for the flat terrain case. This could be explained by a reduction in the turbulence intensity caused by the terrain induced acceleration, even though such a claim requires further investigation.

The Science of Making Torque from Wind (TORQUE 2020) IOP Publishing
Journal of Physics: Conference Series **1618** (2020) 032041 doi:10.1088/1742-6596/1618/3/032041

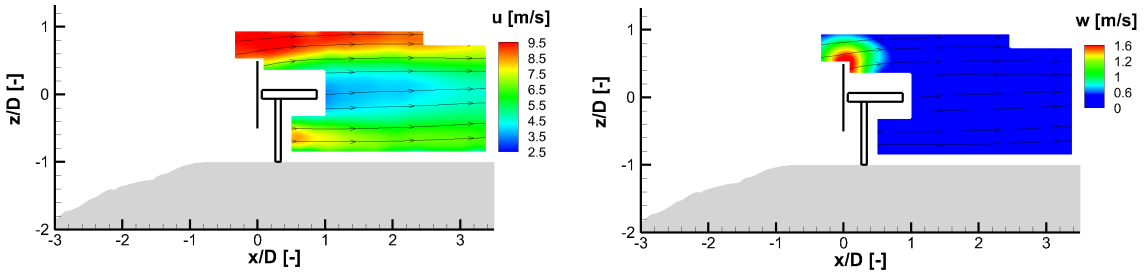


Figure 13: Streamwise (left) and vertical (right) velocity contours with the wind turbine.

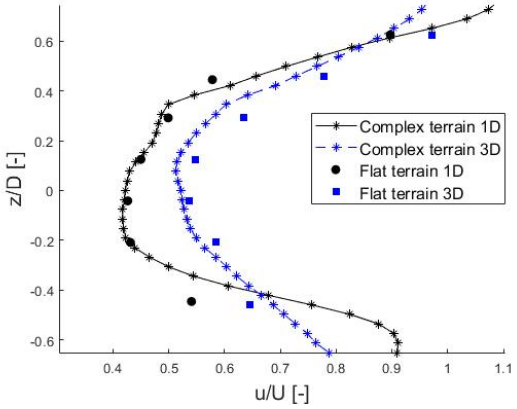


Figure 14: Comparison of vertical wake profiles at 1 D and 3 D between the complex terrain and flat terrain cases.

## 4. Conclusions

A scaled model of a complex terrain test site was designed and manufactured taking flow similarity criteria into consideration. CFD simulations were used for refining the terrain geometry to ease the manufacturing of the wind tunnel model as well as for evaluating the blockage effect of the terrain when placed in the wind tunnel. The resulting terrain geometry ensures a Reynolds independent flow, while it induces a 5% increase of the wind speed caused by the presence of the wind tunnels walls. The flow over the terrain was measured with PIV with and without a scaled wind turbine model. Initial results without the turbine showed that the terrain induces a consistent increase of the free stream velocity component at the wind turbine rotor disk position with respect to inlet flow measurements. Moreover, a considerable vertical velocity component about 1 D upstream of the turbine was observed from the measurements, due to the steep slope of the terrain. Measurement results with the turbine showed that this particular complex terrain geometry has only a limited influence on the wake, mostly apparent in its lower part close to the ground. In addition, there is a slightly weaker recovery rate about three diameters downstream of the rotor compared to a flat terrain case.

Future steps on this study would be to perform hot-wire and stereo PIV measurements in selected areas of the flow field upstream and downstream of the wind turbine, in order to assess the influence of the terrain on the whole wake area including possible effects on the lateral velocity component. Moreover, a future analysis will include second order statistics, such as turbulence intensity and momentum fluxes that can have considerable effects on wake behaviour (such as

recovery rate) and wind turbine performance. Additionally, the terrain will be equipped with a vegetation model, based on the actual vegetation of the test site, with the aim of experimentally evaluating the effect that this terrain feature can have on the inflow.

## 5. References

[1] Alfredsson P H and Segalini A 2017 *Philosophical Transactions of the Royal Society A* **375** 20160096
[2] Lange J, Mann J, Berg J, Parvu D, Kilpatrick R, Costache A, Chowdhury J, Siddiqui K and Hangan H 2017 *Environmental Research Letters* **12** 094020
[3] Politis E S, Prospathopoulos J, Cabezon D, Hansen K S, Chaviaropoulos P and Barthelmie R J 2012 *Wind Energy* **15** 161–182
[4] Ayotte K W and Hughes D E 2004 *Boundary-Layer Meteorology* **112** 525–556
[5] Chock G Y and Cochran L 2005 *Journal of Wind Engineering and Industrial Aerodynamics* **93** 623–638
[6] Conan B, Chaudhari A, Aubrun S, van Beeck J, Hämäläinen J and Hellsten A 2016 *Boundary-layer meteorology* **158** 183–208
[7] Jubayer C M and Hangan H 2018 *Journal of Wind Engineering and Industrial Aerodynamics* **175** 65–76
[8] Li Y, Xu X, Zhang M and Xu Y 2017 *Advances in Structural Engineering* **20** 1223–1231
[9] Lutz T, Schulz C, Letzgus P and Rettenmeier A 2017 Impact of complex orography on wake development: Simulation results for the planned windfors test site *Journal of Physics: Conference Series* vol 854 (IOP Publishing) p 012029
[10] Schulz C, Letzgus P, Weihing P, Lutz T and Krämer E 2018 Numerical simulation of the impact of atmospheric turbulence on a wind turbine in complex terrain *Journal of Physics: Conference Series* vol 1037 (IOP Publishing) p 072016
[11] Schulz C, Lutz T and Krämer E 2018 Aerodynamic response of wind turbines in complex terrain to atmospheric boundary layer flows *New Results in Numerical and Experimental Fluid Mechanics XI* (Springer) pp 753–764
[12] Hyvärinen A and Segalini A 2017 *Journal of Energy Resources Technology* **139** 051205
[13] Tian W, Ozbay A, Yuan W, Sarakar P, Hu H and Yuan W 2013 An experimental study on the performances of wind turbines over complex terrain *51st AIAA aerospace sciences meeting including the new horizons forum and aerospace exposition* vol 7 pp 1–14
[14] Schulz C, Hofsäß M, Anger J, Rautenberg A, Lutz T, Cheng P W and Bange J 2016 Comparison of different measurement techniques and a cfd simulation in complex terrain *Journal of Physics: Conference Series* vol 753 (IOP Publishing) p 082017
[15] Hofsäß M, Clifton A and Cheng P 2018 *Remote Sensing* **10** 1465
[16] Wang J, Wang C, Campagnolo F and Bottasso C L 2018 *Wind Energy Science under review*
[17] Wang C, Wang J, Campagnolo F, Carraón D and Bottasso C L 2018 Validation of large-eddy simulation of scaled waked wind turbines in different yaw misalignment conditions *Journal of Physics: Conference Series* vol 1037 (IOP Publishing) p 062007
[18] Yeow T S, Cuerva-Tejero A and Perez-Alvarez J 2015 *Wind Energy* **18** 153–169
[19] Cermac J E 1970 Laboratory simulation of the atmospheric boundary layer Tech. rep.
[20] Durst F 2008 *An introduction to the theory of fluid flows* (Springer)
[21] Bowen A 2003 *Journal of Wind Engineering and Industrial Aerodynamics* **91** 1859–1871
[22] McAuliffe B R and Larose G L 2012 *Journal of Wind Engineering and Industrial Aerodynamics* **104** 603–613
[23] Snyder W H 1972 *Boundary-Layer Meteorology* **3** 113–134
[24] VDI 2000 Vdi 3783/12, 2000. environmental meteorology—physical modelling of flow and dispersion processes in the atmospheric boundary layer—applications of wind tunnels
[25] Nanos E M, Kheirallah N, Campagnolo F and Bottasso C L 2018 Design of a multipurpose scaled wind turbine model *Journal of Physics: Conference Series* vol 1037 (IOP Publishing) p 052016
[26] Nanos E M, Robke J, Heckmeier F, Jones K, Cerny M, Iungo G V and Bottasso C L 2019 Wake characterization of a multipurpose scaled wind turbine model *AIAA Scitech 2019 Forum* p 2082
[27] Kilpatrick R, Hangan H, Siddiqui K, Parvu D, Lange J, Mann J and Berg J 2016 *Wind Energ. Sci* **1** 237–254

https://doi.org/10.5194/wes-2021-79
Preprint. Discussion started: 19 August 2021


eawe european academy of wind energy
Open Access WIND ENERGY SCIENCE DISCUSSIONS

# Vertical wake deflection for floating wind turbines by differential ballast control

Emmanouil M. Nanos[1], Carlo L. Bottasso[1], Dimitris I. Manolas[2], and Vasilis A. Riziotis[2]

[1]Wind Energy Institute, Technische Universität München, 85748 Garching b. München, Germany
[2]School of Mechanical Engineering, National Technical University of Athens, 15780 Athens, Greece

**Correspondence:** C.L. Bottasso (carlo.bottasso@tum.de)

**Abstract.**

This paper presents a feasibility analysis of vertical wake steering for floating turbines by differential ballast control. This new concept is based on the idea of pitching the floater with respect to the water surface, thereby achieving a desired tilt of the turbine rotor disk. The pitch attitude is controlled by moving water ballast among the columns of the floater.

This study considers the application of differential ballast control to a conceptual 10 MW wind turbine installed on two platforms, differing in size, weight and geometry. The analysis considers: a) the aerodynamic effects caused by rotor tilt on the power capture of the wake-steering turbine and at various downstream distances in its wake; b) the effects of tilting on fatigue and ultimate loads, limitedly to one of the two turbine-platform layouts; and c) for both configurations, the necessary amount of water movement, the time to achieve a desired attitude and the associated energy expenditure.

Results indicate that —in accordance with previous research— steering the wake towards the sea surface leads to larger power gains than steering it towards the sky. Limitedly to the structural analysis conducted on one of the turbine-platform configurations, it appears that these gains can be obtained with only minor effects on loads, assuming a cautious application of vertical steering only in benign ambient conditions. Additionally, it is found that rotor tilt can be achieved in the order of minutes for the lighter of the two configurations, with reasonable water ballast movements.

Although the analysis is preliminary and limited to the specific cases considered here, results seem to suggest that the concept is not unrealistic, and should be further investigated as a possible means to achieve variable tilt control for vertical wake steering in floating turbines.

## 1 Introduction

Power production from wind is typically organized in clusters of turbines, forming a wind plant. By interacting through their wakes within the plant, turbines are subjected to adverse effects that reduce their power capture and life expectancy, both for onshore and offshore installations. While in the latter case typical spacings between turbines are quite large, wake-induced losses can still be significant. In fact, in typical offshore conditions wakes persist many diameters downstream of the rotor because of the low turbulence of the atmospheric boundary layer (Vermeer et al., 2003).

https://doi.org/10.5194/wes-2021-79
Preprint. Discussion started: 19 August 2021


eawe european academy of wind energy
Open Access WIND ENERGY SCIENCE DISCUSSIONS

Several remedies against these effects have been proposed so far, as for example changing the induction factor (Steinbuch et al., 1988), redirecting (or "steering") the wake path in the lateral or vertical directions (Parkin et al., 2001; Fleming et al., 2015; Campagnolo et al., 2016a; Fleming et al., 2019; Campagnolo et al., 2020; Doekemeijer et al., 2021), dynamically exciting the wake to enhance mixing (Frederik et al., 2020b, a), and various possible static and/or dynamic —largely unexplored— combinations thereof (Cossu, 2020c). Among these techniques, it appears that static induction is not very effective as far as power capture is concerned (van der Hoek et al., 2019). On the other hand, dynamic mixing techniques are promising, but further research is needed to address various concerns related to increased loading and actuator duty cycle (Wang et al., 2020) and to loss of effectiveness in turbulent inflows (Munters and Meyers, 2018). Among these various proposed solutions, static wake redirection is the most mature wind farm control technique available today, which has already been demonstrated in field experiments (Fleming et al., 2019, 2020; Doekemeijer et al., 2021) and it is also offered as a market product (Energy, 2019).

Wake redirection is based on purposely misaligning the rotor with respect to the wind vector, thereby creating a force component normal to the wind direction that is responsible for deflecting the wake. *Lateral* wake deflection is based on yawing the turbine out of the wind. Since horizontal axis wind turbines are already equipped with active yaw control, this method does not require any radical hardware modification. This fact, together with the significant wake displacements that can be achieved without excessively increasing the loads on the steering turbine, is one of the reasons for the success of this technique, which in fact has been successfully implemented on wind turbines originally designed without taking wake steering into consideration (Fleming et al., 2019, 2020; Doekemeijer et al., 2021).

*Vertical* wake deflection works in the same way as lateral deflection: when the rotor is tilted about an horizontal axis, its thrust is inclined with respect to the ground; in turn, the equal and opposite reaction on the flow is also inclined, resulting in a vertical force component with respect to the ground that deflects the wake in the vertical direction.

There are, however, some key differences between the lateral and vertical deflection strategies.

First, contrary to lateral wake steering, standard wind turbine configurations do not offer an already existing mechanism that can be employed for deflecting the wake vertically. The only exception is the case of downwind teetering rotors, where vertical wake deflection can in principle be achieved by tilting the tip-path plane through blade flapping; however, there are no large downwind teetering rotors on the market today.

Second, vertical steering presents a strong directional dependence. While also lateral steering is not exactly symmetric between left and right misalignments because of the rotation of the wake (Fleming et al., 2018), deflecting the wake towards the sky or towards the ground has profoundly different effects. In fact, in vertically sheared flows, an upward vertical deflection moves the wake into a higher speed flow region, whereas the opposite happens for a downward deflection. Furthermore, when subjected to a downward deflection the wake eventually interacts with the ground, resulting in a strong deformation of the wake structures and in its accelerated recovery (Scott et al., 2020).

Notwithstanding the technical difficulty of implementing vertical wake deflection, this concept has received some attention in the recent literature. For example, Srinivas et al. (2012) presented an analytical study of vertical steering, and evaluated some engineering models in their ability to predict the vertical motion of the wake. Fleming et al. (2015) used computational fluid dynamics (CFD) to simulate a single column of two wind turbines with tilted rotors, while in the paper of Annoni et al. (2017)

https://doi.org/10.5194/wes-2021-79
Preprint. Discussion started: 19 August 2021


eawe european academy of wind energy
Open Access WIND ENERGY SCIENCE DISCUSSIONS

the authors simulated up to three turbines in a column; both studies reported significant power gains at the cluster level, caused by an improved capture downstream that offsets more limited losses upstream. Simulation studies on more complex layouts were conducted by Cossu (2020a) and Cossu (2020b), where the front two rows of turbines in a farm were tilted, obtaining significant power gains at the wind plant level. The author also studied the effect that rotor size, longitudinal spacing between the turbines and thrust setting can have on the plant power output. These studies have highlighted an interesting phenomenon, whereby downward wake deflection leads to the creation of high-speed streaks in the flow, which again are associated with significant power boosting at the plant level. Su and Bliss (2019) used a free-wake method to study a tilted rotor, reporting power benefits for a two-turbine column when deflecting the wake of the upstream machine towards the sky. Scott et al. (2020) performed wind tunnel measurements of a four-by-three grid layout using scaled wind turbine models, where the machines in the third row were tilted. Among other results, the authors reported a faster wake recovery for downward deflection than in the upward case.

In summary, the literature already reports a significant body of evidence indicating that vertical wake steering can be an effective form of wind farm control. Further potential gains could be possibly achieved by combining vertical and lateral steering, although this problem does not seem to have been explored yet. However, the problem of how vertical steering can be achieved in practice remains at present unsolved, except for the downward teetering turbine configuration.

To address this gap, Nanos et al. (2020) proposed a novel way of implementing vertical wake steering for floating wind turbines. This new idea exploits the fact that semi-submersible platforms, which are among the most popular floating concepts (Liu et al., 2016), require the use of ballast to achieve a desired attitude with respect to the sea surface. Attitude control is commonly obtained by storing and distributing water among the columns of the platform in order to change the center of gravity position. Active ballast control systems are already installed on board semi-submersible platforms used by the oil industry; the same concept is included in some offshore-wind conceptual designs (Roddier et al., 1997), where its purpose is mainly to counteract the pitching moment created by the thrust force of the rotor. With reference to wind farm control, the idea pursued here is to use an active ballast control system to pitch the platform, this way achieving a desired tilting of the rotor disk and, therefore, a vertical deflection of the wake. The concept of vertical wake deflection through platform pitching by active ballast control is illustrated in Fig. 1.

The scope of the present work is to refine the concept first presented in Nanos et al. (2020). The objective here is clearly not to design an actual system implementing vertical wake steering by active ballast control, but to perform a feasibility analysis, with the goal of answering the following basic questions:

- Is it conceptually feasible to use differential ballast control to perform vertical wake steering for wind farm control? and what would be the most and least favourable configurations and operational conditions?
- Can an existing ballast control system be used for this additional purpose (similarly to what has been done with yaw control for lateral wake deflection), or should the system be modified somehow?
- Would such a system be able to reach sufficiently large pitch motions (and, hence, rotor tilt angles)? and what would be the achievable tilt rate and associated energy cost?

https://doi.org/10.5194/wes-2021-79
Preprint. Discussion started: 19 August 2021


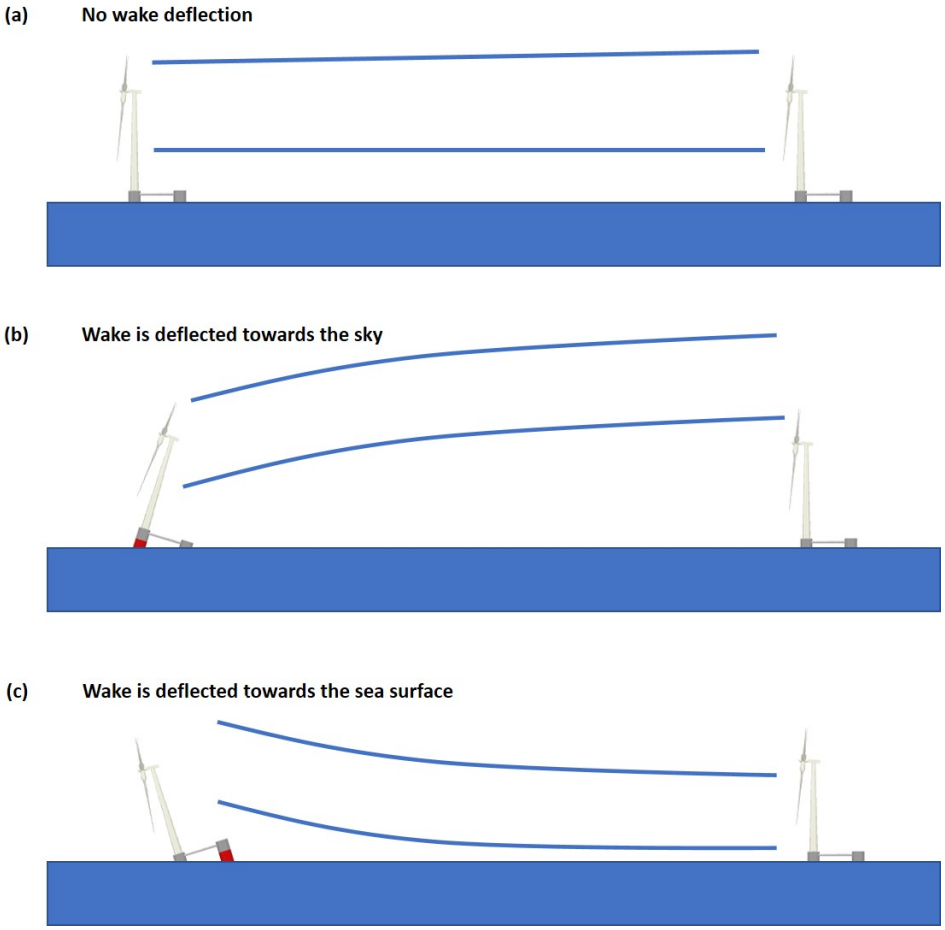


**Figure 1.** Schematic representation of the vertical wake redirection concept.

– Could an existing floating wind system be used for vertical wake steering by ballast control, or would the turbine, platform and/or mooring system need to be partially resized?

More specifically, this paper will:

– Assess the effect of rotor tilt on the wake of a turbine and on the power yield of a column of two turbines. To this purpose, CFD simulations of a scaled wind turbine, validated with wind tunnel experiments, are employed. Expanding on previous tilt misalignment studies, which analyzed streamwise spacings of 6-8 rotor diameters (Fleming et al., 2015; Annoni et al., 2017; Cossu, 2020b; Scott et al., 2020), the present work considers distances up to 12 rotor diameters, which is a more realistic spacing for offshore-wind applications.

https://doi.org/10.5194/wes-2021-79
Preprint. Discussion started: 19 August 2021


eawe european academy of wind energy
Open Access WIND ENERGY SCIENCE DISCUSSIONS

– Make preliminary calculations of the quantity of water ballast that needs to be redistributed for achieving the necessary tilting of the rotor, along with estimating the associated energy expenditure.

– Assess the impact of the proposed method on the structural loading of the turbine, the platform and its mooring system. Although semi-submersible platforms and turbines are designed and certified to withstand significant pitch excursions under extreme weather conditions, a specific assessment of the effects on the structure of this new form of wind farm control is important to evaluate the overall feasibility of the concept. To this end, hydro-aero-servo-elastic simulations of a conceptual wind turbine on a floating platform are utilized.

The article is organized as follows. Section 2 gives a description of two reference platforms and one wind turbine that are used for assessing the feasibility of the proposed concept. Section 3 analyzes the effect of tilting the rotor on the turbine wake and on the power of a two-turbine cluster through CFD simulations, which were first validated against experimental data. Section 4 presents the effects of tilt on the extreme and fatigue loads computed by hydro-aero-servo-elastic simulations. Section 5 assesses the differential ballast control concept on the basis of an hydrostatic analysis, and presents an initial rough sizing of the system for the two different platform configurations. Finally, Sect. 6 presents the main conclusions and outlines possible future steps.

## 2 Reference turbine and platforms

The present analysis is based on one reference wind turbine and two reference floating platforms. Unlike other wake control strategies, ballast control for vertical wake deflection is substantially affected by the design characteristics of the turbine and of the platform.

Regarding the turbine configuration, upwind wind turbines are favored when wake deflection towards the sky is considered, because of the built-in uptilt used to increase rotor-tower clearance (Burton et al., 2001). In fact, since the rotor plane is already tilted nose-cone up (typically by about $5°$), in order to achieve a given misalignment a smaller additional rotation is needed for a nose-up attitude (upward wake deflection, as in Fig. 1b) than for a nose-down one (downward wake deflection, as in Fig. 1c). Therefore, smaller platform rotations are necessary for deflecting the wake towards the sky than towards the sea surface. Exactly the opposite happens for a downwind turbine, where the built-in uptilt used to increase rotor-tower clearance favours downward wake deflections, resulting in smaller platform angles when the wake is steered towards the sea surface than towards the sky.

As shown by previous research (as for example Cossu (2020a, b); Scott et al. (2020)) and later on in this paper, it appears that downward wake deflection is more effective for improving cluster power than upward deflection. From this point of view, a downwind turbine configuration appears to be better suited for this application than an upwind one. Notwithstanding this important difference between the two configurations, an upwind turbine is used in this work, since it represents today's standard offshore configuration and no large downwind turbines are at present available on the market. The following analyses are based on the DTU 10 MW turbine (Bak et al., 2013), whose basic characteristics are reported in Table 1.

https://doi.org/10.5194/wes-2021-79
Preprint. Discussion started: 19 August 2021


eawe european academy of wind energy
Open Access WIND ENERGY SCIENCE DISCUSSIONS

**Table 1.** Basic characteristics of the DTU 10 MW reference wind turbine.

| Data | Value | Data | Value |
|---|---|---|---|
| Configuration | Upwind | Wind class | IEC 1A |
| Rated electrical power | 10.0 MW | Rated thrust | 1 400 kN |
| Hub height [H] | 119.0 m | Rotor diameter [D] | 178.30 m |
| Rotor uptilt angle | 5.0° | Total weight | 1 280 tons |

**Table 2.** Basic characteristics of the two reference platforms.

| | Platform A | Platform B |
|---|---|---|
| Column length | 38 m | 65 m |
| Column diameter | 12 m | 15 m |
| Column to column distance | 56.4 m | 45 m |
| Total weight | 7 000 tons | 30 000 tons |

Since the present wake control concept is based on the pitching of the whole platform, also the characteristics of the floater —in addition to those of the turbine— play an important role. In fact, the ballast distribution that is required for a specific pitch attitude depends on the size, weight and draft of the platform. Additionally, ballast is affected by where the turbine is located with respect to the platform, either close to its center or to its edge. In case the platform is not axially symmetric about the turbine tower, the yaw orientation of the turbine with respect to the platform also plays a role in determining the differential ballast that is necessary for a given attitude. Finally, it should be noted that, depending on the configuration of the system, a change of platform pitch can imply —in addition to a tilting— also a vertical motion of the hub; as a result, the rotor can be exposed to a slightly different wind speed in a sheared inflow.

In order to explore some of these configuration-related effects, the present paper makes use of two different reference platforms. The first one, hereafter called Platform A (Fig. 2a and 2b), is based on the concept developed in the WINDFLOAT project (Roddier et al., 1997). The platform is composed by three columns made out of steel, arranged in a triangular configuration by connecting trusses, with the turbine directly placed on top of one of the columns. The second platform (Fig. 2c and 2d) is the tri-spar floater developed in the INNWIND project (Azcona et al., 2017; Manolas et al., 2018), hereafter called Platform B. This floater was developed to accommodate a 10 MW machine mounted on a steel structure at the center of three columns, and it represents a hybrid configuration between a semi-submersible and a large-draft spar buoy. This design uses concrete for the spars, resulting in a much heavier structure compared to Platform A. The principal characteristics of the two platforms are summarized in Table 2.

Figure 2b defines also the angle conventions adopted in this paper. Tilt indicates the angle between the rotor axis and the wind vector, while pitch refers to the angle between the platform and the water surface. While wind vector and water surface

https://doi.org/10.5194/wes-2021-79
Preprint. Discussion started: 19 August 2021


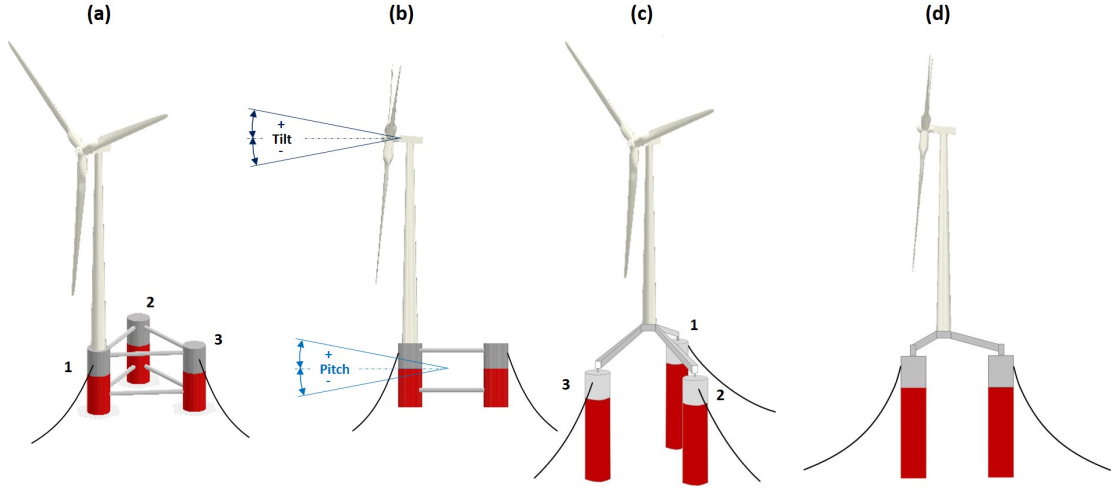


**Figure 2.** Sketch of Platform A, based on the WINDFLOAT concept (Roddier et al., 1997) **(a,b)**. Sketch of Platform B, based on the INNWIND concept (Azcona et al., 2017; Manolas et al., 2018) **(c,d)**.

are assumed to be always parallel, the tilt and pitch angles are not necessarily equal to each other, because of the built-in uptilt used in wind turbines to increase the clearance between rotor and tower with the purpose of relaxing the stiffness requirements on the blade. For a positive tilt, the rotor axis is above the horizon when looking upstream. Hence, an upwind wind turbine has a positive built-in uptilt, whereas a downwind machine has a negative one; additionally, positive tilt implies that the wake is deflected towards the sky, whereas for negative tilt the wake is steered towards the sea surface. Pitch follows the same sign convention. For better readability, instead of referring to positive and negative angles, the text will refer to *wake-up* and *wake-down* angles, respectively, which is a more intuitive terminology.

## 3 Characterization of the wake

The effects of rotor tilt on wake development and downstream power capture were evaluated by a combined simulation-experimental study. The G06 scaled model (Nanos et al., 2021) of the reference 10 MW wind turbine is used for this purpose. Previous work by Wang et al. (2021) has shown that scaled wind turbines, designed according to the same specifications of the G06 model, are capable of producing highly realistic wakes in atmospheric boundary layer wind tunnels. A CFD simulation model of the turbine was first verified based on experimental measurements performed in the wind tunnel in rotor-tilted condition, and then used to explore the characteristics of the wake.

https://doi.org/10.5194/wes-2021-79
Preprint. Discussion started: 19 August 2021


eawe european academy of wind energy
Open Access WIND ENERGY SCIENCE DISCUSSIONS

### 3.1 CFD validation and set-up

CFD simulations were executed with a flow solver based on a large eddy simulation (LES) actuator line method (ALM) implemented in Foam-extend (Jasak, 2009), while the wind turbine lifting-line aerodynamics was modeled in FAST (Guntur et al., 2016). This framework has been validated in previous work (Wang et al., 2019), and it is further verified here in tilted conditions using new ad hoc wind tunnel measurements.

An experimental campaign was conducted in the BLAST atmospheric boundary layer wind tunnel at the University of Texas at Dallas (UTD). Further details on the wind tunnel and the G06 scaled model are available in Nanos et al. (2018, 2019, 2021). The model was operated at its optimum tip speed ratio and pitch angle. With the help of a tilting mechanism inserted between the nacelle and the tower top, the rotor was tested at three different attitudes: $0°$, $20°$ wake-up, and $-20°$ wake-down.

The wake of the G06 was measured on a vertical plane at a 5D downstream distance by Stereo Particle Image Velocimetry (S-PIV). The velocity at hub height was approximatively equal $10$ ms$^{-1}$, the turbulence intensity was $8.5\%$, and the inflow had a vertical shear characterized by an exponent $\alpha = 0.2$.

A first set of CFD simulations mimicked the experimental set-up, including the tilting geometry, the wind tunnel walls and the passive generation of the turbulent and sheared inflow, which was obtained by spires placed at the chamber inlet and roughness elements on the floor. Figure 3 shows the simulated and measured vertical profile of the inflow at the turbine location, which appear to be in very good agreement with each other. Figure 4 shows the absolute percent error between CFD and S-PIV measurements for the three tilt angles at a $x/D = 5$ downstream distance. The error was calculated according to the following formula:

$$\epsilon = \left| \frac{\mathrm{u}^{\mathrm{exp}}/\mathrm{U}^{\mathrm{exp}}_{\mathrm{hub}} - \mathrm{u}^{\mathrm{cfd}}/\mathrm{U}^{\mathrm{cfd}}_{\mathrm{hub}}}{\mathrm{u}^{\mathrm{exp}}/\mathrm{U}^{\mathrm{exp}}_{\mathrm{hub}}} \right| 100, \tag{1}$$

where $u$ is streamwise velocity in the wake and $U_{\mathrm{hub}}$ the inflow velocity at hub height. Results show that the error is for the most part of the domain between $0\%$ and $2\%$, reaching $4\%$ in some limited areas. This error is considered acceptable for the scope of the present analysis. Additional details on the experimental set-up, the S-PIV data and the comparison between experiments and simulations are available in Nanos et al. (2020).

### 3.2 Effects of tilt on the flow

After validating the CFD model for this specific set-up, additional simulations were conducted at different rotor tilt angles. This second set of simulations was based on the configuration of Fig. 2a,b, where the rotor is facing away from the other two columns. This implies that, since the position of the turbine for each tilt angle is determined by the platform kinematics, a wake-up tilt rotation generates a small vertical lifting of the hub, whereas a wake-down tilt comes with a small downward motion.

To compute the power available in the wake, the power coefficient of the untilted configuration was obtained from the CFD results by computing a rotor-effective wind speed. Next, using the computed value of the power coefficient, the power in the wake was obtained from the longitudinal flow velocity component on the area of the rotor disk at various downstream positions,

https://doi.org/10.5194/wes-2021-79
Preprint. Discussion started: 19 August 2021


eawe european academy of wind energy
Open Access WIND ENERGY SCIENCE DISCUSSIONS

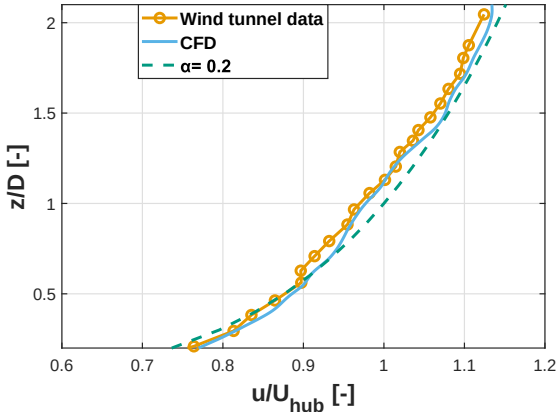


**Figure 3.** Measured and simulated boundary layer profile at the turbine location.

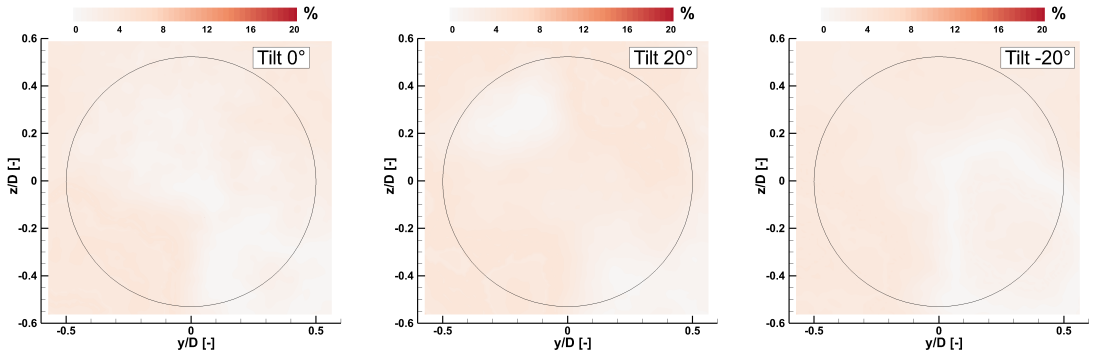


**Figure 4.** Absolute percent error between S-PIV and CFD streamwise flow speed 5D downstream of the rotor, for three tilt angles. The black circle denotes the rotor circumference.

directly behind the wind turbine. Even though, for offshore applications, typical horizontal spacings between two turbines are about equal to 10D, the effects of tilt on downstream power is presented here for distances from 6 to 12D, for the sake of completeness.

Figure 5 shows contours of the normalized streamwise velocity. For brevity, the results are shown only at two downstream distances (namely, $x/D = 6$ and $x/D = 12$) and for three rotor tilt angles ($0°$, $15°$ wake-up and $-15°$ wake-down). The deflection of the wake center is evident at $x/D = 6$, but changes in the flowfield are still noticeable even at $x/D = 12$.

Because of the non-uniformity of the sheared inflow, the wake center is deflected towards the ground by 0.2D even for the aligned rotor case. This effect can also be appreciated in Fig. 6, which shows normalized velocity contours on the $xz$ midplane for the same tilt angles. The flow has a higher momentum above the wake than below it. As a result, turbulent mixing is stronger in the top part of the wake, resulting in a non-symmetrical vertical profile, as already observed in previous studies

https://doi.org/10.5194/wes-2021-79
Preprint. Discussion started: 19 August 2021


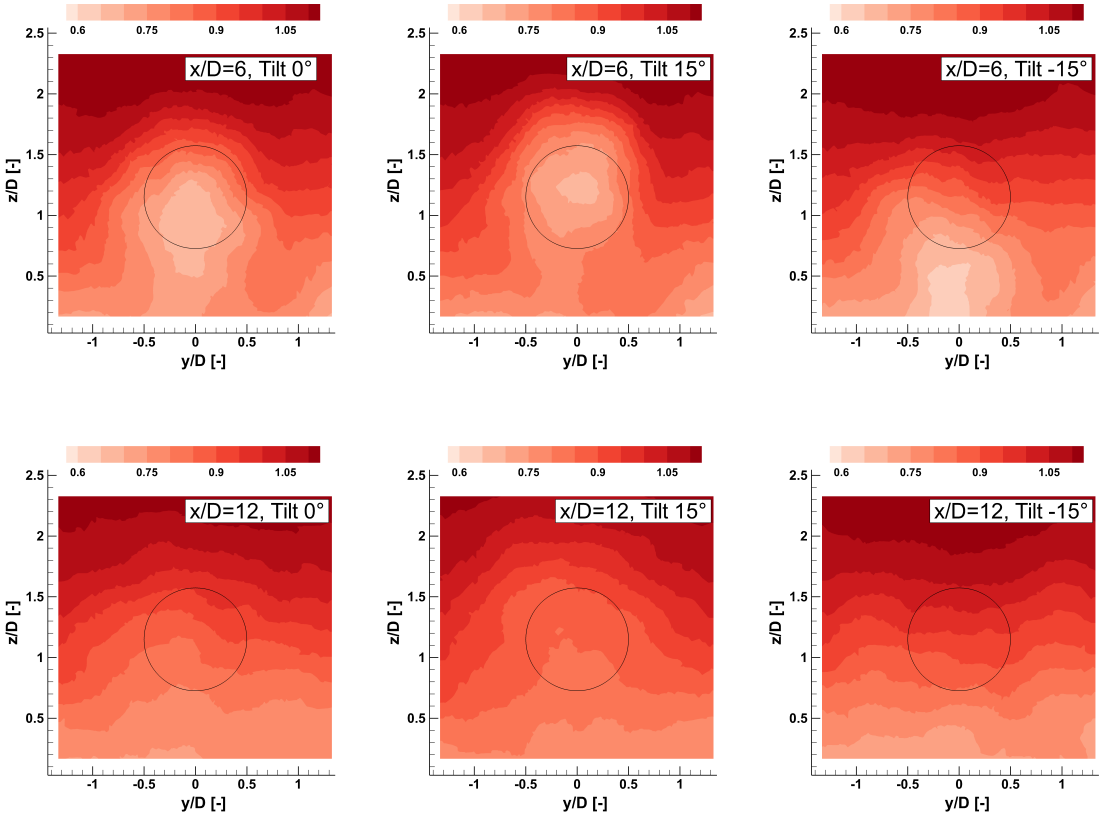


**Figure 5.** Contours of normalized streamwise velocity $u/U_{\text{hub}}$ on $yz$ crossplanes (orthogonal to the flow) for two downstream distances and three rotor tilt angles. The black circle denotes the rotor disk circumference.

(Chamorro and Porté-Agel, 2009; Nanos et al., 2021). Therefore, as shown by the figures, the deflection of the wake towards the sea surface results in a higher energy flow within the downstream rotor area.

Furthermore, it appears that the direction of wake deflection has an effect also on how fast the wake recovers. The recovery rate was calculated based on the integral of the speed $\langle \mathrm{u} \rangle$ computed over a square area of size 2.5D-by-2.5D, centered at hub height. This area is sufficiently large to enclose the wake for all simulated tilt misalignment cases. The value of the integral at $x/D = 2$ was considered as a reference, resulting in the following expression of the recovery rate:

$$\mathrm{R_w} = \frac{\langle \mathrm{u} \rangle}{\langle \mathrm{u} \rangle_{\mathrm{2D}}}. \tag{2}$$

Figure 7 shows the recovery rate for the tilt angles $0°$, $20°$(wake-up), and $-20°$(wake-down). The plot clearly indicates that the recovery for the wake-up (positive) tilt case is essentially the same of the untilted condition. On the other hand, the recovery rate almost doubles for the wake-down (negative) tilt case.

https://doi.org/10.5194/wes-2021-79
Preprint. Discussion started: 19 August 2021


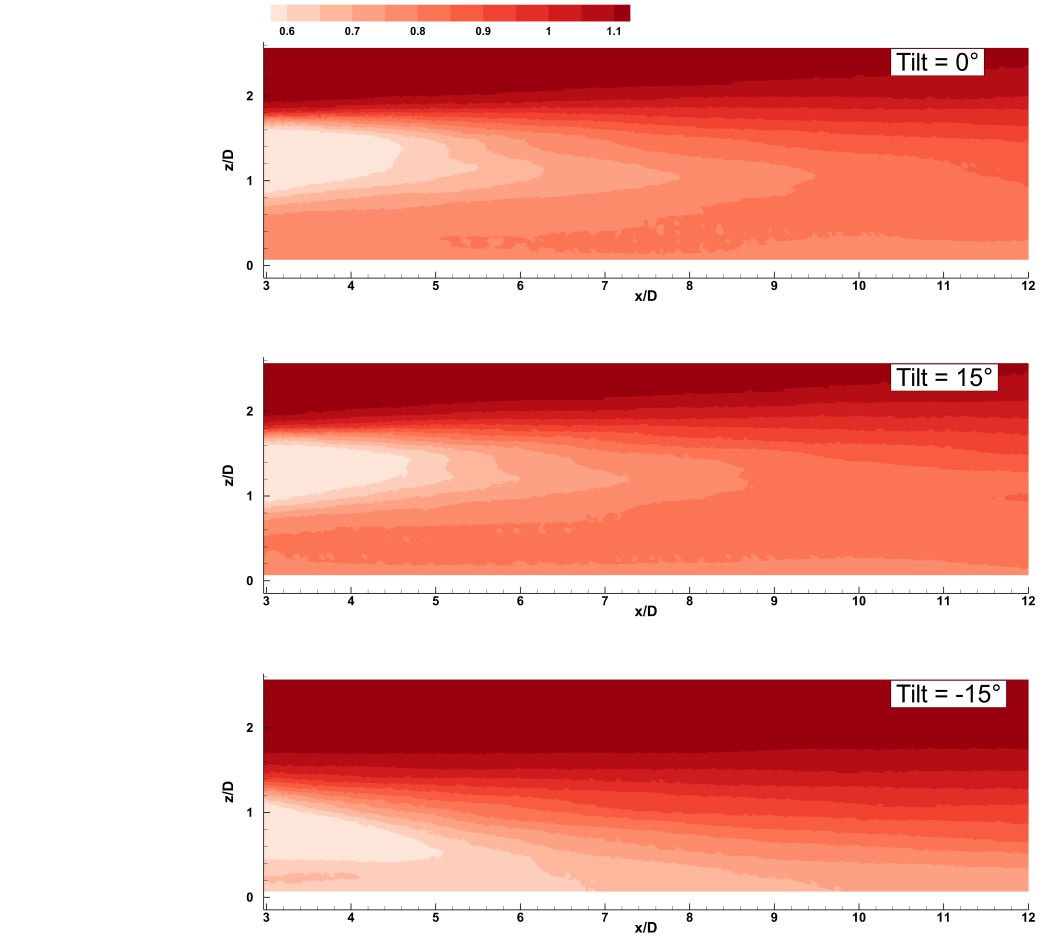


**Figure 6.** Contours of normalized streamwise velocity $u/U_{\text{hub}}$ on the $xz$ longitudinal midplane for three rotor tilt angles.

### 3.3 Effects of tilt on power

Figure 8a reports the percent power drop for the wake-deflecting wind turbine as a function of the rotor tilt angle $\beta$. As expected, tilt misalignment reduces the power capture of the turbine, similarly to the classical yaw misalignment case (Campagnolo et al., 2016b). Best fitting the cosine law $P = P_{\beta=0}\,(\cos\beta)^p$ results in an exponent $p \approx 3.5$. For the same scaled turbine, the power drop cosine exponent in yaw misaligned conditions and laminar inflow is $p \approx 2.01$ (Nanos et al., 2021). The range of exponent values reported in the literature for lateral steering is quite wide (Nanos et al., 2021). The value reported here is relatively high, possibly because of the high turbulence intensity and sheared inflow. Vertical shear also contributes to the noticeable lack of symmetry between wake-up and wake-down tilt angles, in addition to the vertical motion of the hub. The results of the figure

https://doi.org/10.5194/wes-2021-79
Preprint. Discussion started: 19 August 2021


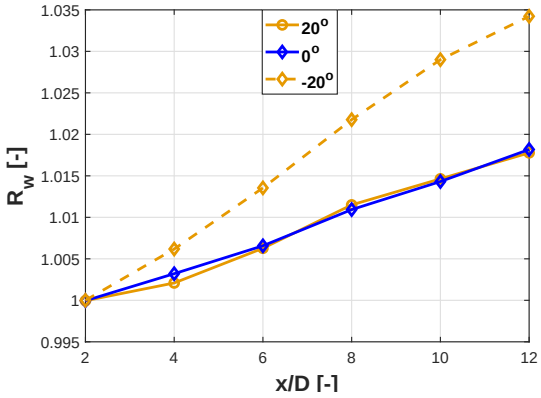


**Figure 7.** Wake recovery rate $R_w$ for $0°$ (untilted), $20°$(wake-up), and $-20°$(wake-down) rotor tilt angle.

correspond to the configuration shown in Fig. 2a, where the rotor is facing away from the other two columns; effects caused by the vertical motion depend on the yaw orientation with respect to the platform and on the platform configuration.

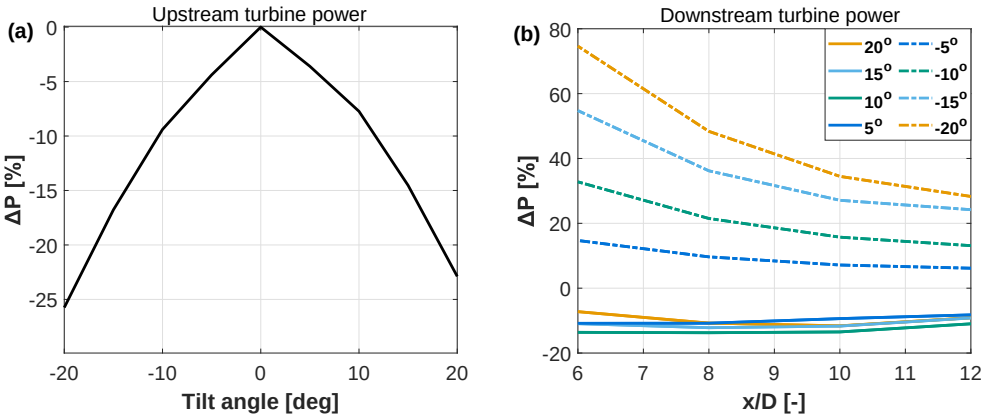


**Figure 8.** Power drop as a function of tilt angle for the wake-steering turbine **(a)**. Power change in the wake as a function of tilt angle and downstream distance **(b)**.

Figure 8b shows the percent power change in the wake as a function of upstream rotor tilt and downstream distance. For wake-down tilt angles, there is a substantial power gain due to the deflection of the wake out of the downstream rotor area, as shown in Fig. 5. The power gain grows with increasing tilt angles, since the wake is further deflected out of the rotor area; at the same time, the upstream machine extracts less power from the flow, resulting in a slightly weaker wake. Furthermore, the power gain decreases with increasing turbine spacing, because of wake recovery.

For wake-up tilt angles, the behavior of the power available in the wake is markedly different, and power drops for all tested tilt angles. In fact, as previously observed with the help of Fig. 6, the upper part of the wake recovers substantially faster than

https://doi.org/10.5194/wes-2021-79
Preprint. Discussion started: 19 August 2021


eawe european academy of wind energy
Open Access WIND ENERGY SCIENCE DISCUSSIONS

the lower part. Hence, by pushing the wake upwards, a lower energy flow is moved into the rotor disk area, reducing power capture downstream.

Additionally, it appears that for wake-up tilt angles the power of the second wind turbine is fairly insensitive to the tilt misalignment of the upstream rotor, in contrast to the wake-down case. This effect can be explained with the help of Fig. 9, which shows vertical profiles of the streamwise velocity for various tilt angles at hub center and $x/D = 6$. The effect of increasing the tilt from $-15°$ to $-20°$ (wake-down) is quite clear, with the larger (negative) tilt angle leading to a higher speed within the rotor disk area. On the other hand, moving from $15°$ to $20°$ (wake-up) has a double-sided effect. On the one hand, the velocity drops in the upper part of the rotor disk area, since the wake center is deflected further up. However, on the other hand the upstream machine extracts less energy from the flow, which results into higher speeds in the lower part of the rotor area. These two effects counteract each other and, as a result, the power production of the downstream machine is relatively insensitive to the tilt angle for wake-up misalignments.

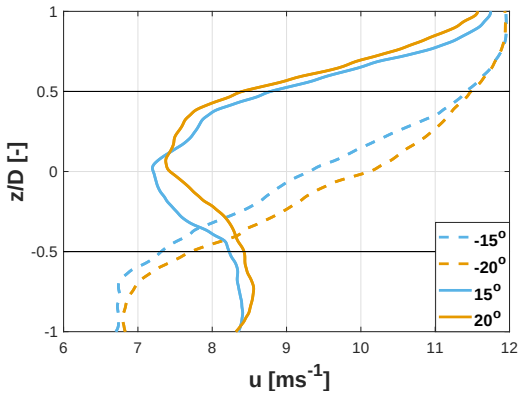


**Figure 9.** Vertical profiles of the longitudinal speed in the wake at $x/D = 6$ for various tilt angles. Black lines denote the rotor upper and lower edges.

Finally, it is interesting to consider the combined gain-loss effects on the power output of the two-turbine cluster, which are shown in Fig. 10. For wake-up tilt angles, the cluster power is always less than the baseline untilted case, which is an expected results since, as shown in Fig. 8, tilt misalignment has a negative impact on both machines. For wake-down tilt angles, the power gain for longitudinal spacings between 10-12D is around 2%, while for closer spacings it can reach up to 7%. The power gain is small but not negligible, considering the fact that it is observed in a cluster of only two turbines. In fact, previous research has shown that wake deflection strategies can multiply their impact in deep arrays (Annoni et al., 2017; Cossu, 2020a, b).

For a comparison with the more popular method of wind farm control by lateral wake deflection, the same simulation set-up was used to implement lateral —as opposed to vertical— misalignment for three different yaw angles, namely $10°$, $15°$, and $20°$. The results are reported in Fig. 10 using black markers, and indicate that —for similar misalignment angles— vertical

https://doi.org/10.5194/wes-2021-79
Preprint. Discussion started: 19 August 2021


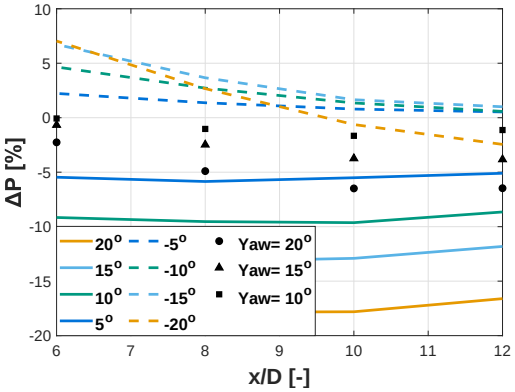


**Figure 10.** Cluster power change as a function of spacing between the turbines, for different tilt misalignment angles (solid and dashed lines). Black markers denote the change in cluster power for different yaw misalignment angles.

deflection towards the ground outperforms lateral deflection. However, this finding is clearly set-up specific, and different layouts might lead to different results. This highlights another important consideration: the two techniques of lateral and vertical steering should not be seen as antagonistic, but rather they could be used together in synergy to achieve the best possible result depending on the layout and operating condition.

### 3.4 Effect of the configuration

The configuration of the floating platform may introduce additional parameters into the problem. For example, with reference to Platform A, pitching results also in a vertical translation of the hub (see Fig. 11). The magnitude of this vertical translation $\Delta z$ depends on the geometric characteristics of the platform-turbine assembly. For the case shown in the figure, the vertical displacement can be computed as

$$\Delta z = \sin\left(\tan^{-1}\left(\frac{l}{m}\right) + \beta\right)\left(\sqrt{l^2 + m^2}\right) - l, \tag{3}$$

where $m$ and $l$ are the horizontal and vertical distances, respectively, between the hub and the center of rotation, and $\beta$ is the pitch angle of the platform (Fig. 11). The center of rotation is considered fixed at the centroid of the platform waterplane area (center of flotation — indicated as CF in the figure), which is a good approximation for small pitch angles (Newman, 2018). The vertical displacement also depends on the turbine orientation with respect to the platform (Fig. 12). For example, consider the situation of Fig. 11, which corresponds to orientation (a) of Fig. 12. In this case, the rotor center is translated downwards for a wake-down pitching of the platform. However, the opposite happens for orientation (c), where a wake-down pitching of the platform moves the rotor center upwards. Clearly, the ensuing effects on the rotor power and its wake also depend on the amount of shear of the inflow.

Figure 13a shows the relation between rotor tilt angle and the normalized vertical translation of the hub, for the three different turbine orientations of Fig. 12; these conditions provide an envelope, within which all other possible conditions are contained.

https://doi.org/10.5194/wes-2021-79
Preprint. Discussion started: 19 August 2021


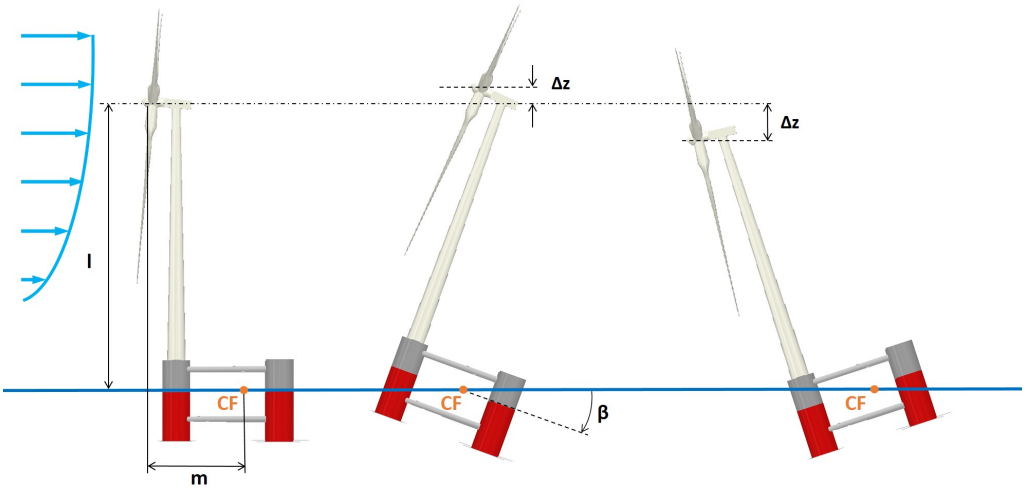


**Figure 11.** Schematic representation of the effects of platform pitch on rotor hub height, considering Platform A. CF: center of flotation; $\beta$: platform pitch angle.

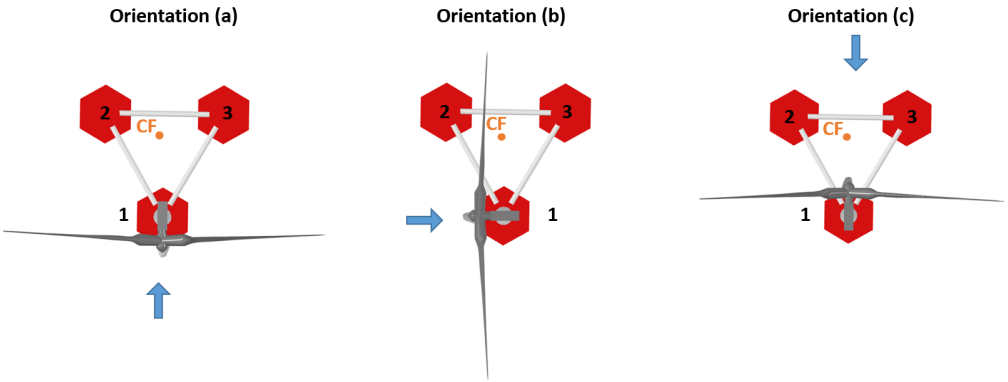


**Figure 12.** Top view of three different turbine orientations with respect to the platform, in the case of Platform A. The blue arrow shows the incoming wind direction. Numbers identify the platform columns.

https://doi.org/10.5194/wes-2021-79
Preprint. Discussion started: 19 August 2021


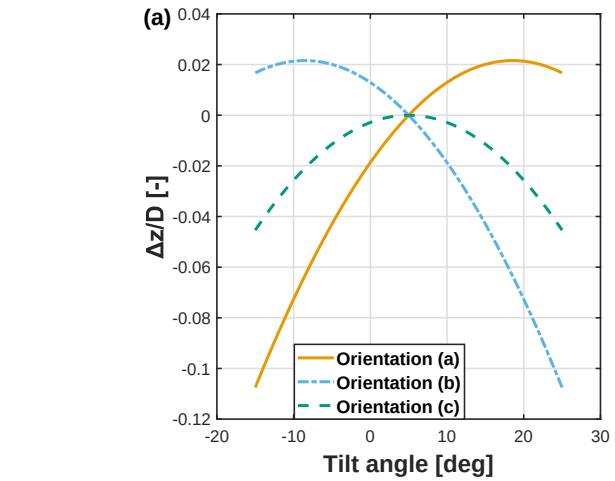

eawe european academy of wind energy
Open Access WIND ENERGY SCIENCE DISCUSSIONS

For Platform B, where the turbine is placed at the center of the floater, this effect is negligible, and all turbine orientations coincide (with a maximum 2% deviation) with orientation (b) of Fig. 12.




**Figure 13.** Normalized vertical translation of the rotor center as a function of rotor tilt angle for three different turbine orientations **(a)**. Percent power change with respect to the baseline untilted case for a $-15^\circ$ (wake-down) deflection at a 10D downstream distance, for three orientations of the turbine with respect to the floater **(b)**.

The vertical translation of the hub caused by platform pitch can have two effects. First, it slightly shifts the wake position in the vertical direction. Second, in case of a sheared inflow, it exposes the rotor to a slightly faster of slower wind speed. In the current set-up and inflow conditions, it was found that the upstream machine looses approximately 5% of power for a 0.1D vertical movement towards the sea surface following an about $15^\circ$ pitching. This loss of power is added to the one caused by tilt misalignment.

It is clear that these effects are strongly dependent on the turbine-platform configuration (for example, they are nearly absent for the Plaform B case), operating conditions and inflow. Therefore, it is difficult to provide a general assessment of their importance. However, in an effort to assess their potential relevance, it was decided to quantify their boundaries in the worst case scenario of Platform A, where the position of the turbine at the very edge of the floater exacerbates these effects. Figure 13b shows the percent power change with respect to the baseline untilted case for the upstream turbine, the downstream turbine, and the whole cluster. The spacing between the turbines is equal to 10D. As expected, results indicate that the different turbine orientations have opposite effects on the upstream and downstream machine. For example, orientation (b) is better for the downstream machine but worse for the upstream one, when compared to orientation (a). For the cluster power, orientation (c) exhibits the best results with a 3.3% power increase, whereas B and A yield increases of 2.6% and 2.3%, respectively. These results apply to a sheared inflow exponent of 0.2, and would be correspondingly reduced/amplified by less/more pronounced shears.

https://doi.org/10.5194/wes-2021-79
Preprint. Discussion started: 19 August 2021


eawe european academy of wind energy
Open Access WIND ENERGY SCIENCE DISCUSSIONS

## 4 Assessment of fatigue and ultimate loads

The feasibility of the proposed vertical wake deflection technique was verified with respect to its effects on structural loading. The goal here is not to precisely characterize the loading of the pitched configurations, but rather to reveal potential unrealistic load increases on the principal structural elements, which cannot be accommodated through confined design modifications.

### 4.1 Simulation set-up

Structural loads were calculated with the comprehensive hydro-aero-servo-elastic analysis tool hGAST (Manolas et al., 2015; Manolas, 2015; Manolas et al., 2020) for the 10 MW reference turbine mounted on the tri-spar concrete floater (Platform B). Mooring lines were modelled using non-linear truss elements, without modifications with respect to the original mooring system of the floater. Load analyses were performed for the baseline untilted configuration, and with the platform pitched by 20° in both wake-up and wake-down directions. The analysis considered medium sea-severity conditions, characterized by a 50-year significant wave height of 10.9 m, a peak period of 14.8 s, and a water depth of 180 m; typical offshore wind conditions were considered, characterized by high mean speeds and moderate turbulence levels, corresponding to wind class IB.

Simulations were conducted for a subset of the most critical design load cases (DLCs) of the IEC 61400-3 standard (IEC, 2008), including both extreme and fatigue conditions. The reduced test matrix is reported in Table 3.

**Table 3.** Definition of DLCs for the time-domain hydro-aero-servo-elastic analysis.

| DLC | Wind | Wave | Bins ($ms^{-1}$) | Yaw (deg) | Wave (deg) | Safety factor |
|---|---|---|---|---|---|---|
| 1.2 | NTM | NSS | 3-25, step 2 | 0 | 0 | - |
| 1.3 | ETM | NSS | 11-25, step 2 | 8 | 0 | 1.35 |
| 1.6 | NTM | ESS | 11-25, step 2 | 8 | 0 | 1.35 |
| 6.1 | EWM | SSS | 50 | 0, 8 | 0, 30 | 1.35 |
| 6.2 | EWM | SSS | 50 | +/- 30 | +/- 30 | 1.10 |

A list of power production (normal operation) cases covering a wide operational range of wind and wave conditions are considered in the 1.x-series. In the table, NTM and ETM refer to the normal and extreme turbulence models, respectively, while NSS and ESS refer to the normal and extreme sea states, respectively. Since wake steering is used only in the partial load region, power production simulations for the pitched platform case are performed for wind speeds up to 13 $ms^{-1}$, to include the next speed bin just above rated (which is equal to 11.4 $ms^{-1}$ for this turbine).

DLC 1.2 corresponds to normal operation of the floating turbine in normal turbulence and sea state, and it is used for estimating the fatigue limit state (FLS). DLCs 1.3 and 1.6 correspond to extreme wind/wave conditions, and are used to estimate the ultimate limit state (ULS). Clearly, there is no actual benefit in energy production from keeping wake steering control in operation when extreme wave conditions are anticipated or encountered (ESS conditions of DLC 1.6). Therefore, it is reasonable to assume that ballast control for wake steering is shut down in these conditions. Weather forecast and sensors (e.g. accelerometers, buoys, etc.) could be used to identify such conditions. However, since the response time of the control

https://doi.org/10.5194/wes-2021-79
Preprint. Discussion started: 19 August 2021


eawe european academy of wind energy
Open Access WIND ENERGY SCIENCE DISCUSSIONS

system is relatively slow (in the order of minutes, as indicated later in Sect. 5), DLC 1.6 was retained in the analyses to assess the effects of a system failure to timely set back the platform to its reference position.

DLC 6.x corresponds to operation under storm conditions, during which the turbine is in idling mode (combined with a grid loss in DLC 6.2). Typically, as a result of the loss of the grid, yaw control is disabled, possibly leading to extreme yaw misalignment angles. In many circumstances, such large angles drive the maximum loads on the rotor and the turbine. In the present analysis, misalignments of 0° and 8° in the wind direction and 0° and 30° in the wave direction were considered in DLC 6.1 (normal idling operation), while +/-30° wind misalignment and co-directional waves were considered in DLC 6.2 (idling operation combined with grid loss). It is noted that independent studies of an onshore version of the DTU 10 MW turbine have shown that yaw angles of +/-30° are the most critical in terms of maximum loads (Wang et al., 2017).

Before conducting the time domain simulations, the hydrostatic stability of the tilted floating turbine was confirmed. Furthermore, a modal analysis of the overall system revealed that pitching has extremely limited changes on the natural frequencies, as shown in Table 4.

**Table 4.** Eigenvalues (Hz) of the coupled floating system for three platform pitch angles (0°, −20°, and 20°).

| Mode | | Pitch=0° | Pitch=−20° | Pitch=20° |
|---|---|---|---|---|
| 1 | Floater Surge | 0.006 | 0.006 | 0.006 |
| 2 | Floater Sway | 0.006 | 0.006 | 0.006 |
| 3 | Floater Yaw | 0.014 | 0.014 | 0.014 |
| 4 | Floater Pitch | 0.043 | 0.047 | 0.046 |
| 5 | Floater Roll | 0.043 | 0.045 | 0.047 |
| 6 | Floater Heave | 0.060 | 0.061 | 0.061 |
| 7 | 1st Tower Side-side | 0.383 | 0.375 | 0.381 |
| 8 | 1st Tower Fore-aft | 0.400 | 0.398 | 0.391 |
| 9 | 1st Rotor Edgewise Symmetric | 0.541 | 0.539 | 0.540 |
| 10 | 1st Rotor Flapwise Yaw | 0.562 | 0.560 | 0.561 |
| 11 | 1st Rotor Flapwise Tilt | 0.600 | 0.599 | 0.598 |
| 12 | 1st Rotor Flapwise Symmetric | 0.646 | 0.646 | 0.646 |
| 13 | 1st Rotor Edgewise Vertical | 0.928 | 0.928 | 0.928 |
| 14 | 1st Rotor Edgewise Horizontal | 0.941 | 0.940 | 0.941 |

The first-order hydrodynamic operators were re-calculated for both tilted floaters. The hydrodynamic problem considers the floater interacting with the incoming waves, and it is modelled using the hybrid integral equation method freFLOW (Manolas, 2015), which solves the 3D Laplace equation using the Boundary Element Method in the frequency domain. The solution procedure provides the exciting loads, the added masses and damping coefficients, the response amplitude operators (RAOs) of the floater, the hydrodynamic pressure on the wet surface of the floater, as well as the linearized hydrostatic stiffness matrix taking into consideration the exact "mean" geometry of the floater. Comparisons of the surge ($F_{\text{surge}}$) and heave ($F_{\text{heave}}$) exciting

https://doi.org/10.5194/wes-2021-79
Preprint. Discussion started: 19 August 2021


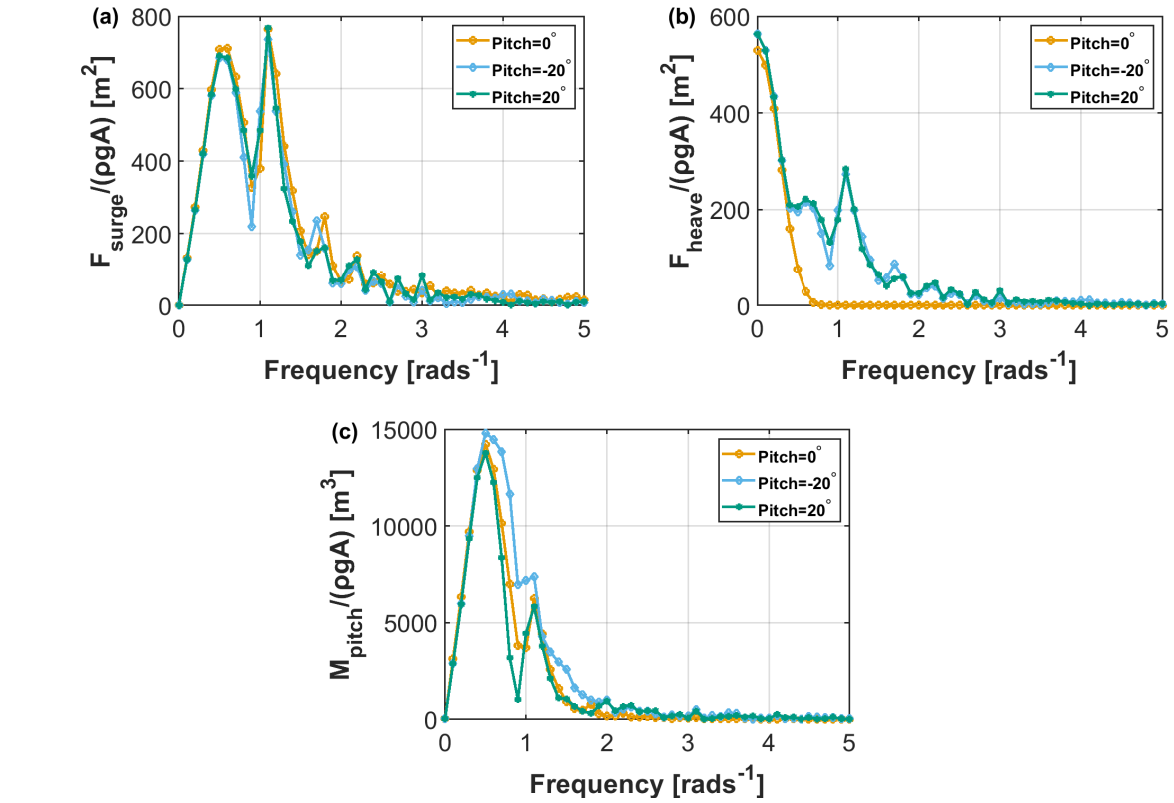


**Figure 14.** Comparison of the wave exciting loads for platform pitch angles $0°$, $20°$ (wake-up), and $-20°$ (wake-down). Surge **(a)**; heave **(b)**; pitch **(c)**.

### 4.2 Effects on damage equivalent and ultimate loads

Table 5 reports lifetime damage equivalent loads (DELs) of the two tilted configurations, comparing them with the ones of the untilted baseline case. DEL calculations are solely based on load time series from DLC 1.2, neglecting parked conditions and startup/shutdown sequences. Lifetime DELs are obtained considering a typical Weibull distribution with $C = 11.3$ ms$^{-1}$ and $k = 2$, $10^7$ reference cycles and a lifetime of 20 years. The S-N curve exponents $m = 4$, 8, and 10 are used for the tower/mooring lines, drive-train, and blades, respectively. Results indicate that blade, drive-train and tower FLS loads are

https://doi.org/10.5194/wes-2021-79
Preprint. Discussion started: 19 August 2021


eawe european academy of wind energy
Open Access WIND ENERGY SCIENCE DISCUSSIONS

barely affected by the tilting of the turbine in either direction. Overall, there is a slight reduction in the edgewise loads, which is higher (5%) for wake-up pitching. This is explained by the fact that the component of the weight load that lies over the rotor plane decreases as the turbine is tilted. The asymmetry between the wake-down and wake-up case is due to the built-in 5° uptilt angle of the rotor, which increases the overall rotor tilt for wake-up inclination of the turbine and visa-versa. Flapwise bending moments remain unaffected. Tower bending moments slightly increase for wake-down pitching, whereas they slightly decrease for wake-up pitching. A maximum increase of 2% is noted on tower base moments. Tower yaw moments slightly decrease in both configurations.

**Table 5.** Comparison of lifetime DELs for platform pitch angles $0^\circ$, $20^\circ$ (wake-up), and $-20^\circ$ (wake-down).

| Sensor | Units | Pitch=0° | Pitch=−20° | Pitch=20° |
|---|---|---|---|---|
| Blade root edgewise moment | kNm | 28 503 | −1% | −5% |
| Blade root flapwise moment | kNm | 31 253 | 0% | 0% |
| Blade root torsion moment | kNm | 454 | 2% | −2% |
| Drivetrain yaw moment | kNm | 28 878 | 0% | 0% |
| Drivetrain tilt moment | kNm | 28 678 | 0% | 0% |
| Drivetrain torsion moment | kNm | 3 356 | 5% | 0% |
| Tower base side-side moment | kNm | 77 492 | 2% | −2% |
| Tower base fore-aft moment | kNm | 272 255 | 2% | −6% |
| Tower base yaw moment | kNm | 27 160 | −1% | −2% |
| Tension at fairleads | kN | 176 | 13% | 1% |
| Tension at anchors | kN | 169 | 12% | 1% |

The main effect of pitching the platform is seen on the mooring line loads, specifically in the case of wake-down pitch. An increase of 13% and 12% is noted on the tension load at fairleads and at the anchor positions, respectively. On the other hand, only a minor increase of 1% is observed for the wake-up pitch case. DEL estimates are derived by averaging over the three mooring lines.

Regarding ultimate loads, it was found that in all cases loads were driven by DLCs outside of the operational envelope of the ballast control system (i.e., DLC 1.6 or DLC 6.x corresponding to extreme sea state or parked/idling operation, or at wind speeds higher than the wake-steering cut-off speed of 13 $ms^{-1}$). Even though the ballast control system will not be used in extreme sea states, it was decided to include DLC 1.6 in the ultimate load analysis with the aim of assessing the effect on loads of the platform remaining pitched under extreme wave conditions.

Results are summarized in Table 6, which also reports the originating DLCs. Changes in loads are null for all cases where ULS are found in DLCs other than 1.6 or 1.3 up to 13 $ms^{-1}$, because the ballast control system is assumed to be deactivated in such conditions. When ultimate loads are originated in DLC 1.6, the load change obtained when this DLC is excluded is indicated in parenthesis.

https://doi.org/10.5194/wes-2021-79
Preprint. Discussion started: 19 August 2021


eawe european academy of wind energy
Open Access WIND ENERGY SCIENCE DISCUSSIONS

**Table 6.** Comparison of ultimate loads for platform pitch angle 0°, 20°, (wake-up) and −20° (wake-down).

| | | Pitch=0° | | Pitch=−20° | | Pitch=20° | |
|---|---|---|---|---|---|---|---|
| Sensor | Units | ULS | DLC | ULC | DLC | ULC | DLC |
| Blade root edgewise moment | kNm | 32717 | $6.2-50$ ms$^{-1}$ | 0% | $6.2-50$ ms$^{-1}$ | 0% | $6.2-50$ ms$^{-1}$ |
| Blade root flapwise moment | kNm | 83212 | $1.6-13$ ms$^{-1}$ | 5% (0%) | $1.6-13$ ms$^{-1}$ | 5% (0%) | $1.6-13$ ms$^{-1}$ |
| Blade root torsion moment | kNm | 1309 | $6.2-50$ ms$^{-1}$ | 0% | $6.2-50$ ms$^{-1}$ | 0% | $6.2-50$ ms$^{-1}$ |
| Blade root combined moment | kNm | 83541 | $1.6-13$ ms$^{-1}$ | 5% (0%) | $1.6-13$ ms$^{-1}$ | 6% (0%) | $1.6-13$ ms$^{-1}$ |
| Drivetrain yaw moment | kNm | 52995 | $1.3-25$ ms$^{-1}$ | 0% | $1.3-25$ ms$^{-1}$ | 0% | $1.3-25$ ms$^{-1}$ |
| Drivetrain tilt moment | kNm | 55680 | $1.6-25$ ms$^{-1}$ | 0% | $1.6-25$ ms$^{-1}$ | 0% | $1.6-25$ ms$^{-1}$ |
| Drivetrain torsion moment | kNm | 17227 | $1.3-25$ ms$^{-1}$ | 0% | $1.3-25$ ms$^{-1}$ | 0% | $1.3-25$ ms$^{-1}$ |
| Drivetrain combined moment | kNm | 63406 | $1.3-25$ ms$^{-1}$ | 0% | $1.3-25$ ms$^{-1}$ | 0% | $1.3-25$ ms$^{-1}$ |
| Tower base side-side moment | kNm | 507594 | $6.2-50$ ms$^{-1}$ | 0% | $6.2-50$ ms$^{-1}$ | 0% | $6.2-50$ ms$^{-1}$ |
| Tower base fore-aft moment | kNm | 808458 | $1.6-13$ ms$^{-1}$ | 19% (0%) | $1.6-13$ ms$^{-1}$ | 39% (0%) | $1.6-11$ ms$^{-1}$ |
| Tower base yaw moment | kNm | 55476 | $1.3-25$ ms$^{-1}$ | 0% | $1.3-25$ ms$^{-1}$ | 0% | $1.3-25$ ms$^{-1}$ |
| Tower base combined moment | kNm | 808458 | $1.6-13$ ms$^{-1}$ | 19% (0%) | $1.6-13$ ms$^{-1}$ | 40% (0%) | $1.6-11$ ms$^{-1}$ |
| Tension at fairleads | kN | 6403 | $1.6-11$ ms$^{-1}$ | 7% (0%) | $1.6-11$ ms$^{-1}$ | −2% (0%) | $6.1-50$ ms$^{-1}$ |
| Tension at anchors | kN | 5965 | $6.1-50$ ms$^{-1}$ | 7% (0%) | $1.6-11$ ms$^{-1}$ | 0% | $6.1-50$ ms$^{-1}$ |

Results indicate that blade extreme loads are only slightly affected by the platform pitching (maximum increase of 5-6%), while drivetrain loads remain unaffected. Larger increases in ultimate loads are noted on tower bending moments. A 19% increase in the combined bending moment is seen in the case of wake-down pitching, whereas a substantially higher increase (40%) is seen in the case of wake-up pitching. The driving load case for tower base loads is DLC 1.6 around rated wind speed, both for the baseline and the pitched configurations. The difference between wake-down and wake-up pitch for tower base fore-aft moment is due to the direction of thrust. For both pitch angles, the moment arm of the weight of the rotor nacelle assembly (RNA) increases, with a corresponding increase of the bending moment at the foot of the tower. However, the fore-aft moment due to the rotor thrust adds to the moment caused by the RNA weight for the wake-up pitch case, whereas it reduces the moment in the wake-down pitch case.

The tension of the mooring lines increases when the platform is pitched wake-down (by 7%, caused by DLC 1.6), whereas slightly decreases (by 2%) in case of wake-up pitching. In the latter case, the tension loads in the mooring lines obtained in DLC 1.6 are smaller than those obtained in DLC 6.1, which becomes the driving load case.

Overall the above results indicate that it is beneficial to deactivate the ballast system when extreme wave conditions occur. This is especially true for the tower base bending moment, which experiences the highest increase. It is worth noting, however, that the observed 40% load increase comes from the wake-up platform attitude, which, as shown in §3.3, is not capable of boosting power output. For the more interesting wake-down pitch case, the increase in tower base combined moment is much

https://doi.org/10.5194/wes-2021-79
Preprint. Discussion started: 19 August 2021


eawe european academy of wind energy
Open Access WIND ENERGY SCIENCE DISCUSSIONS

more contained. Most importantly, based on the reasonable assumption that platform pitching is deactivated for DLC 1.6 conditions, it appears that ballast control will not increase the ultimate loads on the structure.

## 5 Ballast movement estimate

Next, the hydrostatics of floating bodies was used to estimate the differential ballast control necessary to pitch the two floating turbine configurations considered here. For a platform that is resting horizontally, all forces and moments are in equilibrium. If ballast is moved in a specific direction, the center of gravity will move accordingly. As a consequence, the platform will pitch moving the center of buoyancy in the same direction, until a new equilibrium condition is reached (Patel, 1989). The calculations presented here are only indicative and, here again, specific to the configurations considered. For instance, some assumptions have to be made regarding the water ballast pumping system. Moreover, the orientation of the turbine with respect to the floater also plays a role for Platform A, since the ballast movement required for orientation (b) is different from the one necessary for orientations (a) and (c) (see Fig. 12).

The analysis is performed for a rotor tilt angle of $-15^\circ$ (wake-down), which is associated with significant power gains. Given the $5^\circ$ uptilt of the DTU 10 MW turbine, the platform is pitched forward by $20^\circ$ to achieve this attitude. Based on the findings of §3.4, for Platform A the analysis is conducted for orientation (c), which is the most beneficial case in terms of cluster power gain. As previously noted, due to the more symmetric configuration of Platform B, the turbine-platform orientation does not play a role in that case.

For Platform B, the necessary ballast movement was found from static simulations in horizontal and pitched attitudes using the hGAST software (Manolas et al., 2015; Manolas, 2015; Manolas et al., 2020).

Since a similar structural model of Platform A was not available, in this case ballast movement was estimated based on simpler equilibrium of forces and moments for the horizontal and pitched configurations. The analysis considered the mass distribution of the platform and of the turbine, the turbine thrust and torque, and the buoyancy forces from the three columns (Fig. 15). The forces transmitted to the platform by the mooring lines were neglected from the analysis, because the pitch/roll mooring stiffness is small for catenary lines compared to the hydrostatic and gravitational stiffness. This assumption was validated using hGAST for Platform B, where the mooring lines were found to contribute only 5% of the total restoring force. Since no detailed design for Platform A was available, the precise displacement of the column center of gravity and buoyancy could only be estimated. However, the sensitivity of the results to these quantities is relatively low. For example, it was verified that, even with a 30% deviation from the estimated values (which is an exaggerated assumption), the final results of the ballast calculations are affected by less than 4%. To verify the calculation method used for Platform A, the same approach was used also for Platform B, and the results were compared to the ones obtained with hGAST software, yielding only a 6% difference. Such accuracy was deemed sufficient for the preliminary nature of the present investigation.

Results indicate that the necessary ballast movement to achieve a $-20^\circ$ wake-down pitch attitude for Platform A is approximately equal to 500 $m^3$. Considering configuration (c) (Fig. 12c and 15), assuming that water can be moved between each column by dedicated 60 kW pumps, two pumps are used to move water in order to lift column 1 and sink columns 2 and 3. As

https://doi.org/10.5194/wes-2021-79
Preprint. Discussion started: 19 August 2021


eawe european academy of wind energy
Open Access WIND ENERGY SCIENCE DISCUSSIONS

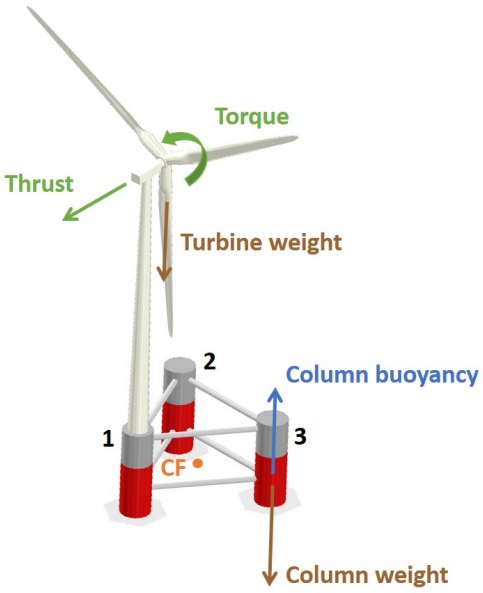


**Figure 15.** Forces and moments considered for the ballast calculations. For clarity, only the forces on one of the columns are shown.

the platform pitches towards a $-20°$ attitude, a height difference between column 1 and columns 2-3 is created. This means that the ballast moves towards a lower position, which facilitates the maneuver. This change of attitude necessitates of approximately 5 minutes and 2 kWh (Menon, 2004). When it is time to return the platform to the horizontal attitude, the situation is different, since the ballast has to move to a higher position. In this case, the maneuver takes approximately 13 minutes and costs roughly 26 kWh.

For the same $-20°$ wake-down pitch attitude, the ballast required for Platform B is equal to $2900\ \mathrm{m}^3$. Given the very large size and weight of this configuration, assuming pumps of triple the power than for case A, the first maneuver (from horizontal position to $-20°$ pitch attitude) takes around 10 minutes, and the energy expenditure is of about 13 kWh. The return to a horizontal attitude requires slightly more than 20 minutes and costs 132 kWh.

Considering two reference turbines spaced 10 rotor diameters apart, exposed to an ambient wind speed of $9\ \mathrm{ms}^{-1}$, the front turbine produces 5 MW and the downstream machine yields 3.5 MW. In such a condition, tilting the first turbine would improve the cluster power production by roughly $3\%$, i.e. 250 kW (which is a conservative assumption, given the results of §3.4). Given that the relation between tilt angle and power gain is approximately linear, Platform A and B would respectively need about 13 and 51 minutes of tilted operation (including the transition time from horizontal to target tilt angle) to break even the energy expenditure caused by tilting, and start having a net energy gain.

https://doi.org/10.5194/wes-2021-79
Preprint. Discussion started: 19 August 2021


eawe european academy of wind energy
Open Access WIND ENERGY SCIENCE DISCUSSIONS

As previously mentioned, the orientation of the turbine with respect to the platform plays a role for Platform A. In fact, the ballast movement required for orientation (b) is three times larger than for orientations (a) and (c); this effect is however negligible for Platform B.

Notwithstanding the variety of possibilities and the room for further optimization, these results indicate that tilt control by differential ballast is a rather slow control input that should be activated in fairly steady wind conditions; possibly, faster changes in ambient conditions could be tracked by lateral yaw misalignment. Additionally, the characteristics of the platform also play a role, with heavy configurations being at a significant disadvantage.

## 6 Conclusions

This paper has presented a technical feasibility assessment of vertical wake steering for floating wind turbines. Today the most mature wind farm control approach is lateral wake steering, a method that is attracting significant attention as the wind energy community is trying to alleviate the adverse effects of turbine wake interaction within wind plants. One of the reasons behind the success of lateral deflection is the fact that it can be implemented without a radical redesign of the turbine. The present study is an attempt at verifying if a similar approach is possible also for vertical steering in floating turbines.

The study is based on two different floating platforms and one reference 10 MW wind turbine. These platforms feature ballast tanks for balancing the structure, and incorporate an active ballast control system for keeping the platform aligned with the water surface (Roddier et al., 1997). The idea explored here is to reuse or adapt such systems in order to tilt the rotor and deflect the wake vertically.

Results obtained with a combined simulation-experimental study indicate that, for two aligned wind turbines spaced 10-12 diameters apart, power gains reach about $3\%$, while for spacings of 6-8 diameters gains can increase to about $7\%$, similarly to the findings of previous research (Annoni et al., 2017; Cossu, 2020a; Bay et al., 2019). These gains are obtained with a $-15^\circ$ wake-down rotor tilt angle that corresponds, due to the rotor uptilt, to a $-20^\circ$ pitch forward of the platform. Because of the direction of rotor uptilt, smaller platform rotations would be necessary for downwind turbine configurations. Nowithstanding this possible advantage, downwind turbines were not considered in this work because they are effectively absent from the current market. However, they have other interesting characteristics for very large rotors that might possibly change this situation in the future (Loth et al., 2017).

The present study has only considered two turbines in full waked conditions, for a specific ambient shear and turbulence intensity. However, previous research has shown that power gains may further increase when considering a larger number of turbines and more complex configurations (Annoni et al., 2017; Cossu, 2020a; Bay et al., 2019). In accordance with prior studies on vertical wake steering (Fleming et al., 2015; Annoni et al., 2017; Cossu, 2020a), the present results confirm that deflecting the wake towards the sea surface is more effective than deflecting it towards the sky. In fact, wake recovery is not axisymmetric when the wake develops within a boundary layer. Due to the vertical non-uniformity of the free stream, turbulent mixing and recovery are faster in the top than in the bottom part of the wake. Therefore, deflecting the wake towards the sea surface results into an air flow of higher momentum moving downwards and into the downstream rotor disk area,

https://doi.org/10.5194/wes-2021-79
Preprint. Discussion started: 19 August 2021


eawe european academy of wind energy
Open Access WIND ENERGY SCIENCE DISCUSSIONS

thereby boosting capture; the opposite happens when the wake is deflected upwards, resulting in a slower flow being lifted up towards the downstream rotor. Additional intra-plant phenomena happen when considering larger arrays and more complex configurations (Cossu, 2020a, b), further increasing power capture.

Another conclusion of the present study is that the geometric characteristics of the platform can have a substantial effect. According to intuition, it was found that a steel platform with smaller draft requires much less ballast movement compared to a concrete platform with greater draft. Specifically, the lighter-weight three-floater configuration of Platform A is able to transition from a horizontal no-steering condition to full steering in about 5 minutes. For a two-turbine cluster, it would take about 13 minutes from the beginning of the maneuver to compensate the expenditure due to tilting and start gaining power; on deeper arrays (Cossu, 2020a, b) this time might be substantially reduced, because of the larger power gains. On the other hand, longer maneuvering times and higher energy expenditures penalize heavy large-draft configurations as the one represented by Platform B. Ballast movement however also depends on additional details related to the geometry of the system. For example, the orientation of the turbine with respect to the platform can have an effect on ballast when the turbine is located directly above a column, because of the strong inertial asymmetry that it creates. Additional effects are related to vertical movements of the hub caused by pitching, resulting in small changes in power capture for sheared flow conditions, which can be beneficial or detrimental depending on the direction of the vertical motion. A more comprehensive analysis, reflecting the latest and most promising configurations, is necessary before final conclusions can be drawn on whether ballast movement is a viable option for implementing vertical steering by pitching. However, this initial study seems to indicate that the amount of water that needs to be moved, the time it will take to pitch and the energy that is required, are not unrealistically high, at least for the lighter-weight Platform A configuration. The present results also indicate that a light-weight steel configuration (like Platform A) with a central arrangement of the turbine (like Platform B) might seem to offer an interesting solution, worth investigating in future studies.

Even in the most beneficial conditions, this preliminary analysis clearly shows that rotor tilting by differential ballast control is a relatively slow control input. Therefore, vertical steering by this method should probably be used only to follow slow changes in wind conditions. On the other hand, lateral steering is able to operate on somewhat faster time scales. This seems to give a strong suggestion towards the study of integrated lateral-vertical steering control, which should try to combine these two complementary methods to maximize their synergies. Of course, steering is only one of the various wake manipulations techniques available, and it could be integrated with —for example— induction control. The optimal combination of techniques for affecting wake behavior is an active area of research in wind farm control, and further progress is anticipated.

Another key aspect related to the feasibility of the present wind farm control method is related to the loading experienced by the steering turbine. This problem was investigated by hydro-aero-servo-elastic simulations with reference to the Platform B concept, for which a complete structural model was available. This heavy platform with a large draft does not seem to be ideally suited to vertical steering, because of the large ballast movements that it requires. In hindsight, a loading study of the lighter weight Platform A would have been more appropriate; this was unfortunately not possible within the scope of the present project, because a detailed design of the Platform A concept was not available. Loads were evaluated for 20° pitch forward and pitch backward attitudes, considering both fatigue and ultimate loads, and they were compared to the design loads

https://doi.org/10.5194/wes-2021-79
Preprint. Discussion started: 19 August 2021


eawe european academy of wind energy
Open Access WIND ENERGY SCIENCE DISCUSSIONS

of the floating system when it is operated without vertical wake steering. The comparison was made under the assumption that steering is used only up to speeds just above rated, and that it would not be used in extreme sea and wind conditions. A detection system with appropriate redundancy might possibly be used to ensure safe behavior in operation, although the characteristics of such a system were not considered in this work. Results indicate that there is only a minor effect on turbine fatigue loads, with an increase of about 5% being experienced by the drivetrain torsional moment. On the other hand, larger increases of about 12-13% were noted on the mooring system, which would have to be accordingly redesigned. Ultimate loads were not affected, since —for this turbine and platform— they are all produced in operational conditions where wake steering is not utilized. These results are promising, but here again more specific analyses are needed before more conclusive answers can be given.

*Data availability.* Data from the CFD and hydro-aero-servo-elastic simulations is available upon request.

*Author contributions.* EMN conducted the experiments, contributed to the CFD simulations, performed all sizing analyses and contributed to the interpretation of the results; CLB devised the original idea of vertical wake steering by differential ballast control, collaborated in the interpretation of the results and supervised the overall work; DIM and VAR performed the hydro-aero-servo-elastic analysis, and contributed to the analysis of the loading conditions on the turbine. EMN and CLB wrote the manuscript, except for Sect. 4 that was primarily authored by DIM and VAR. All authors provided important input to this research work through discussions, feedback and by improving the manuscript.

*Competing interests.* The authors declare that they have no conflict of interest.

*Acknowledgements.* The authors would like to thank Helena Canet at TUM for her input on the load analysis, and Dr. Antonis Daskalakis of Offshore Energy Systems SA for his advice on the platform sizing. Chengyu Wang at TUM contributed to the work on the CFD simulations, while Giacoma Valerio Iungo, Kyle Jones, and Mario Rotea, all at UTD, supported the wind tunnel measurements at UTD.

https://doi.org/10.5194/wes-2021-79
Preprint. Discussion started: 19 August 2021


eawe european academy of wind energy
Open Access WIND ENERGY SCIENCE DISCUSSIONS

## References

Wind Turbines-Part 3: Design Requirements for Offshore Wind Turbines, Tech. rep., IEC 61400-3, 2008.

Annoni, J., Scholbrock, A., Churchfield, M., and Fleming, P.: Evaluating tilt for wind plants, American Control Conference Seattle, pp. 717–722, 2017.

Azcona, J., Vittori, F., Schmidt, U., Savenije, F., Kapogiannis, G., Karvelas, C., Manolas, D. I., Voutsinas, S. G., Amann, F., Faerron-Guzman, R., and Lemmer, F.: D4.3.7: Design Solutions for 10MW Floating Offshore Wind Turbines, Tech. rep., INNWIND.EU, 2017.

Bak, C., Zahle, F., Bitsche, R., Kim, T., Yde, A., Henriksen, L. C., Hansen, M. H., Blasques, J. P., Gaunaa, M., and Natarajan, A.: The DTU 10-MW Reference Wind Turbine, Danish Wind Power Research 2013, Technical University of Denmark, DTU Wind Energy, 2013.

Bay, C. J., Annoni, J., Martínez-Tossas, L. A., Pao, L. Y., and Johnson, K. E.: Flow control leveraging downwind rotors for improved wind power plant operation, in: American Control Conference (ACC), vol. 20, p. 2843–2848, IEEE, 2019.

Burton, T., Sharpe, D., Jenkins, N., and Bossanyi, E.: Wind energy handbook, John Wiley & Sons, 2001.

Campagnolo, F., Petrović, V., Schreiber, J., Nanos, E. M., Croce, A., and Bottasso, C. L.: Wind tunnel testing of a closed-loop wake deflection controller for wind farm power maximization, Journal of Physics: Conference Series, 753, 2016a.

Campagnolo, F., Petrović, V., Schreiber, J., Nanos, E. M., Croce, A., and Bottasso, C. L.: Wind tunnel testing of a closed-loop wake deflection controller for wind farm power maximization, Journal of Physics: Conference Series, 753, 032 006, https://doi.org/10.1088/1742-6596/753/3/032006, 2016b.

Campagnolo, F., Weber, R., Schreiber, J., and Bottasso, C. L.: Wind tunnel testing of wake steering with dynamic wind direction changes, Wind Energy Science, 5, 1273–1295, https://doi.org/10.5194/wes-5-1273-2020, https://wes.copernicus.org/articles/5/1273/2020/, 2020.

Chamorro, L. P. and Porté-Agel, F.: A Wind-Tunnel Investigation of Wind-Turbine Wakes: Boundary-Layer Turbulence Effects, Boundary-Layer Meteorology, 132, 129–149, https://doi.org/10.1007/s10546-009-9380-8, 2009.

Cossu, C.: Replacing wakes with streaks in wind turbine arrays, Wind Energy, https://doi.org/10.1002/we.2577, 2020a.

Cossu, C.: Evaluation of tilt control for wind-turbine arrays in the atmospheric boundary layer, Wind Energ. Sci. Discuss., p. x, https://doi.org/10.5194/wes-2020-106, 2020b.

Cossu, C.: Wake redirection at higher axial induction, Wind Energy Science Discussions, 2020, 1–12, https://doi.org/10.5194/wes-2020-111, 2020c.

Doekemeijer, B. M., Kern, S., Maturu, S., Kanev, S., Salbert, B., Schreiber, J., Campagnolo, F., Bottasso, C. L., Schuler, S., Wilts, F., Neumann, T., Potenza, G., Calabretta, F., Fioretti, F., and van Wingerden, J.-W.: Field experiment for open-loop yaw-based wake steering at a commercial onshore wind farm in Italy, Wind Energy Science, 6, 159–176, https://doi.org/10.5194/wes-6-159-2021, https://wes.copernicus.org/articles/6/159/2021/, 2021.

Energy, S. G. R.: https://www.siemensgamesa.com/en-int/newsroom/2019/11/191126-siemens-gamesa-wake-adapt-en, 2019.

Fleming, P., Gebraad, M., Lee, S., van Wingerden, J., Johnson, K., Churchfield, M., Michalakes, J., Spalart, P., and Moriarty, P.: Simulation comparison of wake mitigation control strategies for a two-turbine case, Wind Energy, 18, 2135—-2143, https://doi.org/https://doi.org/10.1002/we.1810, 2015.

Fleming, P., Annoni, J., Churchfield, M., Martinez-Tossas, L. A., Gruchalla, K., Lawson, M., and Moriarty, P.: A simulation study demonstrating the importance of large-scale trailing vortices in wake steering, Wind Energy Science, 3, 243–255, https://doi.org/10.5194/wes-3-243-2018, https://wes.copernicus.org/articles/3/243/2018/, 2018.

https://doi.org/10.5194/wes-2021-79
Preprint. Discussion started: 19 August 2021


Fleming, P., King, J., Dykes, K., Simley, E., Roadman, J., Scholbrock, A., Murphy, P., Lundquist, J. K., Moriarty, P., Fleming, K., van Dam, J., Bay, C., Mudafort, R., Lopez, H., Skopek, J., Scott, M., Ryan, B., Guernsey, C., , and Brake, D.: Initial results from a field campaign of wake steering applied at a commercial wind farm – Part 1, Wind Energ. Sci., 4, 2135—-2143, https://doi.org/https://doi.org/10.5194/wes-4-273-2019, 2019.

Fleming, P., King, J., Simley, E., Roadman, J., Scholbrock, A., Murphy, P., Lundquist, J. K., Moriarty, P., Fleming, K., van Dam, J., Bay, C., Mudafort, R., Jager, D., Skopek, J., Scott, M., Ryan, B., Guernsey, C., and Brake, D.: Continued Results from a Field Campaign of Wake Steering Applied at a Commercial Wind Farm: Part 2, Wind Energy Science Discussions, 2020, 1–24, https://doi.org/10.5194/wes-2019-104, https://www.wind-energ-sci-discuss.net/wes-2019-104/, 2020.

Frederik, J. A., Doekemeijer, B. M., Mulders, S. P., and van Wingerden, J.-W.: The helix approach: Using dynamic individual pitch control to enhance wake mixing in wind farms, Wind Energy, 23, 1739–1751, https://doi.org/https://doi.org/10.1002/we.2513, 2020a.

Frederik, J. A., Weber, R., Cacciola, S., Campagnolo, F., Croce, A., Bottasso, C., and van Wingerden, J.-W.: Periodic dynamic induction control of wind farms: proving the potential in simulations and wind tunnel experiments, Wind Energy Science, 5, 245–257, https://doi.org/10.5194/wes-5-245-2020, https://wes.copernicus.org/articles/5/245/2020/, 2020b.

Guntur, S., M., J. J., B., J., Q., W., Sprague, A., M., Sievers, R., and Schrek, S. J.: FAST v8 verification and validation for a MW-scale wind turbine with aeroelastically tailored blades, Wind Energy Symp., 2016.

Jasak, H.: OpenFoam: opeN source CFD in research and industry, Int. Nav. Arch. Ocean, 1, 2009.

Liu, Y., Li, S., Yi, Q., and Chen, D.: Developments in semi-submersible floating foundations supporting wind turbines: A comprehensive review, Renewable and Sustainable Energy Reviews, 60, 433–449, 2016.

Loth, E., Steele, A., Qin, C., Ichter, B., Selig, M. S., and Moriarty, P.: Downwind pre-aligned rotors for extreme-scale wind turbines, Wind Energy, 20, 1241–1259, https://doi.org/10.1002/we.2092, 2017.

Manolas, D. I.: Hydro-aero-elastic analysis of offshore wind turbines, Ph.D. thesis, National Technical University of Athens, 2015.

Manolas, D. I., Riziotis, V. A., and Voutsinas, S. G.: Assessing the importance of geometric non-linear effects in the prediction of wind turbine blade loads, J. Comput. Nonlinear Dyn., 10, https://doi.org/10.1115/1.4027684, 2015.

Manolas, D. I., Karvelas, C. G., Kapogiannis, I. A., Riziotis, V. A., Spiliopoulos, K. V., and Voutsinas, S. G.: A comprehensive method for the structural design and verification of the INNWIND 10MW tri-spar floater, J. Phys. Conf. Ser., 1104, https://doi.org/10.1088/1742-6596/1104/1/012025, 2018.

Manolas, D. I., Riziotis, V. A., Papadakis, G. P., and Voutsinas, S. G.: Hydro-servo-aero-elastic analysis of floating offshore wind turbines, Fluids, 5, https://doi.org/10.3390/fluids5040200, 2020.

Menon, S.: Piping Calculations Manual, McGraw-Hill Education, 2004.

Munters, W. and Meyers, J.: Towards practical dynamic induction control of wind farms: analysis of optimally controlled wind-farm boundary layers and sinusoidal induction control of first-row turbines, Wind Energy Science, 3, 409–425, https://doi.org/10.5194/wes-3-409-2018, 2018.

Nanos, E., Robke, J., Heckmeier, F., Cerny, M., Jones, K., Iungo, V., and Bottasso, C.: Wake characterization of a multipurpose scaled wind turbine model, AIAA Scitech 2019 Forum, https://doi.org/10.2514/6.2019-2082, 2019.

Nanos, E., Letizia, S., Barreiro, D., Wang, C., Rotea, M., Iungo, V., and Bottasso, C.: Vertical wake deflection for offshore floating wind turbines by differential ballast control, Journal of Physics: Conference Series, 23, 513–519, https://doi.org/10.1007/s003480050142, 2020.

Nanos, E., Bottasso, C. L., Letizia, S., and Iungo, V. G.: Design, performance and wake characterization of a scaled wind turbine with closed-loop controls, Wind Energ. Sci. Discuss., https://doi.org/10.5194/wes-2020-66, 2021.

https://doi.org/10.5194/wes-2021-79
Preprint. Discussion started: 19 August 2021


Nanos, E. M., Kheirallah, N., Campagnolo, F., and Bottasso, C. L.: Design of a multipurpose scaled wind turbine model, Journal of Physics: Conference Series, 1037, 052 016, https://doi.org/10.1088/1742-6596/1037/5/052016, 2018.

Newman, J.: Marine Hydrodynamics, 40th anniversary edition, [MIT Press], 2018.

Parkin, P., Holm, R., and Medici, D.: The application of PIV to the wake of a wind turbine in yaw, in: DLR-Mitteilung, no. 3 in DLR-Mitteilung, pp. 155–162, qC 20101018, 2001.

Patel, M.: Dynamics of Offshore structures, Butterworth-Heinemann, [S.l.], 1989.

Roddier, D., Cermelli, C., and Weinstein, A.: Windfloat: A Floating Foundation for Offshore Wind Turbines Part I: Design Basis and Qualification Process, Proc. of the ASME 2009 28th Int. Conf. on Ocean Honolulu, 1997.

Scott, R., Bossuyt, J., and Cal, R.: Characterizing tilt effects on wind plants, Journal of Renewable and Sustainable Energy, 12, 2135—-2143, https://doi.org/10.1063/5.0009853, 2020.

Srinivas, G., Troldborg, N., and Gaunaa, M.: Application of engineering models to predict wake deflection due to a tilted wind turbine, European Wind Energy Conference and Exhibition, 2012.

Steinbuch, M., de Boer, W., Bosgra, O., Peters, S., and Ploeg, J.: Optimal control of wind power plants, Journal of Wind Engineering and Industrial Aerodynamics, 27, 237–246, https://doi.org/10.1016/0167-6105(88)90039-6, 1988.

Su, K. and Bliss, D.: A numerical study of tilt- based wake steering using a hybridfree-wake method, Wind Energy, 23, 258–273, https://doi.org/10.1002/we.2426, 2019.

van der Hoek, D., Kanev, S., Allin, J., Bieniek, D., and Mittelmeier, N.: Effects of axial induction control on wind farm energy production - A field test, Renewable Energy, 140, 994 – 1003, https://doi.org/https://doi.org/10.1016/j.renene.2019.03.117, http://www.sciencedirect.com/science/article/pii/S096014811930429X, 2019.

Vermeer, L. J., Sørensen, J. N., and Crespo, A.: Wind turbine wake aerodynamics, Progress in Aerospace Sciences, 39, 467–510, https://doi.org/10.1016/S0376-0421(03)00078-2, 2003.

Wang, C., Campagnolo, F., Sharma, A., and Bottasso, C.: Effects of dynamic induction control on power and loads, by LES-ALM simulations and wind tunnel experiments, IOP Journal of Physics: Conference Series, 1619, 022 036, https://doi.org/doi:10.1088/1742-6596/1618/2/022036, 2020.

Wang, C., Campagnolo, F., Canet, H., Barreiro, D. J., and Bottasso, C. L.: How realistic are the wakes of scaled wind turbine models?, Wind Energy Science, 6, 961–981, https://doi.org/10.5194/wes-6-961-2021, https://wes.copernicus.org/articles/6/961/2021/, 2021.

Wang, J., Wang, C., Campagnolo, F., and L., B. C.: Wake behavior and control: comparison of LES simulations and wind tunnel measurements, Wind Energy Sci., 4, 71–88, 2019.

Wang, K., Riziotis, V. A., and Voutsinas, S. G.: Aeroelastic Stability of Idling Wind Turbines, Wind Energ. Sci., 2, 415–437, https://doi.org/10.5194/wes-2-415-2017, 2017.

## Nomenclature

| | |
|---|---|
| $A$ | Wave amplitude |
| $C_P$ | Power coefficient |
| $D$ | Rotor diameter |
| $F$ | Force |

https://doi.org/10.5194/wes-2021-79
Preprint. Discussion started: 19 August 2021


eawe european academy of wind energy
Open Access WIND ENERGY SCIENCE DISCUSSIONS

| | | |
|---|---|---|
| | $M$ | Moment |
| | $g$ | Gravitational acceleration |
| | $p$ | Cosine law power loss exponent |
| | $P$ | Power |
| | $R_w$ | Wake recovery rate |
| | $U$ | Ambient wind speed (time averaged) |
| | $u$ | Streamwise velocity component (time averaged) |
| | $x$ | Streamwise coordinate (positive downstream) |
| | $y$ | Crosswind coordinate (positive left, looking downstream) |
| | $z$ | Vertical coordinate (positive up) |
| | $\beta$ | Platform pitch angle |
| | $\rho$ | Water density |
| | ALM | Actuator-line method |
| | CFD | Computational fluid dynamics |
| | CF | Center of flotation |
| | DEL | Damage equivalent load |
| | DLC | Design load case |
| | ETM | Extreme turbulence model |
| | EWM | Extreme wind model |
| | FLS | Fatigue limit state |
| | LES | Large-eddy simulation |
| | NSS | Normal sea state |
| | NTM | Normal turbulence model |
| | S-PIV | Stereo-Particle image velocimetry |
| | SSS | Severe sea state |
| | ULS | Ultimate limit state |